FROTH FLOTATION PERFORMANCE ENHANCEMENT BY FEED CAVITATION AND MAGNETIC PLASTIC PARTICLE ADDITION

DISSERTATION

A dissertation submitted in partial fulfillment of the
requirements for the degree of Doctor of Philosophy in the
College of Engineering
at the University of Kentucky

By

Mehmet Saracoglu

Lexington, Kentucky

Director: Dr. Rick Q. Honaker, Professor and Chair of Mining Engineering

Lexington, Kentucky

2013

Copyright © Mehmet Saracoglu 2013

ABSTRACT OF DISSERTATION

FROTH FLOTATION PERFORMANCE ENHANCEMENT BY FEED CAVITATION AND MAGNETIC PLASTIC PARTICLE ADDITION

Froth flotation is the most commonly used process to recover and upgrade the portion of the coal preparation plant feed that has a particle size smaller than 150 microns. Problems that occur when employing froth flotation in the coal industry include i) coal surfaces that are weakly-to-moderately hydrophobic, and ii) flotation systems that are overloaded and limited by insufficient retention time.

Research was performed to evaluate techniques that could be implemented to improve flotation performance under the aforementioned scenarios. Pre-aeration of flotation feed using a cavitation system was extensively evaluated in laboratory and full-scale test programs. The benefits of adding hydrophobic, magnetic plastic particles were also investigated to improve froth stability and increase bubble surface area.

Laboratory tests revealed that pre-aeration through a cavitation tube improved coal recovery by as much as 20 absolute percentage points in both conventional cells and flotation columns when treating difficult-to-float coals. Carrying capacity increased by 32% which was projected to provide a 4 t/h increase in flotation recovery for a typical 4-m diameter flotation column. Product size analyses suggest that the improved particle recovery was more pronounced for the finest coal fractions as a result of particle agglomeration, resulting from the use of the nucleated air bubbles on the coal surfaces as a bridging medium. In-plant testing of a commercial-scale cavitation system found that feed pre-aeration could reduce collector dosage by 50% when no additional air is added and by 67% when a small amount of air is added to the feed to the cavitation system. At a

constant collector dosage, recovery increased by 10 absolute percentage points with cavitation without additional air and 17 absolute points when additional air is provided.

The addition of hydrophobic plastic particles to the flotation feed at a 10% concentration by weight was found to substantially improve froth stability thereby elevating the recovery and enhancing carrying-capacity. Test results showed that the primary flotation improvements were directly linked to the coarsest particle size fractions in the plastic material which supports the froth stability hypothesis. Combustible recovery was increased up to 10 percentage points while producing the desired concentrate quality.

KEYWORDS: Froth Flotation, Coal Recovery, Flotation Size,

Cavitation Pretreatment, Carrying Capacity.

MEHMET SARACOGLU

09/05/2013

FROTH FLOTATION PERFORMANCE ENHANCEMENT BY FEED CAVITATION AND MAGNETIC PLASTIC PARTICLE ADDITION

By

Mehmet Saracoglu

Dr. RICK Q. HONAKER

_____

Director of Dissertation

Dr. THOMAS NOVAK

_____

Director of Graduate Studies

09/05/2013

_____

I would like to dedicate this work to my family whose love and support always found a way to reach me from thousands of miles away. Their never ending guidance, patience, and understanding were inspirations that have profoundly contributed to the completion of this work.

ACKNOWLEDGEMENTS

I would like to express my gratitude to my advisor, Dr. Rick Q. Honaker, for his guidance, enthusiasm, and continual support throughout this work. His mentorship, motivation and friendship guided me during this research to achieve our objectives.

I would like to acknowledge the support of the Center for Advanced Separation Technologies (CAST) who provided the funding for the cavitation project. I am also grateful to Mike Mankosa, Jaisen Kohmuench, Eric Yan, Maoming Fan and other researchers from the Eriez Manufacturing Co. for their technical and hands-on support for the in-plant studies and their assistance for the laboratory tests.

I am extremely grateful to Mr. Edward Thompson for his invaluable help for conducting the tests in the laboratory.

I would also like to thank my entire fellow graduate students without whom conducting the various tests would have been impossible. I am extremely grateful to the whole Mining Engineering department for creating a wonderful atmosphere for me.

Finally, I would like to thank my family for all their support and understanding.

TABLE OF CONTENTS

Acknowledgements iii
Table of Contents iv
List of Tables viii
List of Figures x
Nomenclature xv

CHAPTER 1 - INTRODUCTION 1
1.1. BACKGROUND 1
1.2. RESEARCH OBJECTIVES 10
1.3. METHODOLOGY 13

CHAPTER 2 - FLOTATION RECOVERY: LITERATURE REVIEW 16
2.1. INTRODUCTION 16
2.2. COLLECTION ZONE RECOVERY 16
2.2.1. Probability of Flotation 20
2.2.2. Probability of Collision 21
2.2.3. Probability of Attachment 26
2.2.3.1. Energy Barrier for Attachment 27
2.2.3.2. Kinetic Energy, E_k 31
2.2.3.3. Thermodynamics of Wetting 35
2.2.3.4. Induction Time 39
2.2.4. Probability of Detachment 42
2.2.4.1. Force Balance for Detachment 45
2.2.4.2. Maximum Particle and Bubble Sizes 48
2.2.5. Collection Zone Recovery Rate 52
2.3. FROTH ZONE RECOVERY 54
2.3.1. Froth Zone Recovery Rate 55
2.4. OVERALL FLOTATION RECOVERY 56

CHAPTER 3 - EXPERIMENTAL 60
3.1. CAVITATION FEED PRETREATMENT – LABORATORY STUDIES... 60
3.1.1. Sample Characterization 60
3.1.2. Release Analysis 63
3.1.3. Flotation Rate Tests 65
3.1.4. Column Flotation Tests 66
3.1.5. Laboratory-scale Cavitation Tube 69
3.2. CAVITATION FEED PRETREATMENT – IN-PLANT STUDIES 71
3.2.1. Sample Characterization 71
3.2.2. Full-scale Cavitation Tube System 73
3.2.3. StackCell Flotation Unit 77
3.3. MAGNETIC PLASTIC MATERIAL EVALUATION 79
3.3.1. Sample Characterization 79
3.3.1.1. Coal Samples 79
3.3.1.2. Magnetic Plastic Material 81
3.3.1.3. Grinding and Polishing Process 87
3.3.1.4. Contact Angle Analysis 88
3.3.1.5. Zeta-Potential Measurements 90
3.3.2. Release Analysis 92
3.3.3. Flotation Rate Tests 93
3.3.4. Column Flotation Tests 93

CHAPTER 4 - CAVITATION PRETREATMENT FOR ENHANCED COAL RECOVERY – LABORATORY STUDIES 95
4.1. INTRODUCTION 95
4.1.1. The Cavitation Phenomenon 96
4.1.1.1. Discovery 96
4.1.1.2. Definition 96
4.1.1.3. The Role of Bubble Nuclei 98
4.1.1.4. Classification 100
4.1.1.5. Hydrodynamic Cavitation 102

4.1.2. Role of Cavitation in Froth Flotation 107
4.1.2.1. Effect on Bubble-Particle Collision 107
4.1.2.2. Effect on Bubble-Particle Attachment 110
4.1.3. Fundamental Analysis 113
4.1.3.1. Krasowska and Malysa (2007) 113
4.1.3.2. Sayed-Ahmed (2013) 115
4.1.4. Empirical Studies 117
4.1.4.1. Munoz-Diaz (2007) 117
4.1.4.2. Independent Research Laboratory 119
4.2. RESULTS AND DISCUSSION 120
4.2.1. Conventional Flotation Tests 120
4.2.2. Column Flotation Tests 129
4.3. CONCLUSIONS 137

CHAPTER 5 - CAVITATION PRETREATMENT FOR ENHANCED COAL RECOVERY – IN-PLANT STUDIES 140
5.1. INTRODUCTION 140
5.2. RESULTS AND DISCUSSION 141
5.2.1. Effect of Collector Type 141
5.2.2. Evaluation of Collector Dosage 143
5.2.3. Importance of Collector Application Method 147
5.2.4. Evaluation of Frother Dosage 148
5.3. CONCLUSIONS 151

CHAPTER 6 – APPLICATION OF HIGHLY HYDROPHOBIC PARTICLES FOR ENHANCED COAL RECOVERY 153
6.1. INTRODUCTION 153
6.1.1. Coalescence 155
6.1.2. Drainage 158
6.1.3. Froth Stability 161
6.1.4. Previous Research 163

6.2. RESULTS AND DISCUSSION 167
6.2.1. Conventional Flotation Tests 168
6.2.1.1. Flotation Rate and Recovery Response 168
6.2.1.2. Effect of pH and Surface Forces 173
6.2.2. Column Flotation Tests 176
6.2.2.1. Volumetric Feed Rate Evaluation 176
6.2.2.2. Carrying Capacity Evaluation 179
6.2.2.3. Particle Size-by-Size Flotation 180
6.3. CONCLUSIONS 186

CHAPTER 7 – SUMMARY AND CONCLUSIONS……189

CHAPTER 8 – RECOMMENDATIONS FOR FUTURE WORK…..……...197

APPENDICES
APPENDIX – A: STACKCELL CIRCUIT 200
APPENDIX – B: CAVITATION TUBE SYSTEM 203

REFERENCES……207

VITA .....……226

LIST OF TABLES

Table 1.1. Carrying capacity ranges for different feed size fractions of coal flotation (Christodoulou, 2013). 7
Table 3.1. Particle size distribution and quality characteristics of a preparation plant flotation feed from Winchester seam located in Raleigh County, West Virginia. 61
Table 3.2. Particle size distribution and quality characteristics of a preparation plant flotation feed from Coalburg seam located in Boone County, West Virginia. 62
Table 3.3. Particle size distribution and quality characteristics of a preparation plant flotation feed from Coalburg seam located in Kanawha County, West Virginia. 63
Table 3.4. Operating conditions of the column flotation test program 69
Table 3.5. Random feed size analysis of the Peerless coal used during in-plant studies 72
Table 3.6. Proximate analysis of the Peerless seam on dry basis with 7% surface moisture 72
Table 3.7. Kanawha Eagle preparation plant clean coal proximate analysis for Peerless coal, where AR and DB denote “as received” and “dry basis”, respectively ..73
Table 3.8. Operating parameters for the cavitation tube system during the in-plant testing 77
Table 3.9. Incremental particle size distribution and quality characteristics of a preparation plant flotation feed from Coalburg seam 81
Table 3.10. Information about the EEA plastic coating material used to form PMBP 82
Table 3.11. Size analysis of the magnetic plastic material after being pulverized in the laboratory hammer mill 84
Table 3.12. Magnetic material recovery rates in different stages of recycling after rate tests 86
Table 3.13. Contact angle measurements of coal and magnetic plastic particles using distilled water and Methylene Iodide, where the asterisk (*) represents the measurement from the previous study 90
Table 3.14. Specific parameter values used for the magnetic plastic addition effects on column flotation performance 94
Table 4.1. Improved kinetic rates and the corresponding flotation recovery values using data obtained after one minute of flotation for the Coalburg coal (Munoz-Diaz, 2007) 119
Table 4.2. Improved kinetic rates and the corresponding flotation recovery values after one and two minutes of flotation for the conventional tests conducted by Eriez Flotation Division-USA 120
Table 4.3. Fast and slow flotation rate constants for the BC coal sample 124
Table 4.4. Fast and slow flotation rate constants for the KC coal sample 126
Table 4.5. Notations of the column flotation test points for the different Coalburg coal samples shown in Figures 4.20 and 4.21 130

Table 6.1. Flotation performances after repetitive tests for Coalburg and Pittsburgh No. 8 coals at 0% and 10% magnetic plastics using a residence time of one minute (Munoz-Diaz, 2007).....165
Table 6.2. Flotation rate improvements achieved under varying pH conditions when adding on plastic particles to Pittsburgh No. 8 at a concentration of 10% by weight (Munoz-Diaz, 2007).....165
Table 6.3. Flotation performances with the addition of 5% and 10% magnetic material after one minute of flotation for Coalburg and Eagle coal samples 171
Table 6.4. Flotation rate improvements achieved under varying pH conditions when adding plastic particles to Coalburg coal at a concentration of 10% by weight.....176

LIST OF FIGURES

Figure 1.1. Lower and upper particle size limitations for the effective application of froth flotation on different minerals (Kohmuench et al., 2010) 4
Figure 1.2. Tpical product rate limi (carrying-capacity conditions) for coal flotation at different feed solid concentrations as a result of a pilot-scale test work (Kohmuench and Mankosa, 2006).....6
Figure 1.3. Schematic illustration of the characterization study and the general flotation tests conducted for the evaluation of the cavitation feed pretreatment.…….....14
Figure 1.4. Schematic illustration of the characterization study and the general flotation tests conducted using different coal sources to evaluate the impact of magnetic plastic particles……..…….....15
Figure 2.1. The relationship between the bubble surface area flux and zinc recovery over a range of impeller types and resulting speeds (*after* Gorain et al., 1999) 21
Figure 2.2. Illustration of bubble-particle collision efficiency mechanism with a particle moving past a bubble in a liquid streamline (Yoon and Luttrell, 1989) 23
Figure 2.3. Probability of collision in a flotation column system as a function of bubble size (Yoon and Luttrell, 1993) 25
Figure 2.4. Total interaction (or potential) energy vs. distance diagram for the extended DLVO theory (Sherrell, 2004) 29
Figure 2.5. Grazing streamline for a particle approaching a bubble surface, where u_{tp}, is the tangential velocity (Yoon and Mao, 1996) 33
Figure 2.6. Potential energy and distance relationship for the bubble-particle interaction that determines the work of adhesion, and thus the attachment process (Yoon and Mao, 1996).....34
Figure 2.7. The three-phase contact for a liquid droplet on a solid surface in vapor 35
Figure 2.8. Spreading between solid, liquid and gas interfaces depending on their surface tensions 37
Figure 2.9. Effect of bubble size on the attachment probability of a fine size particle for a range of induction times (*after* Yoon and Luttrell, 1989) 40
Figure 2.10. A solid spherical particle of radius R_1 attaching on a bubble surface in liquid suspension (Yoon and Mao, 1996) 42
Figure 2.11. A cap of particles (R_1) collected at the bottom of a rising air bubble (R_2) (Yoon and Mao, 1996) 44
Figure 2.12. Illustration of the overall flotation recovery showing the interaction between collection and froth zones in a flotation cell rising air bubble 57
Figure 2.13. The impact of collection and froth zone recoveries on selectivity of the flotation process 58
Figure 3.1. Schematic of the release analysis procedure in two-phases using a laboratory-scale conventional Denver flotation cell 64

Figure 3.2. Schematic of the laboratory flotation cell setup employing the cavitation feed pre-aeration during the kinetic rate tests 65
Figure 3.3. Schematic of the laboratory column flotation setup used for the standard testing procedure 67
Figure 3.4. Schematic of the laboratory column flotation setup with the cavitation feed pretreatment 68
Figure 3.5. Venturi cavitation tube and major design parameters for feed pretreatment.. 70
Figure 3.6. Plan view and the plant installation of the cavitation tube system for flotation feed pretreatment 74
Figure 3.7. Schematic view of the air manifold control the airflow prior to the cavitation tube system 76
Figure 3.8. A "see-through" 3-D illustration of the StackCell module with major components of the machine 78
Figure 3.9. Flotation circuit flowsheet of the preparation plant, including a three -stage StackCell unit and a cavitation tube system with the option of air addition 79
Figure 3.10. Chemical structure of ethylene/ethyl acrylate (EEA) copolymer..... 81
Figure 3.11. SEM image of the pulverized magnetic plastic material (minus 180 μm) at 500 μm optical resolution (Munoz-Diaz, 2007) 83
Figure 3.12. Layout schematic of the laboratory magnetic separator with a front and a side view and a picture of the steel grid member located inside the chamber for the recovery of magnetic particles..... 85
Figure 3.13. Laboratory setup of the magnetic separator showing the chamber and the components of the recycling process..... 86
Figure 3.14. Goniometer setup in the laboratory to determine the contact angles 89
Figure 3.15. Brookhaven ZetaPlus analyzer used during the surface charge tests 91
Figure 3.16. Zeta potential as a function of pH for cavitation bubbles and coal and magnetic plastic particles 92
Figure 4.1. TurboFlotation flotation system developed by CSIRO for Australian coal recovery (Firth, 1998). 95
Figure 4.2. Solid, liquid and vapor phase lines for varying conditions of pressure and temperature (Anon., 2011) 98
Figure 4.3. Internal and external forces acting on a cavitation bubble nucleus (Eisenberg, 1950) 99
Figure 4.4. Static equilibrium conditions of cavitation bubble nuclei, where the upper curve has a larger gas content than the lower one (Eisenberg, 1950) 100
Figure 4.5. Classification of cavitation methods based on pressure reduction mechanisms 101
Figure 4.6. Schematic of cavitation flow regimes, where σ and σ_i are denoted as K_c and K_i, respectively (Stinebring et al., 2001) 103
Figure 4.7. Relationship between the bubble diameter and the bubble surface area flux for different sparging systems (Anon., 2010) 107
Figure 4.8. Bubble-particle collision probability as a function of bubble diameter for 400, 600, 900 and 1200-micron particles 109

Figure 4.9. Bridging mechanism of two hydrophobic surfaces with cavitation-generated bubbles (Hampton and Nguyen, 2010).....110
Figure 4.10. Illustration of a wetting film with microbubbles on the solid surface at large film thicknesses that prevent rupture, $h_w > h_{rupture}$ (Stockelhuber et al., 2004) 111
Figure 4.11. Illustration showing the interaction between the wetting film surface and micro-bubbles, at small film thicknesses that results in rupture when $h_w = h_{rupture}$ (Stockelhuber et al., 2004).....111
Figure 4.12. Comparison of the experimental (filled markers) and the predicted (dashed lines) *P* values as a function of bubble size for varying particle sizes (after Luttrell & Yoon, 1992).....113
Figure 4.13. Microscopic photos for Teflon I, II and III, respectively, with varying surface roughness (Krasowska and Malysa, 2007) 114
Figure 4.14. Photo sequences (time interval=0.845 ms) of bubbles during the first collision with hydrophobic Teflon plates of varying and surface roughness (Krasowska and Malysa (2007).....115
Figure 4.15. High-speed photographic sequences of hydrophobic bubble-particle aggregate interaction in the presence of microbubbles on the surface (Sayed-Ahmed, 2013) 116
Figure 4.16. Effects of pre-aeration and cavitation tube performance on BC-Coalburg coal 121
Figure 4.17. Effects of pre-aeration and cavitation tube performance on KC-Coalburg coal 123
Figure 4.18. Release analysis results conducted on the RC coal sample from Winchester seam 127
Figure 4.19. Effects of pre-aeration and cavitation tube performance on the Winchester seam coal 128
Figure 4.20. Effects of flotation performance with cavitation pretreatment of the column flotation feed of a Coalburg coal sample from Boone County, WV 131
Figure 4.21. Effects of flotation performance with cavitation pretreatment of the column flotation feed of a Coalburg coal sample from Kanawha County, WV 131
Figure 4.22. Combustible recovery responses with the increased feed rate for the column flotation tests of the BC-Coalburg coal sample 132
Figure 4.23. Combustible recovery responses with the increased feed rate for the column flotation tests of the KC-Coalburg coal sample.....133
Figure 4.24. Enhanced carrying capacity characteristics realized by cavitation pretreatment of the feed for the BC-Coalburg coal sample at different feed solid contents 135
Figure 4.25. Enhanced carrying capacity characteristics realized by cavitation pretreatment of the feed for the KC-Coalburg coal sample at varying solid contents ranging from 8% to 16%.....136
Figure 4.26. Product particle size analysis for the KC-Coalburg coal following the carrying capacity test for 12% and 14% feed solids content.....137

Figure 5.1. Carrying capacity values for different methods and collectors at around 0.11 to 0.22 kg/t; FL=froth level or depth from overflow lip 142
Figure 5.2. Carrying capacity values for different methods and collectors at around 0.22 to 0.33 kg/t 143
Figure 5.3. Improvement in the product mass flux as a result of feed pre-aeration at a collector dosage of 0.02 kg/t. 144
Figure 5.4. Flotation performance in terms of added recovery gain while taking the conditions without cavitation pretreatment as baseline.....145
Figure 5.5. Collector dosage reduction achievable using cavitation with and without the addition of air 146
Figure 5.6. Additional carrying capacity gain with collector dose while taking the conditions without cavitation pretreatment as baseline.....147
Figure 5.7. The impact of collector application on carrying capacity while employing cavitation pretreatments with and without the air addition 148
Figure 5.8. The impact of frother type and concentration on carrying capacity with the cavitation pretreatments, where (*) denotes a different testing condition ...149
Figure 5.9. The impact of frother concentration under the same conditions on carrying capacity with the cavitation pretreatments 150
Figure 5.10. Visual comparison of the bubble-particle aggregate sizes under different conditions from the first (left) to the third (right) StackCell product 151
Figure 6.1. Illustration of kinetic limiting vs. carrying capacity limiting flotation conditions (Honaker and Ozsever, 2002).....154
Figure 6.2. Variability in plant flotation performance as a function of particle size (Luttrell, 2010) 156
Figure 6.3. Plateau border network in the presence of flotation feed material with different characteristics (Honaker, 2008).....157
Figure 6.4. Profile view of a single foam border showing the high- and low-pressure gradients around Plateau borders for bubbles of different diameters (Dürr-Auster, 2008).....160
Figure 6.5. Liquid drainage between two bubbles and the preventing Marangoni effect in a cross-sectional view (Dürr-Auster, 2008).....161
Figure 6.6. Flotation performances at different concentrations of magnetic plastic material addition using Coalburg and Pittsburgh No. 8 coals (Munoz-Diaz, 2007) 164
Figure 6.7. The impact of plastic particle addition at varying concentrations on carrying capacity characteristics for the Pittsburgh No. 8 coal (Munoz-Diaz, 2007) 166
Figure 6.8. Flotation performances for different concentrations of magnetic plastic material using Coalburg and metallurgical coals; C=collector, F=frother.....169
Figure 6.9. Absolute percent recovery improvements as a function of flotation time for Coalburg and Metallurgical coals with 5% and 10% plastic addition....172
Figure 6.10. Recovery of magnetic plastic particles after the flotation rate tests for different coal types and reagent and plastic concentrations 172

Figure 6.11. Impact of slurry pH on the recovery improvements realized when adding adding plastic particles to a conventional flotation feed containing Coalburg coal 174
Figure 6.12. Absolute percent recovery improvements as a function of flotation time for Coalburg coal under different feed slurry pH conditions.....175
Figure 6.13. Separation performance achieved when treating Coalburg coal in a flotation column with and without plastic particles in the feed; volumetric feed rate=300-1200 ml/min..... 177
Figure 6.14. Flotation performance achieved as a function of volumetric feed rate while treating difficult-to-float coals in a flotation column using 10% plastic particle concentration by weight..... 178
Figure 6.15. The impact of plastic particle addition on carrying capacity characteristics for the Coalburg coal from Kanawha County for different feed solid concentrations 180
Figure 6.16. Improved mass recovery rates for the coarsest and the finest size fractions of Pittsburgh No. 8 coal with and without the plastic particle addition.....181
Figure 6.17. Improved mass recovery rates for the intermediate-to-fine size fractions of Pittsburgh No. 8 coal with and without the plastic particle addition.....182
Figure 6.18. Particle size-by-size weight recovery improvements achieved by the addition of plastic particles at 10% concentration by weight on Pittsburgh No. 8 coal 183
Figure 6.19. Improved mass recovery rates for the coarsest and the finest size fractions of Coalburg coal with and without the plastic particle addition.....184
Figure 6.20. Improved mass recovery rates for the intermediate-to-fine size fractions of Pittsburgh No. 8 coal with and without the plastic particle addition.....184
Figure 6.21. The impact of plastic particle addition on combustible recovery for different size fractions following the carrying capacity tests for the Coalburg coal (KC) .....…..185

NOMENCLATURE

A = Function of surface coverage
A_c = Cross-sectional area (cm^2)
A_{PB} = Cross-sectional area of the Plateau border (cm^2)
b_m = Machine acceleration
C = Constant
C_1 = Empirical constant
c_1 = Fraction of the fast floating component of the mineral
C_d = Drag coefficient
C_{PB} = Viscous drag coefficient of the liquid
D = Diameter of the collection zone (or the flotation unit) (cm)
D_b = Bubble diameter (mm)
$d_{b,\max}$ = Maximum stable bubble size (mm)
$d_{p,\max}$ = Maximum particle size (mm)
E_k = Kinetic energy of a particle approaching a bubble
$E_k^{'}$ = Kinetic energy that tears the particle off the bubble surface (or kinetic energy for detachment)
E_l = Energy barrier for the bubble-particle adhesion
E_2 = Secondary energy minimum
F_{at} = Total attachment force
F_{de} = Total detachment force
F_e = Excess force (or difference between the excess pressure in the bubble and the hydrostatic force)
F_p = Capillary force
F_r = Hydrodynamic resistance (or drag) force
F_w = Particle weight in the liquid medium
g = Gravitational force or acceleration (cm/s^2)
H = Height of the collection zone (cm)
H_c = Particle-particle separation distance
k_B = Boltzmann constant
k_c = Collection zone flotation rate (min^{-1})
K_c = Cavitation number
k_{ci} = Collection zone flotation rate (min^{-1}) of specie i
k_{c1} = Collection zone flotation rate of the fast component in the feed mineral (min^{-1})
k_{c2} = Collection zone flotation rate of the slow component in the feed mineral (min^{-1})
k'_f = Froth transfer constant (min^{-1})

k''_f = Drop-back rate constant (min^{-1})

k_{fc} = Overall flotation constant (min^{-1})

K_i = Inception, or critical, cavitation number

k_1 = Constant for the balance between gravity and viscosity

k_2 = Constant for the balance between capillary suction and gravity

K_{132} = Magnitude of hydrophobic interaction in a three-phase contact

K_{131} = Hydrophobic force parameter for particle-particle interaction

K_{232} = Hydrophobic force parameter for bubble-bubble interaction

L = Length (or height) of the collection zone (or the flotation unit) (cm)

n = Bubble-particle collision rate (sec^{-1})

N_p = Particle concentration in the flotation cell (cm^{-3})

N_t = Total number of mineral particles in the flotation cell

P = Probability of flotation in the collection zone

P_A = Probability of attachment

P_a = Ambient pressure

P_B = Pressure in Bernoulli`s equation

P_{border} = Hydrostatic pressures on the Plateau border

P_C = Probability of collision

P_D = Probability of detachment

P_{film} = Hydrostatic pressures in the liquid film

Pe = Axial dispersion coefficient (Peclet number)

P_i = Power input

P_v = Vapor pressure (Pa)

p_1 = Pressure for the particle at the center of the cap (or cap pressure) (Pa)

Q = Gas flow rate (cm^3/sec)

R_b = Bubble radius (mm)

R_C = Collection zone recovery (%)

R_F = Froth zone recovery (%)

R_i = Radius of the curvature (mm)

R_O = Limiting radius (mm)

$R_{Overall}$ = Overall flotation recovery (%)

R_p = Particle radius (mm)

Re = Bubble/particle Reynolds number

Re_b = Bubble Reynolds number

Re_p = Particle Reynolds number

S = Spreading coefficient

S_b = Bubble surface area flux (cm/sec)

s_1 = Projected area on the bubble surface (cm^2)
s_2 = Curved area of the particle inside the bubble (cm^2)
T = Temperature
t_i = Induction time (milliseconds)
t_s = Sliding time (milliseconds)
u_b = Bubble rise velocity (mm/sec)
u_r = Liquid radial velocity
u_{rp} = Particle (rising) radial velocity
u_p = Particle slip velocity between the water and the particle
U_t = Bubble terminal velocity (cm/sec)
$\bar{U}^2$ = Mean square velocity difference between two points in the turbulent flow from a distance apart from the maximum bubble diameter (cm/sec)
V = Liquid volume in the cell
V_B = Water flow velocity in Bernoulli`s equation
V_D = van der Waals dispersion energy
V_E = Electrostatic interaction energy
V_g = Superficial gas rate (cm/sec)
V_H = Hydrophobic interaction energy
V_K = Kinetic energy supplied by mechanical and thermal agitation (or by Brownian motion)
V_l = Superficial liquid rate (cm/sec)
V_S = Structural interaction energy
V_t = Superficial tailings rate (cm/sec)
V_T = Total interaction energy (potential energy)
$V_{T,\max}$ = Maximum interaction energy occurring between the interfaces upon approach
W_A = Work of adhesion
W_A^d = Dispersion (or the London dispersion) component of work of adhesion
W_A^{nd} = Non-dispersion (or polar) component of work of adhesion
W_C = Work of cohesion
We = Critical Weber number
x = Radial coordinate
ε = Energy dissipation rate per unit mass in the liquid
ΔG = Gibbs free energy of the system (energy of adhesion)
Δp = Density differential between the particle and the bubble
γ = Surface tension
γ_{LV} = Interfacial surface tension at the liquid/vapor interface
γ_{SL} = Interfacial surface tension at the solid/liquid interface
γ_{SV} = Interfacial surface tension at the solid/vapor interface

γ_{SW} = Interfacial surface tension at the solid/water interface

μ = Dynamic liquid viscosity (centipoise)

ρ_l = Liquid density (gr/cm^3)

ρ_m = Medium density

ρ_p = Solid density (gr/cm^3)

ρ_s = Solid density (gr/cm^3)

ρ_w = Water density (gr/cm^3)

θ = Contact angle (degrees)

θ_d = Critical contact angle for the three-phase contact line before detachment (degree)

θ_i = Contact angle of specie i (degree)

θ_O = Limiting (or cap area) angle (degree)

ψ = Stream function

ϑ = Angular coordinate

φ_S = Volumetric concentration of solids (%)

τ_c = Collection zone residence time (min)

τ_L = Liquid retention time (min)

τ_p = Total particle retention time (min)

ϕ = Contact area

Ψ_O = Surface potential

ζ = Zeta (or electrokinetical) potential

CHAPTER 1

1. INTRODUCTION

1.1. BACKGROUND

The froth flotation process has been listed among the top ten inventions of the twentieth century with the first commercial installation occurring in 1906. For more than 100 years after H.L. Sulman, H.F.K. Picard and J. Ballot's first patent (U.S. No. 835,120), froth flotation has been the dominant process for the concentration of various minerals comprising a typical -1 mm ore. Materials concentrated using froth flotation include those containing copper, lead, zinc, gold, platinum, iron, molybdenum, tin, phosphate, talc, rutile, kaolin, fluorspar, coal and many others. It is estimated that froth flotation processes currently treat about 9 billion tons of ore annually. The United States leads the world with the highest total installed capacity of 20.3% attributed to coal flotation circuits compared to other major coal producing countries, such as China (14.0%), the United Kingdom (12.1%), India (11.1%), Canada (9.5%) and Australia (9.4%). Coal cleaning through froth flotation in these countries represents about 13.6% of the total installed capacity, which is estimated to be approximately 160 Mt/year (Kempnich, 2003).

From a fundamental perspective, froth flotation is known as a physico-chemical process that separates solid particles based on their differences in physical and surface chemistry properties. For fine coal cleaning, froth flotation is the most commonly used process to recover and upgrade the portion of the coal preparation plant feed that has a particle size smaller than 150 microns. The typical amount of flotation feed material in run-of-mine coal is 7% to 12% of the total mass flow.

Coal particle surfaces are typically hydrophobic (i.e., dislikes water) whereas the mineral matter is hydrophilic (i.e., likes water). The separation principles of the flotation process involve the use of air bubbles (produced by means of shear) which collide with flotation feed particles thereby allowing an opportunity for hydrophobic particles to attach and

form a particle-air bubble aggregate. As a result, coal-air bubble aggregates, having a density less than the medium, rise to the top of the flotation cell where they overflow into a concentrate launder. On the other hand, hydrophilic mineral matter particles do not attach with a bubble after collision and move downward with the major portion of the volume flow where they report to cell underflow stream.

Fundamental froth flotation principles are basically the same for all flotation machines, however there are differences in the design depending on the operational restrictions and the requirements for a given mineral. There are two main types of flotation devices used today, i.e., conventional mechanical and column flotation cells. Conventional and column flotation cells have been widely used since the early 1900's and the late 1980's, respectively.

Conventional flotation cells are characterized by their relatively low length-to-diameter (L:D) ratio. In the presence of the mineral slurry, conventional flotation cells employ a rotor and stator (or a high-shear impeller) for agitation and bubble generation by drawing air down a hollow shaft. Conventional cells are near perfect mixers and, as such, provide a relatively inefficient bubble-particle collision environment. To reduce the impact, a series of three or more cells are used to form a bank of flotation cells. Due to inherent problems, such as hydraulic entrainment and entrapment of fine particles in the clean coal froth, high quality products are difficult to achieve for the conventional cells.

Flotation columns, on the other hand, provide a relatively efficient bubble-particle collision environment and support a deep froth due to their high L:D ratio design. Columns utilize a counter-current flow of feed slurry and air bubbles to separate coal particles from refuse particles. Wash water injection in the froth phase is also another key feature of the column flotation process by which entrainment of low grade materials are rejected. The use of wash water allowed the column performance to approach the "ideal separation" defined by release analysis data.

The froth flotation process consists of two separate and distinctly different zones, i.e., the collection zone and the froth zone. The overall mineral recovery is the result of the interaction between these two zones. Many of the novel flotation techniques, including the conventional cells, developed since 1980's are aimed at improving methods of contacting air bubbles and treated mineral particles in the collection zone. The collection zone achieves a separation between the valuable and non-valuable minerals based on the bubble-particle attachment process, which takes place below the collection zone-froth zone interface. During this process, a portion of the non-valuable minerals is carried from the collection zone into the froth zone with the mineral-bubble aggregates due to hydraulic entrainment.

The separation of the valuable mineral from the non-valuable mineral components in the collection zone is based on differential flotation rates. The rate at which a particle is recovered due to true attachment is known as the collection flotation rate, k_{ci}. The collection zone flotation rate of a mineral can be quantified by the expression:

$$k_{c_i} = \frac{3V_g}{2D_b} P_c P_a (1 - P_d) \tag{1.1}$$

in which V_g is the superficial gas velocity, D_b the bubble diameter, P_c the probability of collision, P_a the probability of attachment and P_d the probability of detachment. The collection zone flotation rate equation shows that the bubble-particle collision, attachment and detachment sub-processes are the most critical steps in froth flotation. Bubble-particle collision should be maintained at maximum efficiency to ensure a high recovery of the floatable mineral, which makes it a non-selective process. The bubble-particle attachment process, however, is the principal mechanism defining the ability to effectively separate minerals in the collection zone of a flotation process which results in grade profiles and thus selectivity between particles. The probability of detachment is a function of both particle size and density and thus may play a minor role in selectivity.

The flotation rate constant is also a function of the particle size in the flotation feed, through the probabilities of collision, attachment and detachment, which can result in significantly different recovery values for a given residence time. Extensive research indicated that froth flotation performance varies significantly as a function of particle size as shown in Figure 1.1. (Jowett, 1980; Yianatos et al., 2001; Jameson et al., 2008; Jameson, 2010; Kohmuench et al., 2010).

Lower and upper particle size limits exist that varies from material-to-material mainly due to density. Flotation recovery significantly declines for particles larger or smaller than these limits. In coal flotation, a narrow particle size range of approximately 50 to 500 μm typically exists to achieve a high level of separation efficiency. The lower particle size limit for a given mineral is a function of the bubble-particle collision efficiency (P_c) with denser particles having the ability to penetrate the fluid streamlines at smaller particle sizes. For this reason, ultrafine particles (<10 μm) tend to float very slowly due to a tendency to move with the fluid streamlines, which leads to low collision efficiencies.

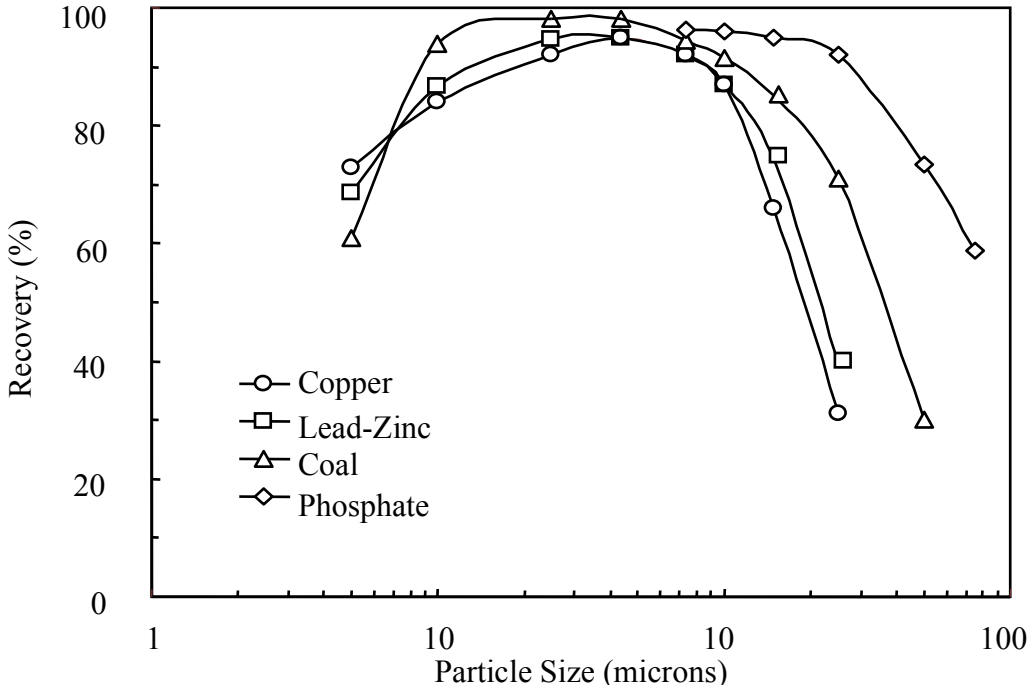


Figure 1.1. Lower and upper particle size limitations for the effective application of froth flotation on different minerals (Kohmuench et al., 2010).

The upper particle size limit is associated with the bubble-particle detachment process (P_d), which is also dependent on the particle density (inertia). Although the coarse particles can penetrate into the streamlines of the rising bubbles, their inability to remain being attached on the bubbles due to the turbulent nature of the flow field reduces the coarse particle (>100 μm) recovery significantly (Jameson, 2010). Schulze (1984) showed that coarse particle size limit could be drawn when the centrifugal force acting on the bubble is higher than the surface tension that keeps the particle attached on the bubble surface.

The throughput capacity of a flotation system is limited on the amount of product mass that can be conveyed by air bubbles through the collection zone to the concentrate launder. This limit is typically referred to as the carrying capacity, which is defined as the mass rate of flotation product per unit time per cell (or column) cross-sectional area, i.e., $t/h/m^2$. When the carrying capacity limit is reached, fully loaded bubbles simply have no space where additional particles can attach, which represents insufficient bubble surface area to carry additional hydrophobic particles in the feed.

Under kinetic limiting conditions, the product capacity (mass flux rate) increases in direct proportion to the increase in the feed solids content. At low feed concentrations, a linear relationship reflects that the amount of floatable material entering in the feed stream has sufficient bubble surface area to be conveyed to the product launder to ensure nearly 100% froth zone recovery, where the separation is based on the differences in flotation kinetic rates as shown in Figure 1.2.

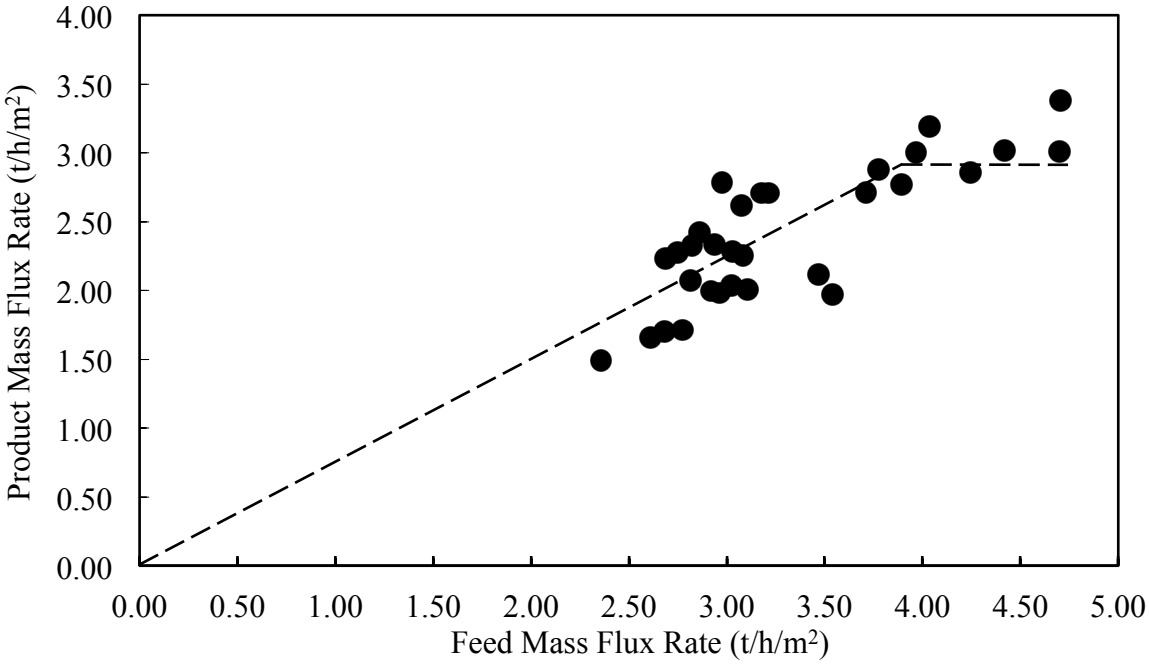


Figure 1.2. Typical product rate limit (carrying-capacity conditions) for coal flotation at different feed solid concentrations as a result of a pilot-scale test work (Kohmuench and Mankosa, 2006).

As the bubble-particle aggregates rise through the froth phase to the top of the cell (or column), bubble surface area declines due to coalescence when the bubble walls thin. When particle population increases by a decrease in particle size and/or increase in solids concentration, the bubbles become loaded and additional amounts of the floatable material are not recovered. At this point, the flotation system becomes carrying capacity-limited when the product rate reaches a maximum and the slope no longer represents a constant. For particles with a near narrow size distribution, the maximum carrying capacity value will remain constant over any further increases in the feed rate. However, for particles with a broad size distribution, insufficient bubble surface area causes the selective detachment of the coarser size fractions, which are associated with higher mass. The result is a decrease in the product mass flux rate with an increase in the feed mass flux. Selective detachment also applies for the weakly hydrophobic particles when particles compete for attachment sites under carrying capacity-limited conditions.

Depending on the bubble surface area availability, the detached particles can re-attach to a bubble at a lower point in the froth zone or in the collection zone. The process of detachment and re-attachment of particles generates a recycling of particles, which is commonly referred to as reflux (Honaker et al., 2006).

In the coal industry, the carrying capacities for the most operating full-scale columns range anywhere from 0.9 to 3 tph/m^2 (Sastri, 1996; Kohmuench and Mankosa, 2006) and from 0.6 to 2.4 tph/m^2 (Luttrell, 2012) with an average of about 0.12 tph/ft^2 for a typical flotation feed particles smaller than 150 microns, as shown in Table 1.1. Smaller particle size distributions have higher overall surface area, which requires more bubble surface area to be covered. However, the total bubble surface area that can be produced in a flotation system is limited. As with belt conveying systems which has limited capacity, a flotation system has a maximum carrying capacity that is determined by the amount of bubble surface area that can be generated and the total surface area of the floatable particles entering in the flotation feed stream.

Table 1.1. Carrying capacity ranges for different feed size fractions of coal flotation (Christodoulou, 2013).

Feed Size (micron)	Target Capacity(tph/m^2)
Minus 600	1.8-2.6
Minus 150	1.0-1.4
Minus 45	0.6-0.9
150x45	1.8-2.2

Using these values, one can estimate that the carrying capacity would be around 12 t/h for a typical industrial column flotation unit (4.6-m diameter) in the case of a flotation feed comprised of a very fine size fraction (minus 45 microns). By increasing the feed size to a typical flotation feed (minus 150 microns), the carrying capacity could be increased by about 10 t/h to obtain an overall product rate of 22 t/h.

An issue that results in poor flotation performance is limited retention time due to increases in the amount of flotation feed that exceed the designed capacity. In this case, increasing the flotation rate of the coal can result in significant flotation recovery improvements despite the limited residence time. By floating fine particles as larger clusters bridging together or by maintaining the coarse particles in the flotation system through reduced drainage, not only the carrying capacity, but also the flotation rate and thus the flotation recovery improves.

Another problem that occurs when employing froth flotation in the coal industry includes bubble surfaces that are insufficient carriers of bubble-particle aggregates with low carrying capacities. As previously discussed, the lower limit is a result of inefficiencies in the bubble-particle collision process while the upper size limit is associated with bubble-particle detachment process. It is well documented in the literature that reducing the bubble size improves the flotation rate, which would ultimately decrease the flotation system size range. Tao (2004) found that the lower size limit could be extended to a few microns, and even sub-microns, by employing micron- to sub-micron size bubbles for ultrafine flotation efficiency. Similarly, the upper limit could also be expanded to upper size limits of 1 to 2 mm, which involves the flotation of relatively coarse particles.

As previously mentioned, froth flotation processes are typically applied toward the treatment of particles having a size smaller than 150 microns. Thus, the large total surface area requires a significant amount of surfactant referred to as collector to convert the surface of a given mineral from one characterized as being hydrophilic to a hydrophobic surface or to increase the surface hydrophobicity for improved flotation characteristics. For example, it is estimated that the collector market associated with froth flotation is worth $6.75 billion annually worldwide. In addition to their cost, environmental concerns regarding the flotation reagents have resulted in operators reducing dosage levels, which resulted in poor application of reagents due to insufficient amounts. Consequently, these problems negatively impact flotation recovery and represent significant energy and economic losses. Fan et al. (2010) found that, in the presence of bubbles generated

through cavitation, the flotation improvement was more significant on the hard-to-float particles than that of the easy-to-float particles especially at lower collector dosages. Zhou et al. (1997) and Tao et al. (2006) have also found that the feed pretreatment through cavitation-generated bubbles can reduce the flotation collector consumption while simultaneously improving the recovery.

In addition to selectivity, the probability of attachment is also directly related to the hydrophobicity of coal particles, which determines the flotation rate response of a given coal type. In some cases, however, the hydrophobicity of a particular coal is relatively weak with a high degree of surface oxidation and thus the response to flotation is poor. An example in the central Appalachia coalfields is the coal from the Coalburg seam. The seam is very prominent and used widely in the utility industry. Due to its poor flotation performance, recovery from commercial flotation circuits is poor to nearly non-existent which explains the lack of flotation circuits in some preparation plants treating Coalburg seam coal. For coals with poor flotation characteristics, the concept of froth stability provided by hydrophobic solid particles, such as naturally hydrophobic plastic particles, offers a solution due to restriction of the drainage of the liquid from the thin water layer surrounding air bubbles, thereby preventing bubble coalescence. Thus, froth stability benefits from the addition of particles having a contact angle up to 90°. In addition to the potential benefit of adding hydrophobic particles in the feed, cavitation-nucleated bubbles have also shown enhanced flotation recovery benefits to an Australian coal by over 15 absolute percentage points (Zhou et al., 1997).

This study details the work performed to evaluate the impact of nucleating submicron-size bubbles onto the surfaces of weakly hydrophobic particles through cavitation feed pretreatment in an effort to increase the flotation rate and thus elevate recovery. Furthermore, the addition of highly hydrophobic magnetic plastic particles in the feed was studied to improve the flotation characteristics of poorly floating coal particles, especially in the froth zone, by reducing water drainage thereby increasing the froth stability.

1.2. RESEARCH OBJECTIVES

The goal of the dissertation research was to provide a potential solution for low flotation recovery performances caused by 1) a low degree of coal surface hydrophobicity in the flotation feed, 2) retention time limited flotation systems and 3) carrying capacity-limited conditions.

One of the proposed concepts involves the use of feed pre-aeration using a cavitation system, which has been proven to enhance flotation recovery in laboratory studies. By injecting feed through a cavitation system, micron-sized bubbles nucleate onto the surface of the coal particles, which results in the pre-aeration of the flotation feed. As a result, when the particles interact with bubbles produced from a conventional bubble generator, the attachment process occurs more rapidly. Due to the finer distribution, the injection of additional air and the production of bubbles on the particle surfaces, flotation rate and carrying capacity are improved which directly results in enhanced flotation recovery.

In a laboratory experimental program, the slurry was injected through a cavitation tube, which causes small air bubbles to nucleate on the coal surface. Afterward, the pretreated slurry was subjected to laboratory-size conventional and column flotation units. During the laboratory studies, weakly floatable coals from the Coalburg seam were obtained from an active coal preparation plant in the Central Appalachian coal region. The effectiveness of this novel method was evaluated under different operating conditions to assess the overall benefit to flotation process. The results were used to quantify flotation rate and compare the value to the performance achieved with no pretreatment.

Following the laboratory tests, in-plant studies were conducted at an operating preparation plant after the installation of the cavitation tube system for feed pretreatment prior to a StackCell circuit. Performance of the froth flotation circuit treating an underground metallurgical coal seam (Peerless) was evaluated under different operating

conditions, such as varying flotation chemicals and dosages, froth depth levels in the StackCells, air injection into the cavitation system, etc. Tests were conducted both while the flotation slurry was flowing through the center pipe (all cavitation tube valves are closed) and through the cavitation tube system (the center pipe valve is closed). In this study, results of both the laboratory and the in-plant studies involving the cavitation pretreatment are given. Comparisons are also made between the findings of the recent study and those of the previous research.

The other concept utilizes highly hydrophobic plastic material with magnetic characteristics. This naturally hydrophobic material is easily recoverable by low-intensity magnetic separators. Prior research (Munoz-Diaz, 2007) has shown promising results indicating a significant enhancement in separation performance thorough the addition of magnetic hydrophobic particles to the flotation process. From the previous research, the detachment process has been shown to be selective toward the rejection of the more weakly hydrophobic solids. However, the most significant discovery was the doubling of the flotation rate and the improvement was the greatest for the coarsest particle size fractions. In the proposed investigation, laboratory conventional and column flotation cells will be used to collect the necessary data needed to fully validate previous findings and quantify the fundamental mechanisms governing the impact of the magnetic plastic material addition to the flotation system. Coal samples of varying degrees of floatability, such as Pittsburgh No. 8 and Coalburg coals, will be used as the test material to evaluate the effect of change in surface hydrophobicity on collision, attachment and detachment processes.

Using well-known fundamental relationships, flotation rates will be quantified for particles of all sizes and particularly the coarsest particle size fraction. In addition, to exploit the change in carrying capacity relationship, experiments will be performed to explain the preferential recovery improvement observed for the coarse particles in the presence of hydrophobic plastic material. Flotation rate improvements related with the surface properties, especially under low and high pH conditions, will be evaluated under

specific characterization studies. In short, the findings of the previous research will be validated and the repeatability of the results will be tested using similar test procedures. The specific objectives of the investigation were:

• To investigate the impact of hydrodynamic cavitation feed pretreatment using especially weakly floatable coals with high middling contents, such as the Coalburg seam. The flotation performance from various flotation feed stocks was conducted to provide benchmarking performances. Flotation rate tests allowed a comparison of rate constants for each coal type in addition to providing comparative values for the response of pretreated feed. Each of the flotation feed stocks was pretreated using a cavitation method and then processed in a laboratory flotation cell. The data from these test provided preliminary estimates of the rate increases that can be expected in a full-scale industrial application. In addition, column flotation tests will be performed to demonstrate the achieved performance enhancement over a range of operating conditions.

• To determine benefits of the full-scale cavitation tube system on the flotation circuit performance after the installation to the preparation plant in the light of the laboratory studies. The existing plant circuitry was fully characterized such that accurate comparisons were made concerning the flotation characteristics of the StackCell circuit prior to and after cavitation pretreatment. Additional value of the cavitation tube system on reducing the flotation reagent consumption, especially collector, was investigated.

• To perform an investigation to validate and duplicate the reported impact (Munoz-Diaz, 2007) of highly hydrophobic magnetic plastic particles on the separation performance achieved by the flotation process in order to bring a better understanding of this unique material for its effect on coal. As such, flotation performance with and without the plastic particles was analyzed over a range of operating conditions (solids concentrations, feed volumetric flow rate, particles size and pH) in the laboratory-scale conventional and column flotation units.

1.3. METHODOLOGY

In the first part of this research involving the feed pretreatment through hydrodynamic cavitation, flotation rates from the corresponding recovery values were determined over a range of operating conditions first for the conventional flotation tests, then for the column flotation tests. During the laboratory studies, flotation feed samples were collected from three different preparation plants in West Virginia, two of which were treating the Coalburg seam and one processing the Winchester seam. Cavitation and the application of air parameters were varied under the same conditions to make a head-to-head comparison. After identifying the baseline conditions through the laboratory-scale conventional cell results, continuous column flotation unit was operated under different variables, such as volumetric feed rate, solids concentration, air flow rate and collector dosages. In order to keep the cavitation bubbles intact on hydrophobic coal particles, pretreated feed samples were taken with caution and the tests were conducted immediately afterwards to optimize the conventional or column flotation tests.

Following the laboratory studies, a full-scale cavitation tube system was installed for the in-plant tests ahead of the StackCell flotation circuit. One variable at a time was varied during the in-plant studies to make a comparison between the operating conditions. During this study, coal from the Peerless seam was evaluated during the in-plant studies, which has significantly better flotation characteristics than that of the Coalburg coal. The overall methodology of the tests involving the cavitation pretreatment in the laboratory and in the field is shown in Figure 1.3. Test results for each coal type with and without the cavitation tube will be presented in comparison and the possible mechanisms involving these differences will be discussed.

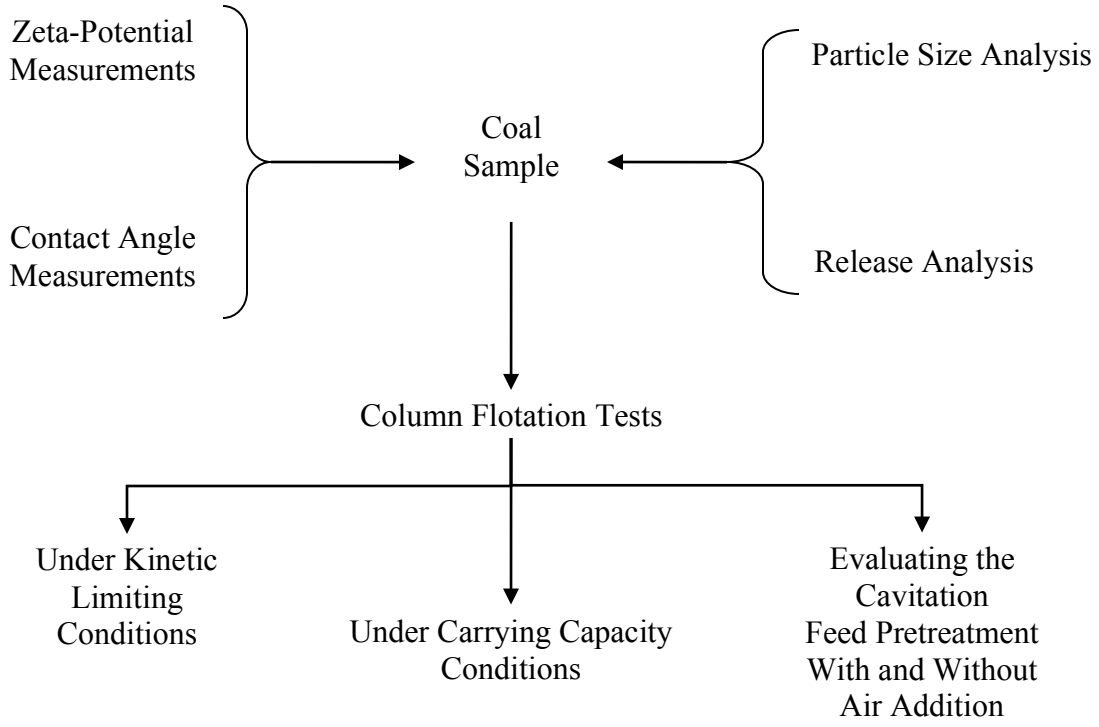


Figure 1.3. Schematic illustration of the characterization study and the general flotation tests conducted for the evaluation of the cavitation feed pretreatment.

During the second part of this research, tests were performed to investigate the impact of highly hydrophobic magnetic plastic particles on the separation performance achieved by the flotation process. The repeatability of the results from the previous research (Munoz-Diaz, 2007) was tested using the same, or similar, procedures to validate the overall impact of the magnetic plastic particles. Coalburg coal samples from a different preparation plant than that of the previous study were utilized during these tests for upgrading the surface hydrophobicity of the coal particles through froth enrichment with the addition of highly hydrophobic plastic particles. Bituminous coal samples used in the flotation tests were analyzed for particle size distribution and proximate analysis following the sample preparation methods shown in Figure 1.4. The results of the release analysis were used to determine the theoretical achievable separation limits of the feed

material by flotation, which were used as a benchmark for comparison purposes in subsequent tasks.

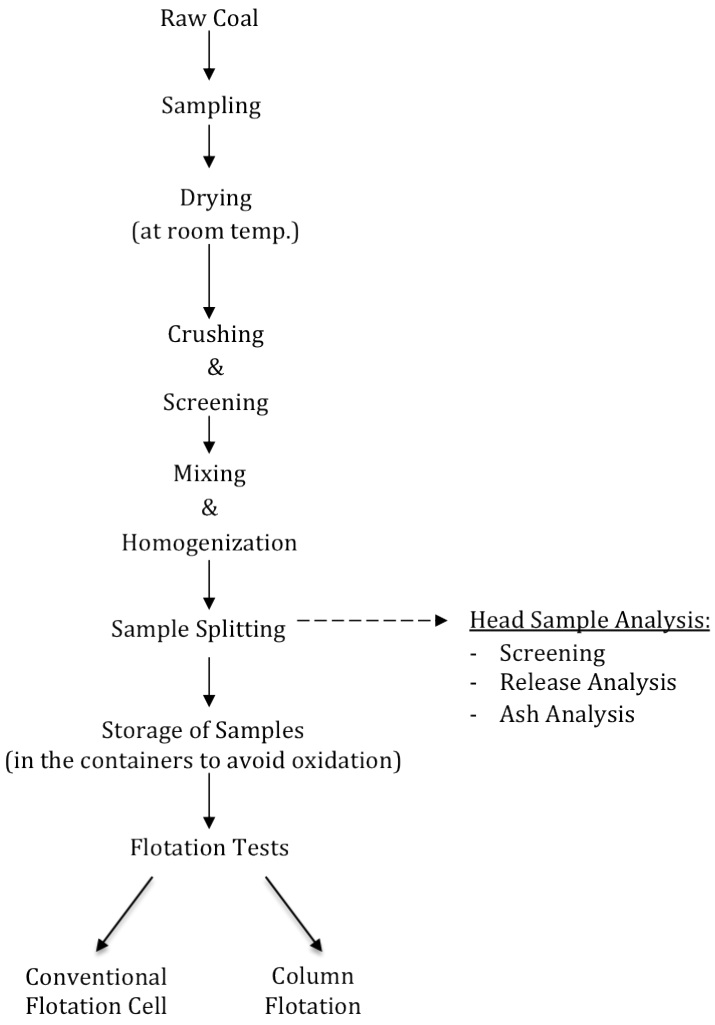


Figure 1.4. Schematic illustration of the feed characterization study and the general flotation tests conducted using different coal sources to evaluate the impact of magnetic plastic particles.

The plastic material contained about 70%, magnetite, which resulted in easy recovery by a magnetic separator. Following each flotation test, concentrate material from the conventional and column flotation tests were passed through the magnetized chamber of the magnetic separator three times to ensure the complete recovery of the magnetic particles that were adhered on the coal surfaces.

The degree of hydrophobicity in the coal changes as a function of particle size, which is related to the various maceral types associated with the coal. Since the density of a particle depends on the coal and mineral matter content, the hydrophobicity of the feed material decreases as the mineral matter content increases due to the density differential. As a result of the hydrophobic material addition, the impact on the flotation characteristics of the weakly floatable Coalburg will be assessed and compared to the findings from the previous research (Munoz-Diaz, 2007).

CHAPTER 2

2. FLOTATION RECOVERY: LITERATURE REVIEW

2.1. INTRODUCTION

The success of the flotation process depends on the capture and transfer of hydrophobic particles by air bubbles from the collection zone to the froth zone. The overall flotation recovery is a function of both the collection recovery and the froth zone recovery, which can be formulized by the following expression (Falutsu and Dobby, 1989):

$$R_{Overall} = \frac{R_C R_F}{1 - R_C + R_C R_F} \tag{2.1}$$

where R_C is the collection zone recovery, R_F is the froth zone recovery and $R_{Overall}$ is the overall recovery.

Although recent research has focused on the recovery mechanisms in the froth zone, a very detailed understanding of the collection zone process has been realized from more than a century of research. The main processes in the collection zone involve collision, attachment and detachment mechanisms between the bubbles and the particles.

2.2. COLLECTION ZONE RECOVERY

Single bubble-particle collision rate in a fluid of zero viscosity, n (sec^{-1}), was first derived by Sutherland (1948) based on the potential flow conditions, which will be discussed later, with the following relationship:

$$n = 3\pi R_p R_b u_b N_p \tag{2.2}$$

in which R_p and R_b are the particle and bubble radii (cm), respectively, u_b is the bubble rising velocity (cm/s) and N_p is the particle concentration in the cell (cm^{-3}).

The rate at which this separation occurs due to true attachment in the collection zone is known as the flotation rate, k (min^{-1}). In other words, the flotation rate is a measurement of how fast a particle is recovered in the collection zone. After manipulating Eq. (2.2) to include several other parameters that contribute to the flotation process, Sutherland (1948) developed the first flotation rate model with the following expression:

$$\frac{dN_t}{dt} = \frac{9R_pQH}{4R_b^2} P_a P_d N_t \tag{2.3}$$

where N_t is the total number of mineral particles in the cell, Q is the gas flow rate (cm^3/sec), H is the height of the collection zone (cm), and P_a and P_d are the probability of attachment and detachment, respectively.

Upon integration of Eq. (2.3) and substitution with the commonly used variables, the more recognized first-order expression is obtained to determine the collection zone kinetic flotation rate, k_c (Yoon et al., 1989; Gorain et al., 1995; Yoon and Mao, 1996; Gorain et al., 1997; Deglon et al., 1999; Heiskanen, 2000):

$$k_c = \frac{3V_g}{2D_b} P \tag{2.4}$$

where V_g is the superficial gas velocity, D_b is the bubble diameter, and P is the probability of flotation.

The ultimate recovery of a given mineral species in the collection zone is a function of flotation rate, retention time and the hydrodynamic parameters combined. The capture and transfer mechanisms controlling the flotation recovery rate, and thus the recovery, are dominated by two factors, i.e., superficial gas velocity and bubble diameter. It is clearly

indicated from Eq. (2.4) that increasing the amount of air (V_g) in the flotation system has a positive effect on flotation rate as well as increasing the probability of flotation.

Superficial gas velocity, V_g, is a measure of the aeration ability of a flotation cell, which is defined as the volume of air passing a unit cross-section of a cell in the pulp per unit time:

$$V_g = \frac{Q}{A_c} \tag{2.5}$$

where Q is the gas flow rate and A_c is the cross-sectional area.

Bubble size is another important factor governing the flotation performance, which is a measure of the air dispersion in the flotation cell. In mechanical cells, bubbles are usually generated by shear action of the impeller; thus, bubble size is dependent on both airflow rate and impeller rotation speed. As such, bubble size cannot be controlled independently of cell turbulence. The bubbles used in a column are usually generated within the size range that maximizes interfacial surface flux and collection intensity through the vessel.

Eq. (2.4) suggests that smaller bubbles result in higher rate values, and thus, increased flotation recoveries, by carrying more mineral particles per unit volume of air. On the other hand, larger bubbles may be caused by the combination of high superficial gas velocities and poor shearing action of the bubble generators (Gorain et al., 1995). Bubble surface area flux, S_b, is the amount of bubble surface area rising up a flotation cell per cross sectional area per unit time and defines the effectiveness of bubble-particle collision and the froth recovery due to attachment. An expression has been derived for S_b, which incorporates both the superficial gas velocity and the bubble size (Yoon et al., 1989):

$$S_b = \frac{V_g}{\pi D_b^3 / 6} \pi D_b^2 = \frac{6V_g}{\pi D_b^3} \pi D_b^2 = \frac{6V_g}{D_b} \tag{2.6}$$

Combining Eqs. (2.4) and (2.6) shows that S_b plays a key role in the flotation efficiency and at shallow froth depths is linearly proportional to the first order flotation rate constant and thus to the flotation recovery. The strong correlation between the bubble surface area flux and the flotation rate constant can be expressed as (Deglon et al., 1999):

$$k_c = \frac{1}{4} S_b P \tag{2.7}$$

Although Heiskanen (2000) questions the validity of this correlation and the relationship between the effect of bubble surface area flux and the particle size, Gorain et al. (1997) clearly showed the overall importance of the bubble surface area flux on the recovery of a flotation process in Figure 2.1. As a result, one can conclude that an increase in bubble surface area flux improves the recovery rate in the pulp zone of a cell. However, in the presence of excessive air, the recovery rate in the pulp zone can decrease due to 'boiling'. Gorain et al. (1995) suggests that it is also important to control both airflow rate and impeller speed to produce correct bubble sizes to perform at high bubble surface area flux values and, in turn, achieve high recovery values. This finding is in agreement with the early studies by Schubert and Bischofberger (1978) and Ahmed and Jameson (1989), which suggest that flotation rate constants are dependent on bubble size and impeller speed. Later studies by Gorain et al. (1999), Deglon et al. (2000), Power et al. (2000) and Yianatos et al. (2001) have advocated that bubble surface area flux and air dispersion are key machine and hydrodynamic variables for flotation cells, respectively.

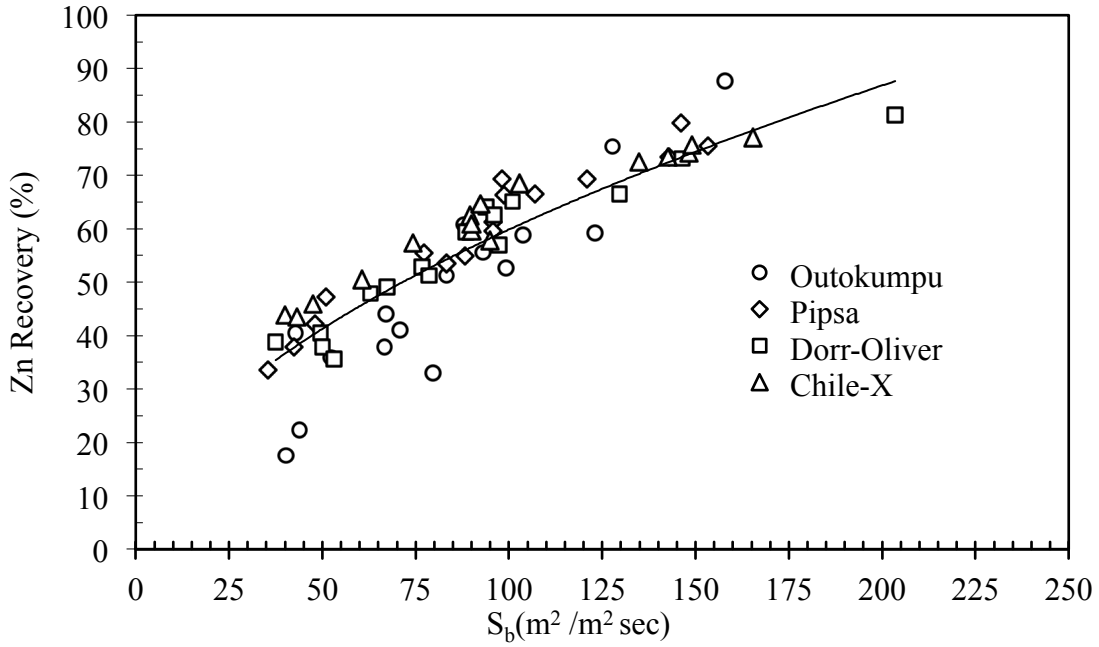


Figure 2.1. The relationship between the bubble surface area flux and zinc recovery over a range of impeller types and resulting speeds (*after* Gorain et al., 1999).

2.2.1. Probability of Flotation

The efficient capture of hydrophobic particles by air bubbles through bubble-particle collision, attachment, and detachment are the most critical steps in the flotation process. The probability of flotation, P, defines these three sub-processes that occur in the collection zone as a stochastic function:

$$P = P_C.P_A.(1-P_D) \tag{2.8}$$

where P_C , P_A and P_D are defined as the probability of bubble-particle collision, attachment and detachment, respectively.

In order to represent the success of effective particle separation by froth flotation using a probability function, Schuhmann (1942) first introduced the bubble-particle collision and attachment concepts. Later, Sutherland (1948) took bubble-particle detachment into account, while Tomlinson and Fleming (1963) considered the probability of a particle to

remain in the froth. The overall effect of P on the flotation rate depends on the individual governing factors and the combined influence of each of these sub-processes.

2.2.2. Probability of Collision

For a bubble moving relative to the liquid, the liquid movement around the bubble forms streamlines. The effectiveness of a bubble sweeping these streamlines completely is related to the probability of bubble-particle collision, P_C, which is also known as the collision efficiency (Sutherland, 1948).

Recovery of fine particles in flotation predominantly depends on the probability of collision. Since ultrafine particles follow the same streamlines due to limited inertia with bubbles, it results in low collision efficiencies, and thus, poor flotation performances (Nguyen et al., 1997; Rubinstein and Samygin, 1998; Yoon, 2000).

According to Sutherland (1948), a bubble rising vertically through the pulp with a radius of R_b will collide with all particles of a radius R_p that are contained within the streamline limiting radius of R_o as shown in Figure 2.2. Particles of sufficient momentum due to their size and/or density will penetrate the streamlines and collide with the bubble, when $R_O = R_b$. As a result, the probability of bubble-particle collision can be written as:

$$P_C = \left(\frac{R_O}{R_b} \right)^2 \tag{2.9}$$

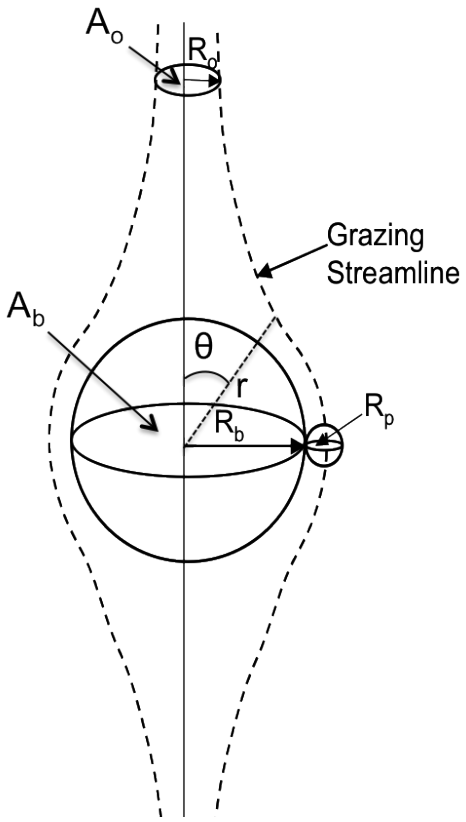


Figure 2.2. Illustration of bubble-particle collision efficiency mechanism with a particle moving past a bubble in a liquid streamline (Yoon and Luttrell, 1989).

The limiting radius associated with the streamlines, R_O, is a function of the resulting hydrodynamic conditions due to three main flow conditions as the fluid passes around the bubble surface. In addition to Gaudin`s (1957) and Sutherland`s (1948) studies on Stokes and potential flows, respectively, Weber and Paddock (1983) and later Yoon and Luttrell (1989) provided a relationship between the bubble size and probability of collision under intermediate flow conditions, i.e.,

Stokes Flow (Gaudin, 1957):

$$P_C = \frac{3}{2}\left(\frac{R_p}{R_b}\right)^2 = \frac{3}{2}\left(\frac{D_p}{D_b}\right)^2 \quad \mathrm{Re} \to 0, \textit{viscous fluid} \tag{2.10}$$

Potential Flow (Sutherland, 1948)

$$P_C = \frac{3}{2}\left(\frac{R_p}{R_b}\right) \quad \mathrm{Re} \to \infty, \textit{inviscid fluid} \tag{2.11}$$

Intermediate Flow (Weber and Paddock, 1983)

$$P_C = \left(\frac{R_p}{R_b}\right)^2 \frac{3}{2}\left[1 + \frac{(3/16)\mathrm{Re}}{1 + 0.249\,\mathrm{Re}^{0.56}}\right] \quad 0<\mathrm{Re}<300 \tag{2.12}$$

Intermediate Flow (Yoon and Luttrell, 1989)

$$P_C = \left(\frac{R_p}{R_b}\right)^2 \left[\frac{3}{2} + \frac{4\,\mathrm{Re}^{0.72}}{15}\right] \tag{2.13}$$

where R_p and R_b are particle and bubble radii, respectively, and Re is the bubble/particle Reynolds number.

The bubble Reynolds number describes the flow around the bubble and can be quantified by the following expression:

$$\mathrm{Re}_b = \frac{\rho_l U_t d_b}{\mu} \tag{2.14}$$

where ρ_l is the liquid density, U_t the bubble terminal velocity, d_b the bubble diameter and μ is the liquid viscosity (centipoise).

The effect of bubble size and Reynolds number on collision probability from Eq. (2.13), can be summarized by the following generalizations in which the trend is, as bubble size gets larger, P_c becomes less dependent on D_b (Yoon, 1993; Yoon, 2000):

- $P_C \alpha D_b^{-2}$ for small bubbles with Re<<1,

- $P_C \alpha D_b^{-1}$ for large bubbles.

- $P_C \alpha D_b^{-0.46}$ for very large bubbles.

The intermediate stream function for quiescent conditions modeled and derived in Eq. (2.13) was verified by Yoon and Luttrell (1993) for P_C by using a very hydrophobic ultrafine coal sample, i.e., 11.4 microns, as shown in Figure 2.3.

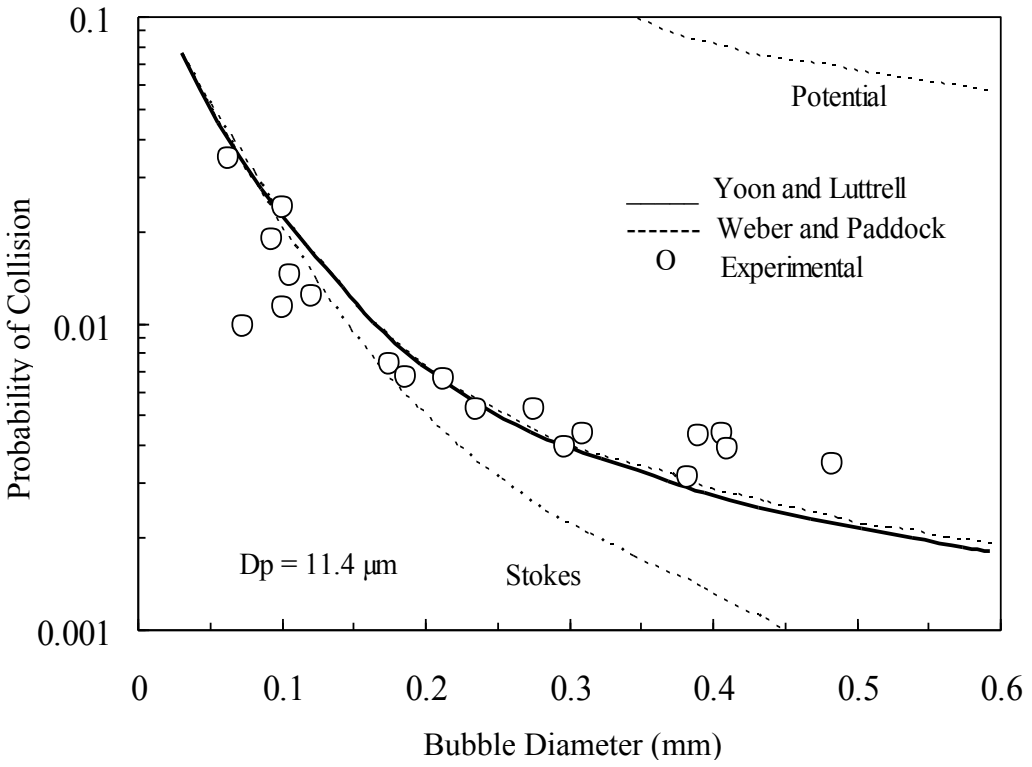


Figure 2.3. Probability of collision in a flotation column system as a function of bubble size (Yoon and Luttrell, 1993).

Although there are differences in their approach, the comparison of Yoon and Luttrell`s (1989) data using Eq. (2.13) was in agreement with Weber and Paddock`s (1983) predictions from Eq. (2.12). The relationship in Eq. (2.13) was also found to be accurate on micro-turbulence models for perfectly mixed conditions (Schubert and Bischofberger, 1979; Yoon, 2000). Derjaguin and Dukhin (1961) described the bubble-particle collision theory based on a model which suggests that, before a particle can adhere on the surface of an air bubble, it must pass through three zones, i.e., hydrodynamic, diffusion-phoretic and wetting zones. The distinct interaction forces in these zones influence the particle first to collide and later to adhere to the bubble (Dai et al., 2000).

Hydrodynamic force is dominant when a big particle moves toward a bubble. In this case, particle inertial and gravitational forces act on such particles. For fine particles near the bubble, diffusio-phoretic forces play a major role on the particles as a result of adsorbed ions (or surfactants) on the bubble surface. The electrical field formed between the bubble and the particle suggests that reducing the particle zeta potential can improve collision properties (Erepan, 2004).

2.2.3. Probability of Attachment

Since maximum collision efficiency is desired between the bubbles and the particles in a flotation system, it is generally agreed that the collision mechanism is the dominant factor controlling the recovery of valuable material. As such, collision mechanism is often regarded as the rate-determining step in froth flotation for ultrafine particles and is not a selective process (Weber and Paddock, 1983; Yoon and Luttrell, 1989).

Although it is desirable for all particles in the feed to collide with a bubble (100% collision efficiency), it is not desired that all collisions result in bubble-particle attachment. As such, the bubble-particle attachment process determines the selectivity of a flotation system in which the probability is a function of hydrophobicity and surface forces that interact between interfaces upon approach and can be represented by the following expression:

$$P_A = A\exp\left(-\frac{V_{T,\max}}{k_B T}\right) \tag{2.15}$$

where A is a function of surface coverage, $V_{T,max}$ is the maximum interaction energy occurring between the interfaces upon approach, k_B is the Boltzmann constant and T the temperature.

Thus, $V_{t,max}$ represents the energy barrier or activation energy to overcome for successful attachment between bubble and particle, which occurs at a particle-particle separation distance, H_C, that is a function of the interfacial and solution chemistry.

In other words the probability of attachment, P_A, is related to the kinetic energy of a particle approaching a bubble, E_k, and the energy barrier for the bubble-particle adhesion, E_1, as given by (Luttrell and Yoon, 1992; Mao and Yoon, 1997):

$$P_A = \exp\left(-\frac{E_1}{E_k}\right) \tag{2.16}$$

To increase the probability of attachment, P_A, Eq. (2.16) suggests that the energy barrier, E_1, needs to be decreased and the kinetic energy, E_k, must be increased. These conditions can be achieved through increased particle hydrophobicity and by providing high-shear mixing in the system, as suggested by Weiss and Schubert (1988) and, Jameson (2010) for increased flotation rates to benefit the fine particle recovery.

2.2.3.1. Energy Barrier for Attachment

The energy barrier for bubble-particle attachment, E_1, comes from surface forces, which are modeled using the extended DLVO (Derjaguin, Landeau, Verwey and Overbeek) theory as shown in Figure 2.4. The magnitude of the surface energies between two interfacial boundaries, or the total interaction energy, can be given by (Israelachvili and Pashley, 1984; Xu and Yoon, 1990):

$$V_T = V_D + V_E + V_S \tag{2.17}$$

where V_T is the total interaction energy (potential energy), V_D the van der Waals dispersion energy, V_E the electrostatic interaction energy and V_S is the structural interaction energy (or V_H, the hydrophobic interaction energy), which is the additional term to the classical DLVO theory modeled by Israelachvili and McGuiggan (1988).

The total potential energy, V_T, interacting between two hydrophobic particles in a medium is equivalent to the Gibbs free energy of the system. Thus, a negative value for any interaction energy represents an attractive interaction and a positive value represents a repulsive interaction.

Upon the approach of a particle and bubble, the existence of a positive electrostatic energy for surfaces of like charge causes repulsion. The repulsive response increases until the attractive hydrophobic force becomes dominant and the maximum interaction energy, E_1, occurs at the separation distance or the critical rupture thickness, H_C. At separation distances below H_C, the surface energy drops continuously. As a result, a successful bubble-particle attachment occurs by overcoming this interaction energy barrier (Sherrell, 2004).

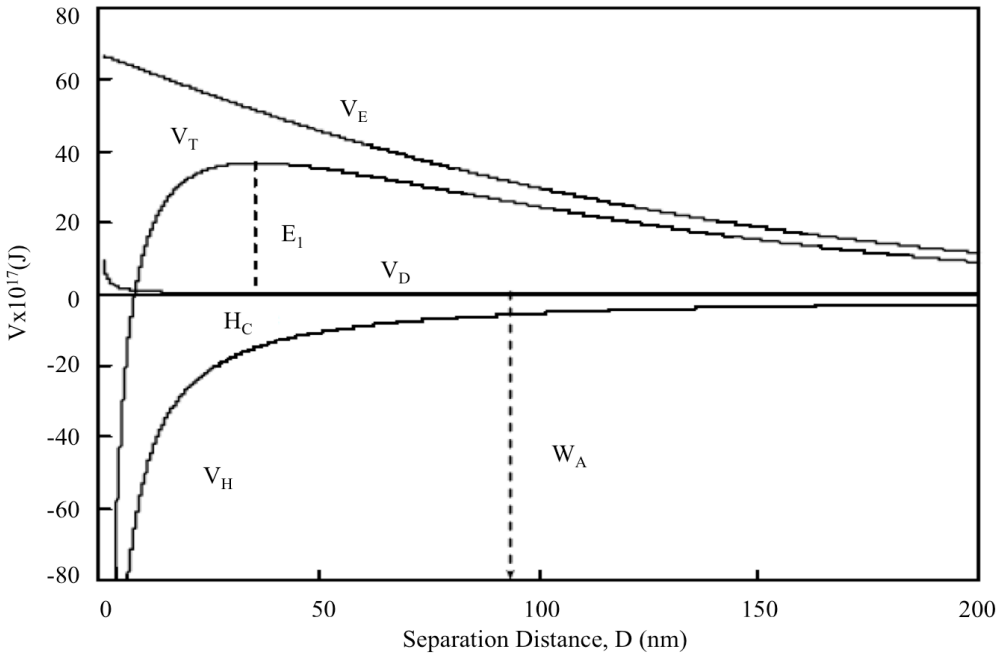


Figure 2.4. Total interaction (or potential) energy vs. distance diagram for the extended DLVO theory (Sherrell, 2004).

The van der Waals dispersion energy, V_D, is a function of the electromagnetic variation between two particles, which has an inverse power law dependence on their separation. In general terms, V_D can be attractive or repulsive, and is always attractive between two similar solid particles immersed in a liquid. When these two solid bodies are adequately close to each other, V_D results in an attractive force, which depends on the geometry of the space separating them (Fan, 2008). When the dielectic constant of the medium is between the dielectic constants of the two interacting bodies, the dispersion force is repulsive. This is the case for bubble-particle interactions.

Another way to decrease the energy barrier for the bubble-particle adhesion is by decreasing the electrostatic repulsion between the particle and the bubble. Fuerstenau (1957) showed that the maximum flotation response is achieved at the point of zero charge (p.z.c.) of a particle, which refers to the pH for which the surface charge, σ_o, is zero. Similarly, Derjaguin and Shukakidse (1960) showed that the particle floatability increases with decreased zeta (or electrokinetic) potential, ζ, which is commonly used as an estimate

of the surface potential, Ψ_O, in colloid chemistry studies by using low electrolyte concentrations.

The electrostatic interaction energy, V_E, is a result of the various mechanisms that cause the development of surface charge phenomenon. For many inorganic and biological surfaces, surface charges are developed dependent upon primarily the pH and also the adsorption of charged ions and the presence of permanent structural charge (especially for clays) (Sposito, 1989). The overall surface charge is represented as the balance of the dissolved counter-ions in the solution. These counter-ions are attracted to a particle surface through an electric field, which forms the electrical double-layer around the particle the surfaces in an aqueous solution (Stumm, 1992; Butt et al., 1995).

The electrostatic interaction energy, V_E, occurs as a result of the osmotic pressure that exists when the ion clouds surrounding a charged particle surface overlap when they approach each other. The resulting interaction may be attractive if the ion clouds are comprised of oppositely charged ions, or repulsive when the ion clouds have the same charged ions. V_E varies exponentially depending on the distance between the two particles and shows a strong correlation with the particle surface charge densities and the ionic strength of the immersed liquid.

In addition to hydrodynamic forces, the movement of fine particles toward a bubble is a function of both diffusional and electrophoretic forces, i.e., diffusiophoretic forces. In the wetting zone, relatively weak forces, such as van der Waals and electrostatic forces, act to encourage collision of fine particles with bubbles. As a result, fine particles with limited inertia may adhere on the surface of air bubbles without penetrating the thin wetting film (Ahmed and Jameson, 1989; Nguyen et al., 1997; Dai et al., 2000; Yoon, 2000).

The structural interaction energy, V_S, results from the structure of the water molecules in the liquid boundary layers around a solid. The structural interaction can be either attractive or repulsive, depending on the nature of the interaction between the solid surfaces and the water molecules (Israelachvili and McGuiggan, 1988). On the other hand, Xu and Yoon (1990) found that hydrophobic interaction energy, V_H, is attractive and decays exponentially. In addition, it operates at much longer separation distances than the van der Waals dispersion energy, V_D. The hydrophobic interaction energy, V_H, is recognized as the major attractive force between bubbles and strongly hydrophobic particles whereas electrostatic interaction energy, V_E, is regarded as the primary repulsive force (Yoon and Mao, 1996; Yoon and Aksoy, 1999).

Rabinovich and Yoon (1994) hypothesized that the attractive hydrophobic interaction force (V_H) can be quantified by the following relationships:

$$V_H = -\frac{R_p R_b}{6\left(R_p + R_b\right)} \frac{K_{132}}{H_C} \tag{2.18}$$

where K_{132} the magnitude of hydrophobic interaction in a three-phase contact (1-particle, 2-bubble, 3-liquid).

The hydrophobic force parameters for particle-particle interaction (K_{131}) and for bubble-bubble interaction (K_{232}) can be combined to determine the magnitude of hydrophobic interaction in a three-phase contact, K_{132} (Yoon and Mao, 1996; Yoon et al., 1997):

$$K_{132} = \sqrt{K_{131} K_{232}} \tag{2.19}$$

2.2.3.2. Kinetic Energy, E_k

The depth of the primary minimum in Figure 2.5 is equal to the Gibbs free energy of the system (ΔG), which is also referred to as the energy of adhesion. In order for coagulation to occur between two interacting bodies in the primary minimum, the energy barrier must be either non-existent or overcome by external energies, i.e.,

$$V_{T,\max} = V_D + V_E + V_S < V_K \tag{2.20}$$

where V_k is the kinetic energy supplied by mechanical and thermal agitation (or by Brownian motion). From this expression, bubble-particle attachment is considered to occur in Eq. (2.16) when the kinetic energy of the particle, E_k, is larger than the energy barrier, E_l, determined by the surface forces involved in the bubble-particle interaction.

The kinetic energy of a particle approaching a bubble, E_k, or kinetic energy for attachment in this case, can be determined by assuming the flotation process under laminar conditions as shown in Figure 2.5. When a particle collides with bubble at the very top, i.e., $\alpha=0$, all the kinetic energy will be utilized to thin the bubble-particle film. However, when the particle hits the bubble with an angle, i.e., $\alpha>0$, only a portion of the kinetic energy will be used for this process. The maximum kinetic energy for the film thinning process may be determined from the radial velocity of the particle, u_{rp}, since the resisting hydrodynamic and surface forces are acting along the radial direction. Particle rising (radial) velocity would be equal to the liquid radial velocity, u_r, when a particle (with no inertia) is located at a sufficient distance to the bubble. For a closer distance between a particle and a bubble, particle radial velocity, u_{rp}, will decrease due to hydrodynamic resistance (drag) force.

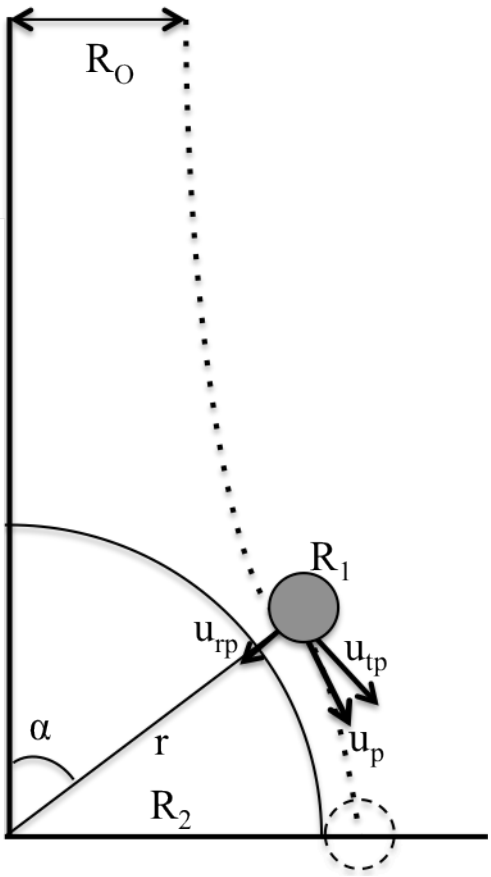


Figure 2.5. Grazing streamline for a particle approaching a bubble surface, where u_{tp}, is the particle tangential velocity (Yoon and Mao, 1996).

Bubble-particle attachment also occurs due to the existence of a secondary energy minimum (E_2), which is depicted in Figure 2.6. In this case, attachment may occur without forming a three-phase contact line at E_2, where the inter-particle equilibrium distance is H_2, when the kinetic energy of a particle approaching a bubble, E_k, is smaller than that of E_1 and E_2 (Derjaguin and Dukhin, 1969). This attachment phenomenon, i.e., contactless flotation, is thought to be limited for very small particles with relatively low hydrophobicity.

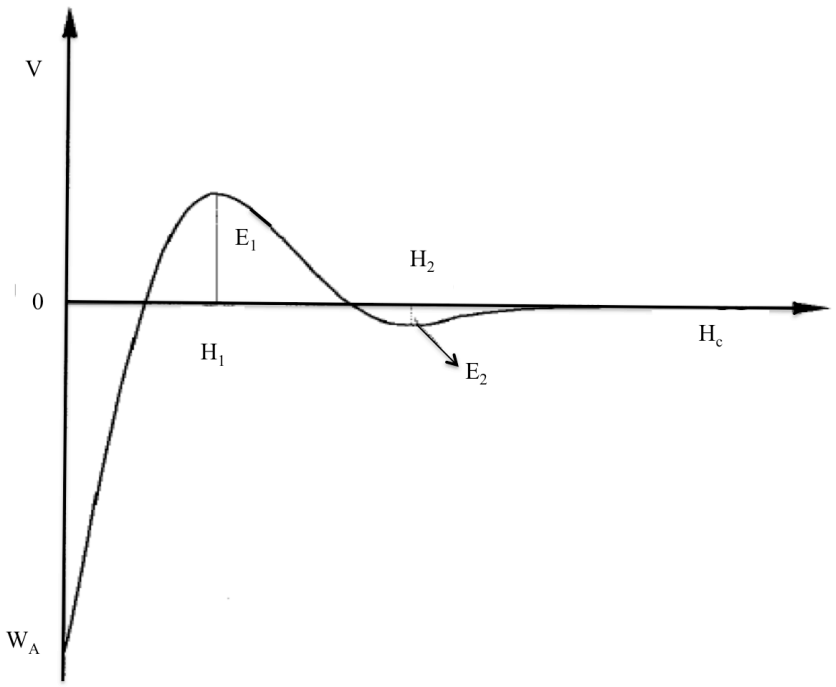


Figure 2.6. Potential energy and distance relationship for the bubble-particle interaction that determines the work of adhesion, and thus the attachment process (Yoon and Mao, 1996).

The three-phase contact line will be formed (at H_c=0) after the thin film ruptures between the bubble and the particle, when the kinetic energy, E_k, is larger than E_1 and E_2, but smaller than the sum of work of adhesion, W_A, and E_1. The thin film ruptures spontaneously when the surface forces become negative (F=-dV/dH_c) between the particles and the bubbles. This is only possible when the particle kinetic energy is equal to or larger than that of the energy barrier within the distance of H_1, which is referred to as the critical rupture thickness. Therefore, $E_k \geq E_1$ is the necessary condition for the bubble-particle attachment to occur (Yoon and Mao, 1996).

The initial kinetic energy term used in the probability of attachment in Eq. (2.16) considers a fraction of the kinetic energy for distributed particle E_k values, which is used to thin the bubble-particle film at H_1. For the particles at various initial locations approaching a bubble from far away distances, Eq. (2.21) was developed to calculate

kinetic energy term, E_k, at H_1 (Yoon and Mao, 1996):

$$E_k = \frac{1}{2}(\rho_s - \rho_m)\frac{4\pi R_1^{\,3}}{3}u_{rp}^{\,2} = \frac{2\pi R_1^{\,3}(\rho_s - \rho_m)}{3}u_{rp}^{\,2} \tag{2.21}$$

where ρ_s and ρ_m are solid and medium densities, respectively.

2.2.3.3. Thermodynamics of Wetting

In order for the bubble-particle attachment to be thermodynamically favorable, for any finite value of the contact angle, there must be a net decrease in the energy of the system. The change in the free energy accompanying the replacement of a unit area of the solid-liquid interface by a solid-gas interface is given by Dupree's equation:

$$\Delta G = \gamma_{SV} - \gamma_{LV} - \gamma_{SL} < 0 \tag{2.22}$$

where ΔG represents the net change in Gibbs free energy and γ_{LV}, γ_{SL}, γ_{SV} are the interfacial surface tensions at the liquid/vapor, solid/liquid and solid/vapor interfaces, respectively, which can be shown in Figure 2.7 after the contact of the interfaces.

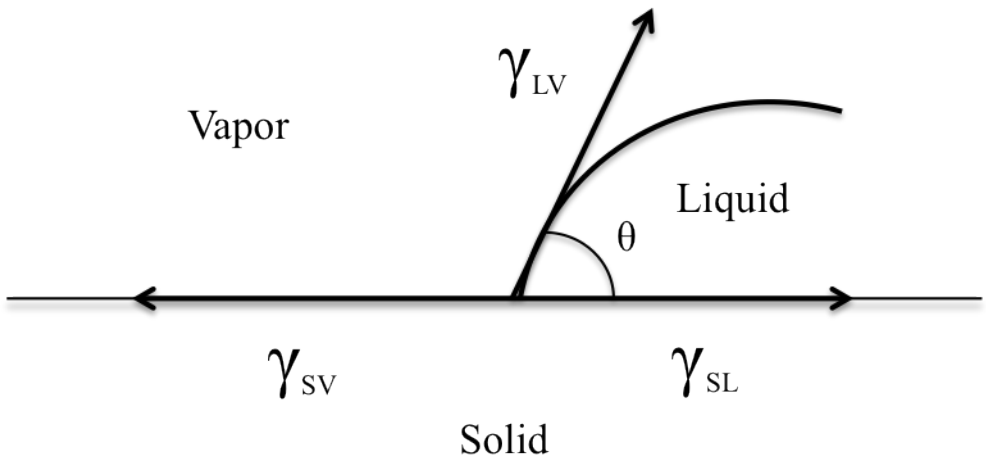


Figure 2.7. The three-phase contact for a liquid droplet on a solid surface in vapor.

The general thermodynamic condition for three-phase contact is defined by Young's equation, which describes the equilibrium between interfacial energies as follows:

$$\gamma_{SV} - \gamma_{SL} = \gamma_{LV} \cos\theta \tag{2.23}$$

in which θ is commonly referred to as the contact angle and is measured through the liquid, as shown in Figure 2.8.

Substituting Eq. (2.23) into Eq. (2.23) yields to the Young-Dupree equation:

$$\begin{aligned} \Delta G &= \gamma_{LV} \cos\theta_i + \gamma_{SL} - \gamma_{LV} - \gamma_{SL} \\ &= \gamma_{LV} \left(\cos\theta_i - 1\right) < 0 \end{aligned} \tag{2.24}$$

This equation can be used as a criterion for flotation, i.e., a negative ΔG value is required for bubble-particle attachment and thus the more negative the value of ΔG, the greater the probability of flotation.

The contact angle has been correlated with flotation for a number of different mineral systems. The floatability of a mineral often increases with increasing contact angle. As shown above, contact angle is a function of the three interfacial surface tensions, i.e.,

$$\cos\theta_i = \frac{\gamma_{SV} - \gamma_{SL}}{\gamma_{LV}}. \tag{2.25}$$

Minerals with θ>0 are hydrophobic to some degree, which means that the solid surface has higher affinity for air than water. Examples of naturally hydrophobic minerals are coal, sulfur, talc, graphite and molybdenite. However, most minerals are naturally hydrophilic (or aerophobic) and require surface chemicals, such as collectors, to become hydrophobic.

For sufficiently hydrophobic particles, the attractive surface forces help the liquid film between the bubble and the particle first to thin and finally to rupture for the attachment to take place, which is followed by the establishment of the three-phase, i.e., solid-liquid-air, contact line, as shown in Figure 2.8.

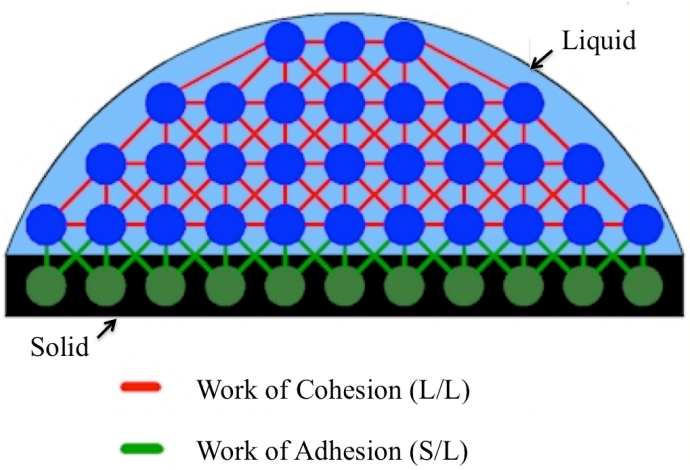


Figure 2.8. Spreading between solid, liquid and gas interfaces depending on their surface tensions.

A hydrophobic solid is defined as one that yields a negative spreading coefficient when in contact with water, which can be identified by the work of cohesion, W_C, and the work of adhesion, W_A, respectively, from the following equation:

$$W_C = 2\gamma_L \qquad \text{and} \qquad W_A = \gamma_S + \gamma_L - \gamma_{SL} \tag{2.26}$$

where γ_L, γ_S, and γ_{SL} are the interfacial surface tensions at the liquid, solid and solid-liquid interfaces, respectively.

Substituting Young's Equation (Eq. (2.24)) into W_A equation yields to:

$$\begin{aligned} W_A &= \gamma_{LV} + \left(\gamma_{LV}\cos\theta + \gamma_{SL}\right) - \gamma_{SL} \\ &= \gamma_{LV}\left(\cos\theta + 1\right) \end{aligned} \tag{2.27}$$

If the liquid is to spread on the solid than

$$S = W_A - W_C > 0 \tag{2.28}$$

or

$$S = \Delta G = \gamma_{SV} - \gamma_{LV} - \gamma_{SL} > 0 \tag{2.29}$$

where S is commonly referred to as the spreading coefficient, which needs to be a negative value for a hydrophobic solid as mentioned above, with the following relationship:

$$W_A < W_C \tag{2.30}$$

The work of adhesion equation can be defined as follows for a solid/water system:

$$W_A = \gamma_S + \gamma_W - \gamma_{SW} = W_A^d + W_A^{nd} \tag{2.31}$$

where $W_A{}^d$ and $W_A{}^{nd}$ are the dispersion (or the London dispersion) and the non-dispersion (or polar) components of the work of adhesion, respectively, and γ_{SW} is the solid-water interfacial surface tension.

The non-dispersion component is a function of the chemical nature of the solid and water and, thus, is the unknown variable. The dispersion component of the work of adhesion can be determined by:

$$W_A^d = 2\sqrt{\gamma_W^d \gamma_S^d} \tag{2.32}$$

where $\gamma^d{}_W$ is the dispersion coefficient on water and $\gamma^d{}_S$ the dispersion coefficient on solid.

Solving Eq. (2.32) for $W_A{}^{nd}$ and substituting Eq. (2.32) yields to:

$$W_A^{nd} = \gamma_S + \gamma_W - \gamma_{SW} - 2\sqrt{\gamma_W^d \gamma_S^d} \tag{2.33}$$

Introducing Young's equation yields to:

$$W_A^{nd} = \gamma_W \left(1 + \cos\theta_W\right) - 2\sqrt{\gamma_W^d \gamma_S^d} \tag{2.34}$$

Since a hydrophobic solid is characterized by $W_A < W_C$ one can generalize that small values of W_A^{nd} denotes a high degree of hydrophobicity (i.e., weak-to-strong) and large values indicates a weakly hydrophobic or hydrophilic solid. Thus, Eq. (2.34) shows that the values of both the contact angle (θ_W) and the dispersion coefficient on solid (γ^d_S) are required characterizing the hydrophobicity of a solid.

2.2.3.4. Induction Time

In addition to determining the probability of bubble-particle attachment from the energy balance of the particle and the bubble surface, i.e., hydrodynamic and surface forces, the attachment mechanism on the bubble surface can be also explained from the illustration in Figure 2.6. Upon collision, particles must penetrate through a water film covering the bubble to achieve attachment. Thus, the rate of penetration is determined by the energy of attraction between the particle and bubble.

During the bubble-particle attachment process, the sliding time, t_s, is known as the period that the particle takes to slide on the bubble surface toward the equator. The induction time, t_i, is known as the time needed both to penetrate, thin and rupture the bubble-particle liquid film and to expand the three-phase contact line to form a wetting perimeter and successfully achieve a bubble-particle attachment process. Flotation as a result of a successful attachment occurs only when the induction time is less than the sliding time (or contact time, with the addition of collision time). As shown in Figure 2.6, R_O represents the limiting radius in which particles with sufficient hydrophobicity will attach to the bubble. For highly-hydrophobic particles, the limiting radius will be quite large due to low induction time values, which can be measured experimentally under a given set of conditions. On the other hand, weakly-hydrophobic particles need to strike the bubble at the top. By adding collectors and/or adjusting solution chemistry, it may be possible to

reduce the induction time of a weakly-hydrophobic solid, thereby improving the probability of attachment as shown in Figure 2.9.

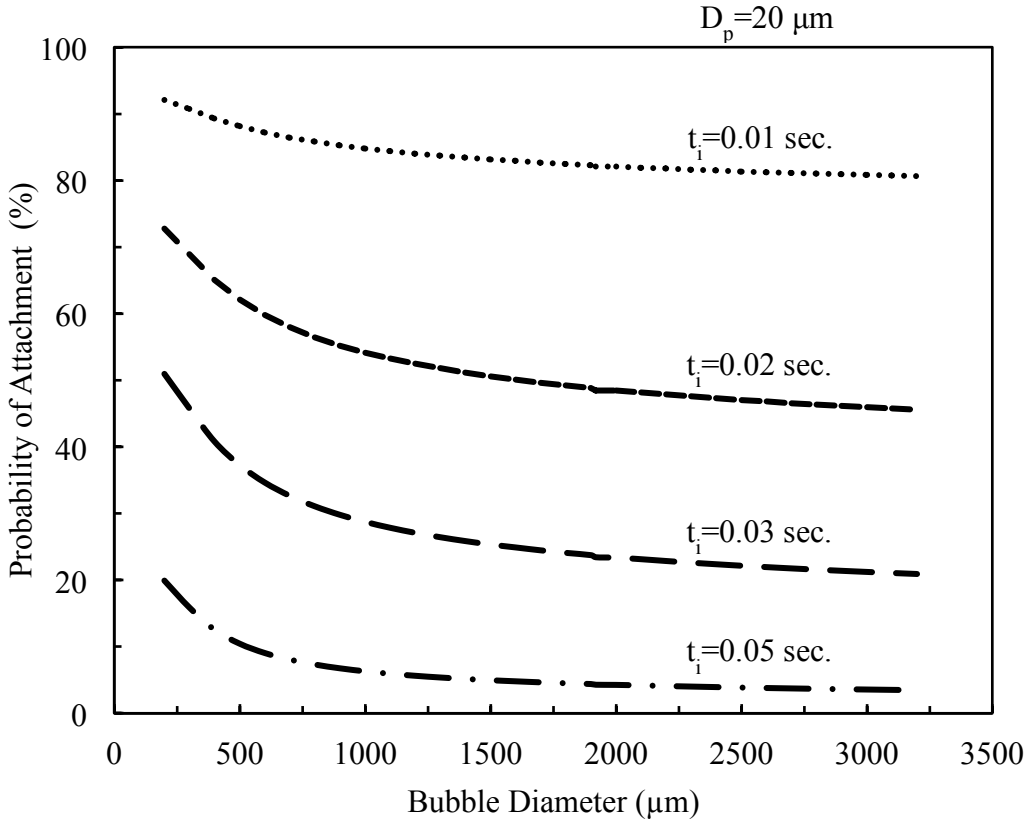


Figure 2.9. Effect of bubble size on the attachment probability of a fine size particle for a range of induction times (*after* Yoon and Luttrell, 1989).

The probability bubble-particle attachment, P_A, can be expressed as the ratio of the limiting radius to the sum of the bubble and particle radii, which was defined as the fraction of particles in the path of the bubble that were actually attaching to the bubble (Yoon and Luttrell, 1989):

$$P_A = \frac{R_O^2}{\left(R_p + R_p\right)^2} \tag{2.35}$$

P_A can be also written in terms of the tangential velocity of the streamline (u_t) passing by the bubble, which is associated with the limiting angle (θ_O):

$$P_A = \sin^2 \theta_O \tag{2.36}$$

Based on the flow conditions characterized by the Reynolds number, appropriate hydrodynamic conditions have been modeled by Yoon and Luttrell (1989) such as in Eq. (2.13) for the intermediate stream function and derived for P_A as:

$$P_A = \sin^2 \left[2 \tan^{-1} \exp \left(\frac{-\left(45 + 8\,\mathrm{Re}^{0.72}\right) u_b t_i}{15 D_b \left(D_b / D_p + 1 \right)} \right) \right] \tag{2.37}$$

where u_b is the bubble rise velocity.

Following conclusions can be made as a result of the predicted trends from the previous studies on bubble-particle attachment (Yoon and Luttrell, 1989; Ralston and Duhkin, 1999; Yoon, 2000):

i. Small induction times and increased particle hydrophobicity result in high P_A values;
ii. P_A decreases with increasing particle size (D_p), which suggests that coarse particles are more difficult to attach the air bubbles. Similarly, lower tangential velocities due to small particle sizes increases P_A.
iii. Smaller the bubble rise velocity, u_b, as a result of decreased bubble size increases P_A, which also increases the sliding time, t_s.
iv. However, for bubble sizes around 350 microns, a further decrease in the bubble size becomes unfavorable for the P_A due to a decrease in the sliding distance, which makes the sliding time smaller than the induction time.

2.2.4. Probability of Detachment

Similar to the attachment process after bubble-particle collision, not all particles report to next successive level in flotation, i.e., the froth phase, upon a successful attachment. Particles detach from the bubble surface drop back into the collection zone when the particle kinetic energy is exceeded by the sum of work of adhesion, W_A, and energy barrier for bubble-particle adhesion, E_i, which can be written similar to that of P_A in Eq. (2.16) (Yoon and Mao, 1996; Mao and Yoon, 1997):

$$P_D = \exp\left(-\frac{W_A + E_l}{E_k'}\right) \tag{2.38}$$

where E_k' is the kinetic energy that detaches the particle from the bubble surface and is not the same as E_k in Eq. (2.16) for bubble-particle attachment.

Consider a solid spherical particle of radius R_p attaching on a bubble surface in liquid suspension as shown in Figure 2.10. Here, the particle radius is much smaller than the bubble surface, which is regarded to be flat compared to that of the particle. In addition, the curved area of the particle inside the bubble is shown as s_2 (after the bubble-particle attachment process), while its projected area on the bubble surface is given as s_1 (Yoon and Mao, 1996).

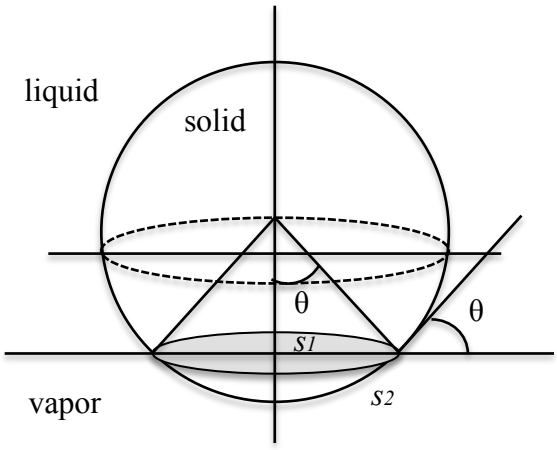


Figure 2.10. A solid spherical particle of radius R_p attaching on a bubble surface in liquid suspension (Yoon and Mao, 1996).

Young`s equation for work of adhesion, W_A in Eq. (2.27) can be rewritten as:

$$W_A = \gamma_{LV}\left(s_1 - s_2\cos\theta\right) \tag{2.39}$$

From the geometric relationship between the bubble and the particle in Figure (2.11), s_1 and s_2 can be written as:

$$s_1 = \pi\left(R_p \sin\theta\right)^2 \tag{2.40}$$

and

$$s_2 = 2\pi R_p^2\left(1-\cos\theta\right)^2 \tag{2.41}$$

which can be substituted into Young`s equation to obtain:

$$W_A = \gamma_{LV}\pi R_p^2\left(1-\cos\theta\right)^2 \tag{2.42}$$

The expression for the probability of detachment can be written after substituting Eq. (2.42) into Eq. (2.38):

$$P_D = \exp\left(-\frac{\gamma_{LV}\pi R_p^2\left(1-\cos\theta\right)^2 + E_l}{E_k{}'}\right). \tag{2.43}$$

As mentioned previously, the particle drop back to the pulp phase takes place when the detachment forces exceed the maximum attachment forces. Similar to the assumption made calculating the kinetic energy for attachment, E_k, laminar flow conditions could be considered to calculate the kinetic energy that tears the particle off the bubble surface, $E_k{}'$.

Most of the particles on the bubble surface would be collected at the bottom, i.e., cap, while it rises through the flotation system, as shown in Figure 2.11. Particles in the cap area will be subjected to increased pressure due to liquid drag force when the angle representing the

cap area, θ_O, is large. French and Wilson (1980) found the pressure for the particle at the center of the cap as follows:

$$p_1 = \frac{\rho_l g R_b^2 \theta_O}{3} \tag{2.44}$$

where g is the gravitational force, and R_b is the bubble radius. The angle representing the cap area, θ_O, is considered to be a function of the bubble and particle size and the particle population in the cap.

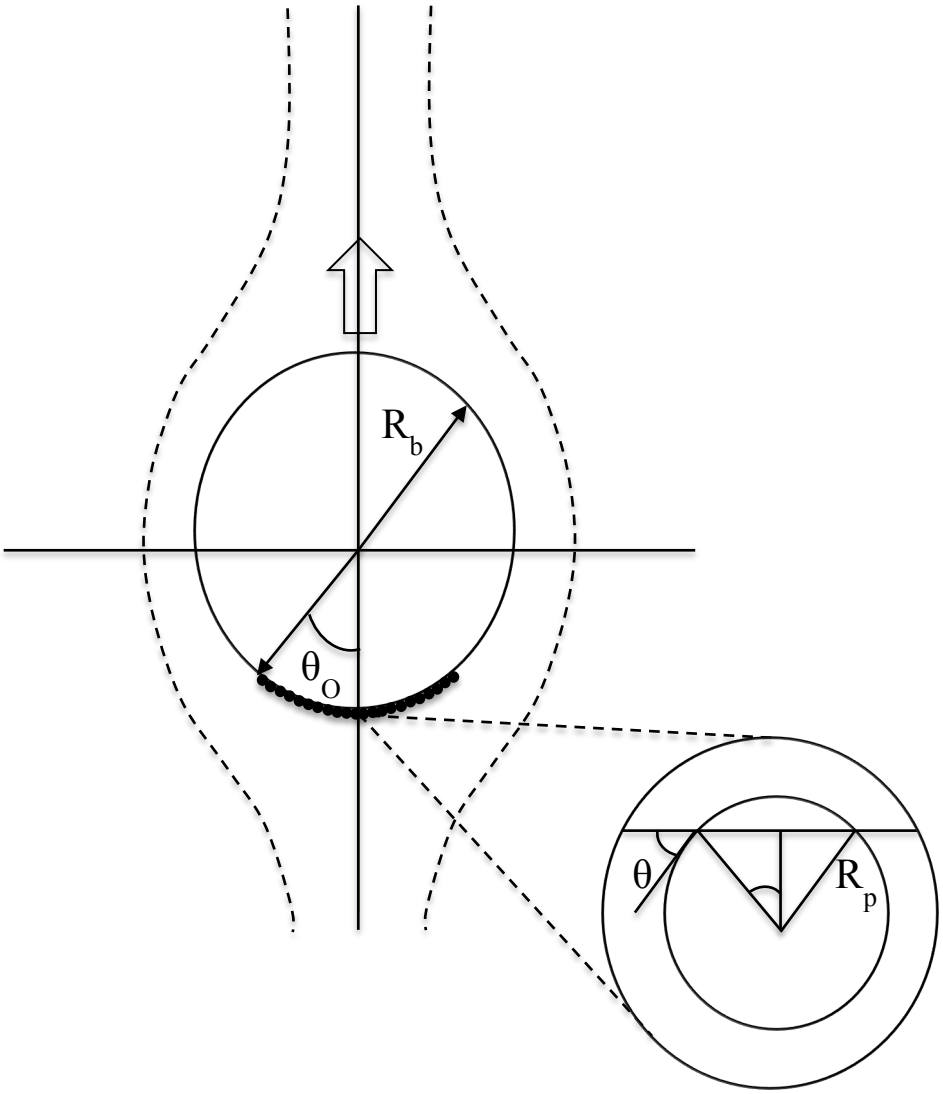


Figure 2.11. A cap of particles (R_p) collected at the bottom of a rising air bubble (R_b) (Yoon and Mao, 1996).

The kinetic energy of particle detachment from the bubble surface, E_k', can be calculated as a function of the contact area, ϕ, between a particle (R_p) and the bubble and the cap pressure:

$$E_k' = p_1 \phi \tag{2.45}$$

where the contact area, ϕ , between a particle and the bubble can be calculated as:

$$\phi = \pi R_p^2 \sin^2 \theta \tag{2.46}$$

where θ is the contact angle of the three-phase contact line between a particle and the bubble. After combining Eqs. (2.44) and (2.46) in Eq. (2.45), one can find out the kinetic energy for detachment, E_k':

$$E_k' = \frac{\rho_l g R_b^2 \theta_O}{3} \pi R_p^2 \sin^2 \theta \tag{2.47}$$

2.2.4.1. Force Balance for Detachment

Similar to the bubble-particle interactions in the attachment process, such as the hydrodynamic resistance (drag) force, F_r, there are other forces between the attached particles and a bubble. In addition to F_r, the capillary force, F_p, the excess force, F_e, and the particle weight in the liquid medium, F_w are the major acting forces (Drzymala, 1994; Cheng and Holtham, 1995; Ralston et al., 1999a, b). Here, F_e is the difference between the excess pressure in the bubble and the hydrostatic force, which favor attachment and detachment, respectively. The following equations represent the force balance for the bubble-particle interactions (Tao, 2004):

$$\begin{aligned} F_r &= 6\pi R_p u_{rp} \\ &= 3\pi D_p u_{rp} \end{aligned} \qquad \text{(Laminar conditions)} \tag{2.48}$$

$$F_r = \frac{C_d \pi}{8} \rho_l D_p^2 u_{rp}^2 \qquad \text{(Turbulent conditions)} \tag{2.49}$$

$$F_p = \frac{\pi D_p \gamma (1 - \cos\theta_d)}{2} \tag{2.50}$$

$$F_p = \frac{1}{4}\pi D_p^2 (1 - \cos\theta_d)\left(\frac{2\gamma}{D_b} - \frac{\rho_w g D_b}{2}\right) \tag{2.51}$$

$$F_w = \frac{1}{4}\pi D_p^3 \rho_p g - \frac{1}{8}\pi D_p^3 \rho_w g\left(\frac{2}{3} + \cos(\frac{\theta_d}{2}) - \frac{1}{3}\cos^3(\frac{\theta_d}{3})\right) \tag{2.52}$$

where γ is the surface tension of the liquid, ρ_l, ρ_p and ρ_w are liquid, particle and water densities, respectively, C_d is the drag coefficient and θ_d is the critical contact angle for the three-phase contact line before detachment.

From these four force categories, the capillary force, F_p, is generally considered as the major attachment force, while particle weight, F_w, and hydrodynamic resistance (drag) force, F_r, are known as the detachment forces. From Eqs. (2.48) and (2.49), it is clear that the drag force, F_r, is dependent on the velocity, which increases as the bubble-particle aggregate rises in a flotation system. In addition, similar to other major forces, F_r is also directly proportional to the particle size, suggesting that coarse particles, or bubble-particle aggregates, are more likely to detach from the bubble surfaces and result in low flotation recoveries compared to fine particles, which has been shown experimentally by Soto and Barbery (1991), Ralston et al., (1999a, b) and Ralston and Dukhin (1999).

The role of excess force, F_e, is related to the relative magnitude of the aforementioned force balance, which is considered as the attachment force, since the bubble diameter in a flotation system is smaller than 5.5 mm under normal conditions (Tao, 2004).

The force balance at the moment of detachment becomes the equilibrium of the sum of the capillary and excess forces and the sum of the particle weight and the drag force:

$$\left(F_p + F_e\right) - \left(F_w + F_r\right) = 0 \tag{2.53}$$

The force balance equation becomes simpler after disregarding F_r, which is relatively negligible compared to F_w (Tao, 2004):

$$F_p + F_e = F_w \tag{2.54}$$

As a result of the attachment and detachment forces acting on bubble-particle interactions, the probability of detachment may be written in terms of that force balance:

$$P_D = \frac{1}{1 + F_{at} / F_{de}} \tag{2.55}$$

where F_{at} and F_{de} represent the total attachment and detachment forces, respectively.

According to Eq. (2.55):

$P_D = 0$ when $F_a >> F_{de}$;
$P_D = 0.5$ when $F_a = F_{de}$;
and $P_D = 1$ when $F_a << F_{de}$.

The total attachment and detachent forces can be calculated by using the Eqs. (2.50) – (2.52) (Tao, 2004):

$$\frac{F_{at}}{F_{de}} \approx \frac{3(1-\cos\theta_d)\gamma}{g\left(\rho_p - \rho_w\left(1/2 + 3/4\cos\left(\theta_d/2\right)\right)\right)} \frac{1 + D_p/D_b}{D_p^2} \tag{2.56}$$

Substituting Eq. (2.56) into Eq. (2.55) gives the probability of particle detachment in terms of the force balance due to the bubble-particle interactions:

$$P_D = \frac{1}{\left[1 + \left(\frac{3(1-\cos\theta_d)\gamma}{g\left(\rho_p - \rho_w\left(\frac{1}{2} + \frac{3}{4}\cos\left(\frac{\theta_d}{2}\right)\right)\right)}\right)\left(\frac{1 + D_p/D_b}{D_p^2}\right)\right]} \tag{2.57}$$

Deglon et al. (1999) empirically showed that the detachment rate constant, and thus the probability of detachment, increases with increased bubble and particle sizes, which can be also seen from Eqs. (2.57) and (2.58). As a result, one may suggest that coarse (plus 150 microns), heavy and less hydrophobic particles, which will first detach from large air bubbles selectively, can be recovered through the use of very fine bubbles. On the other hand, detachment is considered not to be a major problem for ultrafine particles, or even for flotation-size particles (up to 100 microns) (Tao, 2004; Goel and Jameson, 2012). One needs to also remember that most of the abovementioned models are based on the interaction between a single particle and a single bubble, which does not represent the flotation system with countless particles and bubbles. Predicting the behavior of a bubble-particle interface for a real application is further complicated by several other factors, such as the effect of gas holdup, the interaction between the neighboring bubbles and the presence of bubbles on different layers, sizes and shapes. According to Tao (2004), the overall flotation probability, *P*, increases as a result of all these factors, which tend to straighten the liquid streamlines around a bubble.

2.2.4.2. Maximum Particle and Bubbles Sizes

The bubble-particle detachment subprocess ultimately determines the maximum recoverable particle size from a froth flotation process, which is a function of the degree of hydrophobicity and the surface charge. Nguyen (2003) combined the equation derived by Schubert (1999) for the maximum stable bubble size with the work of Schulze (1982) on the maximum size of particle that could remain attached to a bubble that can be given as:

$$d_{p,\max} = \left(\frac{-6\gamma \sin(\pi - \theta/2)\sin(\pi + \theta/2)}{\left(g\Delta\rho + \overline{b_m}\rho_p \right)} \right)^{1/2} \tag{2.58}$$

where $d_{p,max}$ is the maximum particle size, b_m is the machine acceleration and $\Delta\rho$ is the difference in density between the particle and the bubble.

Although it is subject to certain limits, the maximum stable bubble size, $d_{b,max}$, can be generalized by Schubert`s equation (1999):

$$d_{b,\max} = We_c^{3/5} \left(\frac{\gamma^{3/5}}{\left((P/\rho_L V)^{2/5} \rho_L^{3/5} \right)} \right) \tag{2.59}$$

where We_c is the critical Weber number, and V is the volume of the liquid in the cell.

Hinze (1955) suggested that a bubble would burst if the ratio of the inertial and surface tension forces exceeds the critical Weber number:

$$We_c = \frac{\rho \overline{U^2} d_{b,\max}}{\gamma} \tag{2.60}$$

where $\bar{U}^2$ is the mean square velocity difference between two points in the turbulent flow from a distance apart from the maximum bubble diameter, $d_{b,max}$, which can be obtained from Batchelor`s (1951) expression:

$$\overline{U^2} = C_1 (\varepsilon d_{b,\max})^{2/3} \tag{2.61}$$

where C_1 is an empirical constant, and ε is the energy dissipation rate per unit mass in the liquid ($\varepsilon = P_i \rho_L V$, where P_i is the power input).

By combining Eqs. (2.58) and (2.59), Nguyen (2003) improved the accuracy of the solutions to the Young-Laplace equation with the following simple equation to represent the maximum floatable particle size (Jameson et al., 2008):

$$d_{p,\max} = We_c^{3/5}\left(\frac{3\gamma(1-\cos\theta)}{\Delta\rho\left(g+b_m\right)}\right)^{1/2} \tag{2.62}$$

Schulze (1982) assumed that the bubbles in an agitated solution behave as if they are at the center of a vortex and rotating with the vortex. Then, any particle on the surface of the bubble would experience a centrifugal force, which tends to move the particle away from the bubble. The rotational velocity was found using the isotropic turbulence theory and the machine acceleration, b_m, is given by Schulze (1982):

$$b_m = 1.9\frac{\varepsilon^{2/3}}{d_b^{1/3}} \tag{2.63}$$

From this equation, the value of b_m is limitless with the increase in bubble size. However, there has to be a limit to the bubble size that can exist in the turbulent region of the cell. The shear force in the turbulent region, which is responsible for bubble-particle attachment and detachment, also limits the maximum bubble size that can remain stable in the liquid. As a result, it is expected that the shear force in the turbulent environment will limit the bubble size range that are relevant during the particle collection process (Jameson et al., 2008).

It is assumed that the maximum bubble size that is generated in the cell is the limiting factor for the maximum particle size that can be recovered. Therefore, the equation developed by Parthasarathy et al. (1992) for the maximum bubble size (Eq. (2.64)) can be inserted into Eq. (2.63) to find the machine acceleration value (Eq. (2.65)), as follows:

$$d_{b,\max} = \left(\frac{We_c}{C_1}\right)^{3/5}\left(\frac{\gamma^{3/5}}{\left((P/\rho_L V)^{2/5}\rho_L^{3/5}\right)}\right) \tag{2.64}$$

$$b_{m(d_b,\max)} = 1.9\frac{\varepsilon^{2/3}}{d_{b,\max}^{1/3}} = 1.28\frac{\varepsilon_i^{4/5}\rho_L^{1/5}}{\gamma^{1/5}} \tag{2.65}$$

For $b_m >> g$, substituting Eq. (2.65) into Eq. (2.62) yields the following approximate equation for the maximum floatable particle size (Jameson et al., 2008):

$$d_{p,\max} = 1.53\left(\frac{\gamma_{LV}^{6/5}(1-\cos\theta)}{\Delta\rho\varepsilon_i^{4/5}\rho_L^{1/5}}\right)^{1/2} \tag{2.66}$$

The process associated with the probability of detachment reflects a balance between the attractive adhesion forces and the gravitational (or centrifugal) force. According to this equation, coarse particle recovery can be enhanced with increased surface hydrophobicity (contact angle and surface tension) and decreased particle density. The expressions in Eqs. (2.42) and (2.41) clearly reflect the binding force acting to maintain contact, which is weak for particles having a low degree of surface hydrophobicity. In addition, a low-shear flow environment will assist the capture of coarse particles since the energy dissipation rate, ε_i, is inversely proportional with the maximum floatable particle size (Jameson et al., 2008).

The overall first-order flotation rate constant, k, can be rewritten by substituting the probability functions for collision (Eq. (2.13)), attachment (Eq. (2.16)) and detachment (Eq. (2.43)) into Eq. (2.7) to obtain (Yoon and Mao, 1996):

$$k = \frac{1}{4}S_b\left[\frac{3}{2} + \frac{4\mathrm{Re}^{0.72}}{15}\right]\left(\frac{R_p}{R_b}\right)^2 \exp\left(-\frac{E_l}{E_k}\right)\left\{1-\exp\left(-\frac{\gamma_{LV}\pi R_p^2(1-\cos\theta)^2 + E_l}{E_k'}\right)\right\} \tag{2.67}$$

From the first order flotation rate constant (k) model developed by Yoon and Mao (1996), k is given as a function of both hydrodynamic parameters, i.e., radii of particle and bubble (R_1, R_2), kinetic energy of collision and detachment (E_k and E'_k), Reynolds number (R_e), and bubble surface area flux (S_b), and the surface chemistry parameters, i.e., energy barrier for bubble-particle attachment (E_1), contact angle (θ) and surface tension of the flotation slurry (γ_{lv}). Williams and Crane (1983) found that the flotation recovery resulting from the bubble-particle contacting under turbulent conditions is a function of bubble and particle concentrations and the energy input into the system.

2.2.5. Collection Zone Recovery Rate

Collection zone transfer rate of hydrophobic bubble-particle aggregates to the froth zone is as a result of true attachment, which is known as the collection flotation rate, k_c, from Sutherland`s (1948) expression in Eq. (2.2). One should note that k_c and the corresponding recovery, R_C, described in the equations below reflects the collection zone recovery values only.

Levenspiel (1972) defined the collection zone recovery (R_c) of a given component as a function of k_{ci}, particle retention time (τ_P) and the hydrodynamic conditions by the axial mixing equation, i.e.,

$$R_C = 1 - \frac{4A\exp\left(\frac{Pe}{2}\right)}{(1+A)^2\exp\left[\left(\frac{A}{2}\right)Pe\right] - (1-A)^2\exp\left[\left(\frac{-A}{2}\right)Pe\right]} \tag{2.68}$$

where,

$$A = \sqrt{\frac{Pe + 4k\tau_p}{Pe}} \tag{2.69}$$

where Pe is the Peclet number, which is a measure of the axial mixing hydrodynamics of the system that has been quantified by Mankosa et al. (1992), i.e.,

$$Pe = \left(\frac{L}{D}\right)^{0.53} \left(\frac{V_t}{(1-\varepsilon)V_g}\right)^{0.35} \tag{2.70}$$

where L is the length of the collection zone (cm), D the diameter of the collection zone (cm), V_t the superficial tailing rate (cm/sec), V_g the superficial gas velocity (cm/sec), and ε the fractional gas hold-up in the collection zone (generally 20-30%).

For a near perfectly-mixed reactor ($L<<<D$, $P_e \longrightarrow 0$), the collection zone recovery equation becomes:

$$R_C = \frac{k_c \tau_p}{1 + k_c \tau_p} \tag{2.71}$$

For a near a plug-flow reactor ($L>>>D$, $P_e \longrightarrow \infty$), the collection zone recovery expression reduces to:

$$R_C = 1 - \exp(-k_c \tau_P) \tag{2.72}$$

For a flotation system with both fast and slow floating particles, the recovery equation can be modified to incorporate the flotation rate of both components in which multiple flotation rates are typically associated with free and non-liberated minerals as proposed by Jowett (1974) and Lynch (1977):

$$R_C = (1 - c_1)\left[1 - \exp(-k_{c_2} \tau_{p_2})\right] + c_1\left[1 - \exp(-k_{c_2} \tau_{p_2})\right] \tag{2.73}$$

where c_1 is the fraction of the fast floating component of the mineral, k_{c1} and k_{c2} are the flotation rates of components 1 and 2.

The particle retention time, τ_p, can be estimated from the liquid retention time, τ_L, for the majority of the applications, using the following expression:

$$\tau_L = \frac{L(1-\varepsilon)}{V_t} \tag{2.74}$$

For particles with significant settling velocities, the particle retention time, τ_p, can be determined from the following equation:

$$\tau_P = \tau_L \left(\frac{\frac{V_t}{(1-\varepsilon)}}{\frac{V_t}{(1-\varepsilon)+u_p}} \right). \tag{2.75}$$

In Eq. (2.75) u_p $u_b$is the particle slip velocity between the water and the particle, which can be given by:

$$u_p = \frac{gD_p^2(\rho_p - \rho_l)(1-\varphi_S)^{2.7}}{18\mu(1+\mathrm{Re}_p^{0.687})}. \tag{2.76}$$

where φ_S is the volumetric concentration of solids.

The particle Reynolds number, Re_p, in Eq. (2.76) gives a dimensionless measure of the ratio of inertial forces to viscous forces from the following expression:

$$\mathrm{Re}_p = \frac{D_p u_p \rho_l (1-\varphi_S)}{\mu}. \tag{2.77}$$

2.3. FROTH ZONE RECOVERY

In the second phase of recovery in flotation process, the particle-bubble aggregate rises upward through the collection zone and into the froth zone. This is where the froth is formed at the top of the column and the final concentrate is generated. The concentrate in the froth consists of 70% to 80% air, which is a significant increase from 20% to 30% collection zone air fraction (Finch and Dobby, 1990). The retention time of the particles in the froth zone allows drainage of the feed pulp water from the froth which fills the

voids between the bubbles. As a result, the water layer surrounding each bubble thins and bubbles coalesce upon the approach of the liquid-air interfaces, thereby causing a reduction in bubble surface area.

Detachment of the particles occurs if the reduced amount of bubble surface area available in the froth zone is insufficient to carry the solids reporting from the collection zone. Coalescence causes liberation of particles from the bubble-particle aggregates, which have the potential to re-attach at a lower point in the froth o in the collection zone. Detached particles potentially move with the fluid into the collection zone. On the other hand, hydrophilic particles (strong affinity for water) slide over the bubble surface without attaching, descend downward to the tailings stream with the majority of the feed pulp.

2.3.1. Froth Zone Recovery Rate

Froth transfer rates, and thus the froth zone recovery, have a significant effect on the overall flotation kinetics, especially for the flotation systems employing deep froths. A particle may be collected in the collection zone and subsequently report to the froth zone. However, due to bubble coalescence and particle detachment, froth zone recovery may be less than 100 percent. An expression for froth zone recovery is:

$$R_F = \frac{\text{Mass rate of particles reporting to the concentrate via true flotation}}{\text{Mass rate of attached particles at the pulp} - \text{froth interface}} \qquad (2.78)$$

In most commercial flotation columns, R_F is less than 100% due to a reduced launder lip length to unit cross-sectional area ratio as compared to the laboratory and pilot scale units. This causes greater travel distances for the froth, which favors bubble coalescence, reduced bubble surface area and decreased recoveries. Improperly designed conventional cells have areas of stagnation in the froth, which also results in low R_F $R_F$values, which can be also calculated using:

$$R_F = \frac{k_f^{'}}{k_f^{'} + k_f^{''}} \tag{2.79}$$

where $k_f^{'}$ is the froth transfer constant (min^{-1}) and $k_f^{''}$ the drop-back rate constant (min^{-1}) which can be quantified based on semi-batch (Laplante, 1980) and continuous flotation cell tests under steady-state conditions.

2.4. OVERALL FLOTATION RECOVERY

The mass transfer between the collection zone and the froth zone in a flotation cell is used to assess the effect on overall flotation recovery for a given mineral from linear analysis concept (Meloy, 1983) as shown schematically in Figure 2.12 where R_C is the collection zone recovery due to flotation and R_F is the froth zone recovery with respect to solids entering the froth attached to gas bubbles.

Based on the recovery sub-processes and the application of linear analysis, Finch and Dobby (1990) proposed a mathematical expression for the overall flotation recovery, $R_{Overall}$, as a function of R_C and R_F, i.e.,

$$R_{Overall} = \frac{R_C R_F}{R_C R_F + (1 - R_C)} \tag{2.80}$$

From the Eq. (2.81), the effect of R_F on the overall recovery is clearly significant. One should also note that if the froth is operated such that 100% of the material reporting to the froth phase is recovered to the overflow, the $R_{Overall}$ R_{fc} is equal to the R_C.

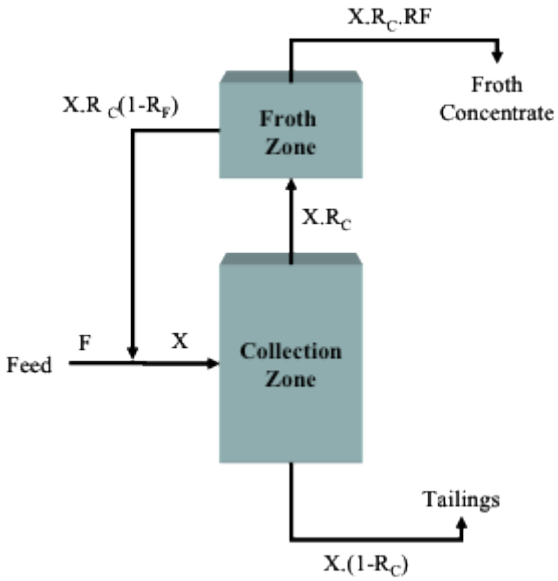


Figure 2.12. Illustration of the overall flotation recovery showing the interaction between collection and froth zones in a flotation cell.

It can be shown that the overall recovery ($R_{Overall}$) in a perfectly mixed continuous reactor can be determined used to expression:

$$R_{Overall} = \frac{k_c R_F \tau_c}{k_c R_F \tau_c + 1} \tag{2.81}$$

As previously discussed, detachment preferentially occurs for particles having a low degree of hydrophobicity which are typically low-grade particles. As such, these particles should experience lower R_F values which should enhance the selectivity process.

For example, consider particle species 1 and 2 with R_C values at 80% and 40%, respectively. Collection zone separation efficiency can be quantified by the difference of R_C values between these species, i.e., 40%. If the froth zone recovery values of species 1 and 2 are 100% and 40%, respectively, the selective detachment in the froth zone increases the overall selectivity of the process to around 60% as shown in Figure 2.13. Unfortunately, coarse and high-density particles are also prone to detach which may

counter the selectivity gain with the loss of valuable coarse particles. The selective recovery of coarse particles is one of the objectives of this study.

From Eq. (2.80) the overall recovery from a plug-flow reactor can be determined considering the two zone recoveries from i.e.,

$$R_{Overall} = \frac{\left[1-\exp(-k_{ci}.\tau_P)R_F\right]}{\left[1-\exp(-k_{ci}.\tau_P)R_F\right]+1-\left[1-\exp(-k_{ci}.\tau_P)\right]} \tag{2.82}$$

Equating Equations (2.80) and (2.82) above and solving for the overall kinetic rate (k_{fc}):

$$k_{fc} = \frac{1}{\tau_P}\ln\left[\exp(k_c.\tau_P)R_F + 1 - R_F\right] \tag{2.83}$$

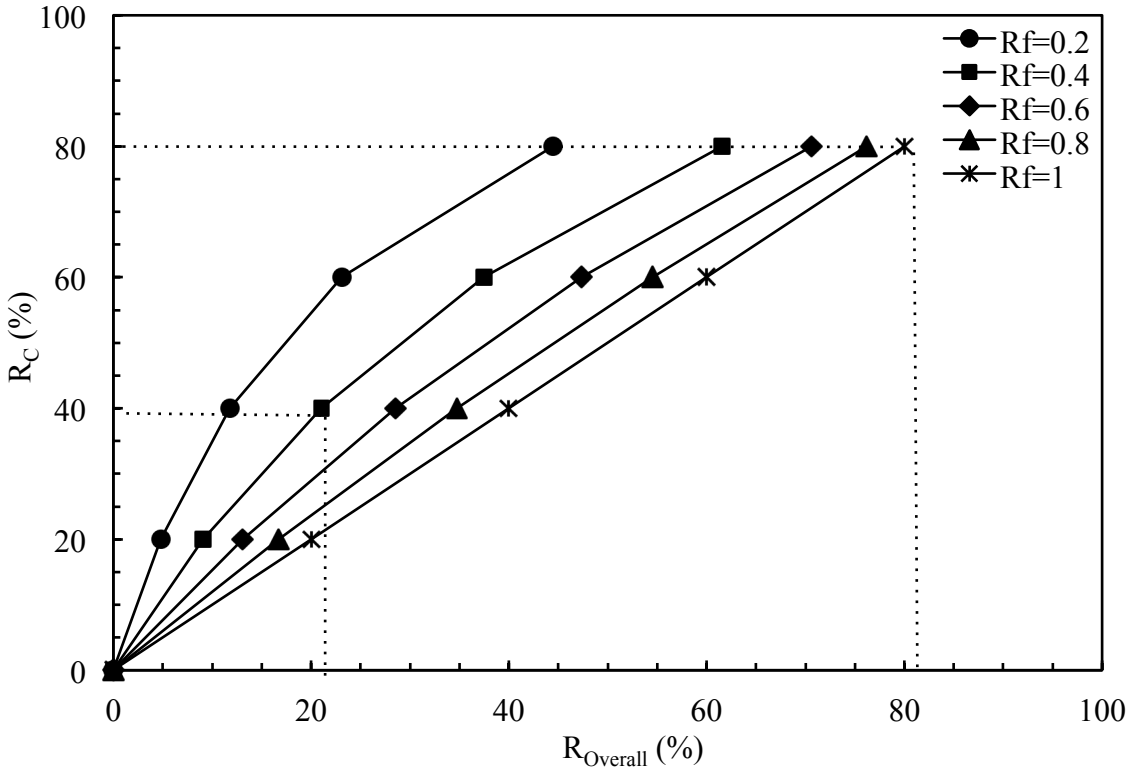


Figure 2.13. The impact of collection and froth zone recoveries on selectivity of the flotation process.

In the design of a flotation system, the overall kinetic flotation rate k_{fc} is most desired, which represents the rates through the collection k_c and froth k_f zones. However, most standard kinetic tests are used with the goal of attaining the value of the collection zone rate since k_{fc} is a function of time and thus not a true rate constant.

The relationship between k_{fc} and k_c is a function of the hydrodynamic conditions. From experimental data, for plug flow conditions with high k_c values, k_c is found to be a good approximation of k_{fc} regardless of the value of R_F. However, due to the non-plug flow nature of commercial columns, typical L:D ratio of 2, R_F is important to consider.

As mentioned above, highly floatable particles that are detached in the froth zone are efficiently recovered in the collection zone. On the other hand, weakly hydrophobic particles have a low collection zone recovery and thus are less likely to be recovered in the collection zone. As a result, reductions in froth zone recovery have a significant impact on the overall recovery of particles that have moderate-to-weak flotation characteristics. Therefore, the differential effect of froth zone recovery values between particles of varying floatability indicates an additional selectivity mechanism provided by the reflux action between the collection and froth zones.

CHAPTER 3

3. EXPERIMENTAL

3.1. CAVITATION FEED PRETREATMENT – LABORATORY STUDIES

3.1.1. Sample Characterization

Coal from two sources with different flotation characteristics were collected for the laboratory studies involving the feed pre-aeration concept using cavitation. Two separate samples from the Coalburg coal seams were collected from two active processing plants in West Virginia. The Coalburg seam coal is known to have difficult flotation characteristics. Coal from the Winchester seam was also collected for the study from a West Virginia preparation plant. The Winchester seam coal has excellent flotation properties and is used in the metallurgical market. The Coalburg coal is high-vol. bituminous coal whereas Winchester is mid-vol. bituminous coal. All three samples were collected in a 19-liter (5-gal.) bucket increments every 30 minutes from a flotation process stream in four 208-liters (55-gal.) drums simultaneously from each preparation plant ensure representative samples for the testing program.

The Winchester coal sample was collected from an active preparation plant located in Raleigh County, West Virginia. The flotation circuit of the 650-t/h plant consisted of flotation columns which processed for about 10% of the plant feed at 150 x 45 micron size range. The overall plant yield was about 40% and the overall plant concentrate ash content was around 7%. Since the collector and the frother were being added into the feed sump before the flotation feed collection pipe, the decision was made to collect the sample from the 38.1 cm (15 inch) classifying cyclone overflow before being fed to a bank of 32 deslime cyclones that were 6.35 cm (2.5 inch) diameter from which the overflow stream feeds into the flotation feed sump. As shown in Table 3.1, Winchester flotation feed had a solids content of 4.5% by weight of which the majority had a particle size smaller than 25 microns.

Table 3.1. Particle size distribution and quality characteristics of a preparation plant flotation feed from Winchester seam located in Raleigh County, West Virginia.

Particle Size Fraction (μm)	Incremental (%)		Cumulative (%)	
	Weight	Ash Content	Weight	Ash Content
+ 180	1.20	5.21	1.20	5.21
- 180x125	1.60	3.88	2.79	4.45
- 125x75	4.32	4.68	7.12	4.59
- 75x45	6.88	10.83	14.00	7.66
- 45x25	7.86	27.17	21.86	14.67
- 25	78.14	72.31	100.00	59.71
Total	100.00	59.71		

The first of the two Coalburg coal samples was collected from a preparation plant located in Boone County, West Virginia with a feed rate of 850 t/h. The flotation circuit in the plant consisted of conventional flotation cells which processes -0.15 mm material representing about 5% of the plant feed. The overall plant yield was nearly 48% and the overall plant product ash content was around 13%. Since the collector was added to the classifying cyclone overflow prior to being fed to the flotation circuit and the frother was added to the flotation feed pipe just prior to the conventional cells, both reagent additions were cut off during the sampling procedure to eliminate any chemicals being present in the feed slurry.

The flotation feed slurry sample contained 6% solids by weight. Similar to the Winchester sample, the Coalburg flotation feed was mostly comprised of particles smaller than 25 microns as shown in Table 3.2. However, a significant quantity of floatable material existed in the coarser size fractions as indicated by the relatively low ash contents.

Table 3.2. Particle size distribution and quality characteristics of a preparation plant flotation feed from Coalburg seam located in Boone County, West Virginia.

Particle Size Fraction (μm)	Incremental (%)		Cumulative (%)	
	Weight	Ash Content	Weight	Ash Content
+ 180	0.45	5.50	0.45	5.50
- 180x125	1.18	6.58	1.62	6.28
- 125x75	5.03	9.31	6.65	8.57
- 75x45	7.49	15.11	14.15	12.03
- 45x25	7.98	25.99	22.13	17.07
- 25	77.87	65.07	100.00	54.45
Total	100.00	54.45		

The second Coalburg coal sample was collected from a preparation plant located Kanawha County, West Virginia which has a feed rate of 700 t/h. During the sampling procedure for the laboratory studies, the flotation circuit was not in operation, which originally consisted of conventional flotation cells until late 2008. As such, the particles finer than 150 microns in the plant feed and reporting to 38.1-cm (15-inch) classifying cyclone overflow was directed to the thickener as the final plant reject. The overall plant yield was about 60% and the ash content of the plant clean coal product was around 13%.

As shown in Table 3.3, the majority of the flotation feed collected from the feed includes ultrafine slime material (minus 0.025 mm). However, this amount is less then the previous two samples, which contained over 75% ultrafine particles. On the other hand, the coarser particle sizes (plus 150 microns) have significantly higher ash contents (over 5 absolute percentage points) compared to the previous samples. The overall feed ash was around 43% which was relatively low compared to the other two samples indicating the presence of a lower amount of slime material. The feed solids content was around 8% by weight.

Table 3.3. Particle size distribution and quality characteristics of a preparation plant flotation feed from Coalburg seam located in Kanawha County, West Virginia.

Particle Size Fraction (μm)	Incremental (%)		Cumulative (%)	
	Weight	Ash Content	Weight	Ash Content
+ 225	2.74	13.03	2.74	13.03
- 225x150	4.38	14.73	7.12	14.08
- 150x75	13.20	20.68	20.31	18.37
- 75x45	11.27	27.75	31.58	21.71
- 45x25	10.04	32.39	41.62	24.29
- 25	58.38	55.52	100.00	42.52
Total	100.00	42.52		

3.1.2. Release Analysis

Release analysis is the main feed characterization test in flotation similar to the washability analysis in gravity-based separations. The goal of the analysis is to obtain the best possible separation performance achievable by any froth flotation process. Release analysis is conducted in two-phases with distinctly different goals. The first phase separates the hydrophobic particles away from the hydrophilic particles. In order to ensure a satisfactory separation, the initial feed material is re-floated 3 times through multiple cleaning stages as shown in Figure 3.1. After each cleaning stage, the remaining material in the cell container is collected as the tailings of the corresponding stage. In Phase I, collector (Fuel Oil No. 2) and frother (MIBC) are added at minimum dosages on an as-needed basis. Feed slurry is mixed with the collector for 5 minutes each time before adding the frother, which was allowed to disperse in the slurry for 1 minute for proper bubble generation before opening the air valve for flotation.

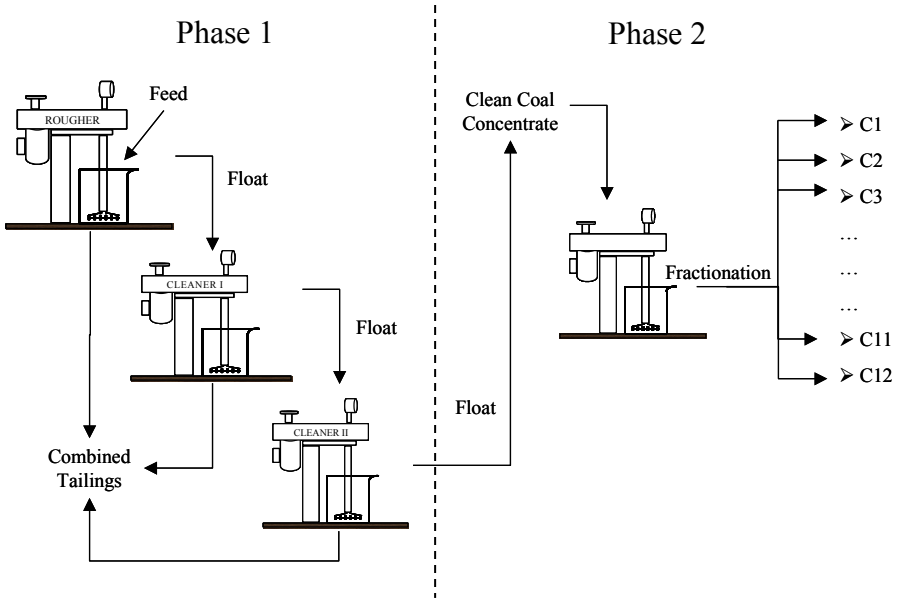


Figure 3.1. Schematic of the release analysis procedure in two-phases using a laboratory-scale conventional Denver flotation cell.

The second phase has the goal of separating hydrophobic particles collected in the first phase into various fractions depending on their degrees of floatability. Fractionated samples are obtained in the second stage by controlling airflow rate (L/min) and rotator revolutions (rpm) in the absence of collector addition. The first concentrate sample is taken under starvation type conditions, i.e. low airflow rates and slow rotator revolutions, to allow the collection of the highly floatable particles. In the following steps, the flotation process is continued to collect the next set of hydrophobic particles by providing more favorable conditions with the progressive increase of air rate and rotation speed. Through the end of the second phase, a small amount of frother was added to float the least hydrophobic particles in the feed.

Release tests were performed in this study using a 4.3-liter laboratory-scale conventional Denver flotation cell. The obtained concentrate and tailings fractions were dried, weighed and analyzed for ash content (%) using the appropriate ASTM procedures. The results of the release analysis were used to determine the theoretical achievable separation limits of the feed material by flotation which were used as a bench mark for comparison purposes.

3.1.3. Flotation Rate Tests

Flotation kinetics of the coal samples were analyzed followed the ASTM D5114 procedure for flotation rate tests with and without employing pretreatment using cavitation principles. For both approaches, a laboratory semi-batch Denver flotation unit equipped with a 4.3-liter cell was used. Flotation feed was conditioned with collector (Fuel Oil No.2) for 15 minutes μmbefore adding an alcohol-based frother (MIBC) to ensure correct adsorption of surfactants on hydrophobic coal particles. During the rate tests, flotation concentrates were collected as a function of time. Samples were filtered, dried, weighed and analyzed for ash content using the appropriate ASTM procedures.

In addition to the standard testing, flotation rate tests were also conducted using the cavitation tube to pretreat the flotation feed in an effort to nucleate micro-bubbles on hydrophobic coal surfaces. The laboratory setup including the cavitation tube consisted of a mixer to keep the slurry in suspension and conditioning, a sump which held around 40 liters, a recirculation pump to direct the slurry flow to go through the cavitation tube, a regulator to control the air pressure, a flowmeter to control the airflow and a pressure gage to observe the amount of pressure going into the cavitation tube as shown in Figure 3.2. The regulator at the air inlet was set to the maximum air pressure of 206 kPa (30 psi) to receive pressurized feed slurry at 138-kPa (20-psi) through the cavitation tube.

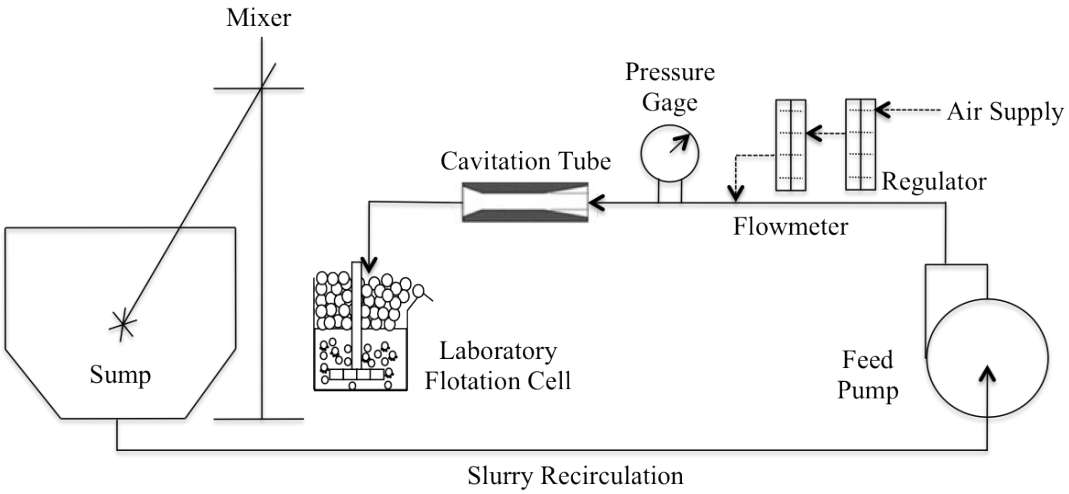


Figure 3.2. Schematic of the laboratory flotation cell setup employing the cavitation feed pre-aeration during the kinetic rate tests.

After conditioning the slurry inside the sump with collector, the feed sample was taken directly from the nozzle of the cavitation tube into the laboratory flotation cell for flotation rate tests. One minute mixing time of frother in the cell was given to the keep the same conditions of a standard kinetic rate test.

The airflow in the conventional flotation cell was controlled during the tests through a flowmeter attached to the adjustable air valve and kept constant at 5 L/min while the rotor speed was maintained at 1200 rpm. The application of the cavitation tube and the addition of air to the feed to the cavitation tube were the parameters that were changed during the rate tests. In select tests, air was added directly into the feed line to the cavitation tube at a constant rate of 1 l/min and monitored through a flowmeter during the tests when both the cavitation tube and air addition parameters were tested. The feed slurry was injected into the cavitation tube and directly transported into the laboratory flotation cell (Figure 3.2). In this manner, the micron-size air bubbles that were formed by cavitation were kept mainly intact as opposed to collecting the treated material in a separate container and transporting a sample of the bulk to the flotation cell. As such, bubble-aggregate stability was enhanced.

3.1.4. Column Flotation Tests

A continuously operated laboratory column unit was used to perform flotation tests over a range of feed volumetric flow rates in order to provide separation performance analysis over a range of retention times, as shown in Figure 3.3. In addition, feed solid concentrations were also varied at a constant volumetric flow rate to assess the impact of the novel recovery enhancement mechanism on carrying capacity. The flotation column used the Microcel™ bubble generator which consisted of a static mixer and a pump configuration whereby a portion of the tailings was circulated back to the column.

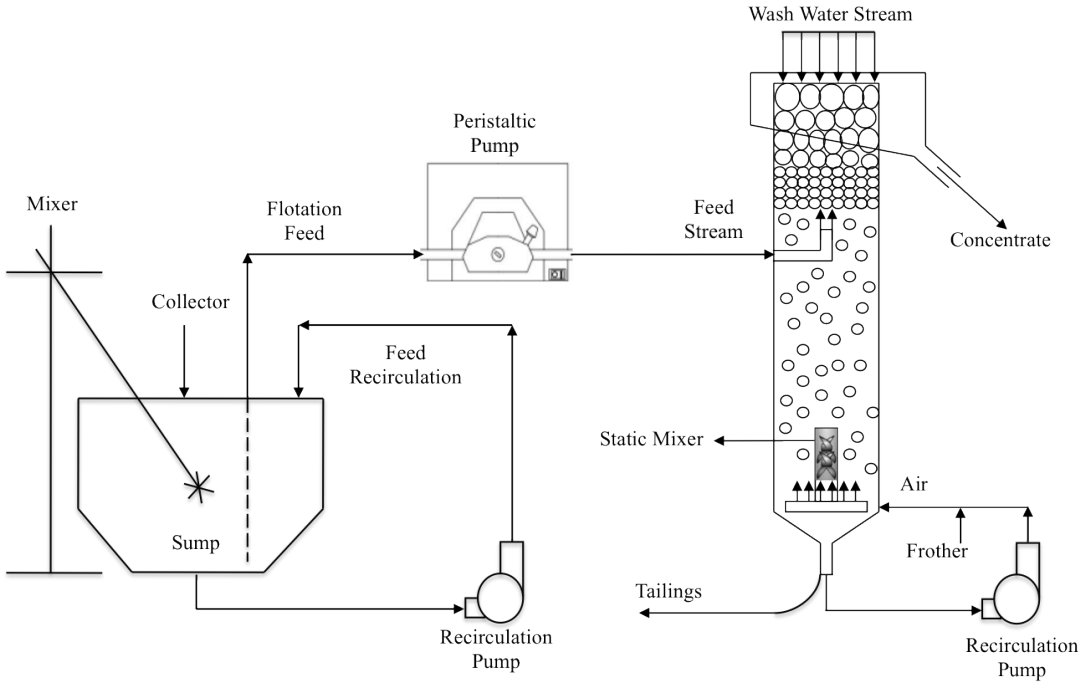


Figure 3.3. Schematic of the laboratory column flotation setup used for the standard testing procedure.

With a column 5 cm column diameter, the flotation column setup provided near plug-flow conditions with the length-to-diameter ratio of around 50:1. The length of the collection and froth zones typically used in the test program were 210 cm and 30 cm, respectively, where the feed slurry inlet was located 45 cm below the overflow lip. Wash water was added in the froth zone at a depth that was 1/3 of the froth zone height below the overflow lip. Frother and air were injected into the recirculation line at the bottom of the column prior to static mixer, which generates conventional-sized bubbles. Collector was added in the sump and conditioned for 15 minutes using the mixer. A constant amount of wash water, which was monitored through a water flowmeter, was used to eliminate the entrainment by minimizing the pulp water from reporting to the froth product.

The feed pre-aeration setup for the laboratory column consisted of a mixer to keep the slurry in suspension and conditioning, a sump which can hold about 40 liters (≈10 gal.), a recirculation pump to direct the slurry flow to go through the cavitation tube and a pressure gage to observe the amount of pressure going into the cavitation tube. Collector was added in the sump and conditioned for 15 minutes prior to initiating the flotation tests. Conditioned feed slurry was then pumped from the sump into a cavitation tube under a pressure of 138 kPa (20 psi) at a volumetric flow rate of 5.7 L/min (1.5 gal/min). The exit stream from the cavitation tube was distributed into two streams. The flow rate of one stream was manipulated to a desired value in the range of 300 to 2000 ml/min and fed into the flotation column. Thus, the majority of the flow was circulated back into the feed sump through a peristaltic pump which was used to draw a pre-determined amount of feed into the flotation column at a point just below the pulp-froth interface as shown in Figure 3.4. As a result, the pretreated coal particles initially move downward in the cell against a rising flow of air bubbles. Upon collision and attachment, the air bubble-particle aggregate rises to the top where they are collected in an overflow launder. The hydrophilic particles remain unattached and flow with the majority of the pulp to the tailings (underflow) stream.

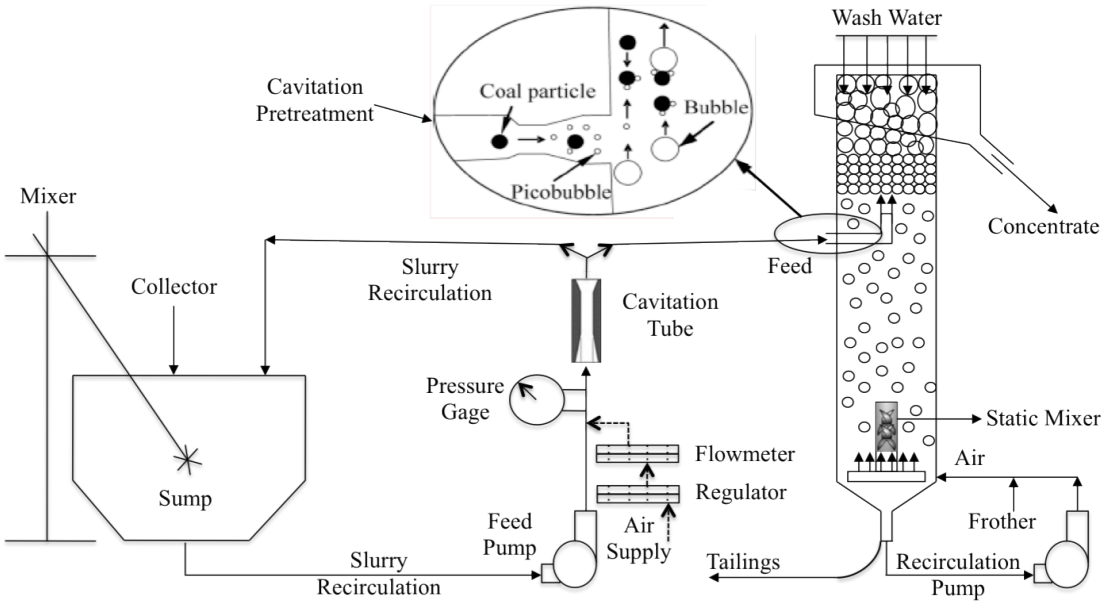


Figure 3.4. Schematic of the laboratory column flotation setup with the cavitation feed pretreatment.

The tailing flow was adjusted with a controllable pinch-valve attached to the tailing pipe. A microprocessor (Love Controls Series 2600) received signals from a pressure transducer located at the bottom of the column. The signal adjusts the air pressure that controls the flow to the tailings pinch valve, which is based on the desired froth level.

A time period of three particle retention times was allowed to achieve steady-state conditions. After reaching the steady-state, samples of the feed, product and tailing streams were collected simultaneously. Afterward, the samples were filtered, dried, weighed and analyzed for the ash content. A summary of the operating parameters used throughout these tests is provided in Table 3.4.

Table 3.4. Operating conditions of the column flotation test program.

Feed rate	300 ml/min to 2000 ml/min
Feed solids concentration by weight	6% for Boone County coal and 8% for Kanawha County coal
Bias factor	0.75
Collector Rate	0.5 kg/t
Frother Rate	30 ppm
Froth depth	30 cm
Superficial gas velocity	2 cm/s
Volumetric wash water	400 ml/min

3.1.5. Laboratory-scale Cavitation Tube

During the conventional and column flotation tests, the slurry was injected through a cavitation tube for feed pre-aeration, which cause small air bubbles to nucleate on the coal surface. Hydrodynamic cavitation, which will be discussed later in detail, occurs whenever the pressure at a point in a liquid is momentarily reduced below its vapor pressure due to the local accelerations of the liquid in a flowing system. For the design of the cavitation tube, three device options were considered, i.e., orifice plate, nozzle and Venturi, which were all capable of producing cavitation at a desired point of the flow.

However, due to their fundamental design differences, they range in their suitability for use in this study. Following advantages made the Venturi design to be chosen as the best option:

1. The gradual reduction and the subsequent gradual expansion reduced the possibility of blockage (plugging) of particles in the throat section,
2. The permanent head loss of the other two options could be as high as 3 to 4 times greater than the Venturi. Very low head loss characteristics of the Venturi design results in a minimal impact on the pump capacity in a plant, and
3. The ability to vary the throat length in the Venturi is also advantageous, which means that the critical pressure can be maintained to allow the expansion of gas nuclei in the fluid.

In the light of these design advantages, the Eriez Flotation Division (USA) engineers developed a Venturi tube, which is the most widely used hydrodynamic cavitation device, to be used for the feed pretreatment of the flotation feed slurry for kinetic and column flotation tests as shown in Figure 3.5. Another Venturi tube design by Australian researchers from CSIRO Energy Technology Division (Hart et al., 2002; 2004) is also provided in Appendix B for more information.

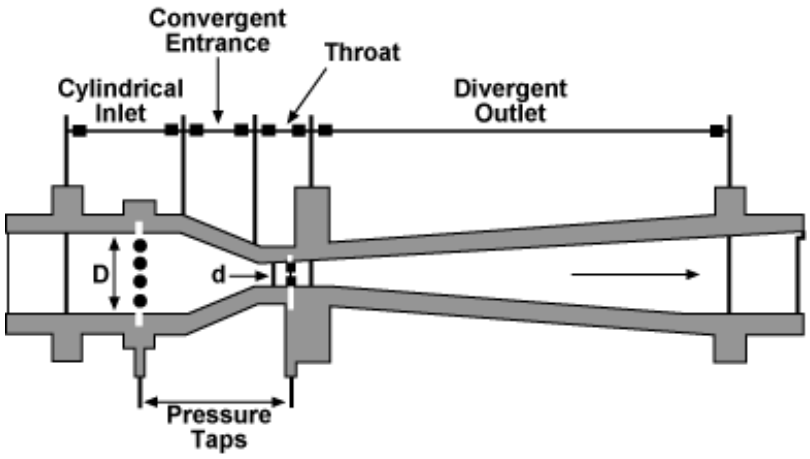


Figure 3.5. Venturi cavitation tube and major design parameters for feed pretreatment.

The laboratory-scale cavitation tube (L=12.7 cm, 5 in.) consists of a gradual contraction from the pipe diameter (D=1.27-cm, 0.5-in.) to the throat diameter (d=0.16-cm, 1/16-in.) and then a gradual expansion to the original pipe diameter. In the conical convergent entrance of the Venturi tube, the liquid flow accelerates due to the narrowing diameter. In the cylindrical throat, the liquid flow is higher in velocity and lower in pressure compared to the liquid flow in the cylindrical inlet which results in cavitation and micro-bubble generation.

3.2. CAVITATION FEED PRETREATMENT – IN-PLANT STUDIES

3.2.1. Sample Characterization

Although it was shown from the laboratory studies that the cavitation feed pretreatment had a significant impact on the flotation characteristics of Coalburg seam coal, the processing of the coal at the preparation plant located in Kanawha County, West Virginia was stopped due to market conditions. The feed to the preparation plant was changed to the Peerless seam coal to produce clean coal for the metallurgical market. The coal was extracted by an underground mine using continuous miners. The flotation characteristic of the Peerless coal was generally considered excellent.

Random feed samples were collected for particle size analysis to assess the variability in flotation feed composition and particle size as shown in Table 3.5. Although there is a good correlation between the weight and ash compositions of the samples, solid concentration in the feed varied somewhat between the tests. The variability in solid concentration implied significant changes in the amount of floatable material in the feed.

Two additional notes of importance were that i) about 70% of the feed was finer than 0.025 mm on average and ii) the ash contents in the same size fraction were around 65% on average. Both facts suggest the presence of a substantial quantity of floatable ultrafine coal particles in the feed. The impact was a greater dependency on retention time to

achieve the desired collection zone recovery and low carrying capacity values. The estimated carrying capacity was projected to be around 0.7 t/h/m^2 (0.07 t/h/ft^2).

Table 3.5. Random feed size analysis of the Peerless coal used during in-plant studies.

Size Analysis (mm)	Feed Sample-1: 9.6% Solids			Feed Sample-2: 9.2% Solids		
	Wt (%)	Ash (%)	Floatable Material (%)	Wt (%)	Ash (%)	Floatable Material (%)
+ 0.15	2.65	1.90	6.13	3.13	2.05	5.74
- 0.15x0.045	13.98	4.13	31.55	19.26	4.60	34.30
- 0.045x0.025	8.05	17.26	17.26	9.97	17.41	15.16
- 0.025	75.32	67.83	46.87	67.64	59.54	48.11
Total	100.00	53.10	53.10	100.00	41.86	100.00

The coal company operating the preparation plant conducted washability analysis and a Hardgrove Grindability Index (HGI) test on feed core hole samples of the Peerless seam at 1.50 S.G. Typical HGI values lie between 30 (increased resistance to pulverization) and 100 (more easily pulverized), which is a measure of coal's resistance to crushing. An HGI value of 49 was obtained for the Peerless coal which indicated that the material is not very easily pulverized. Washability analysis data presented in Table 3.6 indicates that, one quarter of the total sulfur is in the form of pyritic sulfur (0.36%) which is important due to its floatability.

Table 3.6. Proximate analysis of the Peerless seam on dry basis with 7% surface moisture

Proximate Analysis	Dry Basis
Ash (%)	6.2
Volatile Matter (%)	38.4
Fixed Carbon (%)	55.4
Calorie (kcal/kg)	7969
Moisture & Ash Free Calorie (kcal/kg)	8495
Total Sulfur (%)	1.25
- Pyritic Sulfur (%)	0.36
- Sulfate Sulfur (%)	0.01
- Organic Sulfur (%)	0.88

In addition to the feed characterization, incremental samples were collected during a sampling program from the clean coal stream of the StackCells when the preparation plant was treating the Peerless seam. Clean coal samples labeled as No. 1 and 2 were collected incrementally over a 4-hour operating period whereas sample No. 3 was obtained over a 2-hour period. Each sample contained about 13.5 kilograms of material. As shown in Table 3.7, the flotation product quality was consistent over the three sampling periods and very close to the desired value of 7% ash on average.

Table 3.7. Kanawha Eagle preparation plant clean coal proximate analysis for Peerless coal, where AR and DB denote "as received" and "dry basis", respectively.

Proximate Analysis	Sample #1		Sample #2		Sample #3		Composite	
	AR	DB	AR	DB	AR	DB	AR	DB
Ash (%)	6.55	6.89	6.78	7.13	6.9	7.27	6.74	7.10
Sulfur (%)	1.25	1.31	1.27	1.34	1.19	1.25	1.24	1.30
Calorie (kcal/kg)	7505	7890	7521	7910	7455	7857	7494	7886

3.2.2. Full-Scale Cavitation Tube System

In support of the study and in response to the outcome of the laboratory test program, engineers at a major equipment manufacturer (Eriez Manufacturing Co.) developed a full-scale cavitation tube system for the pre-aeration of flotation feed. The unit was installed in an operating preparation plant located in Kanawha County, West Virginia. The cavitation system consisted of four venturi tubes (CT-600) connected to a main pipe, which provides the ability to bypass the entire flow or a portion thereof through the cavitation tube system as shown in Figure 3.6. For the in-plant tests, a 35.5-cm (14-inch) diameter main pipe with a total length of about 3 m (114 inch) was pump-fed into the first StackCell from the feed sump and the cavitation tube system was designed so that it was a direct drop-in placement during the operation. The cavitation tube system was planned to be at knee-high elevation for ease of removal and change-out in the case of bypassing the flow directly into the cell.

The cavitation tube system was designed to allow the system to be added into the operation without alterations to the existing flotation circuit. Four 15.2-cm (6-inch) knife gate valves were placed at knee-high elevation for ease of turning on and off the cavitation tube system (Figure 3.6). The throat (thinnest portion) of the 61 cm (24inch) cavitation tubes were designed to handle the flotation feed slurry without plugging with an 80 mm (3.15 inch) diameter opening. Each cavitation tube line is also equipped with two pressure gages, i.e., one on the inlet and one on the exit side of the tube, to measure the required pressure drop (or back pressure), which depends on the pipe diameter, pump capacity, volumetric flow rate and aeration rate. A detailed design of the cavitation tube system including the knife-gate valves, pressure gauges and air inlet manifolds is shown in Figure B-1.

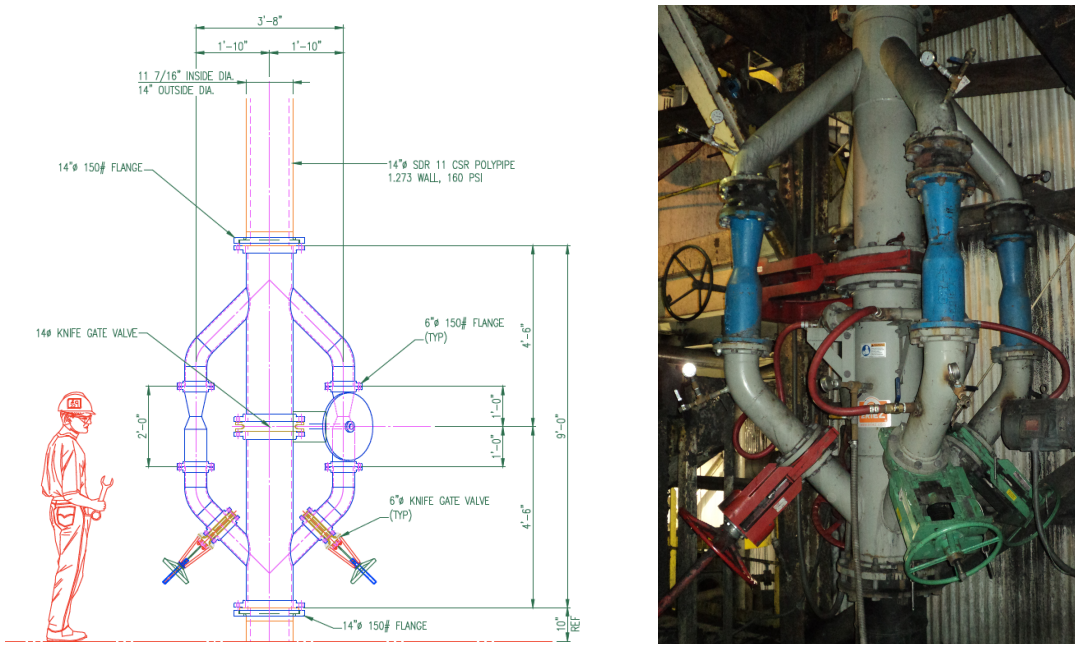


Figure 3.6. Plan view and the plant installation of the cavitation tube system for flotation feed pretreatment.

The cavitation tube system required a minimum of 172-kPa (25-psig) inlet pressure for proper aeration and bubble generation. To provide the required pressure, feeding the flotation material from a sump through a pump to the first StackCell was required. In addition to the minimum 25-psig pressure for aeration, the pump provided sufficient head to handle the static head and in-line losses during the travel of the flow from the sump to the cavitation tube at the feed inlet. As such, a flotation feed sump and a centrifugal pump system was added to the existing StackCell flotation circuit.

Air was added to the cavitation system in some tests using a portable compressor, which was maintained at around 1.4-1.55 m^3/min (50-55 ft^3/min). Airflow was adjusted both using the regulator on the air control assembly and by opening and closing the ball valves on each cavitation tube. When air was employed with the cavitation tests, pressure on the air control assembly was varied through a regulator, which was maintained around 345 kPa (50 psi) or higher than 310 kPa (45 psi) in order to overcome the line pressure existing prior to the cavitation tubes. Air addition prior to the cavitation tubes provided an additional 35-kPa (5-psi) increase to the inlet pressure (reading before the cavitation tubes). However, the outlet pressure (reading after the cavitation tube) did not change noticeably. Thus, the differential pressure drop (or back pressure) increased in the presence of additional air.

Airflow readings were monitored from the PLC screen of the vortex flow meter, as shown in Figure 3.7. Operation density was adjusted based on the line pressure and the temperature at the air control assembly, which was taken through an infrared thermometer. In addition to airflow, pressure and temperature readings, air velocity, frequency and current output (4-20 mA) values were gathered from the flowmeter.

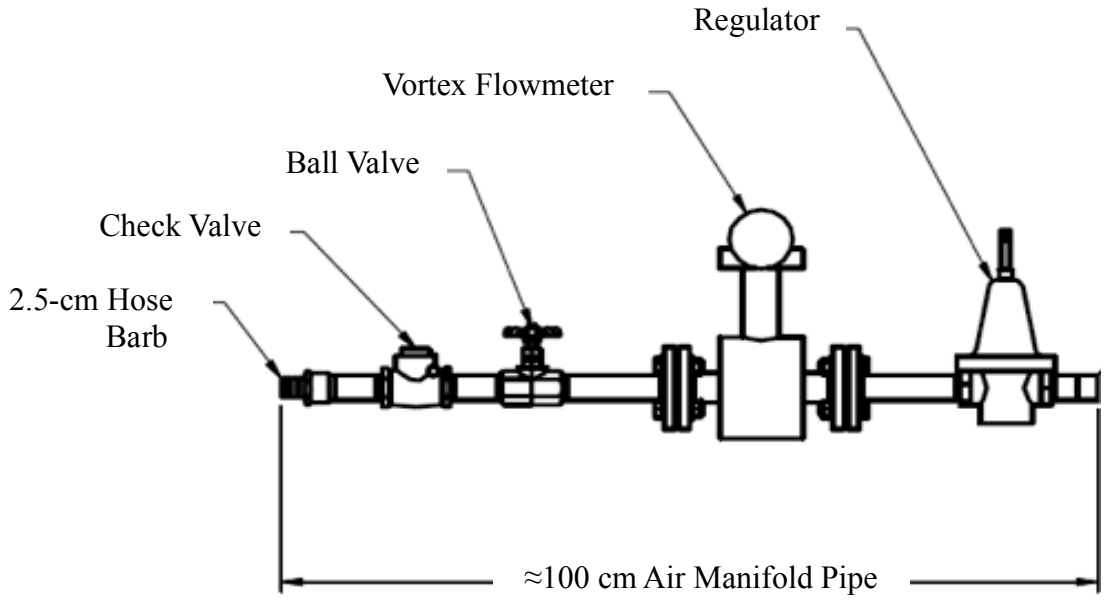


Figure 3.7. Schematic view of the air manifold control the airflow prior to the cavitation tube system.

After installing a Doppler flow meter placed on the Poly pipe that feeds the first StackCell, it was found that the cavitation tube system was designed to handle about two times the flow that was actually reporting to the StackCell circuit. To properly operate the cavitation system with the required pressure drop (inlet and outlet pressure differential), two of the cavitation tubes located across from each other were completely closed**.** As a result, the pressure drop increased from about 70 kPa (≈10psi) to 140 kPa (≈20psi) on each cavitation tube. During the tests using cavitation system, both cavitation tubes were fully opened to achieve about 50% sump level with makeup water level around 25%-30%. However, for tests using air injection into the cavitation system, the center pipe was partially opened (~9 cm) to achieve the feed sump level needed for proper plant operation. It should also be noted that the air addition to the cavitation system was relatively low, i.e. 1.4-1.55 m^3/min (50-55 ft^3/min). In fact, the 2% (Karaman et al., 1996) to 2.5% (Craig et al., 1993) dissolved air already existing within the slurry medium was found to be sufficient to provide a substantial improvement in flotation recovery. The typical operating conditions used for the cavitation system are shown in Table 3.8.

Table 3.8. Operating parameters for the cavitation tube system during the in-plant testing.

Air Flow	~1415 L/min
Air Pressure	~50 psi (345 kPa)
Air Velocity	10 m/s
Temperature	~21 C°
With Cavitation & No Air (Both fully open)	In: 303 kPa Out: 131 kPa
With Cavitation & With Air (Both fully open+~9 cm from center pipe)	In: 310 kPa Out: 138 kPa
Compressor Pressure	827 kPa-Max./620 kPa-W/Air

3.2.3. StackCell Flotation Unit

During the operation of the StackCell, feed slurry enters the separator through a bottom-fed nozzle, where low-pressure air is added through an air manifold, as shown in a "see-through" illustration of a single StackCell machine Figure 3.8. In addition to the installed cavitation tube system prior to the feed of the first StackCell, the slurry is also pre-aerated inside the machine through a sparging device to provide significant shear and bubble-particle contact prior to the arrival into the separation chamber. In fact, all of the necessary bubble-particle contacting is designed to take place in the cavitation tube system prior to injection into the primary tank (feed to first StackCell), which is used only for the phase separation between the pulp and the froth. Thus, the bubble and particle attachment occurs in close proximity to the aeration device in this system, and results in an increase in the rate of reaction for the overall process. As a result there is a corresponding decrease in the required retention time for a given application. This indicates that the same flotation recovery can be obtained in a smaller volume with increased capacity (Kohmuench et al., 2010; Kohmuench and Norrgran, 2011).

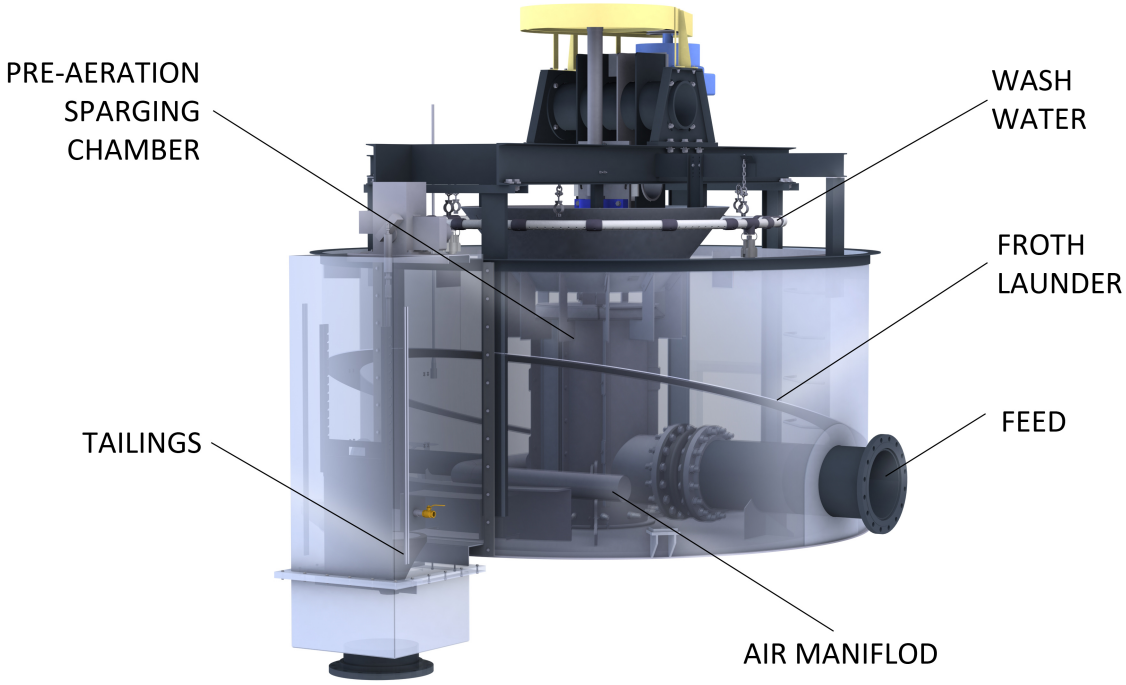


Figure 3.8. A "see-through" 3-D illustration of the StackCell module with major components of the machine.

The flotation circuit in the Kanawha County, West Virginia preparation plant uses a series of three StackCells in a rougher-scavenger-rescavenger arrangement in order to take advantage of improved mixing conditions, and thus, provide a balance between improving recovery due to less back mixing and the added cost of the new cell, as shown in Figure 3.9. The feed is injection through the in-line cavitation system as a flow rate of 11000 L/min. The mass solids flow rate was around 60 t/h with some variations occurring throughout the test program as indicated by changes in the solids concentration. The layout of the StackCell circuit in the preparation plant and the corresponding material and volume balance for slurry and solids flows and concentrations, pulp densities and delivery pressures for wash water units are also shown in Figure A-1 and Table A-1 respectively.

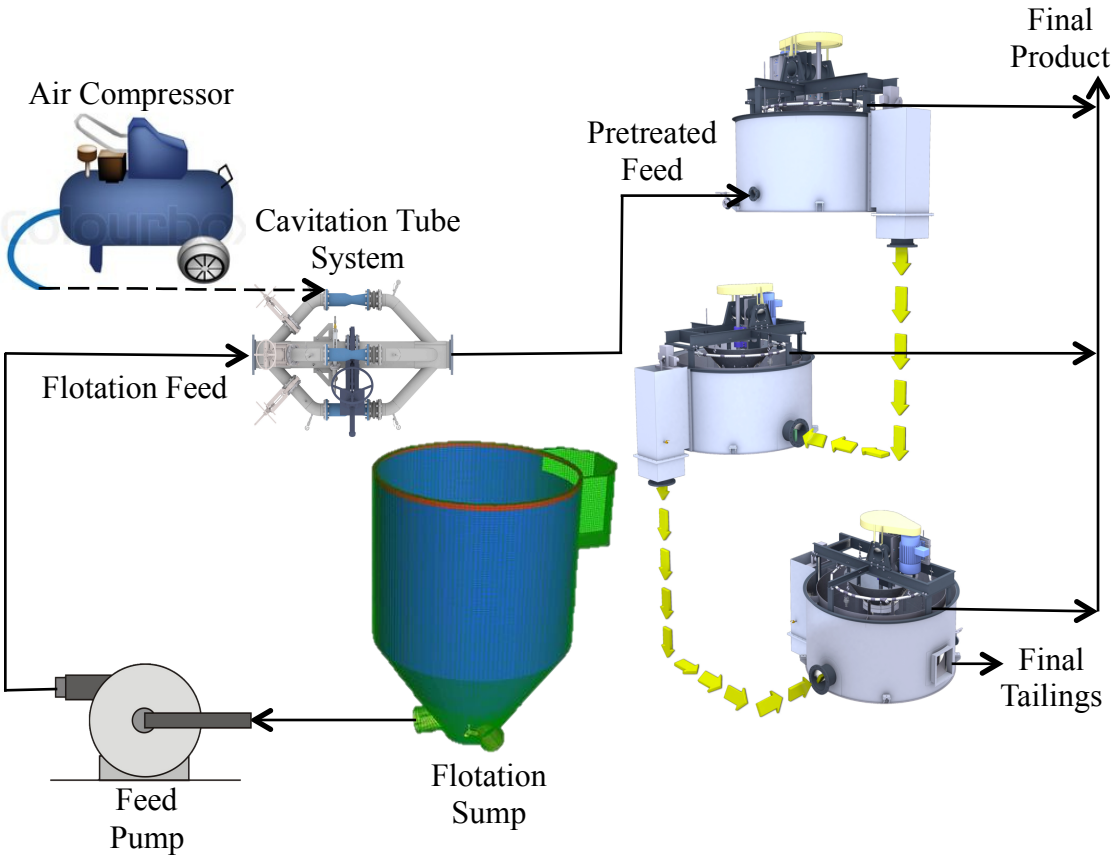


Figure 3.9. Flotation circuit flowsheet of the preparation plant, including a three-stage StackCell unit and a cavitation tube system with the option of air addition.

3.3. MAGNETIC PLASTIC MATERIAL EVALUATION

3.3.1. Sample Characterization

3.3.1.1. Coal Samples

Encouraging results were obtained in a previous study on the use of magnetic plastic material to enhance flotation recovery. One of the objectives of this study was to validate the previous findings and advance the fundamental understanding of the mechanisms involved. In this effort, run-of-mine coal samples from the Coalburg and Eagle seams were collected in bulk and used in the flotation test after crushing and grinding. The Coalburg coal is ideal for this study due to its poor flotation characteristics and relatively

high content of middling (mixed-phase) particles (10% to 20%). Eagle seam, on the other hand, has excellent floatability which produces coal for the metallurgical market.

The bulk sample was collected in 19-liter (5-gal.) buckets from the top deck of a deslime screen in increments of 30 minutes and placed into into four 208-liters (55-gal.) drums. The top size of the particle was 75 mm (3-inches). The operating plant was located in Kanawha County, West Virginia. After arrival at the laboratory, representative coal samples were crushed with a jaw crusher to obtain 100% passing 1.27 cm (1/2-inch). Afterwards, the samples were split using the "cone and quarter" method. Coal samples of around 1-kg (~ 2.2 lbs.) were placed in sealed plastic bags after removing the excess air and stored in a commercial chest freezer to prevent contamination and prolonged exposure to air. Coal samples were pulverized to minus 180μm (80 Mesh) using a laboratory hammer mill just prior to the flotation test to prevent oxidation of the coal surfaces.

Two bags of representative coal samples were taken from the freezer and pulverized to below 180 μm. The samples were subjected to size analysis from which the data is provided in Table 3.9. The data suggests that the particle size distributions generated by the process were relatively equal as well as the ash contents for the Coalburg coal. The overall feed ash content was around 44.43% which indicates the presence of a significant amount of floatable material. The relatively large amount of material coarser than 150 microns is especially noteworthy given the emphasis of this concept to improve coarse coal recovery. Eagle coal sample had lower amount of coarser particles (+150 microns) after crushing compared to that of the Coalburg coal. In addition, ash contents of each size fraction was higher than Coalburg coal which resulted in about 15% higher feed ash contents.

Table 3.9. Incremental particle size distribution and quality characteristics of a preparation plant flotation feed from Coalburg and Eagle seams.

Particle Size Fraction (μm)	Coalburg Coal-1		Coalburg Coal-2		Eagle (Met.) Coal	
	Weight	Ash Content	Weight	Ash Content	Weight	Ash Content
+ 150	18.52	36.36	22.26	36.57	10.76	44.18
- 150x75	24.13	33.00	25.71	36.32	20.34	41.12
- 75x45	11.58	33.59	12.35	37.15	11.42	42.23
- 45x25	11.22	41.27	8.90	41.98	10.24	53.79
- 25	34.56	60.65	30.77	61.37	47.24	75.70
Total	100.00	44.17	100.00	44.69	100.00	59.21

3.3.1.2. Magnetic Plastic Material

Eriez Manufacturing Company currently produces a plastic product, i.e., PolyMag™ Black Pellet (PMBP), which is composed of about 70% magnetite (black iron oxide-Fe_3O_4) and 30% ethylene/ethyl acrylate (EEA). The presence of magnetite in the material provided the ability to recover the plastic particles using a magnetic separator. EEA coating material is a copolymer resin, which consists of ethylene (the simplest alkene) and ethyl acrylate monomers (ester of ethanol and acrylic acid), and is used in the preparation of many polymers. The chemical structure of the material is shown in Figure 3.10.

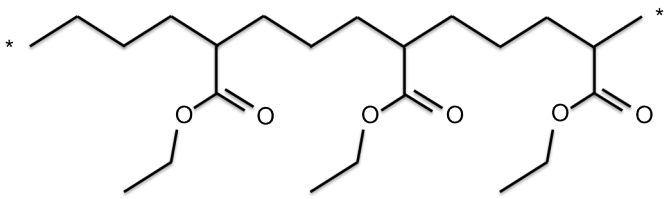


Figure 3.10. Chemical structure of ethylene/ethyl acrylate (EEA) copolymer.

EEA copolymer demonstrates excellent blend compatibility to be used as a bonding layer between polyolefins and for a variety of polar substrates, such as metals, or magnetite in the case of PMBP, to form high strength co-polymer (HSCP) granular particles or pellets (Fire, 1995). Detailed information about the composition of EEA is given in Table 3.10.

Table 3.10. Information about the EEA plastic coating material used to form PMBP.

Chemical Name	Ethylene/Ethyl Acrylate (EEA)
Description	CAS#9010-86-0
Molecular Formula	$C_{21}H_{36}O_6X_2$
Molecular Weight	384.51
Density	0.93 g/ml (at 25 °C)

In literature, other magnetite polymers, i.e., PolyMAG-41/1 and CombiMAG, have also been used in a nanoparticle form to deliver nucleic acids in the cell structure, which were developed by Chemicell GmbH (Berlin, Germany). In this application, polyethylene imines, i.e., PEI, (CAS#: 9002-98-6) are used in the cell culture of weakly anchoring cells as an attachment promoter (Mykhaylyk et al., 2007).

Surface characterization of the magnetic plastic material was performed using a scan electrode image machine, i.e., scanning electron microscope (SEM), at 500μm optical resolution. Figure 3.11 apparently shows a narrow particle size distribution with a granular, irregular and porous surface. However, some of the large particles have distinct, circular/elliptical shapes. Regardless of the size and shape of the magnetic particles, they seem to be well coated with the EEA copolymer resin even after being pulverized in the hammer mill. Compared to that of the PMBP, significantly less coating material was used for PolyMAG-41/1 and CombiMAG nanoparticles, which was 7% and 18%, respectively, based on the PEI/magnetite ratio. However, according to the TEM (Transmission Electron Microscopy) images, PEI coated magnetic nanoparticles showed roughly spherical or ellipsoidal shape cores with some irregularities, which suggests similar observations with the SEM images in Figure 3.11 (Mykhaylyk et al. (2007).

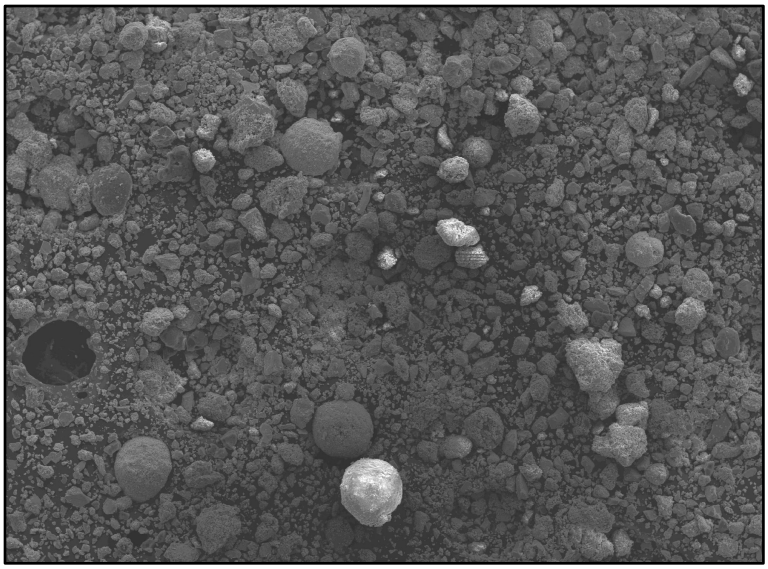


Figure 3.11. SEM image of the pulverized magnetic plastic material (minus 180 μm) at 500 μm optical resolution (Munoz-Diaz, 2007).

The magnetic plastic material, i.e., PMPB, was received as dry pellets with a particle size of 100% minus 6.35 mm (1/4 inch). A representative sample of 200 gr with a nominal size of around 1.7 mm (10 Mesh) was collected and pulverized in a laboratory hammer mill using 180μm screen to obtain the same size material as the coal samples for the flotation test program. The particle size distribution in Table 3.11 shows that very little material existed in the ultrafine size range (minus 25 microns) which minimizes the effect of coating coal particles as a mechanism to enhance surface hydrophobicity.

The naturally hydrophobic magnetic plastic material is comprised of about 70% magnetite, which makes it naturally magnetic and thus recoverable by low intensity magnetic separators. The magnetic strength of the magnetic plastic material was evaluated by using a Davis tube at full magnetic strength of 4000 Gauss. The results showed that 96% of the total sample reported to the magnetite stream, which indicates a high magnetic strength for the plastic material (Munoz-Diaz, 2007).

Table 3.11. Size analysis of the magnetic plastic material after being pulverized in the laboratory hammer mill.

Size Fraction (μm)	Individual Wt. (%)	Cumulative Wt. (%)
+150	47.02	47.02
150x75	32.31	79.33
75x45	12.35	91.68
45x25	5.82	97.50
-25	2.50	100.00
Total	100.00	

The magnetic plastic material was recovered from the flotation slurry samples using a laboratory-scale, high-intensity wet magnetic separator (HIWMS, Series-L, Model-4) from Eriez Manufacturing Co. as shown in Figure 3.12. During the operation, a magnetic field is generated at the center of the separator where a chamber with the highest concentration of the magnetic field is located. The chamber is connected to two stainless-steel pipes on the top and on the bottom to let the flotation slurry pass through the system by gravity. The removable magnetic element box in the chamber contains interchangeable magnetic elements in a form of expanded stainless-steel sheets (medium grid, 18 gauge, 6 mm) for the recovery of the magnetic particles (Figure 3.12.)

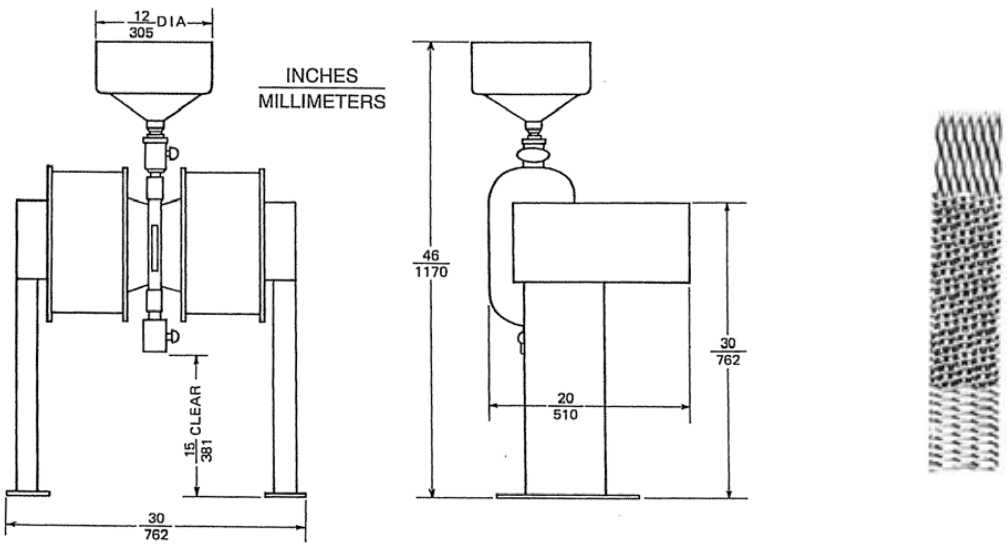


Figure 3.12. Layout schematic of the laboratory magnetic separator with a front and a side view and a picture of the steel grid member located inside the chamber for the recovery of magnetic particles.

When the flotation slurry containing the plastic particles passes through the magnetic separator, the plastic particles become attached to the perforated metallic plates located inside the chamber by the magnetic gradient fields while the non-magnetic coal particles follow the liquid streamlines and report to the bucket blow the chamber as shown in Figure 3.13. After the recycling process, water is flushed through the magnetic separator in order to make sure that all of the particles in the feed have passed through the chamber and only magnetic particles are attached to the metallic plates. After capturing the magnetic plastic particles in the chamber, the magnetic field is turned off and water is flushed into the chamber to recover the magnetic plastic particles.

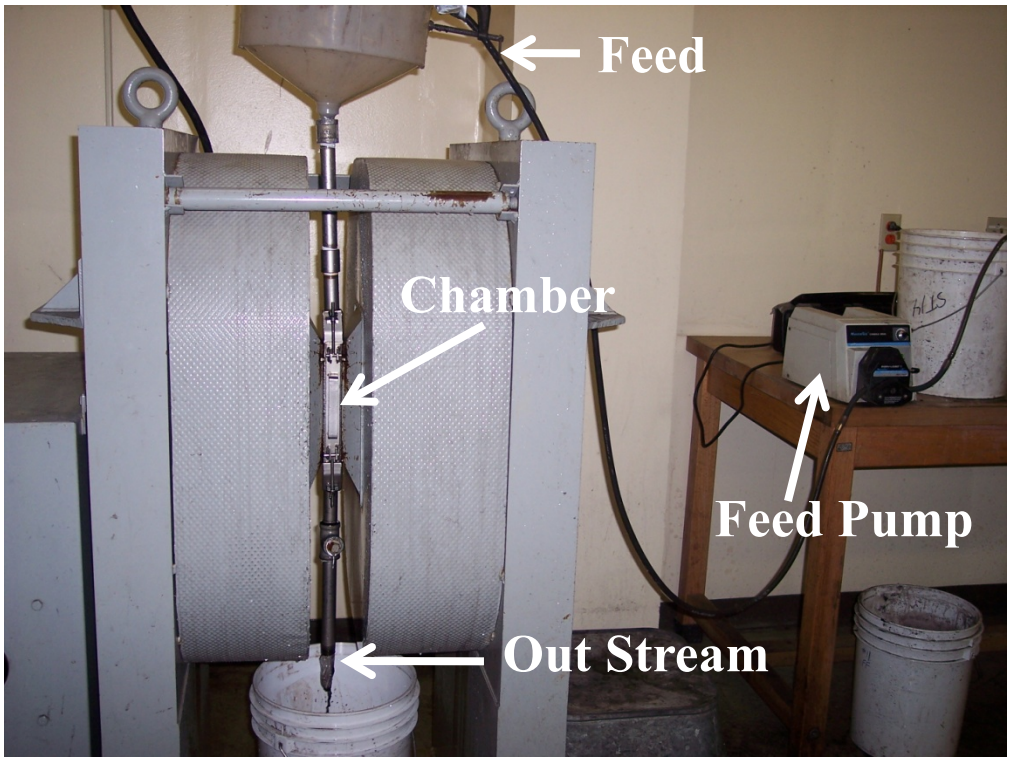


Figure 3.13. Laboratory setup of the magnetic separator showing the chamber and the components of the recycling process.

The magnetic plastic recovery process was repeated three times for each sample to ensure near 100% recovery of the magnetic particles. The average magnetic particle recovery values achieved in each step of the recovery process was reported in the previous study (Munoz-Diaz, 2007) and the recent study are shown in Table 3.12.

Table 3.12. Magnetic material recovery rates in different stages of recycling after rate tests.

Test Identification	1st Recycle	2nd Recycle	3rd Recycle
Munoz-Diaz, (2007)	87.6%	96.1%	99.9%
Current Research	87.0%	94.7%	99.6%

3.3.1.3. Grinding and Polishing Process

Clean coal samples were collected in large chunks from the top deck of the clean coal screens. The particle size was reduced in the laboratory to obtain approximately 1 cm x 1 cm x 0.5 cm-sized cubes which were used for contact angle measurements. A long-cure epoxy kit (#812-523-HAZ) was used from LECO Corp. that contains both a liquid resin and a hardener to securely mount the samples in phenolic ring molds (3.8-mm diameter–#811-229) for the grinding and polishing process. Seven parts of liquid resin was mixed with 1 part hardener in a paper cup and poured on the coal samples which were placed in the ring molds that were mounted on a wax paper with a glue stick. After 4 hours of curing in the room temperature, sample ID stickers were placed in each ring mold and filled using the same mixing procedure of the resin and the hardener for half of the amount. Ring molds were then cured for 4 to 8 hours (or left for overnight) and later the mounted specimens were ground and polished using Buehler Euromet-I Power Head machine.

At the beginning of the grinding process, the cured ring molds were removed from the wax paper and placed, secured and leveled in the specimen holders, which apply a central force (constant pressure) to ensure consistent grinding and polishing on the surface of the ring molds. During the grinding and polishing process, water was continuously poured on the rotating disc to remove impurities and grinded material. In the first step for initial grinding, a diamond-impregnated disc (10μm) was used for 4 minutes at around 200-250 rpm. In the second step, a silicon carbide paper (25μm) was used for 4 minutes at around 200-250 rpm. In the third step, TexMet®-C Micro cloth surface was used after wetting the surface with water. In addition to cleaning the surfaces with water, 1μm aluminum oxide slurry (Alpha C Alumina-#810-818) was used for 90 seconds at the beginning of the final grinding process at 40psi (at around 200-250 rpm) with low water spray. Subsequently, water was flushed for 30 seconds to remove all impurities associated with the aluminum oxide slurry. Next, 0.3μm aluminum oxide slurry (Alpha A Alumina-#810-832) was used for the next 90 seconds with reduced pressure of 30psi, which is followed by flushing water for the next 30 seconds to finalize the grinding process. For all three

steps, the water flow was increased in the last 30 seconds for a thorough cleaning of the surfaces.

In the polishing process, Imperial cloth (#810-546-010) was used with 0.05μm colloidal silica slurry (#812-121-300). Similar to the Micro cloth, Imperial cloth was also used after wetting the surface with hand while flushing water. Polishing process was started at 30psi (at around 200-250 rpm) for 90 seconds, and then the pressure was decreased to 20psi for the next 60 seconds. The polishing disc was flushed with water for the following 30 seconds to remove any adhering colloidal silica. To further eliminate the remaining silica residue on the surfaces, clear household ammonia was poured on the polishing disc for 30 seconds. For the last 30 seconds of the polishing process, water flow was increased for a thorough cleaning of the surfaces. At the end of this process, air was gently blown on the surfaces to get rid of the remaining droplets to eliminate the watermarks. Afterward, the polished surfaces were dried for the next hour in the drying owen. The specimens were quickly transferred to the goniometer for contact angle measurements. Latex gloves were used throughout the experiments to avoid contamination of the surfaces. As grinding and polishing processes can have drastic effects on the contact angle value, both procedures were kept constant for all ring molds to ensure the integrity of the measurements.

3.3.1.4. Contact Angle Analysis

As discussed previously, particle size and hydrophobicity have significant effects on froth flotation. The contact angle at the solid-liquid-vapor interface is generally used to evaluate the hydrophobicity of a solid surface. A good knowledge of particle contact angles is important in defining the role of particle size, since there is a critical contact angle above which flotation response is strong for particles of a particular size (Crawford and Ralston, 1988; Kitchener, 1992). As previously reported in Eq. (2.44), contact angle is an important parameter to establish the probability of detachment and the maximum particle size that can be floated.

Contact angle measurements were conducted using a goniometer (Rame-Hart Model 100-00) with two rotatable cross hairs. The setup consists of a goniometer, a specimen stage and a variable intensity illuminator which were mounted on an optical bench as shown in Figure 3.14.

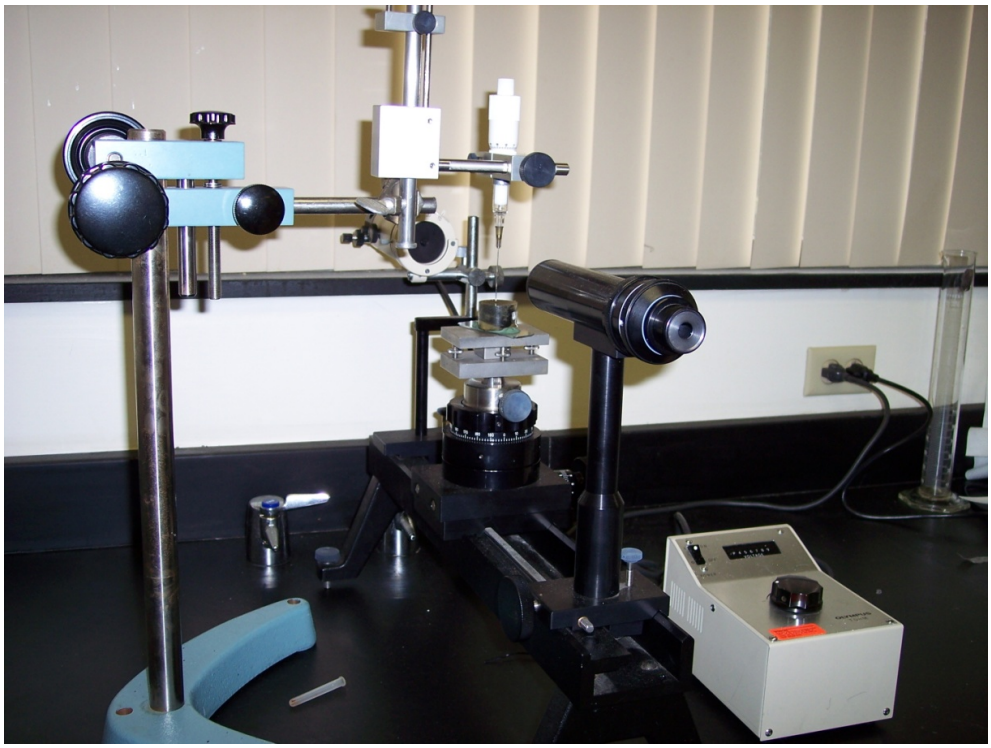


Figure 3.14. Goniometer setup in the laboratory to determine the contact angles.

The contact angles of coal and magnetic plastic particles were measured with distilled water at neutral pH using a calibrated syringe. The equilibrium contact angle of the liquid droplet was measured for both right and left sides in three different positions. All measurements were conducted at the room temperature (25° ± 2° C) with a standard deviation of ± 3^{o} for a single contact angle. Contact angle measurements show a close correlation between the previous and the recent study for the magnetic plastic surfaces, which clearly indicate that they are much more hydrophobic than any of the coal surfaces, as shown in Table 3.13.

Table 3.13. Contact angle measurements of coal and magnetic plastic particles using distilled water and methylene iodide, where the asterisk (*) represents the measurement from the previous study.

Sample (Contact Angles, Degrees)	Distilled Water	
	(Left)	(Right)
Pittsburgh No. 8 Coal*	54.6	55.3
Magnetic Plastic*	81.7	84.4
Magnetic Plastic	85.6	87.3
Coalburg Coal	47.0	47.6
Peerless Coal	58.4	59.0
Eagle Coal	59.8	60.1

3.3.1.5. Zeta Potential Measurements

In an aqueous solution, one of the most important forces favoring stability is the electrostatic repulsion force. When a charged particle is placed in an electrical field, it will move toward an electrode of opposite sign. During the particle transport process, the counter ions that form a rigid layer around the surface will remain with the particle while counter ions that are loosely attached will be lost to the bulk. As a result, a shear plane exists at the solid surface at a distance of say delta (Δ) into the bulk. The potential at this shear plane is called the zeta (ζ) potential or electro-kinetic potential. Electrostatic repulsion between two particles occurs as a result of an electrostatic surface charge of same sign. The magnitude of the repulsion force depends on the zeta (ζ) potential, the ionic strength of the medium and the distance between the particles. Zeta potential is commonly used as an estimate of the surface potential (ψ_o) in colloid chemistry studies where low electrolyte concentrations are used.

The surface charge of the coal and magnetic plastic particles were studied after pulverizing and wet screening to a particle size below 25μm (500 Mesh) using a Brookhaven ZetaPlus system as shown in Figure 3.15. The procedure consisted of preparing 4 liters of potassium chloride (KCl) solution with double distilled water at 10^{-3}

M concentration for the entire set of tests. Six beakers of solution were prepared for each solid type while adding 0.1 grams of solid into a 50 ml potassium chloride solution (10^{-3} M concentration). In addition, hydrochloric acid (HCl) and sodium hydroxide (NaOH) solutions were prepared at 3.25 M and 1.73 M concentration, respectively, to adjust the potassium chloride solution pH values within the range of 2 to 12. Solutions containing solid particles with varying pH values were agitated to ensure the solid dispersion in the beakers and were left to reach an equilibrium pH for approximately 24 hours.

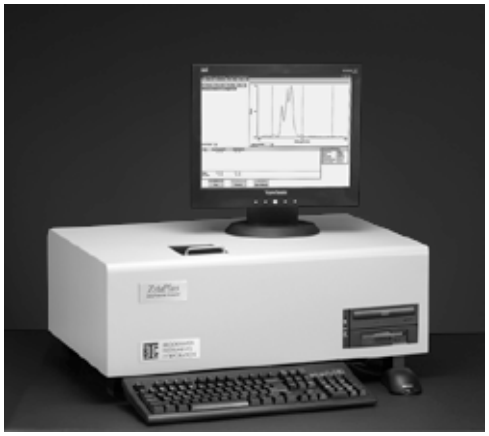


Figure 3.15. Brookhaven ZetaPlus analyzer used during the surface charge tests.

Following the solution preparation, representative samples (1.5 ml) were taken from each beaker and analyzed by using the Brookhaven ZetaPlus system. An average value of 10 measurements was taken for each solid type to achieve a range of zeta potential values with varying surface charges based on slurry pH as shown in Figure 3.16. Similar to the contact angle analysis, zeta-potentials of the magnetic plastic and Coalburg coal particles also showed a close correlation. In addition to measuring the magnitude of electrostatic repulsion and attraction between the particles through Zeta potential analysis, Fan (2008) also quantified the surface charge of the bubbles generated by a cavitation tube.

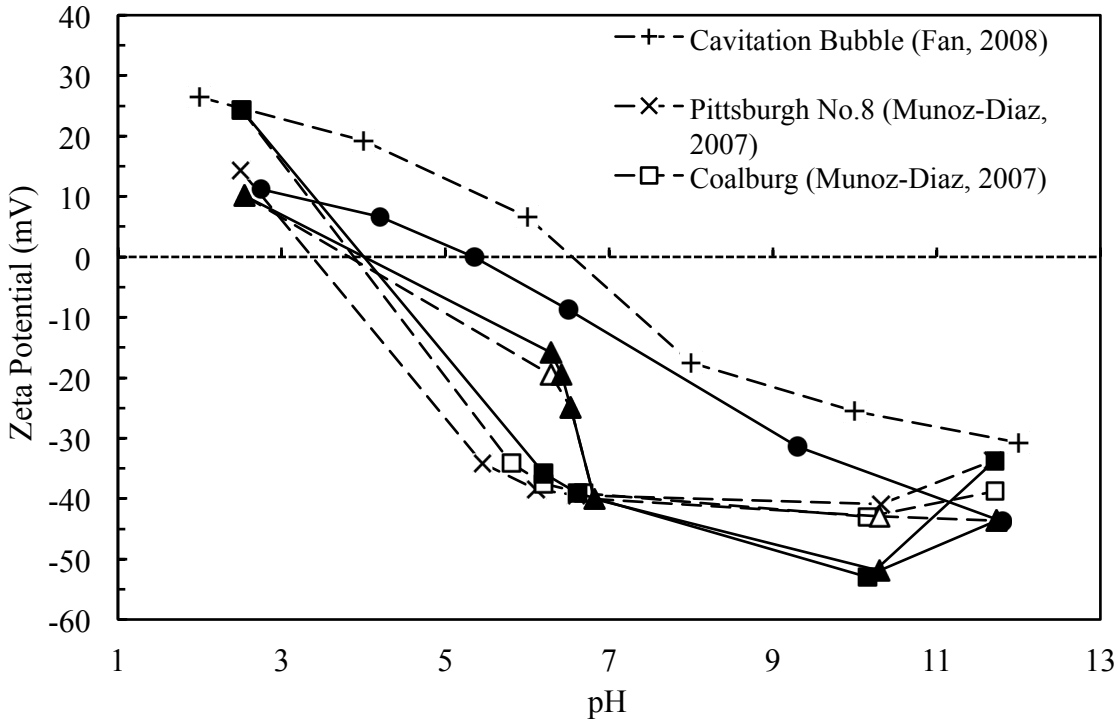


Figure 3.16. Zeta potential as a function of pH for cavitation bubbles and coal and magnetic plastic particles.

Other than the cavitation bubble and the Peerless coal, the surface charges were all negative for any pH measurements greater than about 3. Among all the samples, the Peerless coal gave the highest isoelectric point (or point of zero charge) at around pH 5.35, which is an indicative of good floatability since the best flotation takes place around neutral pH (≈7) conditions. The Zeta potential of the cavitation bubbles decreased through increased pH values with an isoelectric point at pH 6.7.

3.3.2. Release Analysis Test

Release analysis tests were conducted as part of the sample characterization for the Coalburg coal in the same manner as described in Section 3.1.2. However, coarse and dry coal samples were pulverized to a particle size finer than 180 μm (80 Mesh) for the tests involving the magnetic particle evaluation. Later, pulverized coal particles were mixed with water to obtain the desired solids concentration for conventional and column flotation tests.

3.3.3. Flotation Rate Test

Flotation rate tests were conducted with and without the addition of magnetic plastic material using the Coalburg coal sample in the same manner as described in Section 3.1.3. The solid concentration in the 4.3 L flotation cell was maintained at 5% by weight. Thus, the amount of magnetic plastic particles added at different concentrations (2%, 5% or 10% by weight) was subtracted from the total amount of solids (215 grams) which varied the amount of coal particles in the cell depending on the magnetic plastic concentration. Flotation rate tests were conducted as a function of time and the collected samples were separated from the magnetic plastic particles following the procedure described in Section 3.2.1.2. Afterwards, the floated coal fractions and the remaining tailings were filtered, dried and weighed and subsequently analyzed for ash content.

3.3.4. Column Flotation Test

Laboratory column flotation tests were performed to further investigate the empirical data obtained from conventional flotation tests. Experiments were conducted over a range of feed solid concentrations to establish the carrying-capacity limits associated with the addition of magnetic plastic particles to the slurry. At a given solid concentration, a range of volumetric feed flow rates were evaluated to provide the necessary information for the development of the recovery versus product ash curve. Representative samples from each stream were collected and processed through the magnetic separator to remove the magnetic plastic material and the non-magnetic portions of the samples were analyzed for ash content. The specific column operating parameters are provided in Table 3.14 while the other parameter values were maintained at the same levels listed in Table 3.4.

A baseline performance was established for the column flotation tests by conducting tests without the use of the magnetic plastic material. Afterward, a series of tests were conducted to study the impact of various amounts of plastic particles added directly into the feed slurry.

Table 3.14. Specific parameter values used for the magnetic plastic addition effects on column flotation performance.

Feed rate	300 ml/min to 1200 ml/min
Feed solids concentration by weight	2% to 16%
Percent of Plastic Added Relative to Feed	5%-10%
Frother concentration (MIBC)	30 ppm
Collector concentration (Fuel oil No. 2)	0.5 kg/ton

CHAPTER 4

4. FEED PRE-AERATION USING CAVITATION - LABORATORY STUDIES

4.1. INTRODUCTION

In this study, the concept of feed pre-aeration using a cavitation system was evaluated, which has been shown to enhance flotation recovery from the previous studies. Laboratory studies were performed to evaluate the impact of nucleating submicron-size bubbles onto the coal surfaces of varying flotation characteristics which results in the pre-aeration of the flotation feed. For the weakly hydrophobic particles, especially, increasing the flotation rate and thus elevating recovery were the main focus through cavitation feed pretreatment.

Cavitation pretreatment has previously studied by Ofori and Firth (1998) as a bubble generation mechanism through a vertical jet mixer ejector. Upon the bubble formation with the air addition into the jet ejector chamber, bubble-particle contact and attachment were realized during the passage of an in-line mixer. For the proposed concept in this study, however, cavitation mechanism was utilized for the feed pre-aeration based on the hydrodynamic cavitation principles which are detailed in the following subsections.

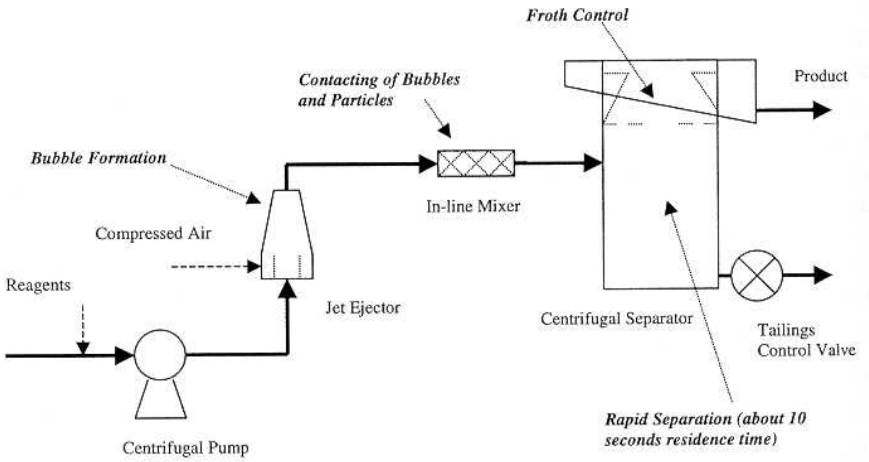


Figure 4.1. TurboFlotation flotation system developed by CSIRO for Australian coal recovery (Firth, 1998).

4.1.1. The Cavitation Phenomenon

4.1.1.1. Discovery

During the trials of the torpedo boat destroyer HMS *Daring* in 1893, the performance of a ship was found to be well below her design speed. Barnaby (1897) and Parsons (1897) discovered that the reduced speed was caused by the poor propeller performance caused by the formation of water vapor bubbles on the blades, which caused similar difficulties for first turbine ship *Turbinia* shortly afterwards (Parsons, 1906). Barnaby and Thornycroft (1895) described this phenomenon and pointed out that the propellers generated voids and clouds of bubbles when the lowest pressure around the blade dropped to a particular value. This phenomenon appeared to manifest itself when the mean negative pressure exceeded 0.46 atm (6 ¾ psi), which was termed as *cavitation* for the first time by R.E. Froude (Barnaby and Thornycroft, 1895).

4.1.1.2. Definition

The term cavitation comes from the Latin word *cavus*, which means a hollow space or a cavity. The formation or birth of cavities is regarded as the first stage of cavitation, which was defined as *nucleation* by Westwater (1964). Cavitation refers, first, to the formation and growth, and then, the collapse and rebound of tiny bubbles, or holes, in liquids filled with gas and/or vapor. These tiny-size gas-filled cavities are often referred to as microbubbles, nanobubbles or picobubbles depending on their size (Robertson, 1969; Zhou, 1996; Young, 1999; Yang et al., 2003; Tao, 2004; Tao et al., 2006; Hampton and Nguyen, 2009).

Cavitation is a general fluid mechanics phenomenon, which can occur whenever a liquid used in a machine inducing pressure and velocity fluctuations in the fluid (e.g. pumps, turbines, propellers, bearings, even the heart and knee joints). When cavitation occurs the liquid changes its phase into vapor at certain flow region, where local pressure is very low due to the high local velocities. This can be explained by Bernoulli's equation:

$$P_B + \frac{1}{2}\rho_l V_B^2 = C \tag{4.1}$$

in which V_B is the water flow velocity at a point where the pressure is P_B, ρ_l is the liquid density and C is constant.

The above equation can be rearranged as:

$$V_B^2 + \frac{2P_B}{\rho_l} = \frac{2C}{\rho_l} \tag{4.2}$$

Eq. (4.2) indicates that if the water flow velocity, V, exceeds $\sqrt{2C/\rho_l}$, the pressure will be negative at that point of the water stream. At this point, water tends to form cavities to expand and relieve the negative pressure (Young, 1999).

By definition, the cavitation process is the formation of these submicroscopic gas bubbles in a liquid structure due to the rupture of a liquid-liquid or a liquid-solid interface from a hole by external forces and is directly related to the pressure reduction below a certain critical value, which makes it different from boiling due to its generating mechanism. As shown in Figure 4.2, there are two types of vaporization, i.e., the well-known process of vaporization by increasing temperature (boiling) and vaporization under nearly constant temperature due to reduced pressure (cold boiling) as in the case of cavitation. The cold boiling process, and hence cavitation, depends on the purity of water. Pure water can withstand considerable low pressure, i.e., negative tension, without undergoing cavitation (Anon., 2011).

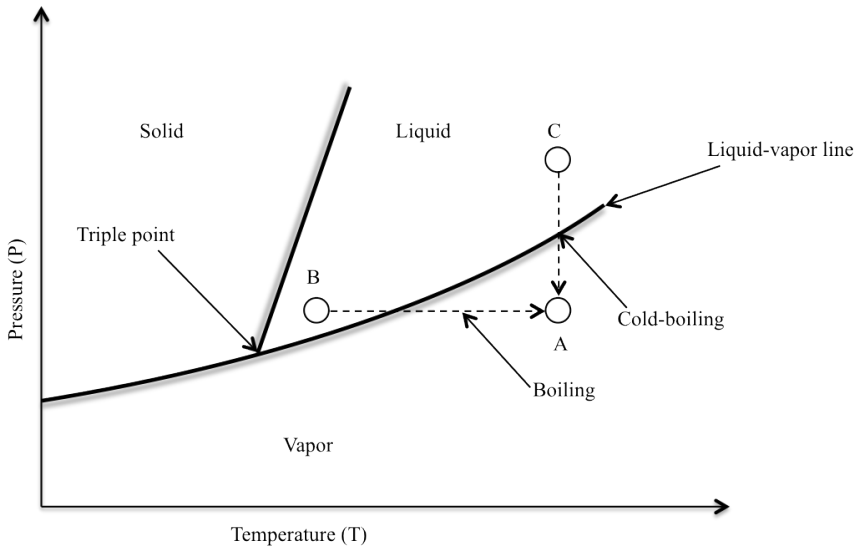


Figure 4.2. Solid, liquid and vapor phase lines for varying conditions of pressure and temperature (Anon., 2011).

If water contains a significant amount of dissolved air, then as the pressure decreases, the air comes out of the solution and forms cavities in which the pressure will be greater than the vapor pressure. This effect applies also when there are no visible bubbles. Submicroscopic gas bubbles can provide suitable nuclei for cavitation purposes. Hence cavitation can either be "*vaporous*" or "*gaseous*" or a combination of both, which will be discussed later in detail (Anon., 2011).

4.1.1.3. The Role of Bubble Nuclei

The process of beginning of cavitation is called "cavitation inception". A necessary condition for the inception is the presence of "weak" spots in the water, which break the bond between the water molecules where the intermolecular forces momentarily approach to zero. These weak spots are generally tiny gas bubbles called "nuclei" (Pease and Blinks, 1947). Cavitation inception at pressures near the vapor pressure requires the presence of nuclei, which contain minute amounts of vapor, gas or both. Cavitation is expected to occur only when these nuclei becomes unstable and grow when subjected to a pressure reduction. The static equilibrium conditions for a spherical nucleus can be analyzed to understand the bubble growth mechanism, as shown in Figure 4.3.

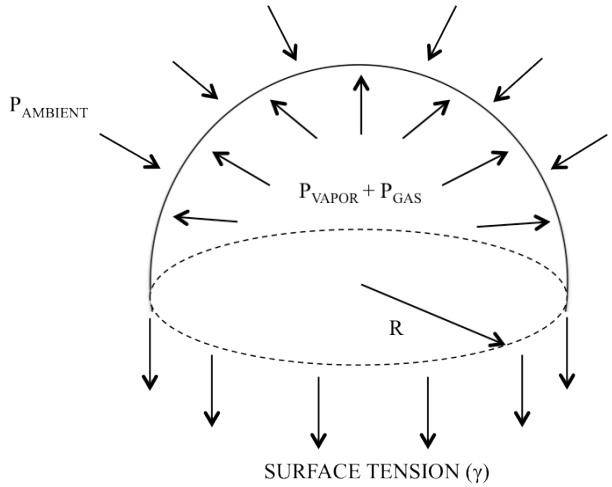


Figure 4.3. Internal and external forces acting on a cavitation bubble nucleus (Eisenberg, 1950).

The ambient pressure and the surface tension pressure at the nucleus-liquid interface must balance the internal forces, which are produced by the partial pressures of the gas and vapor within the nucleus. Thus, the static equilibrium condition can be written as:

$$P_a + \frac{2\gamma}{R} = P_v + \frac{C}{R_b^3} \tag{4.3}$$

where P_a is the ambient pressure, P_v the vapor pressure, where C constant, γ the surface tension and R_b the bubble radius. This equation can be plotted with two gas contents as shown in Figure 4.4.

The pressure adjacent to the cavitation bubble nuclei has a minimum value, which is below the liquid vapor pressure. From the curve, the bubble will stay stable as long as the ambient pressure is above this minimum pressure and the initial bubble radius is smaller than the radius associated with it. Additionally, the bubble tends to reach an equilibrium radius along the left-hand portion of the curve, where the slope is negative. However, if the pressure drops below the critical value, the bubble becomes unstable and grows without bound. As shown in the figure, for smaller gas contents, even lower pressures are required (Eisenberg, 1950).

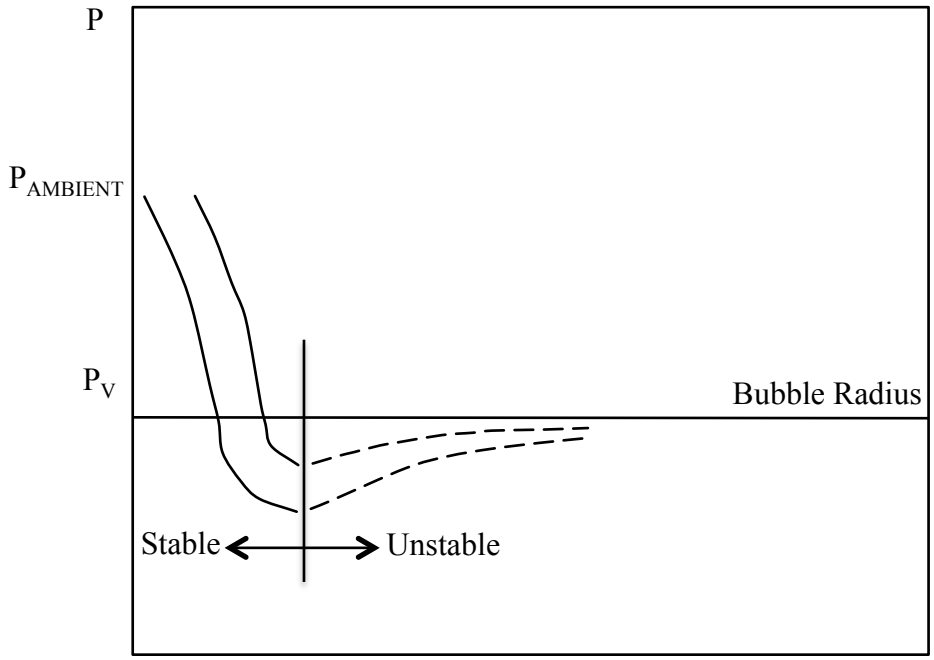


Figure 4.4. Static equilibrium conditions of cavitation bubble nuclei, where the upper curve has a larger gas content than the lower one (Eisenberg, 1950).

4.1.1.4. Classification

The effect of surface tension in the nucleation stage is through the control of the stable gas or vapor nuclei size that can be present in the liquid, which are often the weak points in the liquid that in turn affects the cavitation threshold. According to Gogate and Pandit (2001), liquids with the highest surface tension values, such as water, experience the maximum cavitation intensity. As the surface tension forces increase, the gas nuclei dissolution rate into the liquid increases, the number of nuclei present in the liquid at any moment decreases before being subjected to cavitation, and thus the inception, or critical, pressure for cavitation increases.

Wu (1969) photographically showed that the addition of the organic surfactants produced smaller and many cavities, due to the stabilization of the cavity by the adsorption of an organic film on the bubble surface. Later, Mason (1991) confirmed that the surfactant addition during the cavity generation phase of the cavitation process worked as a

"lubricant" during the difficult process of pulling the molecules apart, and thereby facilitated the cavitation. From these observations, it can be concluded that the addition of organic surfactants, such as frother in the flotation process, produces smaller and more copious cavities by stabilizing the gas nuclei present in the liquid, which would otherwise re-dissolve in the liquid due to surface tension forces, significantly reduces the cavitation threshold, prevents bubble coalescence and protects the cavities from immediate and violent collapse through their adsorption on the bubble surface (Fan, 2008).

There are two ways by which the pressure can be reduced through surface tension. One is by a fluid flow, where the velocity variations in a flowing liquid causes pressure variations in the system, and is often referred to as hydrodynamic cavitation. The other is by an acoustic field, which is often referred to as acoustic cavitation. From the cavitation methods classified as in Figure 4.5, tension methods are easy to scale up, operate and control by geometric parameters and operating conditions, such as velocity (Lauterborn, 1979). Hydrodynamic cavitation is a cheap and energy efficient method to generate cavitation due to its simple equipment requirements and low maintenance cost (Li, 2000; Fan, 2008). Hydrodynamic cavitation is therefore used for the pretreatment of the flotation feed in this study.

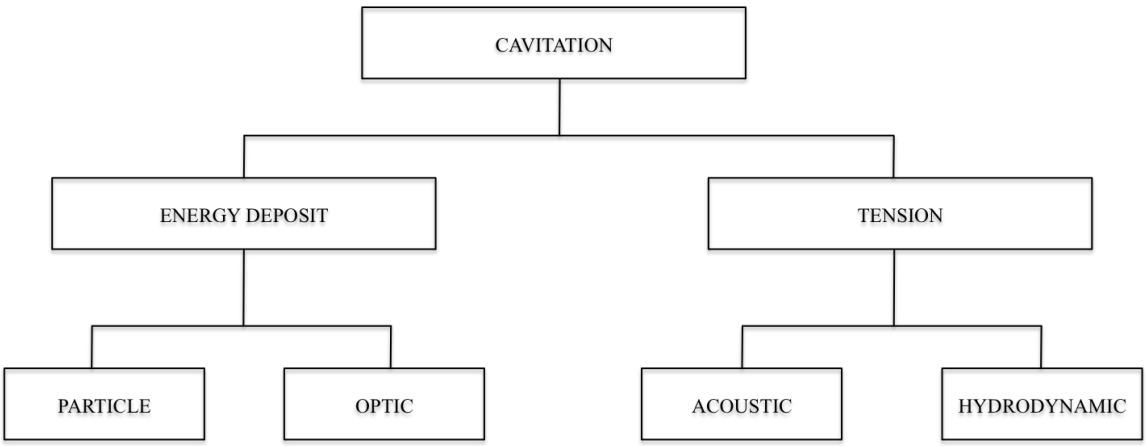


Figure 4.5. Classification of cavitation methods based on pressure reduction mechanisms.

4.1.1.5. Hydrodynamic Cavitation

Cavitation, in general, takes place in the form of gas super-saturation or hydrodynamic cavitation. Through gas super-saturation, tiny bubbles may be formed in inhomogeneous liquids containing pre-existing gas nuclei, gases trapped in crevices of solid particles and cracks in the container walls (Flynn, 1964). Solid particles with rough and hydrophobic surfaces are also known to promote bubble formation in liquid (Gerth and Hemmingsen, 1980; Ryan and Hemmingsen, 1993).

On the other hand, hydrodynamic cavitation is the process of formation and growth of gas bubbles in a liquid due to the rupture of a liquid–liquid or a liquid–solid interface under the influence of external forces. Hydrodynamic cavitation occurs whenever the pressure at a point in a liquid is momentarily reduced below its vapor pressure due to the local accelerations (high flow velocity) of the liquid in a flowing system (Hayward, 1970). O. Reynolds first observed this phenomenon about 100 years ago, when he found out that at the highest points of flow velocity, low, or even negative, pressures may exist, which can allow minute air or vapor-filled bubbles to open up and carried on by the flow regions of higher pressure (Trevena, 1987).

In addition, it is well known from ships and other hydraulic machines that their propellers, which rotate at high speeds, produce numerous amounts of bubbles, even though no external gas is drawn or bubbled in. Dean (1944) concluded this observation that bubbles can always be produced as a result of a turbulent circulation of the liquid or by active stirring. On the other hand, for hydrodynamic cavitation, a change in the direction or a convergence of the streamlines is necessary, which makes it different from a rectilinear flow, i.e., simple parallel non-shear flow without turbulence (Daily and Johnson, 1956; Young, 1999).

In order to measure the resistance of the flow to cavitation, Young (1999) introduced the cavitation number, K_c:

$$K_c = \frac{P_a - P_v}{\frac{1}{2}\rho_l V_a^2} \tag{4.4}$$

where V_a is the local flow velocity.

The cavitation number, K_c, is a dimensionless number, which expresses the relationship between the difference of a local absolute pressure from the vapor pressure and the kinetic energy per volume, and is used to characterize the potential of the flow to cavitate. One can observe different kinds of cavitation by holding the velocity constant and varying the reference pressure in a cavitation experiment as shown in Figure 4.6.

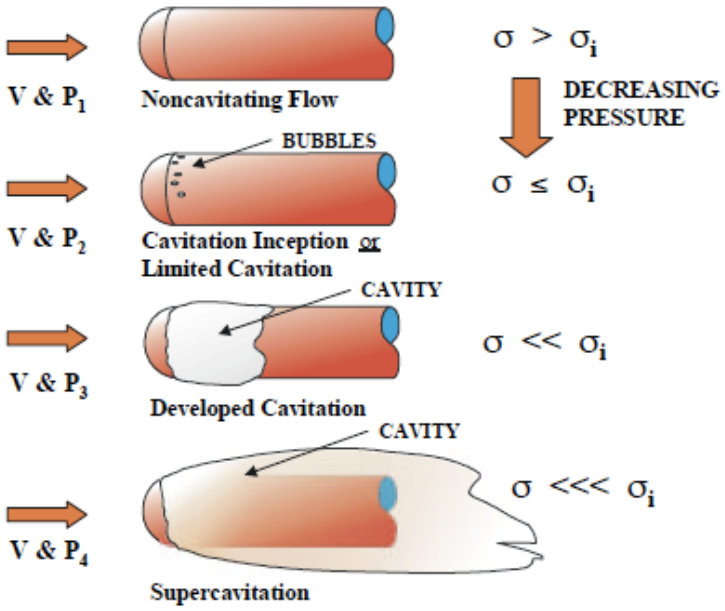


Figure 4.6. Schematic of cavitation flow regimes, where σ and σ_i are denoted as K_c and K_i, respectively (Stinebring et al., 2001).

At sufficiently high pressures, non-cavitating flows occur, where there is no evidence of bubbles. At very low pressures, super-cavitation occurs, where a very long vapor cavity exists and in many cases the cavity wall appears glassy and stable, except near the end of the cavity. Between these two flow regimes, limited and developed cavitation occurs. The lifetime of the small transient cavitation bubbles is measured in milliseconds. They grow while passing through the low-pressure region and then collapse as they enter the high-pressure region. If the bubbles have a relatively high initial gas content, they will collapse and then rebound. If such cavitation bubbles remained spherical throughout their lifetime, extremely high pressures, in the order of thousands of atmospheres, would be developed upon collapse. However, shape distortions occur when the bubble collapses in an unsymmetrical pressure field, e.g. in a gravity gradient or near a wall (Eisenberg, 1950).

Cavitation occurs when the local value of K_c approaches to, or falls below, the inception, or critical, cavitation number K_i, which can be determined experimentally and is typically less than 3. Cavitation is more easily initiated at the higher values of K_i. If cavitation is occurring, lowering the cavitation number, K_c, will increase the extent of cavitation, which can be achieved by decreasing the static pressure or by increasing the flow speed (Young, 1999).

Although there is no simple dimensionless number describing the effect of dissolved gas content on cavitation, three types of streaming cavitations have been distinguished by Knapp et al. (1970) and Hennessy (1989) according to the variations in the amount of dissolved gas and the pressure:

1. Vaporous cavitation:

Under normal pressure and low dissolved gas content, K_i is low and there is a time delay in the first appearance of micron-sized bubbles after reaching the cavitation threshold. This type of cavitation is caused by the explosive growth of bubbles due to the rapid conversion of liquid to vapor at the bubble wall, where the local static pressure is less than the vapor pressure of the liquid (Stinebring et al., 2001).

2. Gaseous cavitation:

Under normal pressure and high dissolved gas content, cavitation depends on the amount of dissolved gas content and the existing population of gas nuclei. The time delay decreases with increasing dissolved and free gas content, and more undissolved gas would form more gas nuclei. For high gas content K_i increases and gaseous cavitation number becomes larger than vaporous cavitation number. This type of cavitation is due to the slower mode of bubble growth caused by the transport of noncondensible gas into the bubble, where the local static pressure is less than the saturation pressure of the gas (Stinebring et al., 2001).

3. Hyperbaric cavitation:

Under high pressure and high dissolved gas content, the inception of gaseous cavitation threshold will occur at a lower flow speed and for a smaller pressure drop, compared to vaporous and gaseous cavitation.

According to this classification, one can conclude that cavitation is much easier under high pressure and high dissolved gas content, as in the case of dissolved air flotation. In addition, the air content in liquid has a significant effect on the occurrence of cavitation. In his research, Holl (1960a,b; 1969; 1970) also found that cavitation was directly proportional to the dissolved air content when he investigated the effect of air content on the occurrence of cavitation in a water tunnel. This suggest that although there is a benefit of air addition to the prior to a cavitation system, it is not a crucial component for the micro-bubble generation on hydrophobic particle surfaces, since bulk water contains from 2% (Karaman et al., 1996) to 2.5% (Craig et al., 1993) dissolved air (under room temperature and atmospheric pressure), which would serve to originate those bubbles from the flotation slurry. High dissolved gas content greatly enhances the cavitation by supplying the nuclei for the process. Solubility of the gas affects the number and the size of the nuclei. As the gas content decreases, the violent collapse of the cavities increases. Suspended solids in a liquid significantly enhance the cavitation efficiency by acting as the major source for nuclei generation. Solid particles with rough and hydrophobic

surfaces are known to promote bubble formation in liquids by entrapping gas in crevices and thus greatly reducing the cavitation threshold to facilitate nuclei/cavity generation, where gas molecules dissolved in water may occupy some of these structural voids (Schroder, 1969). On the other hand, hydrophilic solids usually entrap water and thus cannot enhance cavitation (Gerth and Hemmingsen, 1980; Ryan and Hemmingsen, 1993; Fan, 2008).

The efficiency of the hydrodynamic cavitation and the overall cavitation yield are affected by various important parameters, such as the liquid pressure/velocity entering into the system through the cylindrical inlet, physico-chemical properties of the liquid, geometry of the constriction used in the cavitation (Venturi) tube, i.e. diameter of the constriction used and the percentage of the free area offered for the flow, and the initial radius of the nuclei (Gogate and Pandit, 2001). As the inlet pressure and the pressure drops across the Venturi tube increase, the energy dissipation rate, intensity of the turbulence and the violent collapse of the cavity cluster increase.

It was found that, the presence of minute pockets of undissolved gas in crevices on mineral particles in a flowing stream assisted cavitation as a result of the expansion of these gas pockets under low or negative pressures at that point (Finkelstein and Tamir, 1985; Flynn, 1964). In addition, the existence and the shape of the particles present in water and the roughness of the inner wall of the venturi tube also influence the occurrence of cavitation due to the increased pressure fluctuations in the stream (Daily and Johnson; Holl, 1960a, 1960b, 1969; Arndt and Ippen, 1968). To maximize the bubble surface area generation, a sparging system (CT-600) has been developed based on hydrodynamic cavitation principles (Anon., 2010) which has shown a significant impact on bubbles surface area flux (S_b) due to reduced bubble size (D_b). This relationship is shown in Figure 4.7 by using Eq. (2.6) while keeping the superficial gas velocity (V_g) constant. Compared to jetting and porous sparging systems, sub-micron sized bubbles generated by cavitation principles show the highest surface area available for particles to collide, attach and be conveyed to the concentrate launder.

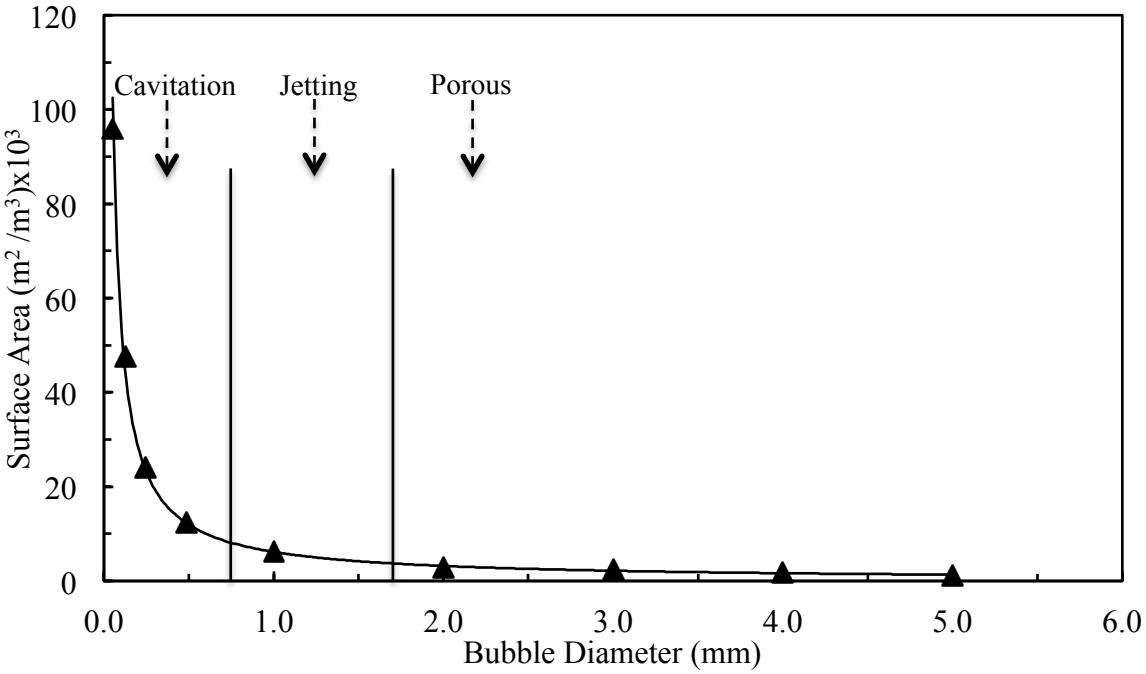


Figure 4.7. Relationship between the bubble diameter and the bubble surface area flux for different sparging systems (Anon., 2010).

4.1.2. Role of Cavitation in Froth Flotation

4.1.2.1. Effect on Bubble-Particle Collision

As previously shown in Eqs. (2.72) and (2.73) for both the perfectly-mixed and plug-flow reactors, respectively, collection zone recovery is a function of the flotation rate constant, k, which, in turn, is a function by the bubble surface flux (Eq. (2.6)) and the probability of flotation after incorporating Eq (2.8) into Eq. (2.7):

$$k = \frac{1}{4} S_b P = \frac{1}{4} S_b \left[P_c . P_a \left(1 - P_d \right) \right] \tag{4.5}$$

Eq. (4.5) shows that S_b plays a key role in the flotation efficiency and thus the flotation recovery. As shown in Figure (4.6), cavitation is the most efficient mechanism among others in producing the smallest size bubbles which results in the highest surface area flux, S_b, available for an effective bubble-particle collision and the froth recovery due to

attachment. As a result, one can conclude that increased in bubble surface area flux through cavitation mechanism would improve the recovery rate in the pulp zone of a cell. In addition to the S_b, probability of collision, P_c, is another factor determining the flotation rate and thus the recovery. As previously shown in Eqs. (2.10), (2.11), and (2.13), for the three main flow types representing each hydrodynamic condition in a liquid, respectively, to achieve the maximum probability of collision, P_c, smaller bubble sizes and larger particle sizes are preferred. In this concept, micron-sized bubbles generated by introducing the cavitation mechanism are being utilized as the bridging medium between the ultrafine particles. As a result of agglomerating these ultrafine particles, bigger and more particles would be floated per unit of bubble surface area, which would in turn increase the flotation rate and the product mass flux rate, or carrying capacity.

Further simulations for a range of bubble and particle size using Eq. (2.13) clearly show that as the bubble diameters decreased, the probability of collision increased for all size fractions as shown in Figure 4.8. Similarly, fine particles have a low probability of collision with bubbles and are thus difficult to catch by bubbles, particularly by large size bubbles. According to Ahmed and Jameson (1989), for the same gas flow rate and agitation, the actual number of collision increase with decreasing bubble size because of the increase in the number of bubbles.

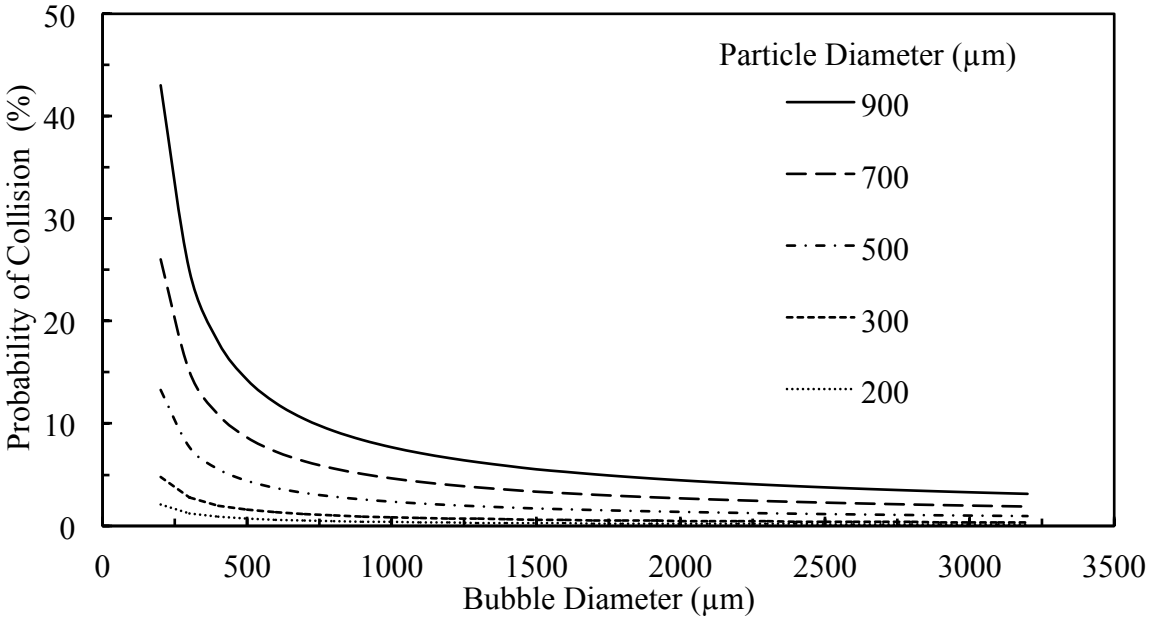


Figure 4.8. Bubble-particle collision probability as a function of bubble diameter for 400, 600, 900 and 1200-micron particles.

Recent studies have provided evidence of a long-range, attractive hydrophobic interaction force between micron-sized bubbles on a particle surface and conventional bubbles. The formation of a gaseous capillary bridge was reported to be detected using an atomic force microscopy (AFM) after the coalescence of microbubbles existing on two hydrophobic surfaces as shown in Figure 4.9 (Parker et al., 1994; Attard, 2003). Upon bringing the two surfaces together, a concave capillary bridge was formed thereby creating a very stable aggregate with a strong binding energy due to the attractive nanobubble bridging capillary force (Schubert, 2005; Hampton and Nguyen, 2010; Palmer et al., 2011; Ishida et al., 2012). The existence of microbubbles on hydrophobic particles surface causing fine particle aggregation through a bubble-bridging mechanism enhances the collision, and thus the collection, probability of hydrophobic particles. This evidence suggests the potential of improving recovery by the cavitation pretreatment of a flotation feedstock.

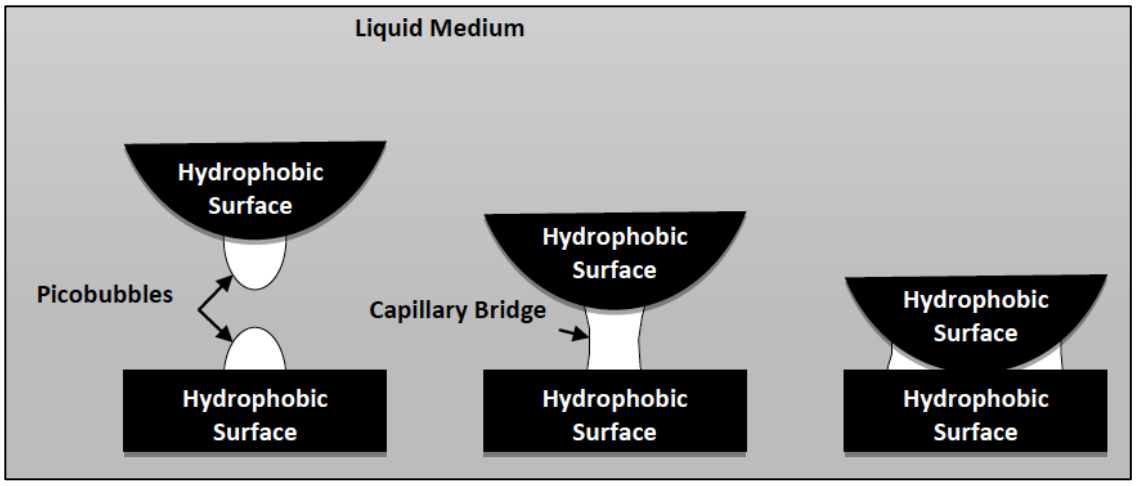


Figure 4.9. Bridging mechanism of two hydrophobic surfaces with cavitation-generated bubbles (Hampton and Nguyen, 2010).

4.1.2.2. Effect on Bubble-Particle Attachment

Improving hydrophobicity of the particle by using higher collector dosage increases the bubble particle attachment probability, P_A. As a result, however, increased operating cost of the flotation circuit and decreased selectivity and separation efficiency would negatively affect the overall performance. Stockelhuber et al. (2004) and Simonsen et al. (2004) suggested a better approach by generating micron-sized bubbles on the solid surfaces through cavitation in order to increase their hydrophobicity instead of increasing collector dosage. During the film thinning process of the attachment mechanism, when the film thickness was greater than the height of the micro-bubbles, no significant impact was seen in the film behavior (rupture) from the illustration in Figure 4.10. However, as the film thickness became closer to the bubble height, the interaction of the surface forces began between the micro-bubble and the wetting film, as shown in Figure 4.11. It is also suggested that the film rupture occurs by the larger micro-bubble on the surface, which has the thinnest foam film to break for the same interaction force.

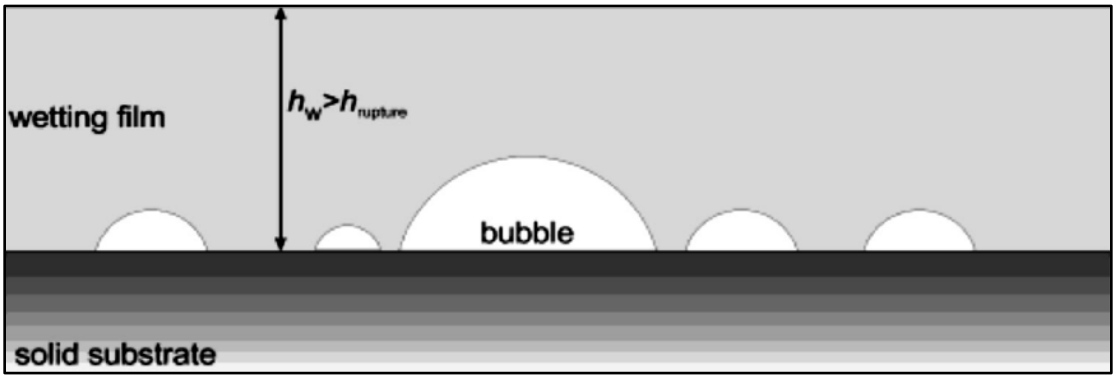


Figure 4.10. Illustration of a wetting film with microbubbles on the solid surface at large film thicknesses that prevent rupture, $h_w > h_{rupture}$ (Stockelhuber et al., 2004).

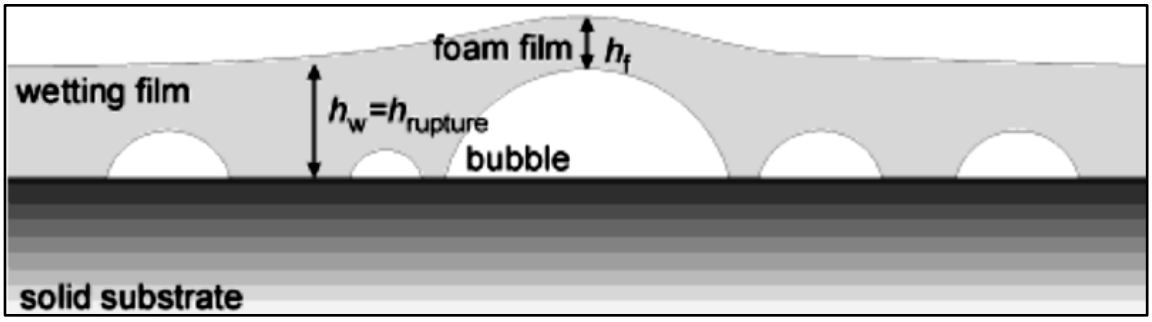


Figure 4.11. Illustration showing the interaction between the wetting film surface and micro-bubbles, at small film thicknesses that results in rupture when $h_w = h_{rupture}$ (Stockelhuber et al., 2004).

Evidence also exists that indicates bubble nucleation at the hydrophobic surface could also increase the probability of attachment and thus the flotation rate. The existence of micro-bubbles in flotation slurry reduces the rising velocity of conventional-sized bubbles. This could result in increased bubble-particle sliding times, decreased tangential velocities of particles sliding on bubble surfaces, and increased bubble-particle attachment probability (Ralston and Dukhin, 1999; Yoon 2000). If the attachment rate is increased, the efficiency of the bubble-particle attachment process is improved and thus recovery is enhanced. In addition, elevated flotation rates can be realized which could increase unit capacity. The mechanism is believed to be due to the added surface

roughness from the concave bubble sites on the particle surface which helps penetrate the water film that coat the conventional bubble surfaces. Also, the attractive force between two bubble surfaces may be greater than the particle-bubble interactive forces that assist during film thinning (Honaker, 2006).

Preliminary tests involving the treatment of slurry through a Venturi tube that contains an opening to the atmosphere at the narrow throat location has found that the collector dosage required during the flotation process could be potentially reduced, since the pretreatment serves a collector role and flotation rate of materials that traditionally have slow flotation characteristics could be improved (Tao et al., 2006; Tao et al., 2010).

In addition to the models for different induction times (Figure 2.10), the experimental data in Figure 4.12 clearly show that P_A increases with increased particle size and decreased bubble size. For fine particles, probability of collection, and thus the flotation recovery, is low due to, especially with large size bubbles. By generating micron-sized bubbles in the liquid, the flotation probability can be greatly enhanced. Considering the abovementioned effects of bubble and particle size on flotation efficiency, pretreatment of the flotation feed was studied in this research through laboratory- and full-scale cavitation tubes.

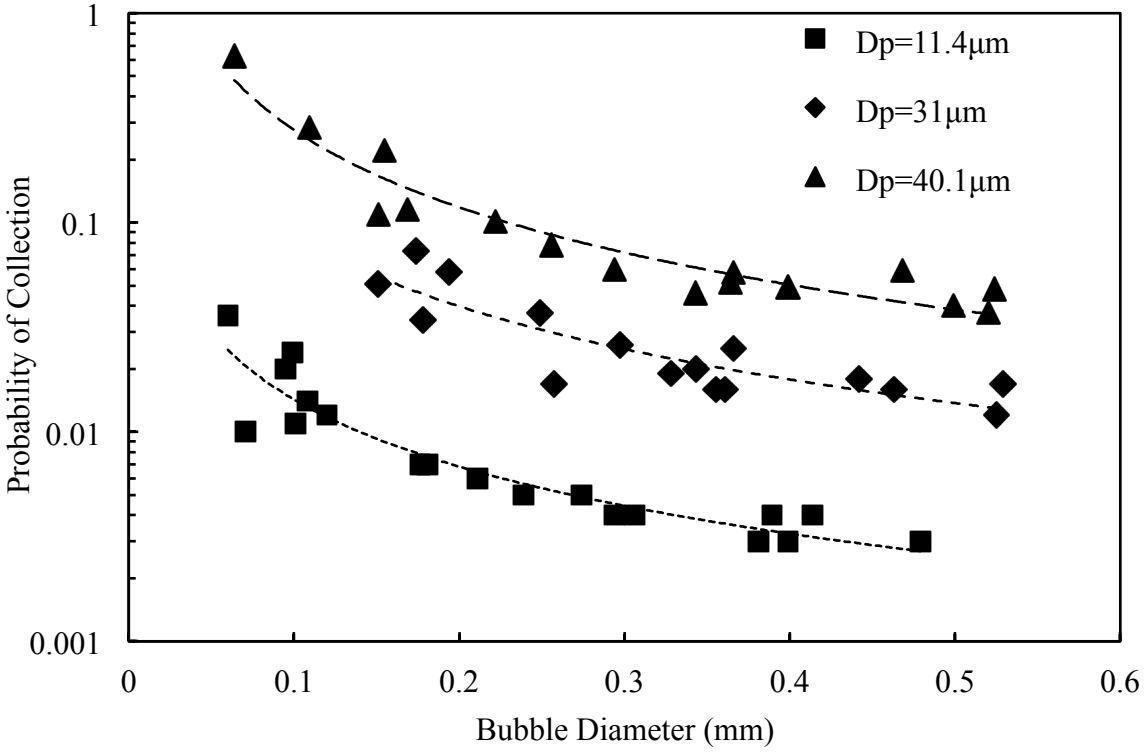


Figure 4.12. Comparison of the experimental (filled markers) and the predicted (dashed lines) *P* values as a function of bubble size for varying particle sizes (*after* Luttrell & Yoon, 1992).

4.1.3. Fundamental Studies

4.1.3.1. Krasowska and Malysa (2007)

The concept of using pre-aeration to improve flotation recovery was originally born from observations reported from a study by Krasowska and Malysa (2007) in which high-speed video showed significantly faster bubble-particle attachment rates when a hydrophobic surface was pre-coated with micron-sized bubbles. During these tests, the researchers used Teflon plates of different surfaces roughness to determine the collision and attachment kinetics of bubbles rising in water. As such, the influence of surface roughness on bubble collision, the formation of three-phase contact and bubble attachment were determined as a result of air presence of on Teflon plates.

Both Teflon plates of I and II were treated with a smooth abrasive paper (No. 2400) and Teflon I surface was further modified by using diamond polishing paste (DP-1/4 μm). As a result, Teflon I and II were finished with smooth surfaces, with scratch dimensions smaller than 1 μm. On the other hand, Teflon III surface was not modified and used as it was received from the mechanical shop with scratch dimensions estimated to range between 30 and 60μm, as shown in Figure 4.13.

The time-scale sequences of bubbles approaching to Teflon plate surfaces prior to bubble attachment in Figure 4.14 showed that for Teflon I and II plates, the bubbles bounced off the surfaces at least 4 times without attachment before coming to rest on the surface. Even after coming to rest, several milliseconds passed before attachment occurred due to the film thinning processes. On the other hand, for the same test, Krasowska et al. (2007) showed that a "necking" was formed at t=4.2ms between Teflon III and the detaching bubble during the initial bounce from the surface. Microphotographs showed that the "necking" was ruptured at t=5.1ms and sub-microscopic air bubble was left on the Teflon III surface (see photo 10 of Fig. 4.14C). Consequently, the interaction of the small hemispherical air pockets on the rough Teflon III surface with the air bubble during the second interaction facilitated an almost instantaneous attachment. As a result of these tests, the total bubble attachment time on Teflon surfaces of I, II and III were found to be 84, 80 and 40 ms, respectively. This suggests that the time required for particles to attach to a bubble after collision can be significantly reduced, about 50% in this experiment, if the particle (or the surface) is pretreated with small micron size bubbles.

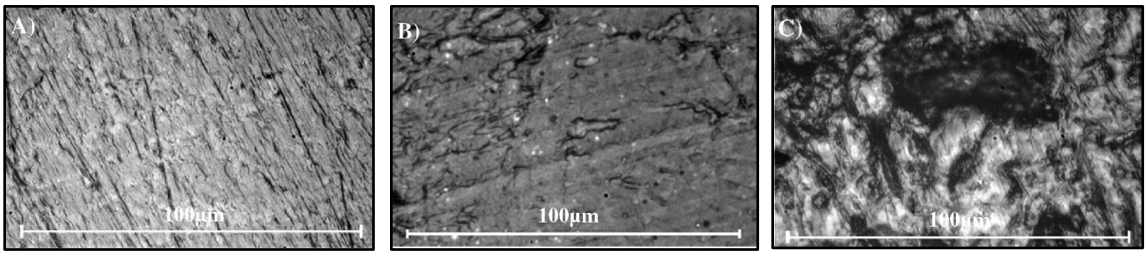


Figure 4.13. Microscopic photos for Teflon I, II and III, respectively, with varying surface roughness (Krasowska and Malysa, 2007).

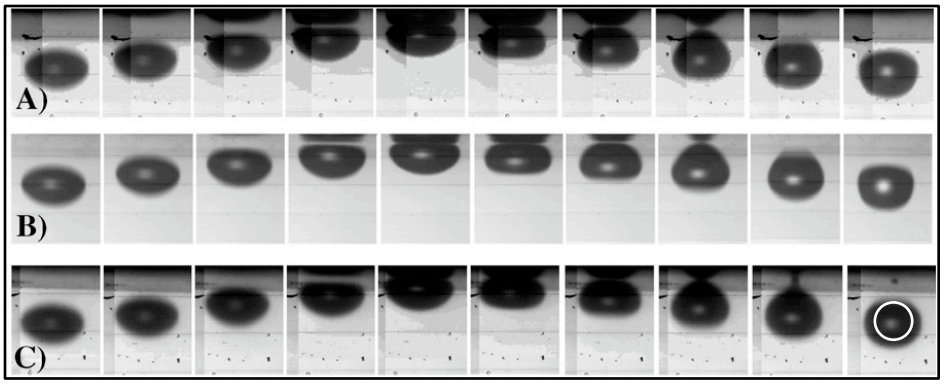


Figure 4.14. Photo sequences (time interval=0.845 ms) of bubbles during the first collision with hydrophobic Teflon plates of varying surface roughness (Krasowska and Malysa, 2007).

4.1.3.2. Sayed-Ahmed (2013)

A more recent study was conducted on the effect of micro- or nano-bubbles on bubble-particle interaction using hydrophobic particle trajectories around a bubble surface under different testing conditions (Sayed-Ahmed, 2013). During these tests, 110-180 micron glass (silica) spheres were made hydrophobic (contact angle ≈ 110°) by methylation in cyclohexane solution (ratio<1:8). Particle with different hydrophobicities were dropped freely on bubble surfaces (1-1.4 mm) in a glass cell setup, which can be visualized through a high-speed video microscope. Solvent exchange method using ethanol, which contains more dissolved air than that of water, was used to form micro- or nano-bubbles on hydrophobic glass surfaces.

From the high-speed video images in Figure 4.15, it can be clearly seen that the micro- or nano-bubble coated particle surfaces form a bridge between the hydrophobic particles and form large aggregates, which in turn, enhances the bubble-particle interaction and the attachment probability through a long-range hydrophobic attraction. In addition to this attraction, Sayed-Ahmed (2013) claims that an additional attractive force exist, which is larger than the van der Waals attraction between the hydrophobic surfaces without micro- or nano-bubbles. This can be attributed to the nanobubble bridging capillary force

(NBCF) concept (Hampton and Nguyen, 2010). When two hydrophobic surfaces approach each other, the gas-filled micro- or nano-bubbles attached to the surfaces, which are filled with gas, are forced to coalesce. As a result, a concave gas bridge is fomed either between the two micro- or nano-bubbles due to an attractive capillary force or due to the interaction of a micro- or nano-bubble and a hydrophobic solid. The resulting bridge is claimed to generate a strong and long range attraction between the surface due to a lower pressure associated with the gas bridge and the interfacial tension between the gas and the liquid phases (Hampton and Nguyen, 2010).

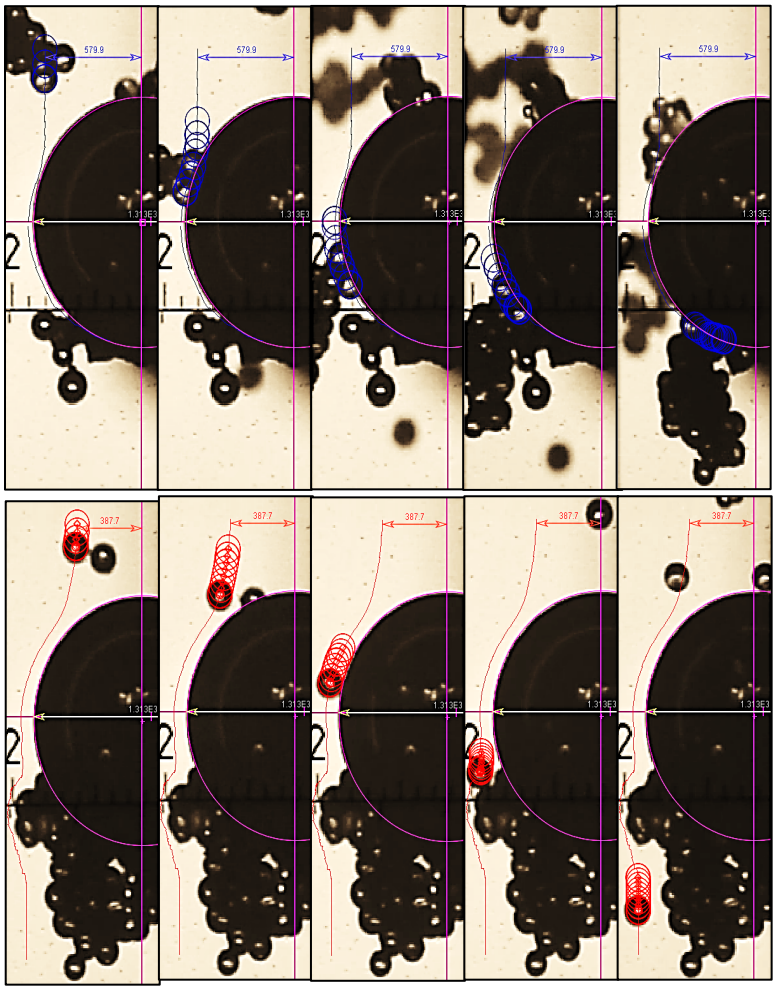


Figure 4.15. High-speed photographic sequences of hydrophobic bubble-particle aggregate interaction in the presence of microbubbles on the surface (Sayed-Ahmed, 2013).

Bubble-particle aggregates formed with hydrophobic surfaces coated with micro- or nano- bubbles increase the collision efficiency through widening the collision limiting area around a bubble, which enables the aggregates to penetrate the liquid streamlines more easily, which in turn enhances the carrying capacity of the bubble surfaces. Enhanced bubble particle attachment is due to the reduced induction time, which is should be less than the sliding time, in the presence of micro- o nano-bubbles on the particle surfaces. In the presence of micro- or nano-bubbles, more attractive sites are shown to be available for attachment, which may due to the attractive force as mentioned above that is claimed to be higher than that of the centrifugal force (Sayed-Ahmed, 2013).

In the light of these findings, flotation feed pretreatment through a cavitation tube was studied in this research to optimize and quantify the improvements for the conventional and column flotation systems. Laboratory- and full-scale studies were carried out to evaluate the impact of cavitation tube tests on coal of varying degrees of hydrophobicity and to assess the potential of using cavitation to improve the top size of the flotation process.

4.1.4. Empirical Studies

4.1.4.1. Munoz-Diaz (2007)

The observations and the fundamental analysis mentioned above led to a hypothesis that the pretreatment of flotation feed potentially could benefit the recovery of difficult-to-clean coals. In the past, most of the attention was paid to develop new collectors to improve the floatability of these coals. However, Munoz-Diaz (2007) employed a more practical and an inexpensive technique by studying the pretreatment of flotation feed through a cavitation tube (or air eductor). Initial flotation tests were conducted using representative feed samples from an active preparation plant in Boone County, West Virginia, which was treating coal from the Coalburg seam with poor flotation characteristics. The flotation feed with 5% solids concentration (by weight) was

comprised of about 84% minus 45μm (325 Mesh) material, which contained the largest amount of floatable material (66.6% of the total amount).

Laboratory conventional and column flotation tests were performed to investigate the impacts of hydrodynamic cavitation on coal recovery using a cavitation tube in an effort to nucleate fine bubbles on the surface of the weakly hydrophobic coal particles prior to flotation. After conditioning with collector, the slurry was pumped through a cavitation tube of 1.27-cm (1/2-in) inner diameter at a volumetric flow rate that provided a pressure of 2.72 atm (40 psi). Pre-aeration of the slurry prior to the cavitation tube was also evaluated by injecting air at a rate of 1 L/min. The feed slurry was processed through the cavitation tube for a single pass and for multiple passes before the flotation rate experiment to quantify flotation rate and compare the value to the performance achieved with no pretreatment. Afterward, the pretreated slurry was first subjected to conventional flotation rate tests. As shown in Table 4.1, subjecting the flotation feed either one time or multiple times through the cavitation tube increased the recovery by about 18 absolute percentage points after one minute of flotation.

The comparison shown in Table 4.1 indicates that the flotation rate during the first minute of flotation nearly doubled as a result of using the cavitation tube. These results are in agreement with those reported by Attalla et al. (2000) and Zhou et al. (1997), which have shown improved recovery responses due to reduced induction times and faster attachment rates in the presence of micro-bubbles on coal surfaces, as originally hypothesized by Krasowska and Malysa (2007) and Krasowska et al. (2007).

Table 4.1. Improved kinetic rates and the corresponding flotation recovery values using data obtained after one minute of flotation for the Coalburg coal (Munoz-Diaz, 2007).

Test Identification	Flotation Rate (min^{-1})	Flotation Recovery (%)
Standard	0.65	61.0
Cavitation (Single Pass)	1.25	78.4
Cavitation (Multiple Passes)	1.24	78.2

4.1.4.2. Independent Research Laboratory (2011)

Considering the notable positive effects of cavitation pre-aeration observed by Munoz-Diaz (2007) from laboratory conventional and column flotation tests, an industrial research laboratory showed interest to potentially utilizing their existing cavitation system technology on full-scale flotation systems to achieve enhanced flotation performances, especially for flotation feedstocks with low floatability. Thus, an internal exploratory test program was conducted to confirm the initial findings by pretreating a difficult-float flotation feed source which mainly (over 60%) consisted of ultrafine particles smaller than 45 microns.

During the flotation rate tests, collector (Fuel Oil No. 2) and frother (polyglycol) additions were at 0.5 kg/t and 10 ppm, respectively. A significant improvement can be seen with tripled flotation rate and recovery values at the end of 1 minute, where the majority of the highly hydrophobic particles are floated, as shown in Table 4.2. Even after 2 minutes of flotation, there is 10 absolute percentage point increase in the recovery and 50% improvement in the rate compared to the standard test without cavitation and air.

Table 4.2. Improved kinetic rates and the corresponding flotation recovery values after one and two minutes of flotation for the conventional tests conducted by Eriez Flotation Division-USA.

Test Identification		Flotation Rate (min^{-1})	Flotation Recovery (%)
Standard	0-1 min.	0.12	11.3
	0-2 min.	0.39	59.6
Cavitation and Air	0-1 min.	0.43	35.1
	0-2 min.	0.57	70.1

4.2. RESULTS AND DISCUSSION

4.2.1. Conventional Flotation Tests

The coal produced from Coalburg seam is well known for its relatively difficult cleaning properties and poor flotation characteristics. As a result, low flotation recovery is often realized in preparation plants treating this coal source. During this research, cavitation pretreatment was further evaluated following the promising results from the initial research to find a solution for low flotation recovery performances caused by a low degree of surface hydrophobicity associated with the Coalburg coal. Flotation feed samples were collected from two active preparation plants located in Boone and Kanawha Counties, West Virginia, to test the repeatability of the data and to reduce the bias of testing from one coal source. Flotation rate tests were conducted in order to assess the kinetic flotation characteristics of the sample following the experimental procedure described in Section 3.1.3.

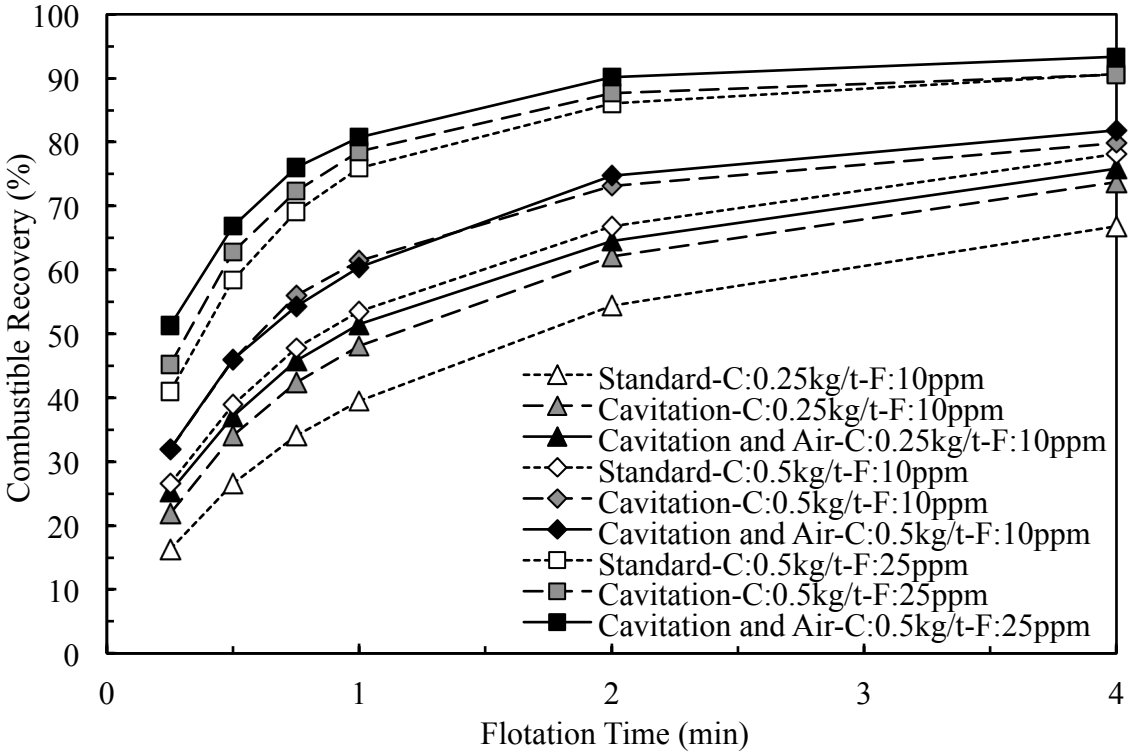


Figure 4.16. Effects of pre-aeration and cavitation tube performance on BC Coalburg coal.

For the Boone County (BC) coal sample, the combination of cavitation pretreatment and air addition with the least reagent consumption gave almost the same performance with the one that employed no feed pretreatment for higher collector additions (0.5 kg/t collector and 10ppm frother), as shown in Figure 4.16. These results suggest that the pre-aerated cavitation pretreatment acted as a secondary collector to improve the flotation recovery, which has the potential to reduce the collector consumption up to 50% under the same conditions.

When the amount of collector was raised up to 0.5 kg/t at low frother concentrations (10ppm), the improvement in the flotation response due to pre-aeration was not found to be as significant. In comparison, the flotation responses were almost identical between these two different conditions for the first four samples (at 15, 30, 45 and 60 seconds, respectively) and the pre-aeration showed only slight improvement in flotation

characteristics after 60 seconds. This suggest that although there is a benefit of air addition to the prior cavitation tube, it is not a crucial component for the micro-bubble generation on coal surfaces, since bulk water contains from 2% (Karaman et al., 1996) to 2.5% (Craig et al., 1993) dissolved air (under room temperature and atmospheric pressure), which would serve to originate those bubbles from the flotation slurry.

Although the impact of the frother concentration was more significant than that of the pre-aeration and cavitation pretreatment at higher reagent additions for BC coal, when the frother concentration was increased from 10ppm to 25ppm under the same collector dosage, the improvement in combustible recovery values due to cavitation pretreatment remained around 5 and 10 absolute percentage points on average, without and with pre-aeration, respectively, across the flotation period.

For the coal sample from Kanawha County (KC) West Virginia, when the frother concentration was increased from 10ppm to 20 ppm under same collector dosages (0.5 kg/t), the increase in the combustible recovery response was more significant than the recovery increase when the collector dosage was increased from 0.25 kg/t to 0.5 kg/t under the same frother concentrations (20 ppm), as shown in Figure 4.17. Since the impact of the frother concentration was more significant than that of the pre-aeration and cavitation pretreatment at higher reagent additions, the difference in combustible recovery values were still substantial but less than ten absolute percentage points from 15 seconds to 2 minutes and the results were almost identical after 2 minutes even for the sample without any feed pretreatment techniques.

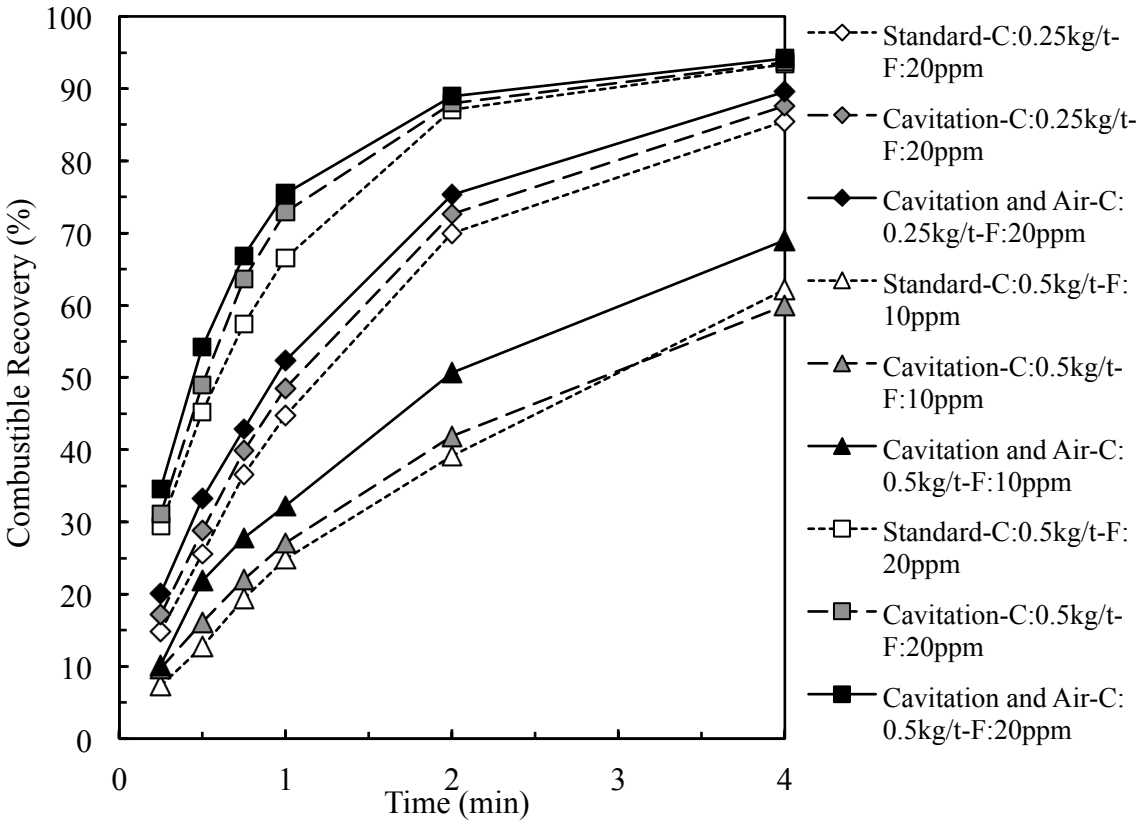


Figure 4.17. Effects of pre-aeration and cavitation tube performance on KC-Coalburg coal.

Flotation rate constants were calculated from Kelsall`s (1961) flotation model, which was proposed to incorporate a fast floating and a slow floating rate constant. The use of two rate constants was considered to give better approximation to the distribution of particle floatability than that with a single rate constant. The mathematical description of the model was later modified by Jowett (1974) and Lynch (1977) as given in Eq. (2.73). Using this equation, the difference of the sum of squares between the actual and the predicted recovery values for each time interval was minimized using Solver in the Excel. Fast and slow flotation rates and the slow floating fraction were chosen as the variables to be optimized to minimize the difference between the sum-of-squares.

From the two-constant flotation rates for BC coal, there is a significant difference in the fast flotation rate values between the tests that employ the pre-aeration and cavitation pretreatment and those with no feed pretreatment, as shown in Table 4.3. It is important

to note that, similar fast flotation rates were achieved between Tests 3 and 4 (0.79 min^{-1} and 0.84 min^{-1}, respectively) using cavitation and pre-aeration under low frother concentrations while reducing the collector consumption by one half, i.e. from 0.5 kg/t to 0.25 kg/t. In addition, at low reagent dosages while employing the cavitation pretreatment only, the fast flotation rate is increased by 30%, which was later reduced to 21% and 9% for higher collector dosages, under low and high frother rates, respectively, which suggest that the cavitation pretreatment is providing a significant benefit to the flotation systems under chemically constrained conditions. Addition of air prior to the cavitation tube (pre-aeration) improved the fast flotation rate constants by about 10% between Tests 11 and 12 and Tests 17 and 18 under different collector and frother concentrations. However, at low frother and high collector dosages, the improvement was only around 5% between Tests 14 and 15, which is also apparent from Figure 3. This finding suggests that the need for additional frother to recover the "slow-to-float" material and pre-aeration is not enough to replace the impact of frother on middlings recovery.

Table 4.3. Fast and slow flotation rate constants for the BC coal sample.

Test No.	Test Conditions	Fast Flotation Rate (min^{-1})	Slow Flotation Rate (min^{-1})
1	Standard C: 0.25 kg/t - F:10ppm	0.54	0.22
2	Cavitation C: 0.25 kg/t - F:10ppm	0.71	0.19
3	Cavitation and Air C: 0.25 kg/t - F:10ppm	0.79	0.23
4	Standard C: 0.5 kg/t - F:10ppm	0.84	0.25
5	Cavitation C: 0.5 kg/t - F:10ppm	1.02	0.21
6	Cavitation and Air C: 0.5 kg/t - F:10ppm	1.07	0.25
7	Standard C: 0.5 kg/t - F:25ppm	1.53	0.29
8	Cavitation C: 0.5 kg/t - F:25ppm	1.67	0.25
9	Cavitation and Air C: 0.5 kg/t - F:25ppm	1.84	0.33

A similar trend to that of the BC coal was apparent for the fast flotation rate values of KC coal due to pre-aeration and cavitation pretreatment, especially at higher collector (0.5 kg/t) dosages, as shown in Table 4.4. Similar to the BC results, very fast flotation rates were achieved in Tests 15 and 16 (1.43 min^{-1} and 1.46 min^{-1}, respectively) using cavitation and pre-aeration under high frother concentrations while using 50% less collector, i.e., 0.5 kg/t to 0.25 kg/t. The increase of frother dosage from 10 ppm to 20 ppm at high collector dosages (0.5 kg/t) showed comparable results for the fast flotation rate, which was increased by two times by doubling the frother rate. On the other hand, increasing the collector dosage from 0.25 kg/t to 0.5 kg/t at high frother dosages (20ppm) did not showed the same rate of increased response for the fast flotation rates, which suggest that frother concentration was more prominent in determining the flotation performance than the collector. As a result of the kinetic rate tests it can be concluded that high amounts of collector, and especially frother are required to float this type of Coalburg coal with more coarse- and intermediate-size particles, i.e., plus 0.15 mm and plus 0.075 mm, respectively, compared to that of the BC coal. In addition, it is shown that the middling particles in both coal samples with low flotation characteristics can only be recovered with high collector and frother dosages, which suggest that there is a chance to see an improvement with the pretreatment of the feed through cavitation in column tests.

In order to assess the flotation characteristics of a coal sample from a different coal source, i.e., Winchester seam, from Raleigh County (RC), West Virginia, release analysis were conducted. The “grade vs. recovery curve” in Figure 4.18 shows a tyical “easy-to-clean” coal, where the concentrate ash is only ranging from 6.6% to 10%, while the feed ash is 62%. This “black and white” separation shows us that there is a very small chance to see a significant improvement with the pretreatment of the feed through cavitation tube. One can reference this hypothesis to the small amount of plus 45-micron material, i.e. 14%, at around 8% ash from the size analysis (Table 3.1). Since the sample was taken

prior to the desliming cyclones, due to the location of the reagent addition, around 80% of the slurry contains high-ash minus 25-micron slimes.

Table 4.4. Fast and slow flotation rate constants for the KC coal sample.

Test No.	Test Conditions	Fast Flotation Rate (min^{-1})	Slow Flotation Rate (min^{-1})
10	Standard C: 0.5 kg/t - F:10 ppm	0.77	0.19
11	Cavitation C: 0.5 kg/t - F:10 ppm	0.86	0.18
12	Cavitation and Air C: 0.5 kg/t - F:10 ppm	1.02	0.22
13	Standard C: 0.25 kg/t - F:20 ppm	1.13	0.23
14	Cavitation C: 0.25 kg/t - F:20 ppm	1.33	0.20
15	Cavitation and Air C: 0.25 kg/t - F:20 ppm	1.46	0.26
16	Standard C: 0.5 kg/t - F:20 ppm	1.43	0.26
17	Cavitation C: 0.5 kg/t - F:20 ppm	1.66	0.23
18	Cavitation and Air C: 0.5 kg/t - F:20 ppm	1.95	0.30

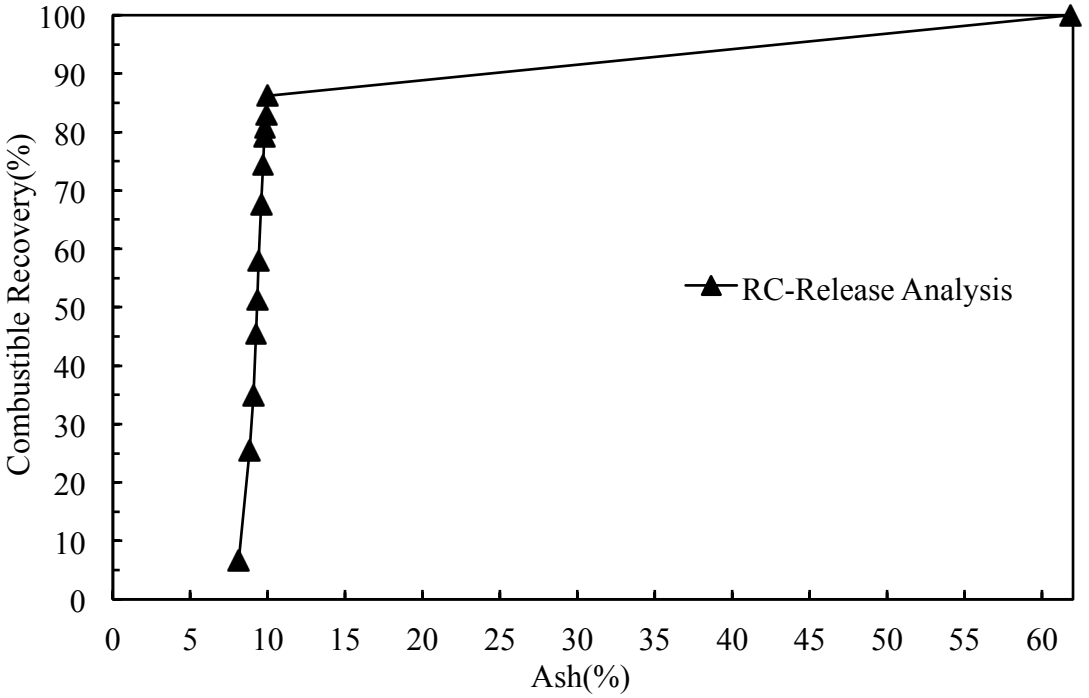


Figure 4.18. Release analysis results conducted on the RC coal sample from Winchester seam.

In addition to the release analysis, kinetic rate tests were conducted over a period of flotation time using very small amounts of flotation reagents, i.e., 0.25 kg/t collector (Fuel Oil No.2) and 10ppm frother (MIBC). The results in Figure 4.19 shows that even at these concentrations, a significant difference in the flotation performance between the tests that employ both the pre-aeration (air addition) and cavitation pretreatments and the one without any feed pretreatment, which represents the standard rate test that was conditioned in the cell only.

Standard rate tests and the cavitation pretreated rate tests were repeated to analyze the variability and the repeatability between the two tests. Results show that the response values for both conditions were relatively close to each other, especially for the cavitation pretreatment tests. Data points were almost the same at the beginning of the test (from 15 seconds to 1 minute), which showed about 4% difference on average in the later part of the rate test (from 2 to 8 minutes). This might be attributed to the amount of stable

bubble-particle aggregates formed as a result of a multiple treatments of the remaining sample in the sump through the cavitation tube. On the other hand, the combination of the cavitation and the pre-aeration resulted in faster flotation responses throughout the testing period, which helped to improve the floatability of the moderately hydrophobic particles.

While testing the effect of only cavitation and only pre-aeration on the flotation performance, both of the responses were similar from 15 seconds to 1 minute of the flotation. The improvement with the cavitation tube was larger in the later part of the rate test (2 to 8 minutes) even though it was not very significant (4% on average). This was very similar to the difference in the flotation performance between the standard rate test and the test both employing the cavitation and pre-aeration. The former started with a higher flotation rate in the first sample (at 15 seconds), the flotation responses were almost identical for the second, third and the fourth samples (at 30, 45 and 60 seconds, respectively) and the latter showed better flotation characteristics after 60 seconds. This might be attributed to a better frother mixing and bubble generation at the beginning of the test for the standard rate test.

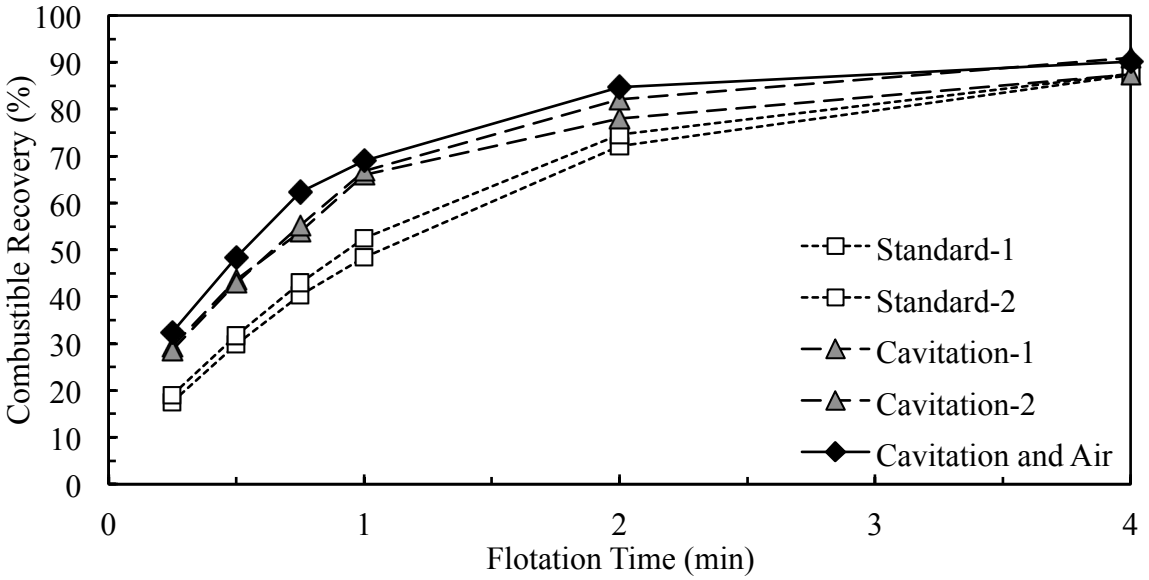


Figure 4.19. Effects of pre-aeration and cavitation tube performance on the Winchester seam coal.

The release analysis (Figure 4.18) showed that the ultrafine particles in the feed can be effectively rejected from the concentrate, which limited the further enhancement using the column flotation and testing the impact of the cavitation tube.

4.2.2. Column Flotation Tests

A continuously operated laboratory flotation column setup (Section 3.1.4.) was used to further investigate the effect of the cavitation pretreatment on retention time limited flotation systems employing Coalburg coal sources from Boone (BC) and Kanawha Counties (KC), West Virginia. The column flotation tests were performed over a range of feed volumetric flow rates, which yielded a range of particle retention time conditions. Flotation feed was pretreated through the cavitation tube, which was located near the feed point of the column. Here, the flow was divided and directed to two different locations by adjusting the peristaltic pump, i.e., a predetermined amount of feed rate (ranging from 300 ml/min to 2000 ml/min) going into the column feed, and the rest of the flow circulating back to the sump. The operating parameters of the laboratory column flotation tests are given in Table 3.4, which were based on the findings of previous University of Kentucky Mining Engineering researchers (Ozsever, 2005; Munoz-Diaz, 2007). At the same operating conditions, Table 4.5 gives the notations on the points with regards to their feed rate values, which were very similar for both column tests.

For the Boone County (BC) coal sample, the combination of cavitation pretreatment and air addition with the least reagent consumption gave almost the same performance with the one that employed no feed pretreatment for higher collector additions (0.5 kg/t collector and 10ppm frother), as shown in Figure 4.16. These results suggest that the pre-aerated cavitation pretreatment acted as a secondary collector to improve the flotation recovery, which has the potential to reduce the collector consumption up to 50% under the same conditions.

Table 4.5. Notations of the column flotation test points for the different Coalburg coal samples shown in Figures 4.20 and 4.21.

Feed Rate (ml/min)	Boone County (BC) Coal		Kanawha County (KC) Coal	
	With Cavitation	Without Cavitation	With Cavitation	Without Cavitation
300	---	A	---	A
450	---	B	---	---
600	c	C	b	B
750	d	D	c	C
900	e	E	d	D
1050	f	F	e	E
1200	g	G	f	F
1350	h	H	---	---
1500	i	I	g	G
1750	j	J	h	H
2000	k	K	i	I

Release analysis for both BC and KC coals show a typical example of a "relatively hard-to-clean" Coalburg coal sample. The concentrate ash range for BC and KC coals were from 3.5% to 8.5% and from 5% to 9% on average, respectively. However the feed ash contents were around 52% for the former and around 46% for the latter, which were in the close proximity with their size analysis from Tables 3.2 and 3.3. For the KC sample in particular, which showed that there are more coarse- and intermediate-size particles, plus 0.15 mm and plus 0.075 mm, respectively, with higher ash contents due to middling particles, represent a chance to see an improvement through the feed pre-aeration.

As a result of the column flotation tests, cavitation feed pretreatment provided a significant effect on column flotation when the separation performance is compared with the release analysis, as shown in Figures 4.20 and 4.21. The pretreated sample resulted in significantly higher recovery values for higher feed rates compared to the sample without any pretreatment. Close proximity of the test results at different feed rates to the release analysis for both coal types suggest that the laboratory column flotation unit was operating at nearly optimum conditions.

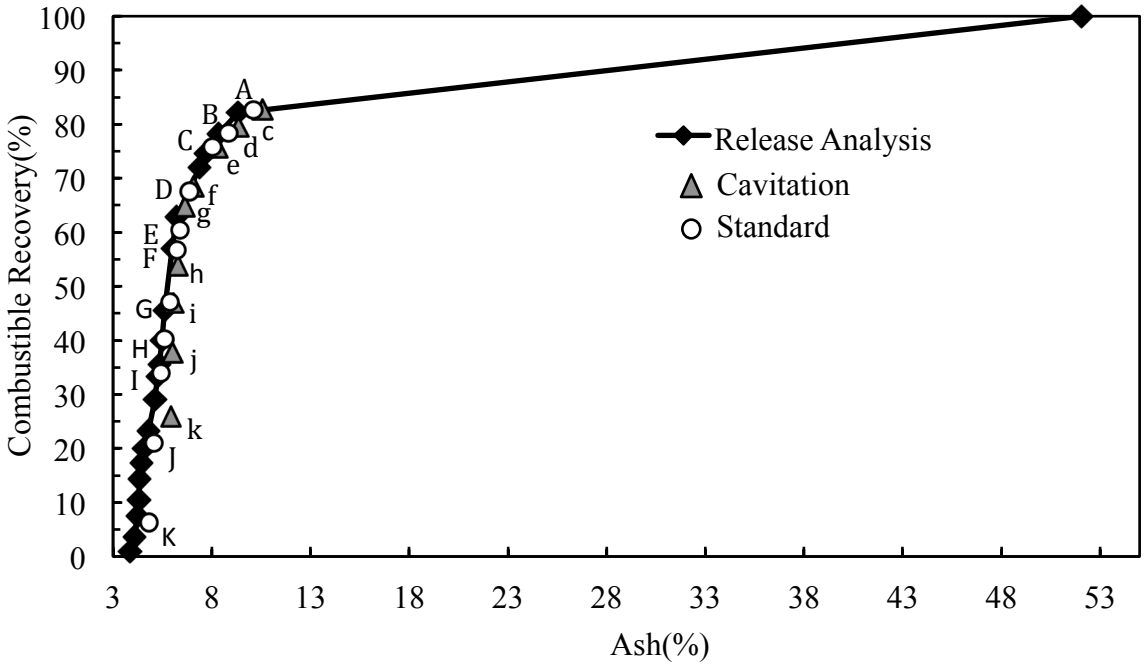


Figure 4.20. Effects of flotation performance with cavitation pretreatment of the column flotation feed of a Coalburg coal sample from Boone County, West Virginia.

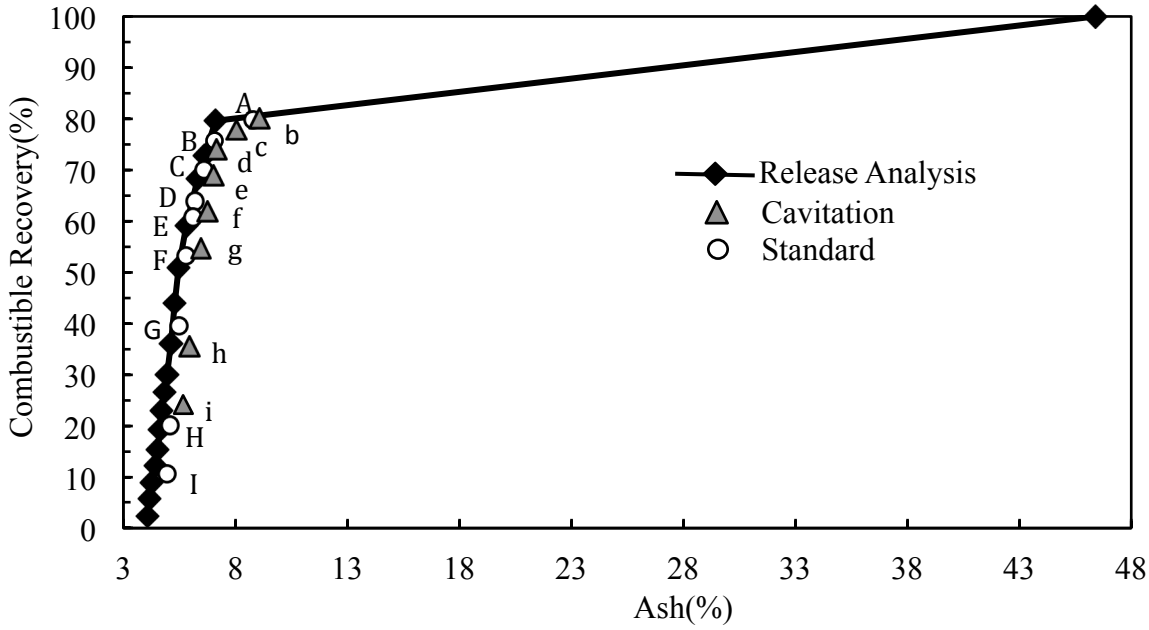


Figure 4.21. Effects of flotation performance with cavitation pretreatment of the column flotation feed of a Coalburg coal sample from Kanawha County, West Virginia.

The impact of the cavitation pretreatment was even more apparent when the combustible recovery values were plotted against the volumetric feed flow rate, which showed recovery improvements over the entire range of flotation rates, as shown in Figures 4.22 and 4.23. The recovery response with the increased feed rate was almost stable up to 600 ml/min with the cavitation-pretreated feed for both coal samples. On the other hand, the standard column flotation recovery values dropped steadily and significantly with the increased feed rate. Especially after the 600-ml/min mark, the difference in the recovery values jumped from 7% to around 12% and from 5% to around 10% for the Boone and Kanawha County coals, respectively, and kept increasing as the feed rate increased. At a flow rate of 1050 ml/min, recovery combustible recovery increased by 12 and 8.5 absolute percentage points when using feed pretreatment for the Boone and Kanawha County coals, respectively. The incremental improvement in recovery increased to values around 10 absolute percentage points when the volumetric flow rate was increased.

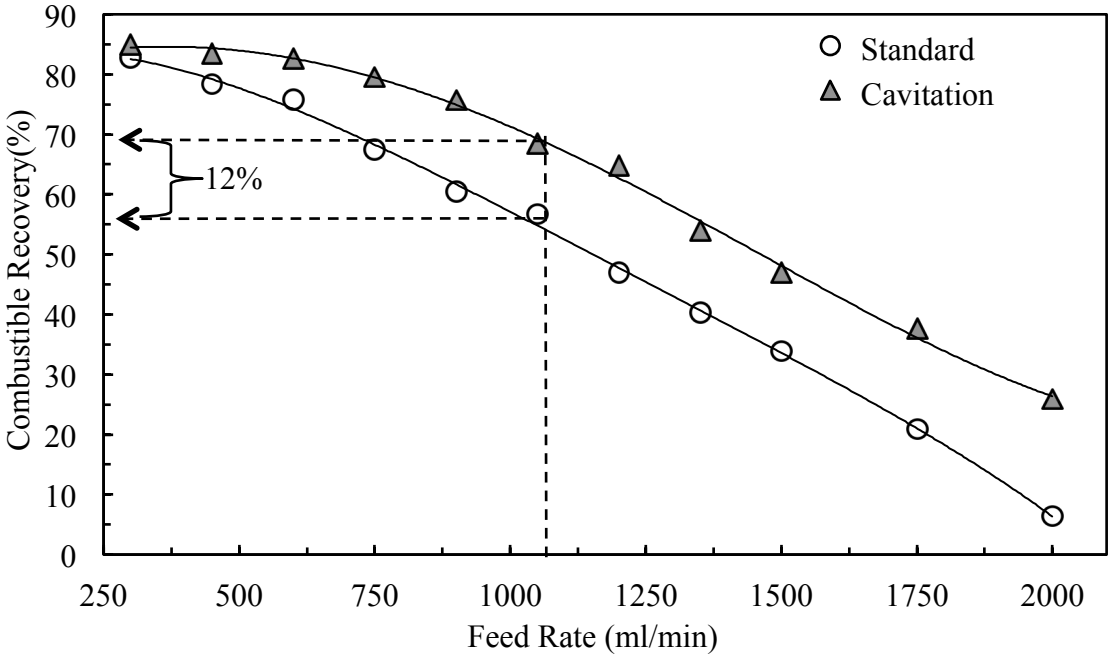


Figure 4.22. Combustible recovery responses with the increased feed rate for the column flotation tests of the BC-Coalburg coal sample.

The increase in the recovery improvement with an elevation in volumetric flow rate is likely a result of both improved flotation rates and carrying capacity. It should be noted that the recovery values achieved under low feed flow rates were impacted by particle flotation rates whereas the high flotation rates were likely more affected by carrying-capacity constraints. This finding is especially important for the flotation systems that are retention time constrained.

Another problem occurring during the flotation of difficult-to-float coals, such as Coalburg coal, is due to the inadequate number of particles carried by the bubbles, which results in poor carrying capacities. With the pretreated sample the recovery responses showed that the capacity could be increased while maintaining high recoveries. This hypothesis is further tested through tests with varying solid contents under the same volumetric feed rate.

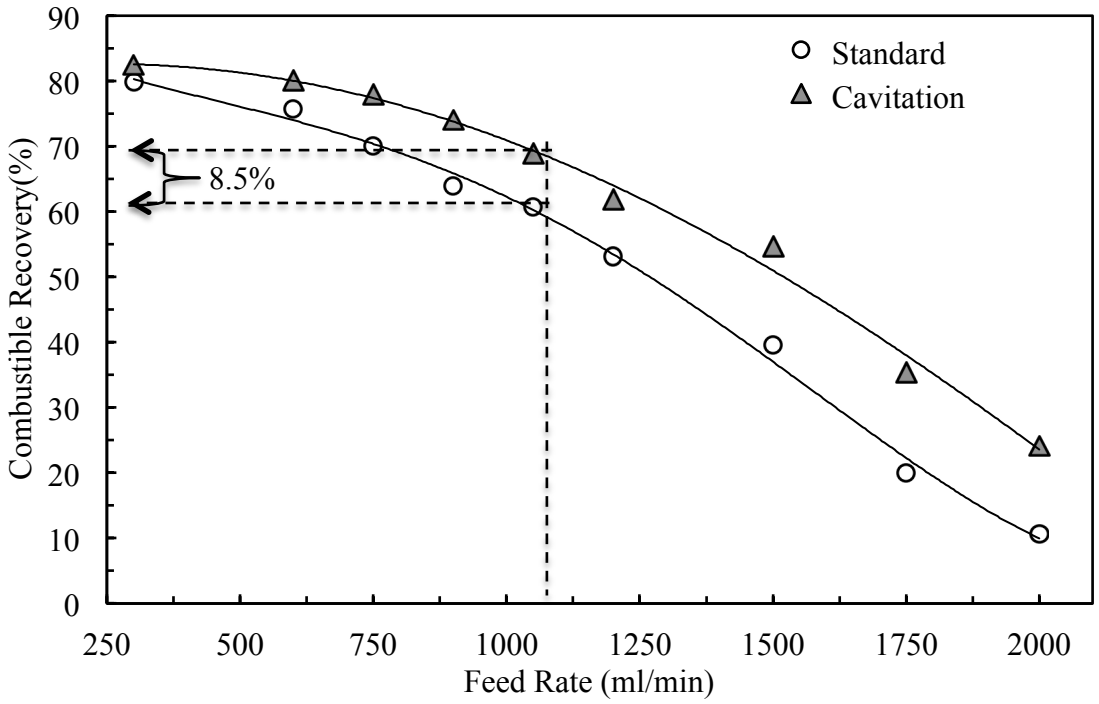


Figure 4.23. Combustible recovery responses with the increased feed rate for the column flotation tests of the KC-Coalburg coal sample.

Following the column flotation tests, the carrying capacity tests were conducted for both coal samples by increasing the feed solids concentration while holding the volumetric feed rate constant at 1050 ml/min. Original feed solid contents of 6% and 8% for Boone and Kanawha County coals, respectively, in Figures 4.31 and 4.32 reflect the data at this feed rate from the column tests.

Carrying capacity achievable for the BC coal sample was assessed by varying the feed solid concentration from 6% to 20% while maintaining the volumetric feed rate to the column cell at a constant value. The limited amount of sample constrained the number of tests and the feed solid concentration levels tested for 6%, 15% and 20% by weight. At 6% and 15% solids, the product rate was increase due to the cavitation pretreatment was 0.08 t/h/m^2 and 0.12 t/h/m^2, respectively, as shown in Figure 4.24. This means that an additional 1.2 t/h and 1.8 t/h can be recovered for a common industrial column (4-m diameter) application for 6% and 15% solids content, respectively, which represent a significant improvement especially for high feed solids concentration. From an economic standpoint, this might be a significant finding for the company to consider while making the decision on installing the cavitation pretreatment to the existing flotation circuit. However, at 20% solids, which was the highest solids content tested, the effect of cavitation was negligible due to heavy loading on the bubble surfaces where the product rate has decreased significantly and both tests resulted in about 0.3 t/h/m^2 product rates.

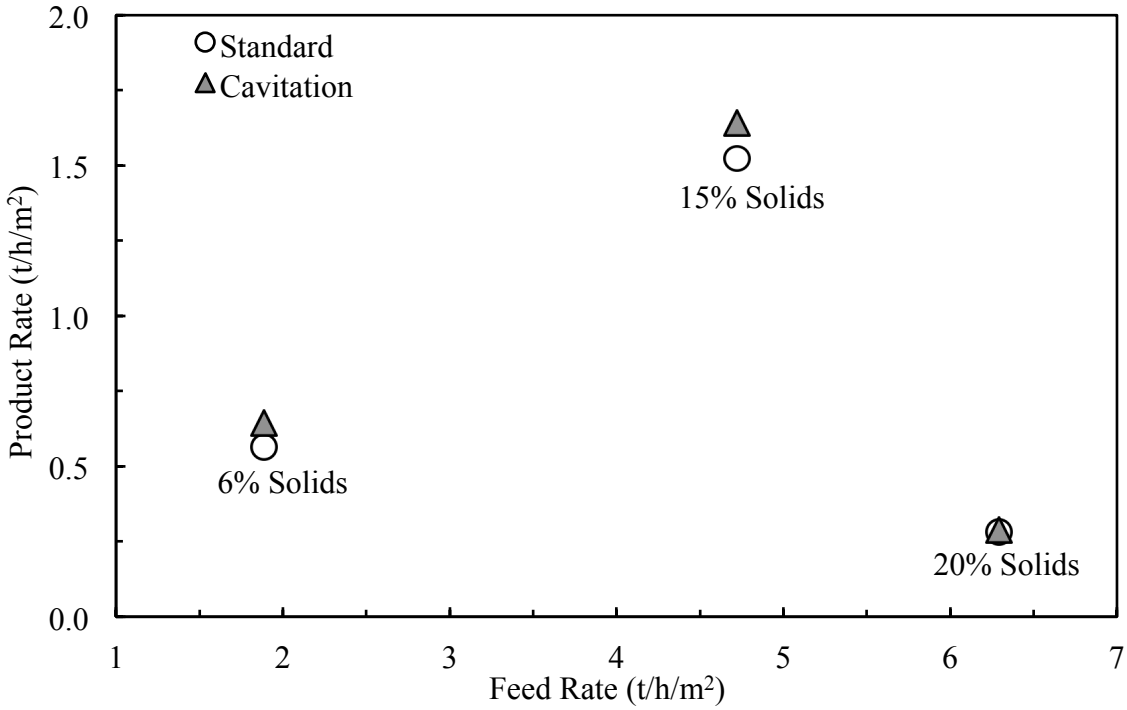


Figure 4.24. Enhanced carrying capacity characteristics realized by cavitation pretreatment of the feed for the BC-Coalburg coal sample at different feed solid contents.

The expected trend of carrying capacity for different solid concentrations in the feed can be clearly seen for the Kanawha County sample, which represents an increase in product mass flux with feed mass flux up to a maximum, as shown in Figure 4.25. A significant increase in carrying capacity was achieved at higher solid concentrations of 12% an 14%, which showed increased product rate values of 0.27 t/hr/m^2 and 0.22 t/hr/m^2, respectively, due to the cavitation pretreatment. For a common industrial column, the difference would equate to additional 4t/h and 3.3 t/h that can be recovered with cavitation pretreatment at a solids concentration of 12% and 14%, respectively. Although the difference in increased product mass flux is not as significant compared to 12% and 14% solids, the same trend of improved carrying capacity due to feed pretreatment follows for the other feed solids concentrations. The reduced carrying capacity after 12% feed solid concentration can be associated with the preferential detachment of coarse particles, which cannot find enough bubble surface area to be conveyed to the concentrate launder.

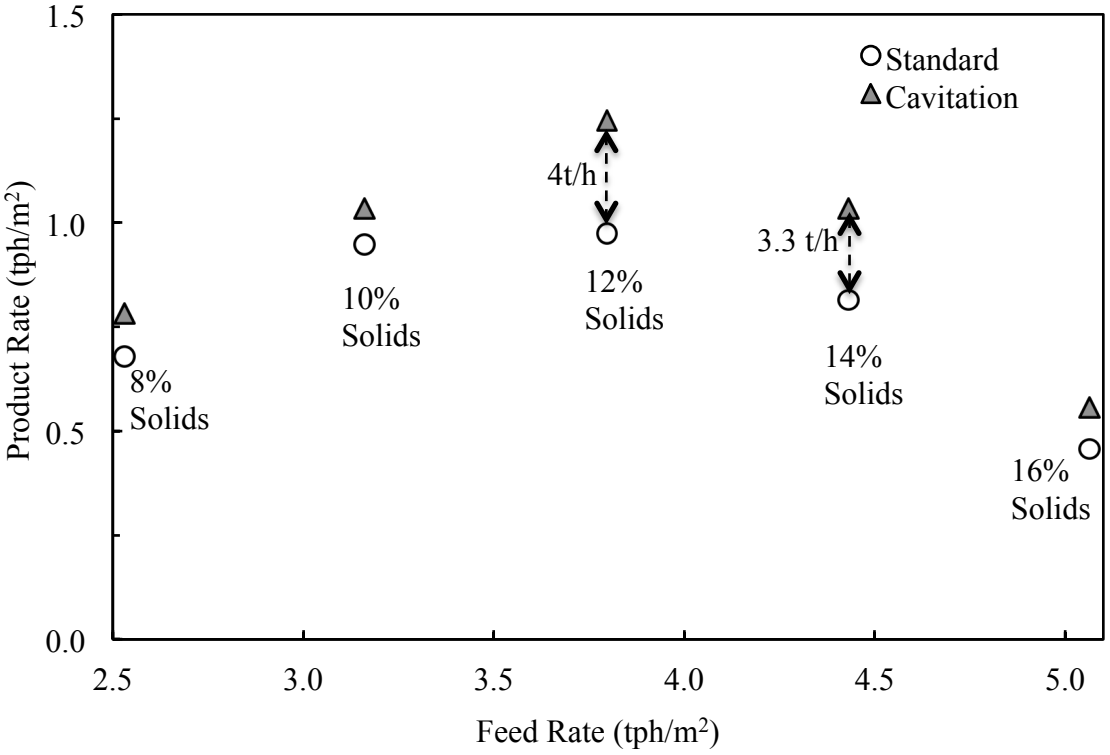


Figure 4.25. Enhanced carrying capacity characteristics realized by cavitation pretreatment of the feed for KC-Coalburg sample at varying solid contents ranging from 8% to 16%.

Carrying capacity test results were further investigated for Kanawha County coal sample by conducting product size analysis for the selected tests, which showed the most significant difference in recovery values with cavitation pretreatment, i.e., 12% and 14% solids. As shown in Figure 4.26, the recovery improvement was preferentially achieved on the ultrafine particle size fractions of the feed. These results point out to the impact of the pre-aeration in causing ultrafine particle aggregation whereby a strong binding energy is formed by the air bridges between the hydrophobic coal particles.

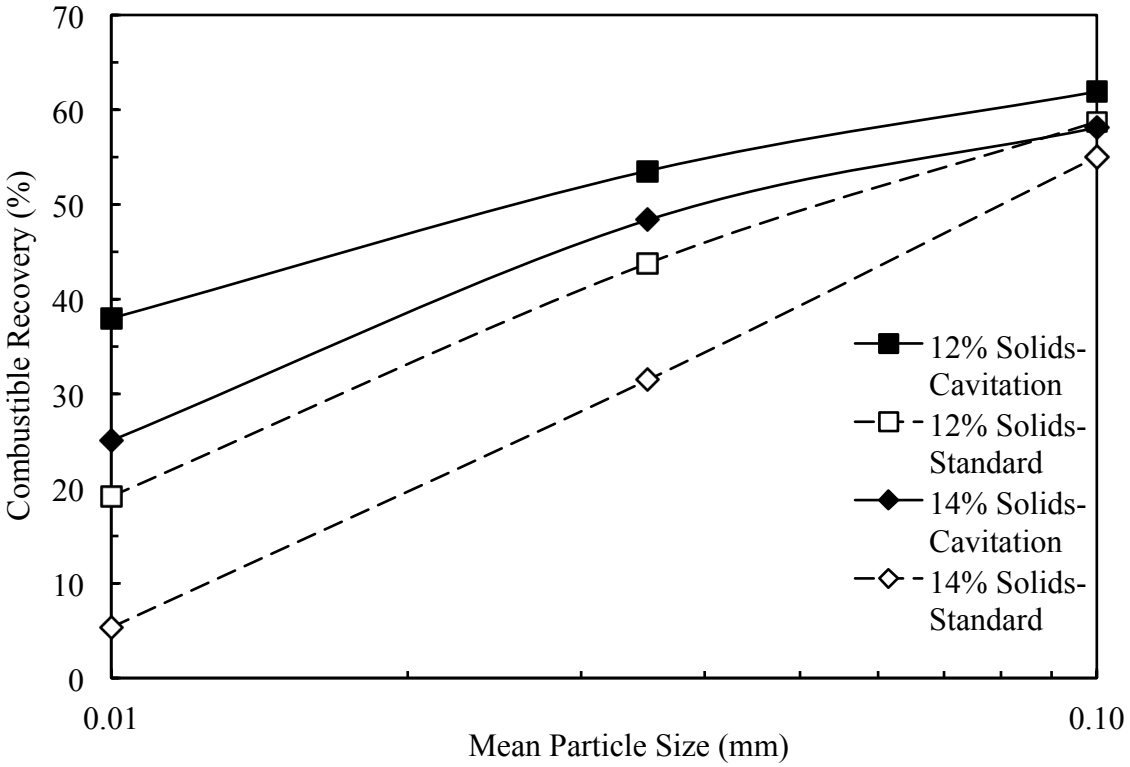


Figure 4.26. Product particle size analysis for the KC-Coalburg coal following the carrying capacity test for 12% and 14% feed solids content.

4.3. CONCLUSIONS

The proposed concept of pre-aerating the flotation feed using a cavitation tube in this study aimed to provide a potential solution for low flotation recovery performances caused by 1) a low degree of coal surface hydrophobicity in the flotation feed, and 2) retention time limited flotation systems. By injecting feed through a cavitation system, micron-sized bubbles nucleate onto the surface of the coal particles, which results in the pre-aeration of the flotation feed. As a result, when the particles interact with bubbles produced from a conventional bubble generator, the attachment process occurs more rapidly. Due to the finer distribution, the injection of additional air and the production of bubbles on the particle surfaces, flotation rate and carrying capacity are improved which directly results in enhanced flotation recovery.

During the laboratory studies, first, two kinds of Coalburg seam coals with poor flotation characteristics were sampled from different preparation plants located in Boone (BC) and Kanawha Counties (KC) in West Virginia to see the real impact the pre-aeration and the cavitation feed pretreatment methods on difficult-to-float coals. As a result of the flotation rate tests, flotation recovery achieved from conventional flotation was improved by about 10 and 8 absolute percentage points on average for BC (at lowest reagent dosages) and KC (at lowest frother dosage) samples, respectively, when subjected to flotation feed pretreatment by passage through a cavitation tube with air addition. Although pre-aeration prior to the cavitation tube had a significant impact on the KC coal at the lowest frother concentrations to recover coarse- and intermediate-size particles, i.e., plus 0.15 mm and plus 0.75 mm, respectively, additional air to the system had a little-to-no positive impact for the BC coal sample. This point out to the fact that the dissolved air in plant water would be sufficient enough to generate micron-size bubbles on coal surfaces through the cavitation tube, although additional air may further benefit the feed pretreatment due to the micro-bubble population in the system. It is also important to see that when the collector dosage was increased for the BC coal, the cavitation feed pretreatment with air has the potential to reduce the collector consumption by 50%. For the KC coal, the amount of slow floating fraction was significantly higher at low frother concentrations, which was the prominent parameter to achieve high recoveries, due to the slow-floating behavior of the Coalburg coal.

In addition to the Coalburg coal samples, Winchester coal sample with good flotation characteristics was collected from Raleigh County (RC), West Virginia. Although recovery improvements of up to 4 absolute percentage points were seen with the pre-aeration and cavitation treatments, easily cleanable nature of this coal made it difficult to draw major conclusions since it was not evaluated further through laboratory column studies.

Following the positive outcomes from the kinetic rate tests, continuous laboratory column flotation tests were performed to test the effect of cavitation pretreatment on volumetric feed rate and carrying capacity while minimizing the effect of micro-bubble collapse during sampling. While increasing the flotation feed rate from 500 to 2000 ml/min and from 600 to 2000 ml/min, the improvement in recovery rose from 5 to around 20 and from 5 to around 15 absolute percentage points for BC and KC coals, respectively. These results clearly indicate the potential to significantly improve flotation performance for the Coalburg coal using feed pre-aeration. Following the column flotation tests, the carrying capacity tests were conducted by increasing the feed solids concentration while holding the volumetric feed rate constant at 1050 ml/min. Results revealed that at 6% and 15% solids, additional 1.2 t/h and 1.8 t/h could be recovered, respectively, for a common industrial column application for the BC coal. The projected product rate improvements for the KC coal were equivalent to around 3.3 t/h and 4 t/h for feed solids content of 14% and 12%, respectively. Further analysis on the product size distribution of the KC coal suggests that the improved particle recovery is more pronounced for the finest coal fractions as a result of particle agglomeration, which occurs due to cavitation feed pretreatment. The improvement is likely due to aggregation of the ultrafine coal particles using the micron-sized bubbles generated by cavitation as the bridging medium. Recently published data also suggests the possibility of enhanced attractive interactions between a micron-sized bubble attached to a particle surface and a bubble produced by a conventional generator. This mechanism would provide enhanced flotation rates by improvements in the probability of attachment.

As a result of the laboratory test programs, feed pre-aeration to a flotation system was found to provide enhanced flotation rates and carrying capacities. Based on these positive outcomes, a full-scale cavitation system developed by Eriez Manufacturing Co. was installed into a three-stage StackCell flotation circuit. After installing the cavitation pre-aeration system in the feed pipe to the first StackCell, a detailed full-scale in-plant test program was conducted to optimize the flotation performance, to quantify the recovery improvements and to evaluate the potential of reducing the collector dosage.

CHAPTER 5

5. FEED PRE-AERATION USING CAVITATION – IN-PLANT STUDIES

5.1. INTRODUCTION

The improvements in recovery and carrying-capacity observed from using pre-aeration of flotation feed in laboratory studies led to the development of a commercial scale cavitation system for in-plant studies. The plant chosen for the in-plant evaluation was identified based on carrying-capacity limits that were impacting flotation recovery and the expressed need to reduce collector consumption. A cavitation tube unit, which was detailed in Section 3.2.2,was placed in the flotation feed pipe of a three-stage flotation circuit treating 60 t/h and 11000 L/min (2900 gal/min) of slurry in an operating coal preparation plant that cleans coal from an underground source for use in the metallurgical market.

Choosing this preparation plant had an additional advantage due to the currently commissioned three-stage StackCell flotation circuit from Eriez Flotation Group. The flotation circuit is comprised of three StackCells placed in series, in which the tailings stream produced by one unit is the feed to the next, as described in Section 3.2.3. A characteristic of the StackCell design employing the cavitation tube system in the feed line is the ability to efficiently pre-aerate the pulp before injecting it into the separation vessel. In this system, the bubble and particle attachment occurs in close proximity to the aeration device and results in an increase in the rate of reaction for the overall process. As a result, there was a corresponding decrease in the required retention time for a given application. This indicates that the same flotation recovery can be obtained in a smaller volume with increased capacity. From the laboratory and pilot scale tests, it was found that the preferred arrangement of the StackCell technology is the sequential placement of three cells in series to provide a balance between improving recovery due to less back mixing and the added cost of the new cell (Kohmuench et al., 2010).

Prior to the installment of the StackCells, the flotation circuit of the plant has not been in operation for the last three years. The abandoned flotation circuit consisted of a bank of three 100-ft^3 conventional flotation cells. Since then, the flotation feed material, comprised of the overflow stream of 15" raw coal classifying cyclones, was sent directly to the thickener, which represents a significant loss in revenues. Through the current expansion of the plant with StackCells and cavitation tube system combination, the goal was to minimize this inefficiency by improving the separation performance of the ultrafine circuit.

Flotation feed to the cavitation feed inlet was a pump-fed system in order to meet the pressure specifications of the cavitation tube for the pre-aeration of the feed particles, which required an additional flotation feed sump and pump configuration, along with the piping for the circuit. Performance of the froth flotation circuit was evaluated under different operating conditions, such as flotation chemicals and dosages, froth depth levels in the StackCells, air injection into the cavitation system, etc. Tests were conducted both while the flotation slurry was flowing through the center pipe (all cavitation tube valves closed) and through the cavitation tube system (the center pipe valve closed). The results of the in-plant study are presented and discussed in the following sections.

5.2. RESULTS AND DISCUSSION

5.2.1. Effect of Collector Type

One of the ways to look at the enhanced flotation performance is through the increased capacity of the bubbles that carry the coal particles to the overflow launder of the flotation cell, which is known as the carrying capacity. Throughout the in-plant studies at the preparation plant, three different collectors were used with varying compositions and characteristics. Collector No. 1 was known as mineral (peanut) oil, which was watery and clear in appearance. Collector No. 2 was a type of pine oil with a molasses-like viscosity dark brown-colored liquid. Collector No. 3 was a blend of four lipids (with carboxyl groups) and heavy naphthenics, which was also watery and brown-colored liquid. For

both lower and higher collector dosages, collectors No. 2 and No. 3 showed the best performance for increased capacity.

As shown in Figure 5.1, feed pre-aeration provided a significant increase in carrying capacity regardless of collector type, dosage and froth level (denoted as FL in the figures). In the tests involving collector No. 1, the solids content in the feed and hence the amount of floatable material was higher compared to the tests with the other two collectors and the froth level was low, which lowered froth zone recovery. Under this condition, air addition in the cavitation system had a significant impact on increasing the carrying capacity as a result of a more stable froth phase. For the samples with cavitation only, data points were shifted away from the associated test points due to high feed solid concentrations. The dashed lines in Figure 5.1 show where the data points would have been for similar feed solid contents when using feed pre-aeration with no additional air.

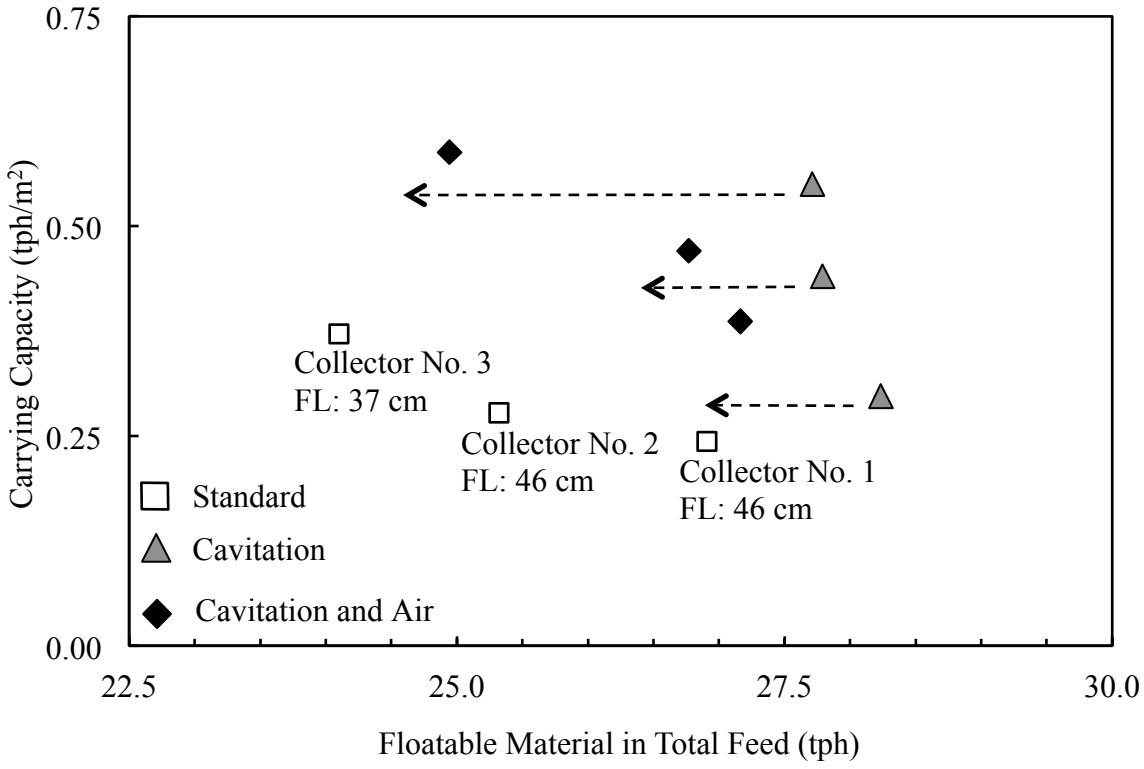


Figure 5.1. Carrying capacity values for different methods and collectors at around 0.11 to 0.22 kg/t; FL=froth level or depth from overflow lip.

For higher collector dosages, the feed solids contents in all tests were nearly equal. As such, the results in Figure 5.2 clearly show a direct comparison of carrying capacity performance under similar conditions. Carrying capacity is increased by nearly 40% over the entire range of feed mass flux values and collector types.

5.2.2. Evaluation of Collector Dosage

At the beginning of the in-plant studies, the preparation plant was employing very little collector to treat the flotation feed material. The dosage of collector No. 1 was around 0.02 kg/t. As a result of the cavitation and air pretreatment techniques, significant improvements were seen even at this low collector rates as shown in Figure 5.3. Relative gains for recovery and carrying capacity were calculated based on the comparison to the tests without cavitation and air pretreatment. Enhanced rates in recovery and carrying capacity were likely a result of the micron-size bubbles nucleated on the surfaces of the coal particles which caused agglomeration and subsequently an elevated flotation rate through enhanced collision efficiency.

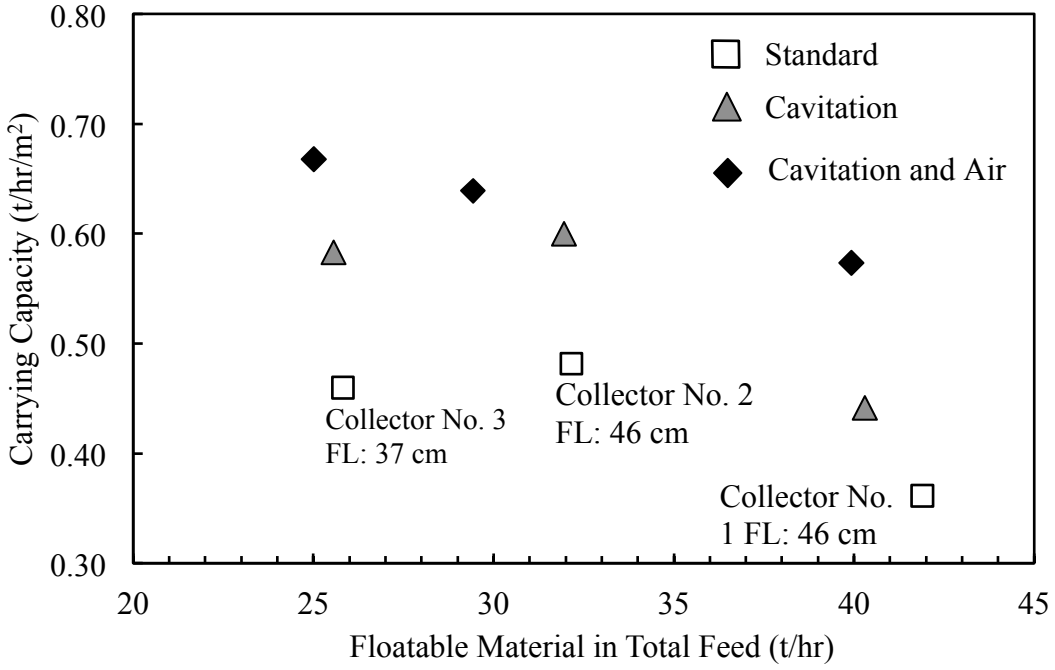


Figure 5.2. Carrying capacity values for different methods and collectors at around 0.22 to 0.33 kg/t.

Similarly, the agglomeration due to the bridging action between the coal particles and micro-bubbles improved the amount of bubble-particle aggregates that can be carried on the bubble surfaces, which resulted in higher carrying capacity values. After discovering the low collector dosage, the collector addition was increased to 0.11 kg/t, which was the lowest rate of collector addition throughout the remaining test program. Subsequently, collector dosages were incrementally increased for different brands to make a comparative study with and without the feed pretreatment methods.

To evaluate the impact of collector dosage, tests were performed using collector No. 3 at three dosage levels of 0.11, 0.22 and 0.33 kg/t (0.25, 0.50 and 0.75 lbs/t, respectively) with and without air added to the feed of the cavitation system and without feed pre-aeration. Operating at these low dosages was required due to the strong frother characteristic of this non-viscous collector, which reacts very fast to form numerous bubbles in the flotation circuit. A polyglycol type of frother, which is a stronger surface tension reducer that forms a more stable froth compared that of alcohol type, was added at a total concentration of 13.5 ppm.

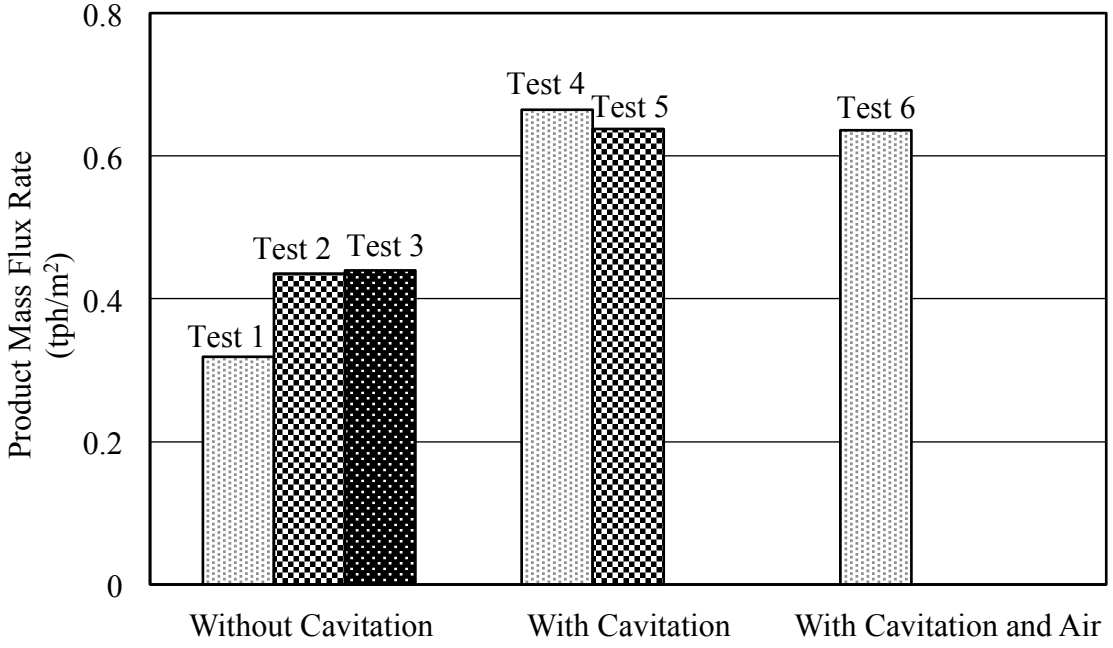


Figure 5.3. Improvement in the product mass flux as a result of feed pre-aeration at a collector dosage of 0.02 kg/t.

The recovery gained after turning on the cavitation system is shown in Figure 5.4 as a function of collector dosage. The standard test without feed pre-aeration is shown as the baseline of zero recovery gain. For the tests with the cavitation only, the recovery gain is around 10 absolute percentage units for all three collector dosages. On the other hand, with the addition of air, an increasing trend of recovery gain with the elevated collector dosage was realized when air was added to the cavitation system. A nearly 17 absolute percentage unit increase in recovery was obtained at a collector dosage of 0.33 kg/t.

The improvement in recovery can be seen more clearly from the collector dosage relationship shown in Figure 5.5. Recovery can be enhanced by about 16 absolute percentage points at the highest amount of collector from the test without cavitation to that with cavitation and air addition. Without the use of feed pre-aeration, the combustible recovery achieved at a collector dosage of 0.33 kg/t was about 20%. A nearly equal recovery value was achieved at 0.11 kg/t of collector when using feed pre-aeration with air added to the cavitation system. This means that the collector cost can be cut to 1/3 while using the cavitation and air together, which would have a significant impact on the reagent cost of a plant. Without air addition to the cavitation system, the same recovery values were obtained with 50% less collector as compared to no feed pre-aeration.

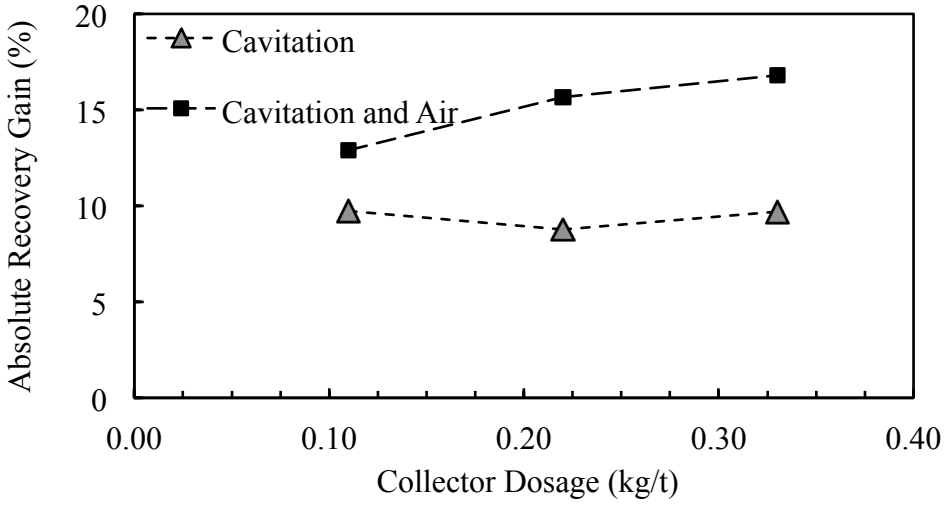


Figure 5.4. Flotation performance in terms of added recovery gain while taking the conditions without cavitation pretreatment as baseline.

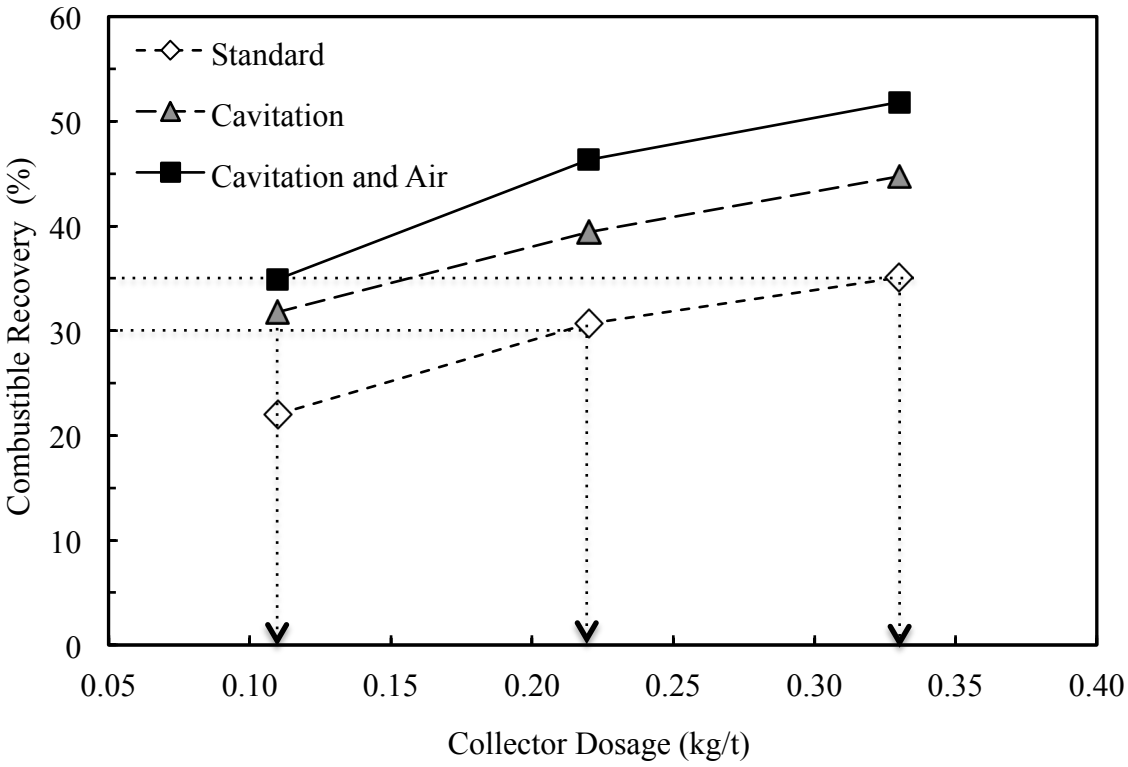


Figure 5.5. Collector dosage reduction achievable using cavitation with and without the addition of air.

Another way to look at the enhanced flotation performance is through the increased capacity of the bubbles to carry the floatable coal particles to the overflow launder of the flotation cell. As shown in Figure 5.6, the cavitation process (with and without air addition) had a substantial impact on the carrying capacity especially when using low collector dosages. These results clearly indicate that feed pre-aeration has a significant impact on both flotation rate and carrying capacity of the ultrafine particle given that collector enhances surface hydrophobicity. The aggregates formed by the micron-sized bubbles on the ultrafine particle improve the flotation rate through the probability of collision, which may counter the drop in the probability of attachment caused by the decrease in collector dosage. There is also the possibility of an elevated probability of attachment when surface nucleated bubbles interact with conventional bubbles. Regardless of the fundamental reason, the positive impact provided by feed pre-aeration on carrying capacity at any collector dosage is clearly evident by the plant data.

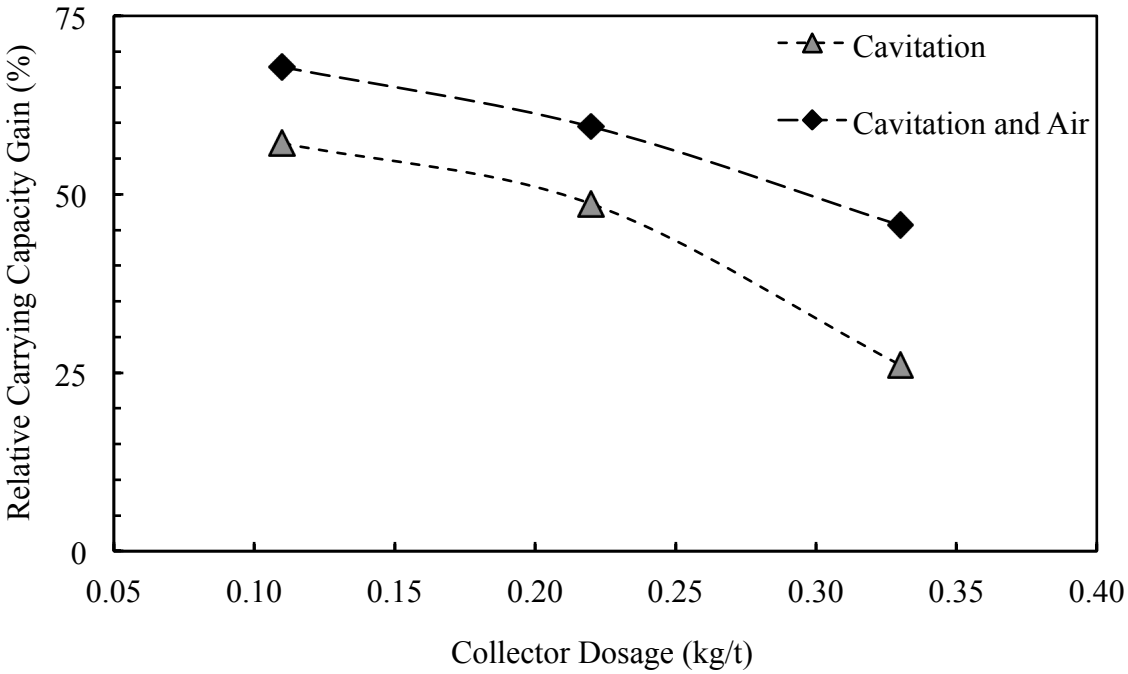


Figure 5.6. Additional carrying capacity gain with collector dose while taking the conditions without cavitation pretreatment as baseline.

5.2.3. Importance of Collector Application Method

One of the adjustments made during the in-plant tests involved the way in which collector was added to the flotation circuit. Initially, collector and frother were injected into the flotation feed stream at the same location, which was one floor above the flotation sump. Later, the collector pipe was diverted to drip on top of the flotation sump and placed closer to the flotation feed for better mixing conditions. Finally, the collector line was taken from this location extended to the top floor of the plant where the raw coal classifying cyclones were located. Collector flow was directed into the center of the cyclone overflow tub which was the feed to the flotation circuit. This step was taken in order to allow more time for the collector to be conditioned with the coal particles prior to its way to the StackCells.

Under the same operating conditions, application of collector showed a significant importance on the amount of product material reporting to the concentrate as shown in Figure 5.7. Carrying capacity was increased by about 60% on average for both cavitation methods, i.e., with and without air.

5.2.4. Evaluation of Frother Dosage

In addition to the analysis conducted on collector, frother addition to the flotation circuit was also studied to evaluate potential benefits of the cavitation feed pretreatment. In this evaluation, collector No.1 was applied at a rate of 0.11 kg/t for all tests through the injection to the feed pipe. The test without cavitation was conducted using an alcohol type frother at a total concentration of 14 ppm. Cavitation pretreatments, however, were applied using a polyglycol type frother at a total concentration of 12.5 ppm. As shown in Figure 5.8, carrying capacity values for the tests with and without the cavitation pretreatment were almost equal. However, in the case of cavitation pretreatment, 12% less frother was used. The addition of air provided around 60% increased carrying capacity, which might be due to a better dispersion of frother with the additional air.

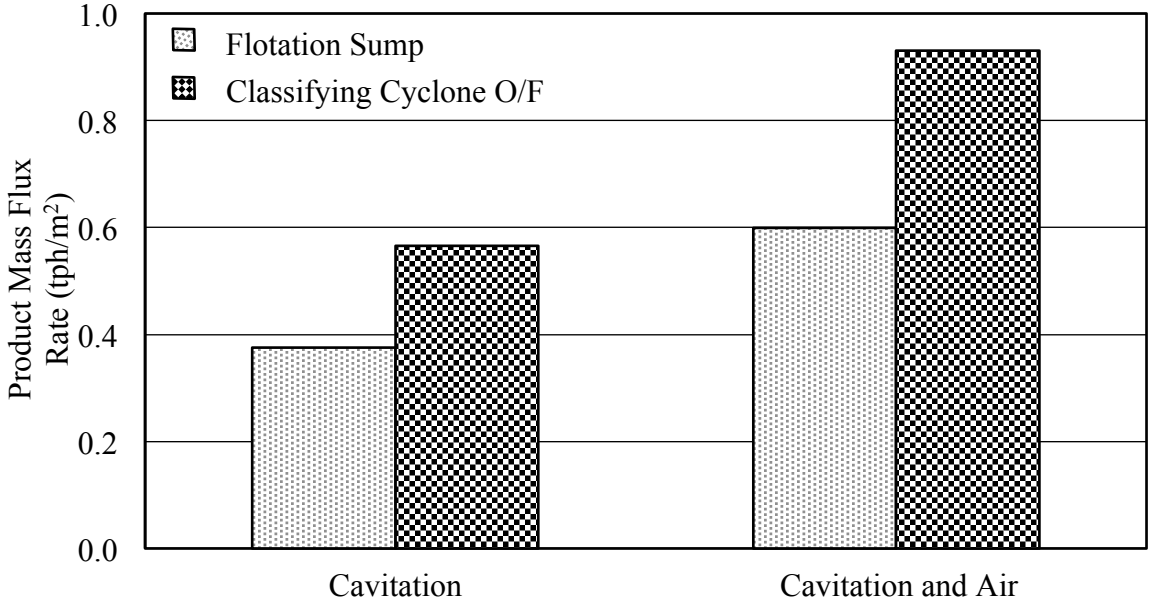


Figure 5.7. The impact of collector application on carrying capacity while employing cavitation pretreatments with and without the air addition.

Although both the frother type and the dosages were changed in this test, a combination of cavitation pretreatment and a stronger frother showed improved flotation performances while employing less frother to the cell.

To achieve a head-to-head comparison for the impact of polyglycol frother with the cavitation pretreatments, another test was conducted under the same conditions in which the collector was added in the flotation sump at a rate of 0.3 kg/t. For the test without the cavitation pretreatment, the total frother concentration was 20.5 ppm. For the cavitation tests with and without the air addition, the total frother concentration was only 13.5 ppm. As shown in Figure 5.9, pre-aeration using the cavitation system without air addition performed better than the test without pretreatment. This suggests that, under the same operating conditions, the frother consumption can be reduced by more than 30% in the presence of cavitation pretreatment. Air addition prior to the cavitation tube system gave an additional 50% increase in the carrying capacity response, which is similar to the previous test.

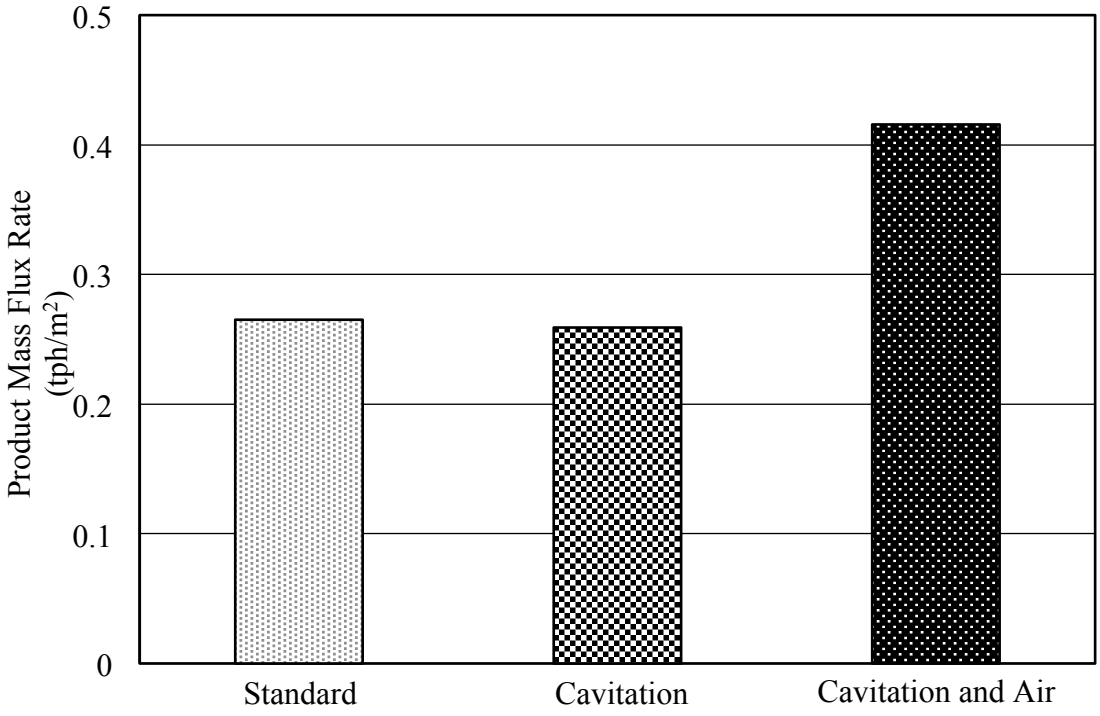


Figure 5.8. The impact of frother type and concentration on carrying capacity with the cavitation pretreatments, where (*) denotes a different testing condition.

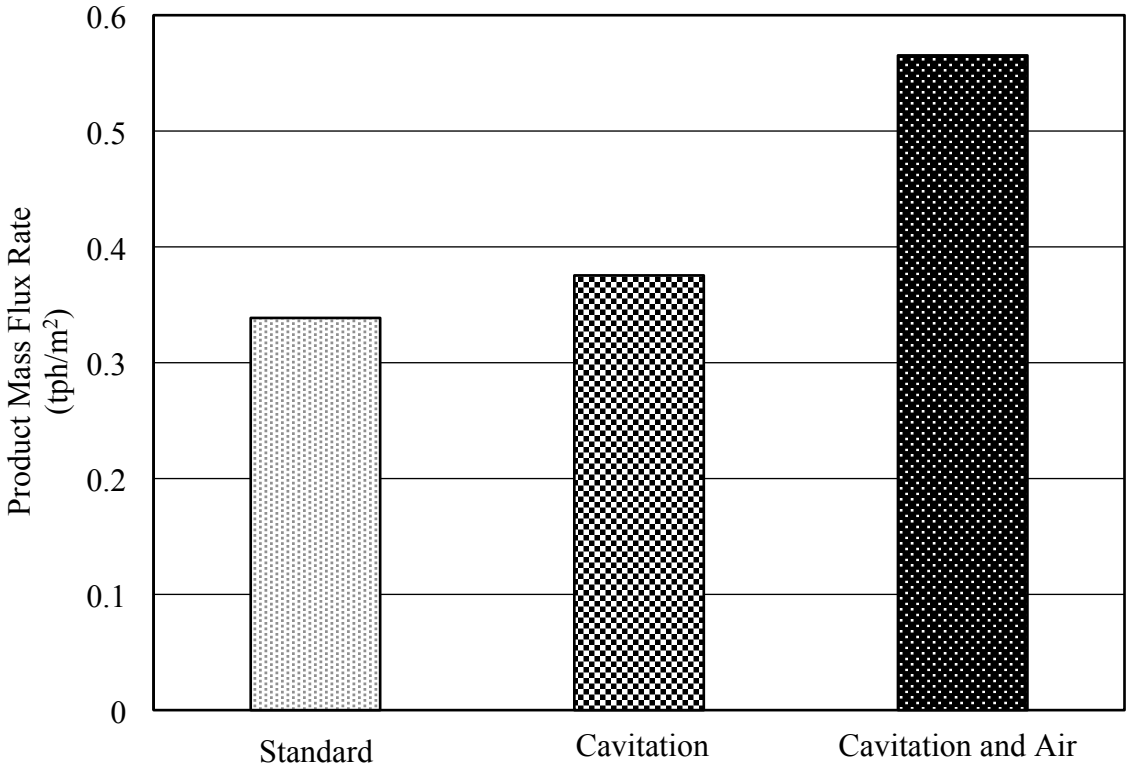


Figure 5.9. The impact of frother concentration under the same conditions on carrying capacity with the cavitation pretreatments.

The impact of cavitation pretreatment with air addition is even more apparent when the bubble-particle aggregates from StackCell products were compared visually as they were taken to buckets for sampling, as shown in Figure 5.10. Pictures for all product streams (left-#1, center-#2 and right-#3 StackCell product) show a clear distinction between bubble-particle aggregate sizes of the tests that employ both cavitation and air addition and the test without any pretreatment. This evidence also confirms the findings of the carrying capacity and the consequent product size analysis during the laboratory studies (Figure 4.30), which suggest that the cavitation pretreatment allows fine particles to be agglomerated through the bridging mechanism of the micron-sized bubbles.

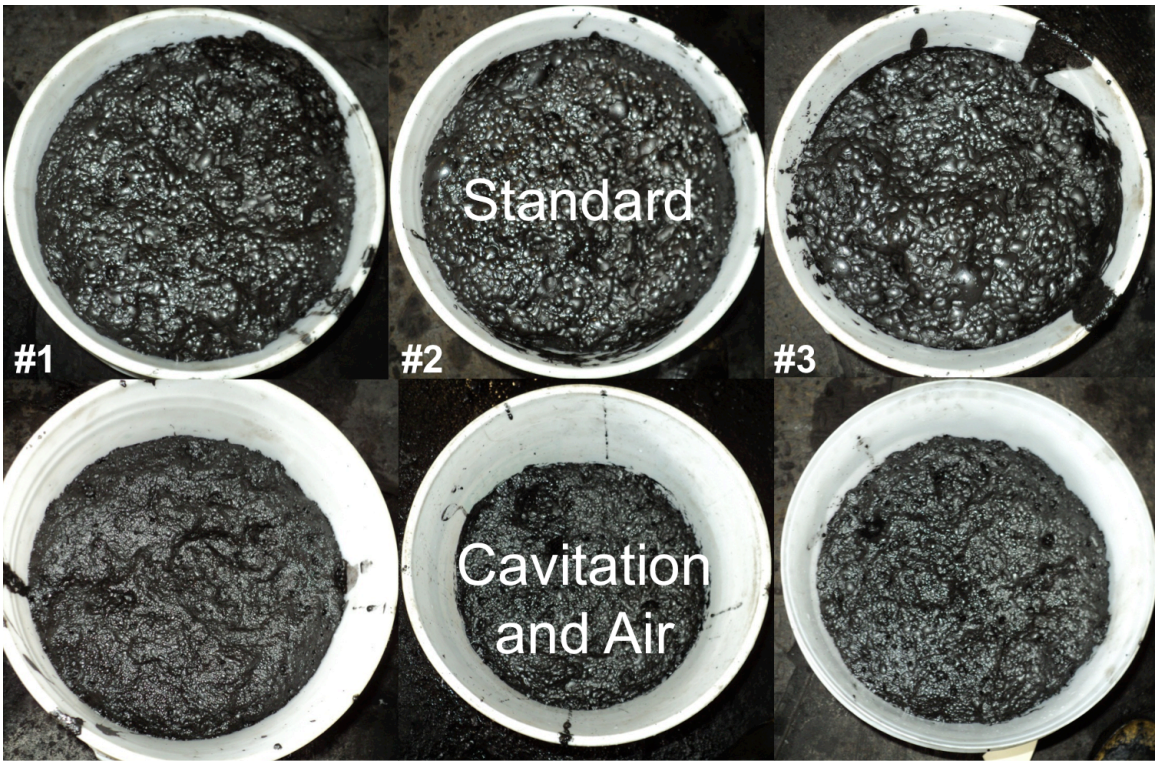


Figure 5.10. Visual comparison of the bubble-particle aggregate sizes under different conditions from the first (left) to the third (right) StackCell product.

The bubble size also indicates the impact of bubble size on improved recovery values, which is several times smaller for the test that employ both cavitation and air addition pretreatment. Air addition was applied at very small volumetric rates (1.4- to 1.55-m^3/min, 50- to 55-ft^3/min) through a portable air compressor. However, as shown from the comparative studies above, air addition is not required for the improved performance.

5.3. CONCLUSIONS

Based on the positive laboratory results, a full-scale cavitation system developed by Eriez Flotation Divison-USA was installed into a flotation circuit that was comprised of three StackCells placed in series in which the tailings stream produced by one unit is the feed to the next. After installing the cavitation pre-aeration system in the feed pipe to the first StackCell, a detailed full-scale in-plant test program was conducted to optimize

performance, quantify recovery improvement and evaluate the potential of reducing the amount of flotation reagents.

Prior to the start of the in-plant tests, the preparation plant changed the coal feed source to the Peerless seam to produce coal for the metallurgical market. The volumetric feed rate to the circuit was around 11000 L/min with a solids flow rate of 60 t/h under standard solid concentrations (≈8.5%). Identical recovery values were achieved using 50% less collector when utilizing the cavitation system with no air and 67% less collector when injecting 1.4-1.55 m^3/min (50-55 ft^3/min) of air in the feed to the cavitation system. At a constant collector dosage, recovery increased by 10 absolute percentage point with cavitation without additional air and 17 absolute points when additional air is provided to the feed of the cavitation system. Carrying capacity improved by 46% to 68%.

The industrial cavitation tube system used in this research can be easily installed into existing flotation circuits given the spacing and piping diagram of the plant. In addition, a pump-fed system is required to ensure the minimum 172-kPa (25-psi) pressure drop at the entrance of each cavitation tubes for proper micro-bubble generation on coal surfaces in the feed slurry. Air addition to the system is not required but can be implemented using a small external air compressor as an additional way to increase the micro-bubble population prior to the cavitation tubes. The amount of air addition was minimal compared to the feed flow rate when it was employed, i.e., 1.4-1.55 m^3/min air addition for 11000 L/min feed slurry flow.

As a result of the in-plant testing, feed pre-aeration to a flotation system was found to provide enhanced flotation rates and carrying capacities. The improvement was found to be preferentially achieved on the ultrafine particle size fractions of the feed. The improvement is likely due to aggregation of the ultrafine coal particles using the micron-sized bubbles generated by cavitation as the bridging medium. Recently published data also suggests the possibility of enhanced attractive interactions between a micron-sized bubble attached to a particle surface and a bubble produced by a conventional generator.

CHAPTER 6

6. APPLICATION OF HIGHLY HYDROPHOBIC PARTICLES FOR ENHANCED COAL RECOVERY

6.1. INTRODUCTION

As previously mentioned in Sections 1.1 and 2.1, the amount of mass being carried by a bubble during the flotation process is a function of particle size, particle density and the packing density of the particles on the bubble surface. The maximum capacity reporting to the top of the flotation cell can be estimated from the bubble surface area flux, S_b, in Eq. (2.6) after neglecting the effects of particle agglomeration. At low feed solid contents, the separation is based on differences in flotation rates, which is commonly referred to as rate-limited conditions where sufficient bubble surface area is available throughout the froth zone to ensure nearly 100% froth zone recovery as shown in Figure 6.1. When the bubble surfaces reporting to the top of the cell are completely full, the product mass rate reaches a maximum which is known as carrying capacity limiting conditions.

The maximum carrying capacity value will be maintained over any further increases in feed mass flux if the floatable material has a narrow particle size distribution (mono-size). However, for floatable material with a broad size distribution a further elevation of the feed mass flux will result in a drop in the product mass flux due to the selective detachment of the coarse particles, which have more overall mass than the fine particles that remain on the bubble. Since the amount of mass being carried by a bubble is a function of particle size, particle density and the packing density of the particles on the bubble surface, coarse particles are hypothesized to preferentially detach first from the bubble.

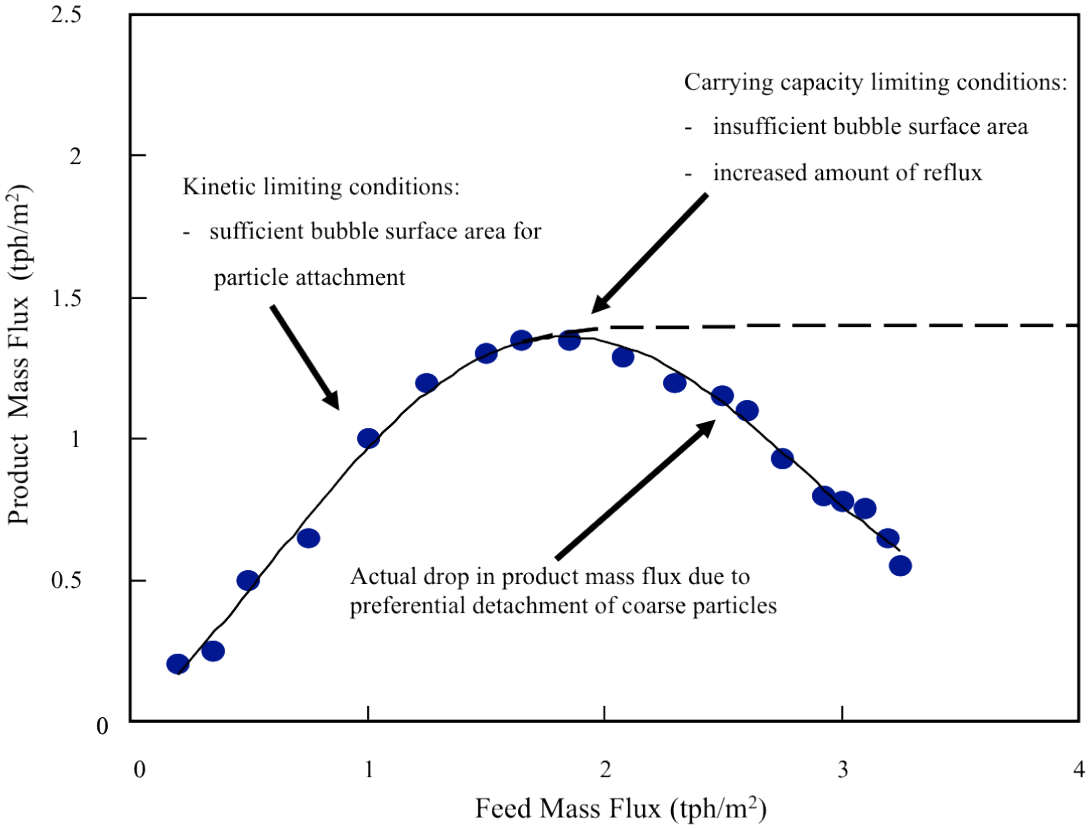


Figure 6.1. Illustration of kinetic limiting vs. carrying capacity limiting flotation conditions (Honaker and Ozsever, 2002).

With the addition of plastic particles in the feed, the recovery responses showed that the carrying-capacity may be maintained at a given product mass flux rate with no selective detachment of coarse particles. This hypothesis was evaluated through carrying capacity tests by varying the feed solids content while holding the volumetric feed rate constant. As a result, the particle retention time is effectively held constant over the range of feed solid concentrations.

Extensive research indicated that froth flotation performance varies significantly as a function of particle size. As previously discussed in Section 1.1, the upper particle size limit is associated with the detachment process of the bubble-particle aggregates from the

bubble surfaces. Therefore, the probability of detachment, P_d, is higher for coarse particles, which is around 500 microns for coal.

Luttrell (2010) provided evidence of the selective detachment of coarse particles using data collected from an operating flotation circuit. Samples were collected from the flotation circuit on a daily basis and analyzed for particle size distribution and ash content which allowed the calculation of size-by-size recovery as shown in Figure 6.2. Recovery of coal in particle size fractions greater than 250 μm (65 Mesh) was significantly sensitive to plant operating conditions, which may be caused by the changes in the plant operation such as increased feed solids concentration. Thus, maximizing flotation recovery requires limiting coarse (+250 μm) material in the feed or developing an alternative that will provide a consistent recovery of coarser particles. Stabilizing the flotation froth by minimizing bubble coalescence is a potential method to reduce particle detachment and thus increase coarse particle recovery. The proposed method achieves this task through the addition of hydrophobic ($\theta \approx 85°$) plastic particles. The plastic material is comprised of a significant amount of magnetite which makes the material recoverable by a low intensity magnetic separator. Stabilization of the froth and maximizing bubble surface area rate (S_b) to maximize coarse particle recovery is the focus of the wok presented in this chapter.

6.1.1. Coalescence

In a three-phase froth structure, the network of interconnected thin liquid films in the froth, i.e. lamellae, separating the bubbles contain the selectively attached hydrophobic particles. In addition, Plateau borders are known as the intersection of three thin films (or lamellae) in froth and four Plateau borders form a vertex which contain the liquid slurry and freely moving particles (Neethling and Cilliers, 2003; Cilliers, 2007; Dürr-Auster, 2008).

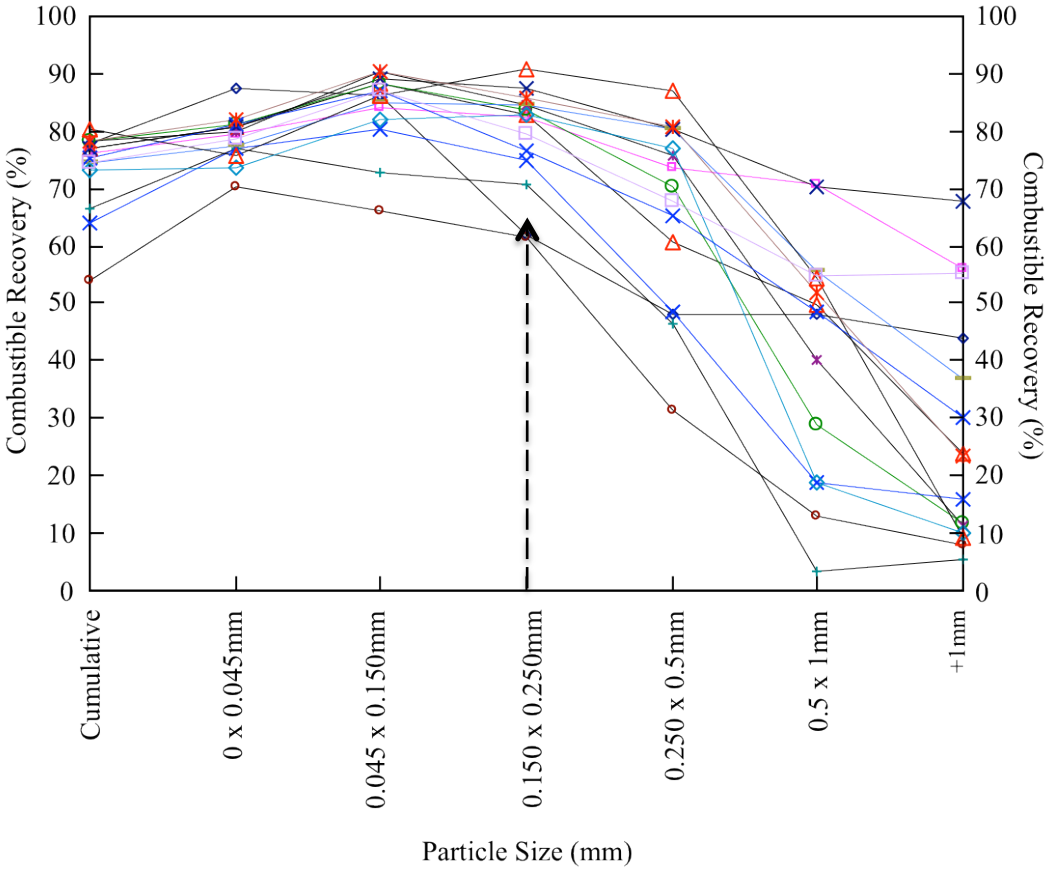


Figure 6.2. Variability in plant flotation performance as a function of particle size (Luttrell, 2010).

As the particle-bubble aggregates rise through the froth phase, the bubble walls thin due to water drainage thereby inducing bubble coalescence. Bubble coalescence within the froth or bursting on the surface occurs when two bubbles first collide and trap a small amount of liquid with some hydrophobic particles between them in the lamellae. Particles that are not attached to lamellae move freely through the Plateau borders and can drain back into the pulp. Liquid drainage continues until the liquid film separating the bubbles reaches a critical thickness. The thinning and ultimately the rupture of the liquid film beyond this critical value results in the coalescence of two neighboring bubbles with the release of attached particles into the Plateau borders and the destabilization of liquid foams. Since the time for the film rupture to take place is generally faster than that of the film thinning process by the trapped liquid, enough time should be given to the latter for

coalescence to occur. In other words, a particle needs to stay at the interface sufficiently longer than the liquid drainage time between the interfaces in order for coalescence to take place (Marrucci, 1969; Pince and Blanch, 1990; Chhabra, 1993; Lin et al, 1998; Dürr-Auster, 2008; Yang et al., 2012).

The importance of the Plateau borders and vertex network on flotation is well known from the relationship between the gangue recovery and water recovery. Entrainment from the pulp is solely responsible for the gangue particles entering the Plateau border network as shown in Figure 6.3. However, hydrophobic particles are both entrained from the pulp and enter the Plateau borders by coalescence or lamellae failure. The motion of both the hydrophobic and hydrophilic particles is determined only by their physical properties when they are within the Plateau borders, not due to surface properties. Since the flotation froths are unstable and the bubbles coalesce in the froth and burst on the surface, the froth rapidly undergoes significant structural change, which makes the prediction of coalescence and bursting is highly complex (Neethling and Cilliers, 2003; Cilliers, 2006; Cilliers, 2007).

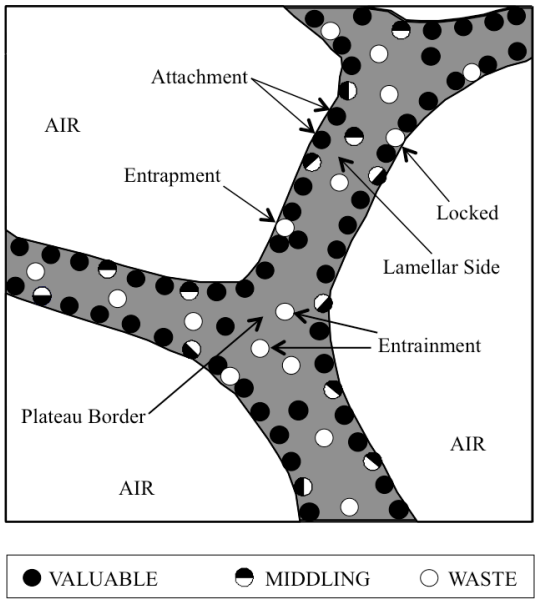


Figure 6.3. Plateau border network in the presence of flotation feed material with different characteristics (Honaker, 2008).

As a result of the coalescence mechanism, the total bubble surface area of the froth declines over time as the aggregate rises to the top of the cell. In addition to the coarse particles, selective detachment of the weakly hydrophobic particles also occurs when particles compete for attachment sites. Depending on surface area availability, the detached particles can re-attach to a bubble at a lower point in the froth zone.

Overall, coalescence is a thermodynamically favored process since it involves surface area reduction by joining two bubbles in a liquid to form one larger bubble. As mentioned above, bubble coalescence takes place in three successive steps: 1) approach of the bubbles and bubble-bubble collision and thin film formation, 2) film drainage and 3) film rupture. These steps need to take place during the collision process to realize bubble coalescence. Among the three steps, film drainage is interrelated both to the bubble collision and the film rupture (Henry, 2009).

6.1.2. Drainage

One of the key processes in froth flotation is the transportation of particles by being attached to the bubble lamellae or by remaining unattached to move through the Plateau borders and become drained. This is determined by the change in bubble size from the pulp-froth interface to the froth launder in addition to the air fraction entering the froth bursting on the surface. The drainage (or recovery) of liquid depends on the motion and distribution of liquid throughout the Plateau borders, which represent significantly different flow behaviors between the liquid draining through foams (and froths) and a packed bed of solid particles. This is because the Plateau borders in the foam, through which the liquid drains, change dimension with the variation in liquid velocity. However, in the packed beds, the channel diameters are fixed (Cilliers, 2007).

The one-dimensional drainage equation based on a force balance on the liquid in the Plateau borders was originally reported by Leonard and Lemlich (1965) and independently extended for two-dimensional flowing foams by Verbist et al. (1996).

For flotation froths with low volumetric liquid fractions, the two-dimensional foam drainage equation (Eq. (6.1)) can be used which represents a balance between the gravity, viscous drag and capillary forces. In the froth phase, gravity acts downwards, viscous drag occurs as the liquid moves relative to the air bubbles and capillary suction depends on the changes in the curvature of the Plateau border interfaces. This is the key difference between foam drainage and drainage through a packed bed of solids in a froth (Neethling and Cilliers, 2003; Cilliers, 2007). The expression to quantify the liquid drainage velocity, v_1, is:

$$v_1 = -k_1 A_{PB} - \frac{k_2}{\sqrt{A}} \frac{dA}{dy} + V_g , \tag{6.1}$$

where A_{PB} is the cross-sectional area of a Plateau border, which changes with froth height, v_g is superficial gas rate, k_1 constant is the balance between gravity and viscosity and k_2 constant is the balance between capillary suction and gravity.

The constants k_1 and k_2 can be defined as:

$$k_1 = \frac{\rho g}{3 C_{PB} \mu} , \qquad k_2 = \frac{\left(\sqrt{\sqrt{3} - \frac{\pi}{2}} \right) \gamma}{6 C_{PB} \mu} , \tag{6.2}$$

where ρ, γ, μ, and C_{PB} are the density, surface tension, viscosity and viscous drag coefficient of the liquid (or slurry in the case of flotation froths) in the Plateau borders, respectively. C_{PB} decreases with increased interface mobility, however, in the case of solid-coated flotation froths, the interface can be considered as immobile, where $C_{PB} \approx 50$.

According to Haas and Johnson (1967), the main driving forces for drainage are gravity and capillary suction and there are indeed two types of drainage: drainage of liquid from films to borders due to capillary suction and drainage of liquid through the network of borders due to gravity. Capillary suction is a function of the pressure difference between the foam film and the border, as shown in a Figure 6.4 of a single border and the pressure gradient induced by capillary suction (Dürr-Auster, 2008).

The pressure gradient results from the curvature of the liquid-gas surfaces and can be expressed by:

$$\Delta P = P_{film} - P_{border} = \frac{\sigma}{R_i} \tag{6.3}$$

where P_{film} and P_{border} are the hydrostatic pressures in the liquid film and the border, respectively, σ the surface tension and R_i is the radius of curvature. In froth flotation, the dimensions of the network of liquid channels vary with the liquid content and the bubble size. Eq. (6.3) also indicates that the rate of film (lamellae) drainage is a function of the bubble size distribution which is proportional to the bubble curvature (Dürr-Auster, 2008).

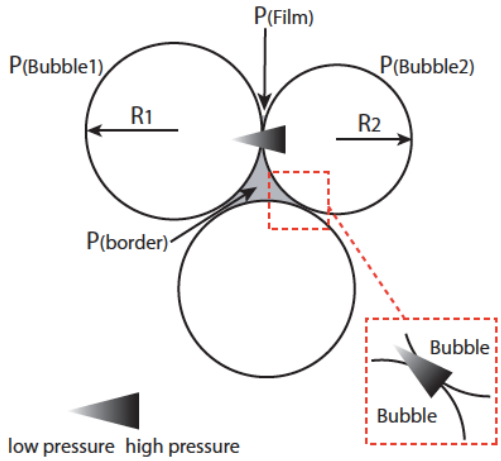


Figure 6.4. Profile view of a single foam border showing the high- and low-pressure gradients around Plateau borders for bubbles of different diameters (Dürr-Auster, 2008).

6.1.3. Froth Stability

Froth stability is an essential component of a flotation system for the achievement of satisfactory separation. An overly stable (metastable) froth is difficult to handle, and results in hydraulic entrainment of undesired particles. On the other hand, an unstable froth may not be able carry the attached hydrophobic particles to the froth launder. Froth stability is defined as the ability of building a froth depth without causing coalescence.

There are a number of variables that can affect the froth stability of a flotation system. These variables can be classified under three categories, i.e., hydrodynamic conditions, particle properties and chemical regime. Avery-Edwards et al., (1994) provided a breakdown of the key effects as:

1. Viscous Effects:

Under high bulk viscosity conditions, every motion, including that causing the drainage of the bubble-wall, slows down. In addition, high surface viscosity delays the drainage of the thin bubble film and the surface deformation that can result in bubble breakage.

2. Marangoni Effect:

Gibbs surface elasticity, which is commonly referred to as the Marangoni effect, is the surface tension gradient along the air-liquid interface that acts to preserve the film thickness and to prevent bubble coalescence as shown in Figure 6.5.

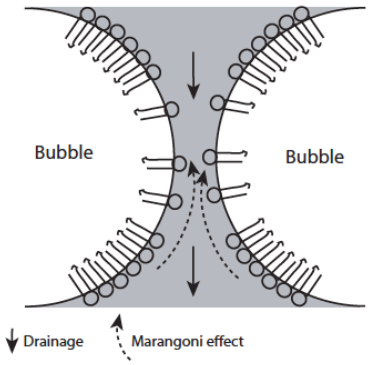


Figure 6.5. Liquid drainage between two bubbles and the preventing Marangoni effect in a cross-sectional view (Dürr-Auster, 2008).

3. Repulsive Effects:

In ionic systems, foam film stability can be maintained by the repulsion of electric double layers. In nonionic systems containing adsorbed polymer chains, entropic repulsion has a stabilizing effect for very thin films.

4. Other Effects:

In addition to the abovementioned effects, the bubble collapse can be delayed by slowing down the bubble size changes and the mechanical stress through reduced gas diffusion between bubbles. Also, film elasticity plays a role in order to recover from the force applied on the bubble thin film.

As reported by many researchers, the stability and drainage of a three-phase (gas-liquid-solid interface) froth depends strongly on the hydrophobicity of the particles present in the froth. Cho and Laskowski (2002) and Tan et al. (2005a, b) showed that the froth stability also depends on the size, shape and wetting properties of the particles.

Froth stability provided by hydrophobic solid particles reportedly occurs due to restriction of the drainage of the liquid from the thin water layer surrounding air bubbles. In short, the stronger the particle adsorption to the bubble, the more stable the froth becomes. Thus, froth stability benefits from the increase in the contact angle of particles to a certain critical value. Experimental data suggests that hydrophobic particles with contact angles between 65° and 90° enhance froth stability and those with contact angles greater than 90° destabilize the froth (Dippenaar, 1982b; Garrett, 1993). In the latter case, the particles begin to work as bridges between bubbles that eventually are drawn together by the highly hydrophobic solid surface. As a result, the water thin film thins and bubble coalescence occurs. However, in the case of partial wetting, the particles trap the liquid and make the film more stable (Ip et al., 1999). Large concentrations of small hydrophobic particles were found to stabilize the froth through a closely packed monolayer bed that prevents the particles going out of the film and keeps the interfaces contacting each other for film rupture (Dippenaar, 1982a). In terms of the viscosity, the

presence of hydrophobic particles adsorbed on floatable particles significantly increase the froth phase, which in turn slows down the drainage process (Jiang, 1998). Froth stability for coarse coal particles is determined exclusively by the additional collector dosage in the flotation system, which reduces the selectivity between the particles of different qualities. As an alternative approach, improvements in coal recovery, especially for coarse sizes, was evaluated in the presence of recoverable plastic particles in the feed.

6.1.4. Previous Research

The study reported by Munoz-Diaz (2007) was initially performed to assess the flotation rate and the corresponding recovery improvement realized by the addition of hydrophobic plastic material at different concentrations (0%, 2%, 5% and 10% by weight) in a laboratory conventional flotation cell. The results presented in Figure 6.6 summarizes the average results obtained from repetitive tests for both Pittsburgh No. 8 and Coalburg coals under the same conditions. The results from the multiple tests indicated excellent repeatability. For both Pittsburgh No. 8 and Coalburg coals, the addition of 10% (by weight) plastic material significantly improved the flotation recovery by about 10 and 15 absolute percentage points, respectively, after one minute of flotation.

The data presented in Figure 6.6 was used to assess the effect of the plastic addition on the flotation rate achieved in the first one minute. Table 6.1 is the average one-minute flotation rate and recovery values achieved with and without plastic material. The plastic addition increased flotation rate by 45% for the Coalburg coal and 26% for the Pittsburgh No. 8 coal which provided a significant recovery increase for both coal sources. The contact angle of the plastic material was reported to be around 84° which was ideal for froth stability.

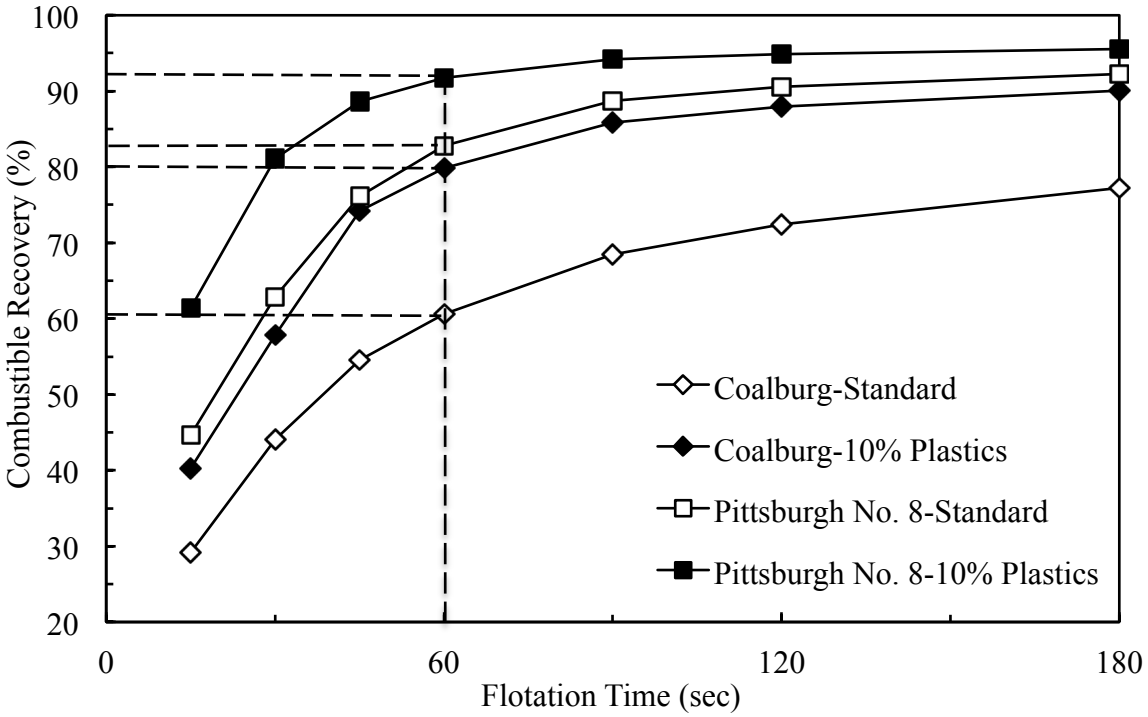


Figure 6.6. Flotation performances at different concentrations of magnetic plastic material addition using Coalburg and Pittsburgh No. 8 coals (Munoz-Diaz, 2007).

The data presented in Figure 6.6 was used to assess the effect of the plastic addition on the flotation rate achieved in the first one minute. Table 6.1 is the average one minute flotation rate and recovery values achieved with and without plastic material. The plastic addition increased flotation rate by 45% for the Coalburg coal and 26% for the Pittsburgh No. 8 coal which provided a significant recovery increase for both coal sources. The contact angle of the plastic material was reported to be around 84° which was ideal for froth stability.

In order to determine the flotation rate, the recovery data achieved within the first minute of flotation were used. The average of the recovery values from the repetitive tests showed that, the flotation rate of the Coalburg and Pittsburgh No. 8 coals were increased by 45% and 26%, respectively, by the addition of the magnetic plastic particles at a concentration of 10% by weight, as shown in Table 6.1.

Table 6.1. Flotation performances after repetitive tests for Coalburg and Pittsburgh No. 8 coals at 0% and 10% magnetic plastics using a residence time of one minute (Munoz-Diaz, 2007).

Test Identification	Coalburg Coal		Pittsburgh No. 8 Coal	
	Flotation Rate (min^{-1})	Flotation Recovery (%)	Flotation Rate (min^{-1})	Flotation Recovery (%)
Standard	0.51	61.1	1.04	80.7
10% Plastic	0.74	77.4	1.31	91.7

During the initial study by Munoz-Diaz (2007), Pittsburgh No. 8 coal was used to assess the impact of 10% plastic material addition (by weight) while the slurry pH was varied from 3.9 to 10.1. Neutral pH conditions, which was found to be slightly lower than 7.0, have shown the best separation performances compared to significantly depressed flotation recovery values obtained under pH values of 3.9 and 10.1. The addition of plastic particle at 10% concentration (by weight) increased the flotation recovery by about 50 absolute percentage points for both low and high pH conditions. The improved recovery response is a direct result of the increased flotation rate values, as shown in Table 6.2.

Table 6.2. Flotation rate improvements achieved under varying pH conditions when adding plastic particles to Pittsburgh No. 8 coal at a concentration of 10% by weight (Munoz-Diaz, 2007).

Test Identification		Flotation Rate (min^{-1})	Flotation Recovery (%)
pH 7.4	Standard	0.66	60.5
	10% Plastic	1.32	96.0
pH 3.9	Standard	0.30	32.8
	10% Plastic	1.51	85.8
pH 10.1	Standard	0.30	32.8
	10% Plastic	1.33	82.7

Using a coal source with good flotation characteristics, the feed solids content was varied from 2 to 12% in the previous study while maintaining the volumetric feed rate at 800-ml/min flow rate. Similar to the proposed mechanism illustrated in Figure 6.1, the product mass flux rate increased in direct proportion to the amount of floatable material entering the feed stream as the feed solid content is increased as shown in Figure 6.7. However, after the carrying capacity limit is reached at around 1.2 t/h/m^2, a further increase in the feed solids concentration significantly reduced the amount of material that can be carried on bubble surface, which in turn sharply decreased the amount of product reporting to the concentrate. With the addition of plastic particles at 5% and, especially, at 10% concentration, improved the carrying capacity conditions were seen compared to that with no plastic particles. In fact, additional increase in the feed solids concentration indicated a near constant product mass rate after reaching carrying capacity in the presence of 10% (by weight) plastic particles in the feed slurry.

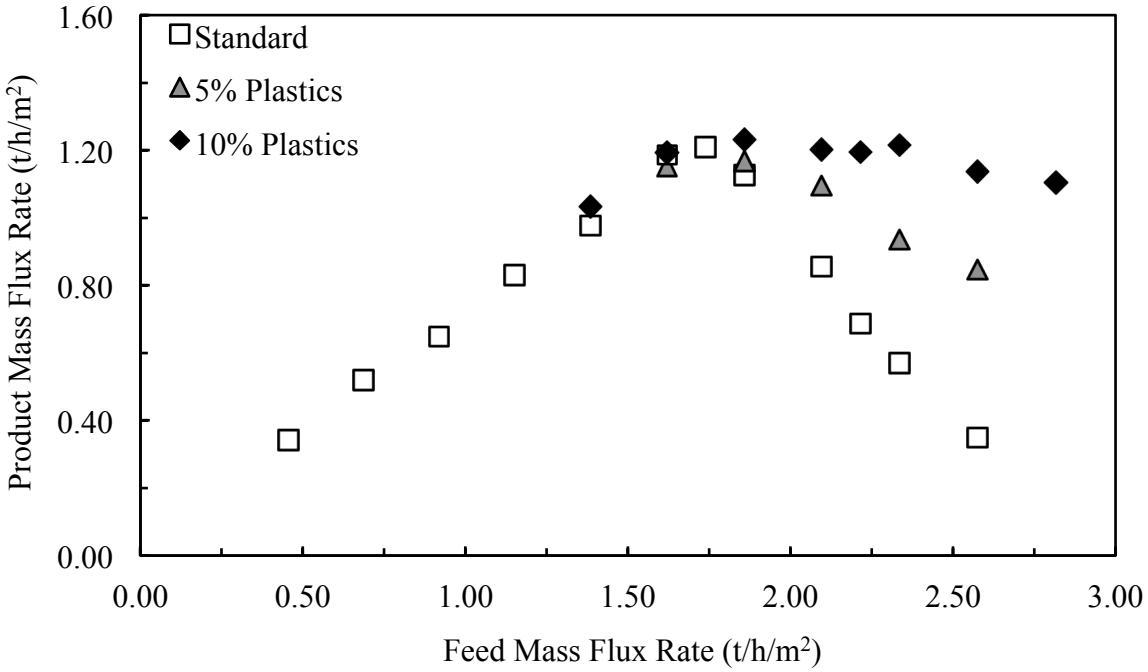


Figure 6.7. The impact of plastic particle addition at varying concentrations on carrying capacity characteristics for the Pittsburgh No. 8 coal (Munoz-Diaz, 2007).

In conclusion, the previous study reported by Munoz-Diaz (2007) has shown promising results indicating a significant enhancement in separation performance thorough the addition of magnetic hydrophobic particles to the flotation process. From the previous research, the detachment process has been shown to be selective toward the rejection of the more weakly hydrophobic solids. However, the most significant discovery was the doubling of the flotation rate and the improvement was the greatest for the coarsest particle size fractions.

In the current research, laboratory conventional and column flotation cells were used to collect the necessary data needed to fully validate previous findings and quantify the fundamental mechanisms governing the impact of the magnetic plastic material addition to the flotation system. Coal samples of varying degrees of floatability were used in the preliminary study and in the current research, respectively, as the test material to evaluate the effect of change in the flotation processes.

Using well-known fundamental relationships, flotation rates and the resulting recovery responses were quantified. In addition, to exploit the change in carrying capacity relationship, experiments were performed to explain the preferential recovery improvement observed for the coarse particles in the presence of hydrophobic plastic material. Flotation rate improvements related with the surface properties, especially under low and high pH conditions, were also evaluated under specific characterization studies.

6.2. RESULTS AND DISCUSSION

The impact of external hydrophobic material addition on the flotation performance was initially studied and promising results were reported by Munoz-Diaz (2007) using Pittsburgh No. 8 and Coalburg coal samples from Monongalia and Logan Counties in West Virginia, respectively. From these two different bituminous coal samples, Pittsburgh No. 8 coal was characterized as very floatable (easy-to-float) with relatively high amount of coal pyrite (FeS_2) while the Coalburg coal had a relatively high content of middling (mixed-phase) particles (10% to 20%) with poor flotation characteristics.

PolyMag™ Black Pellet (PMBP) was used as the external hydrophobic material, which is a plastic product that contains a significant amount of magnetite that can easily be recovered using a low intensity magnetic separator.

The current research study aims to validate the previous findings and advance the fundamental understanding of the mechanisms involved for the improved flotation performance from the addition of hydrophobic plastic particles. This section is divided in two subsections to describe the results obtained from flotation rate tests conducted in a laboratory conventional cell followed by experiments performed in a continuously operated flotation column. The flotation tests were performed over a range of feed, operating and surface chemistry conditions.

6.2.1. Conventional Flotation Tests

The addition of magnetic plastic particles was initially evaluated in a laboratory conventional flotation cell to provide an indication of the effect on flotation rate. The external hydrophobic material was added in the feed slurry at concentrations expressed as total solid mass percentage. The flotation tests were performed under varying operating conditions as a function of time on two different coal samples.

6.2.1.1. Flotation Rate and Recovery Response

The investigation was initiated with conventional flotation tests to validate and confirm the flotation rate response and the corresponding froth recovery improvement previously reported by Munoz-Diaz, (2007). Different concentration combinations of collector (C) and frother (F) were used depending on the flotation characteristics of these coal types. For the Coalburg coal, the addition of 5% (by weight) magnetic plastic material showed approximately the same results compared to that with no plastics addition at the very beginning of sample collection (0 to 30 seconds) as shown in Figure 6.8. However, improvement increased considerably relative to the flotation performance of the sample with no plastics after 30 seconds, which was consistently higher at around 8.5 absolute percentage points on average from 30 seconds to 2 minutes. Similarly, the addition of

10% (by weight) plastic material to Coalburg flotation feed showed a significantly improved combustible recovery response from the start of sample collection up to one minute flotation time, which was steady at around 15 absolute percentage points on average compared to that with no plastics. These results compare well with those reported by Munoz-Diaz, (2007) and presented in Figure 6.6.

In addition, the recovery improvements were still significant even after the first minute, at both plastic concentrations compared to the results with no plastics added. This may also suggest that the magnetic plastic material is improving the floatability and recovery of the slow-floating fraction of the Coalburg coal. After 2 minutes of flotation, very similar recovery responses were obtained between the tests with 5% and 10% magnetic plastic material addition and all data points were converged at after 4 minutes of flotation, which were higher than 90% combustible recovery.

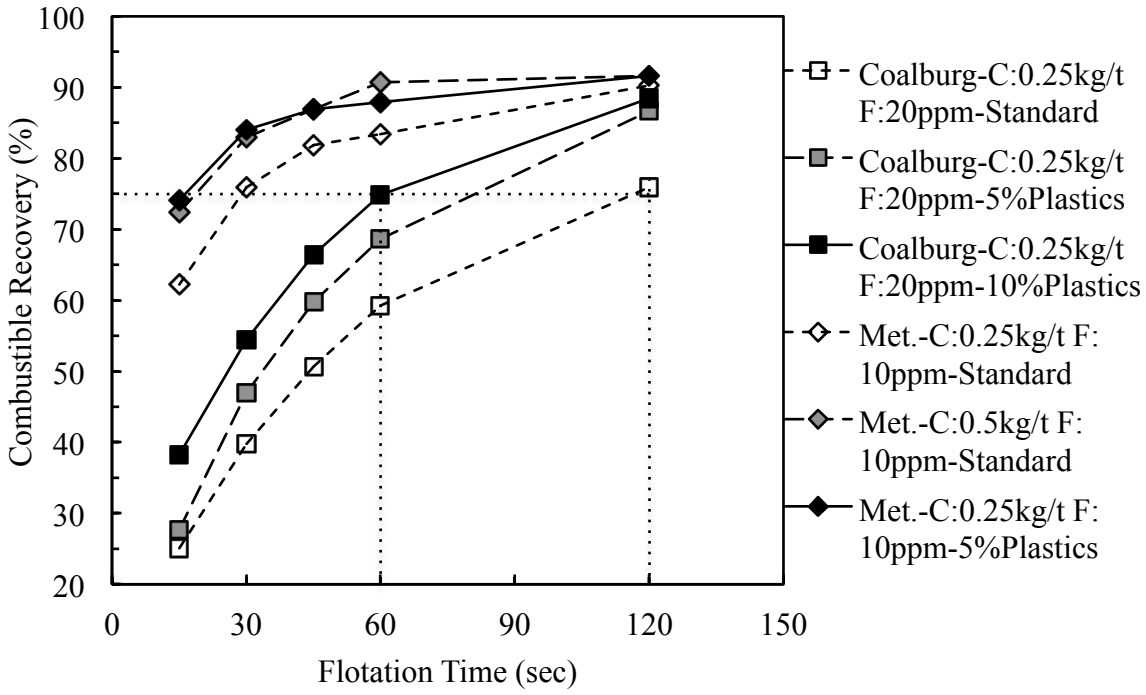


Figure 6.8. Flotation performances for different concentrations of magnetic plastic material using Coalburg and metallurgical coals; C=collector, F=frother.

One might note from Figure 6.8 that, with the addition of 10% magnetic plastic material, the retention time to achieve similar recovery values was reduced to one half compared to that of no plastics addition. Kinetic flotation test results revealed that the addition of highly hydrophobic particles to the flotation feed have a potential benefit in recovering difficult-to-clean coals, such as Coalburg coal, through reduced retention times, which is a major constraint during industrial flotation of these coals.

For metallurgical coal with very good flotation characteristics, the plastic material addition and the flotation reagent dosages were maintained at a lower concentration compared to that of the difficult-to-float coal source. Figure 6.8 clearly shows that the test with the high collector dosage with no plastics and the one with low collector dosage and 5% (by weight) plastics resulted in nearly equal flotation responses which may suggest that the plastic material was acting to counter the effect of the lower collector dosage. The recovery improvement was about 10 absolute percentage points at the beginning of the flotation period (0 to 30 seconds) for both tests. However, a difference of about 3 absolute percentage points in recovery was noted at one minute of flotation which suggests that a portion of the slow-floating particles responded faster in the presence of the magnetic plastic particles. An increase in plastic addition beyond 5% was not found to provide a significant improvement in flotation performance.

Since the metallurgical coal was already an excellent floating coal the recovery gains were significant but lower than that achieved on the Coalburg coal shown by the summary in Table 6.3. The flotation rate for the Coalburg coal increased by 56% using 10% plastic addition which provided about 15 absolute percentage point increase in recovery. For the metallurgical coal the flotation rate increase was 21% with 5% plastic addition. As shown from the feed characterization analysis (Table 3.3), KC Coalburg sample had a greater amount of coarse particles (+150 microns) in the feed. Since the metallurgical coal has a higher contact angle than that of the Coalburg coal (Table 3.13), coarse particles would be more readily floated than the Coalburg coal.

Table 6.3. Flotation performances with the addition of 5% and 10% magnetic material after one minute of flotation for Coalburg and Eagle coal samples.

Test Identification	Coalburg Coal C: 0.25 kg/t, F: 20ppm		Metallurgical Coal C: 0.25 kg/t, F: 10ppm	
	Flotation Rate (min^{-1})	Flotation Recovery (%)	Flotation Rate (min^{-1})	Flotation Recovery (%)
Standard	0.93	59.2	2.14	83.4
5% Plastic	1.19	68.6	2.60	87.9
10% Plastic	1.45	74.9	N/A	N/A

The significant improvement in combustible recovery in terms of absolute percentage gains is more clearly shown in Figure 6.9 for the two coal types and conditions with the addition of hydrophobic particles. The recovery improvement is around 15 absolute percentage points on average after one minute of flotation at 10% plastic particle concentration. This value was around 7.5 absolute percentage points on average after one minute of flotation for both coal sources at 5% plastic material concentration by weight.

The majority of the plastic particles were recovered in the froth concentrate within the first 15 seconds of flotation as shown in Figure 6.10. To obtain this information, the flotation concentrates and tailing samples were processed through a magnetic separator for a total of three times each. Around 65% of the plastic particles were recovered in 15 seconds of floating the Coalburg coal and nearly 80% were floated when treating the metallurgical coal. Over 95% was recovered in one minute of flotation for both coal sources. It is interesting to note that coal recovery gains were realized much past the one-minute flotation time as shown in Figure 6.9.

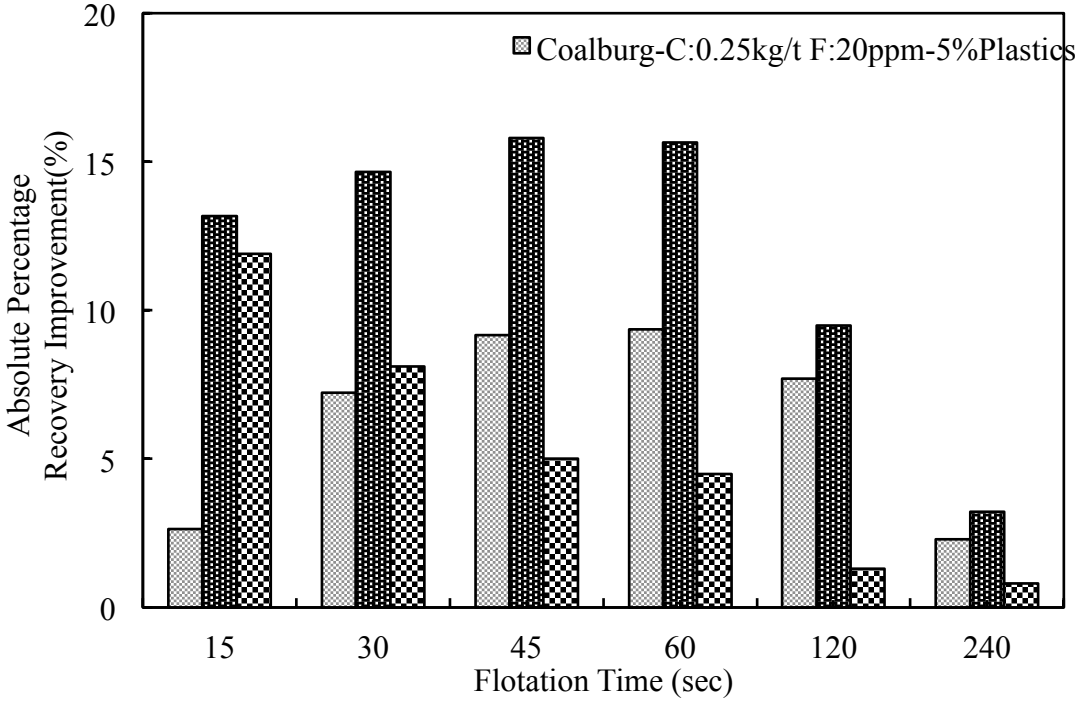


Figure 6.9. Absolute percent recovery improvements as a function of flotation time for Coalburg and Metallurgical coals with 5% and 10% plastic addition.

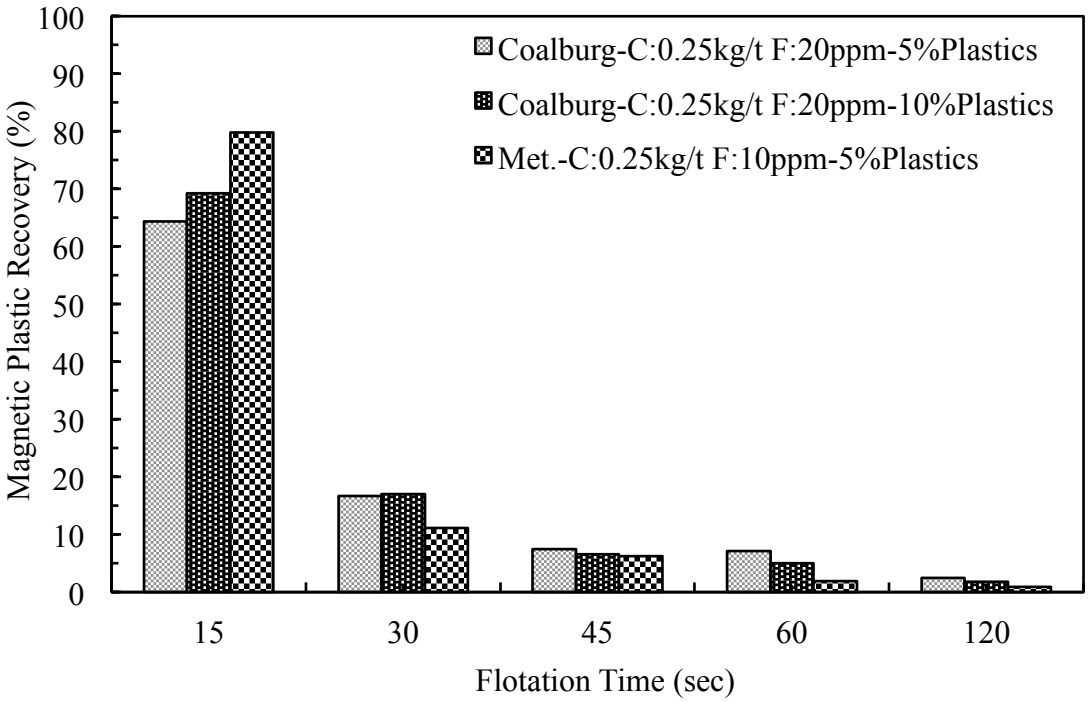


Figure 6.10. Recovery of magnetic plastic particles after the flotation rate tests for different coal types and reagent and plastic concentrations.

Although it may not be the primary reason for the enhanced coal recovery, plastic particle addition may also improve surface hydrophobicity which in turn result in increased flotation rate values. The improved flotation performance based on this hypothesis may be due to the hydrophobic force, as discussed before in Sections (4.1.2.1) and (4.1.3.2), which is a very strong attractive force that exists between hydrophobic particles (including air bubbles) such as the plastic particles (Yoon and Mao, 1996; Yoon and Aksoy, 1999).

6.2.1.2. Effect of pH and Surface Forces

During the bubble-particle attachment process, the electrostatic charge of the particle and the bubble surfaces play a significant role in addition to surface hydrophobicity. The zeta-potential measurements were used to measure the surface charge as a function of pH and the results were presented in Section 3.3.1.5. The surface chemistry study indicated that coal particles and plastic material are negatively charged through most of the typical operating pH values of 3 to 10. This points to the existence of a significant repulsive force which increases in magnitude with an increase in pH. It is well established that higher surface charges lead to significant repulsive forces between the bubbles and the particles which typically slows and even prevents the bubble-particle attachment. Previous studies have suggested that the optimum coal flotation recovery usually occurs under neutral (pH≈7) pH conditions (Parekh and Miller, 1998).

The effect of slurry pH on the recovery gains achieved by the plastic article addition was investigated using the more difficult-to-float Coalburg coal. Similar to previous findings, the best flotation performance was achieved at a near neutral pH of 7.5. In fact, little to no flotation occurred at slurry pH values of 4 and 10. However, the addition of 10% plastic particles provided flotation recovery under all pH conditions with the optimum occurring at pH 7.5 as shown in Figure 6.11. The results were especially impressive at pH 4 where the recovery gain was around 40%. The lack of flotation at pH 4 with no plastic particle addition is mainly due to the adsorption of clay particles due to electrostatic attraction forces.

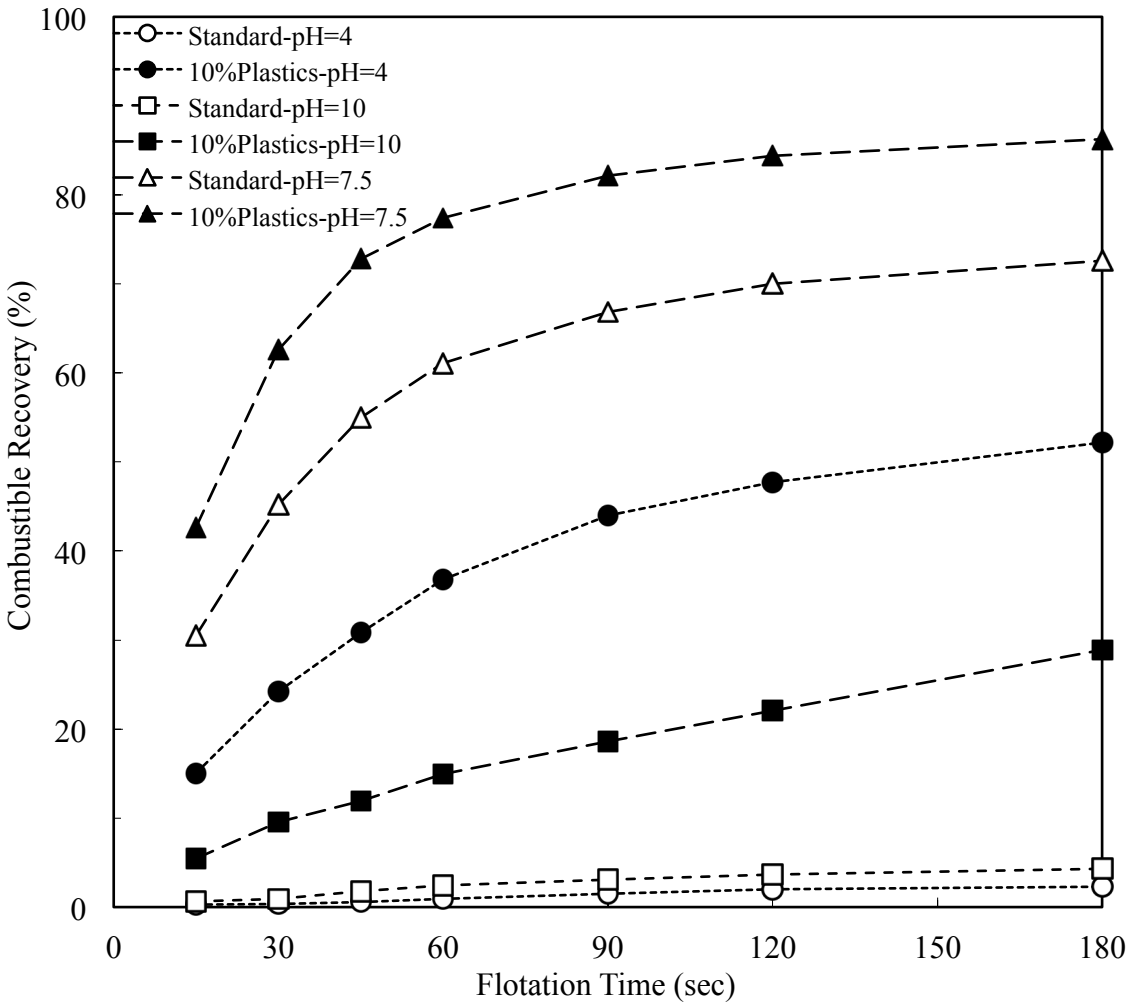


Figure 6.11. Impact of slurry pH on the recovery improvements realized when adding plastic particles to a conventional flotation feed containing Coalburg coal.

Given that the plastic particles have an isoelectric point (point of zero charge) at around pH 4, the lack of clay adsorption and the reason for the sharp recovery gain is unknown. The recovery gain at the high pH value of 10 is likely a result of the very attractive hydrophobic interaction energy which may be linked to the highly hydrophobic nature of the plastic surfaces. The resulting hydrophobic force is attractive to interact between the particle surfaces to overcome the electrostatic repulsive forces.

Flotation recovery gains can be highlighted more clearly as a function of flotation time in Figure 6.12 for different pH conditions studied. Nearly equal flotation recovery gains of around 15 absolute percentage points were realized over the entire flotation time for pH value of 7.5. On the other hand, under low and high pH conditions, the overall improvement increased with flotation time. Particularly under pH 4, the largest increase was realized in the later stages of the flotation period. This trend can be explained with the smaller negative charges on the particle surfaces at pH 4 compared to that at pH 10, which results in relatively favorable electrostatic interactions in addition to the hydrophobic interaction force due to the plastic particles.

Recovery improvement can be linked to the increased flotation rate values, as shown in Table 6.4, which are based on the flotation data after one minute. The results show significantly enhanced flotation kinetics, especially for the depressed flotation responses under low and high pH conditions with the addition of plastic particles.

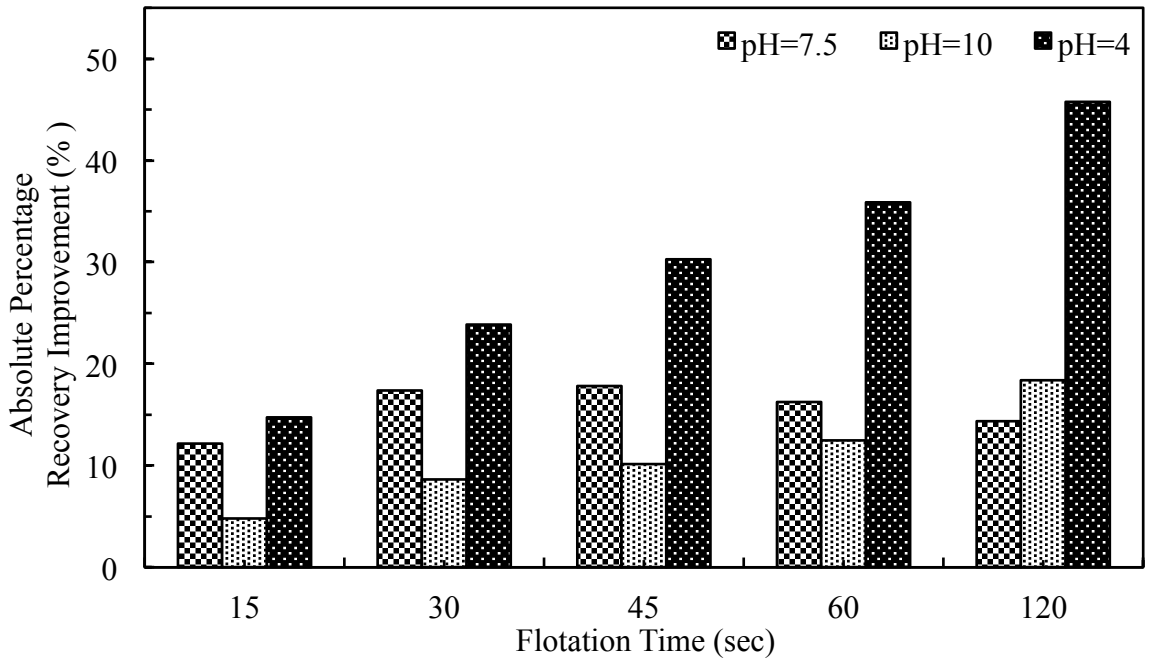


Figure 6.12. Absolute percent recovery improvements as a function of flotation time for Coalburg coal under different feed slurry pH conditions.

Table 6.4. Flotation rate improvements achieved under varying pH conditions on Coalburg coal with 10% plastic particle addition.

Test Identification		Fast Flotation Rate (k_f, min^{-1})	Flotation Recovery (%)
pH=7.5	Standard	0.70	66.8
	10% Plastic	1.06	82.1
pH=10	Standard	0.02	2.43
	10% Plastic	0.13	14.9
pH=4	Standard	0.01	0.94
	10% Plastic	0.38	36.8

6.2.2. Column Flotation Tests

Continuously-operated, laboratory column flotation tests were performed using the setup detailed in Figure 3.3 to further investigate the overall impacts of the addition of plastic particles on the flotation performance. As mentioned before, the hydrodynamic conditions affecting the flotation performance for the conventional cell and the flotation column are different due to the geometric dimensions of the units. The length-to-diameter (L:D) ratio is higher for the column flotation units compared to that of the conventional cell, which provides near plug-flow mixing conditions which are optimum for recovery. As a result, lower overall recovery improvements were expected compared to those from the conventional cells since the mixing conditions are more ideal for the flotation columns.

6.2.2.1. Volumetric Feed Rate Evaluation

The column flotation tests were performed over a range of volumetric flow rates which provided a range of particle retention time conditions. Plastic particles were added to the flotation feed containing Coalburg coal in the sump and mixed thoroughly before being fed to the flotation column through a peristaltic pump at a predetermined rate (300 to 1200 ml/min). The operating parameters of the column tests (Table 3.4) were based on

the findings of previous studies (Ozsever, 2005; Munoz-Diaz, 2007). When the separation performance is compared with the release analysis, the flotation feed including 10% (by weight) plastic particles resulted in nearly equal selectivity as achieved with no plastic addition as shown in Figure 6.13. The recovery versus product ash content relationship is essentially the same and close to the ultimate performance predicted by the release analysis curve. However, the results from the tests including plastic addition were higher on the recovery-grade curve. Given that the volumetric feed rates used with and without plastic addition were the same, the trend indicated improvements in flotation recovery.

The impact of the plastic particle addition was evident when the combustible recovery values were plotted as a function of volumetric feed flow rate as shown in Figure 6.14 which also includes the column flotation test results reported from a previous study using coal from the same seam. Test results from both analyses revealed that the recovery response with increased feed rate was nearly steady up to 600 ml/min with and without the plastics addition.

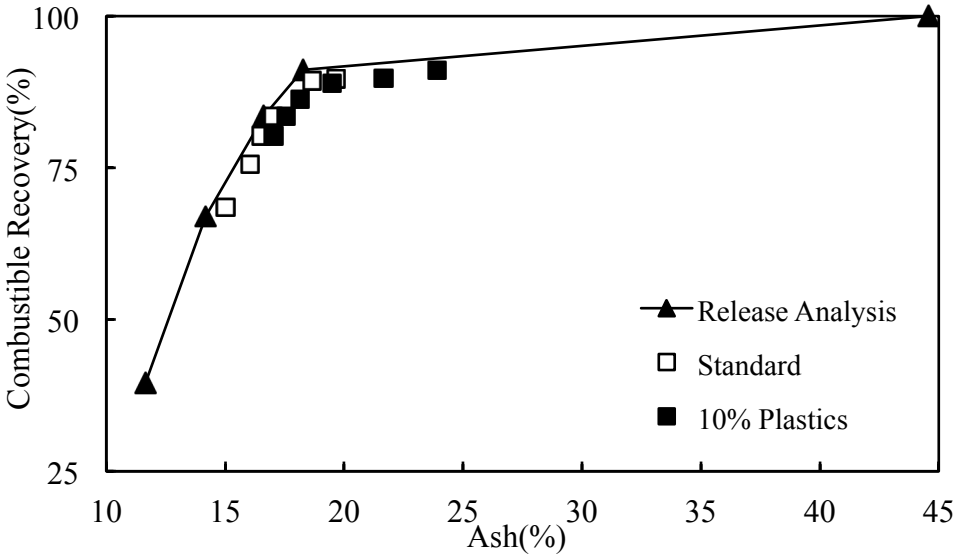


Figure 6.13. Separation performance achieved when treating Coalburg coal in a flotation column with and without plastic particles in the feed; volumetric feed rate=300-1200 ml/min.

Further increases in the volumetric feed rate after this point, however, resulted in a significant drop of the recovery values for the standard column flotation conditions. With the addition of 10% plastic particles by weight, a recovery improvement of about 5 absolute percentage points was achieved on average for the feed rates between 600 and 800 ml/min in the Munoz-Diaz (2007) study. Similarly, improved recovery values were found for the current study with average gains of nearly 6 absolute percentage points for the feed rates between 750 and 900 ml/min. In both cases, the addition plastic particles had a minimal effect on product ash content.

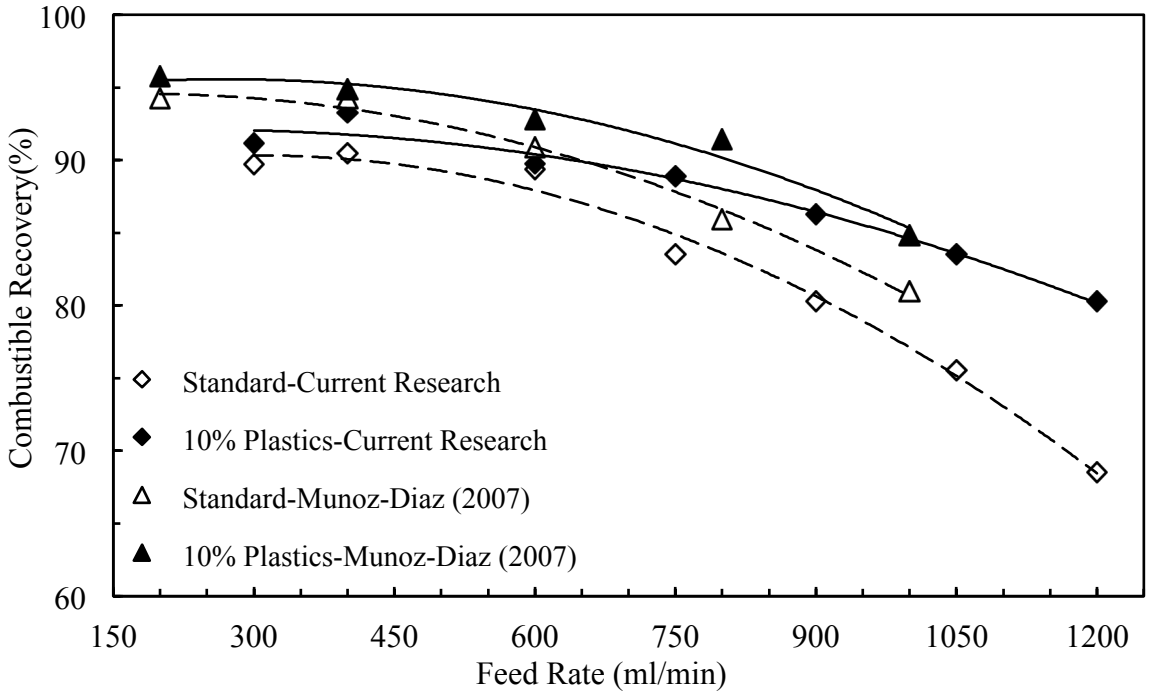


Figure 6.14. Flotation performance achieved as a function of volumetric feed rate while treating difficult-to-float coals in a flotation column using 10% plastic particle concentration by weight.

The data from the two studies in Figure 6.14 provide significant evidence that the addition of the plastic particles substantially increased flotation rate. The recovery differential with the addition of 10% (by weight) plastic particles increased up to 12.5 absolute percentage points at 1200-ml/min flow rate. Although aggregation of plastic particles onto coal surfaces may not be the primary reason for the enhanced coal recovery, the results are especially important for the retention time constrained flotation applications such as those typically associated with the difficult-to-float Coalburg coal source.

6.2.2.2. Carrying Capacity Evaluation

As previously noted, it was believed that the primary impact of adding the hydrophobic plastic was to improve froth stability which would increase carrying capacity. This advantage was investigated using the Coalburg coal sample. During the testing procedure, feed solid concentration was varied from 2% to 16% by weight while maintaining the volumetric feed rate at 1050 ml/min. As shown in Figure 6.15, carrying capacity conditions were reached at around 12% solid concentration (by weight) feed. With 10% (by weight) plastic particle addition to the feed slurry, the carrying capacity conditions were maintained up to 16% feed solids content, which was the highest concentration tested. The product rate decreased noticeably without the plastic particle addition after reaching carrying capacity. This finding suggested a preferential impact on the coarsest particle size fractions in the flotation feed.

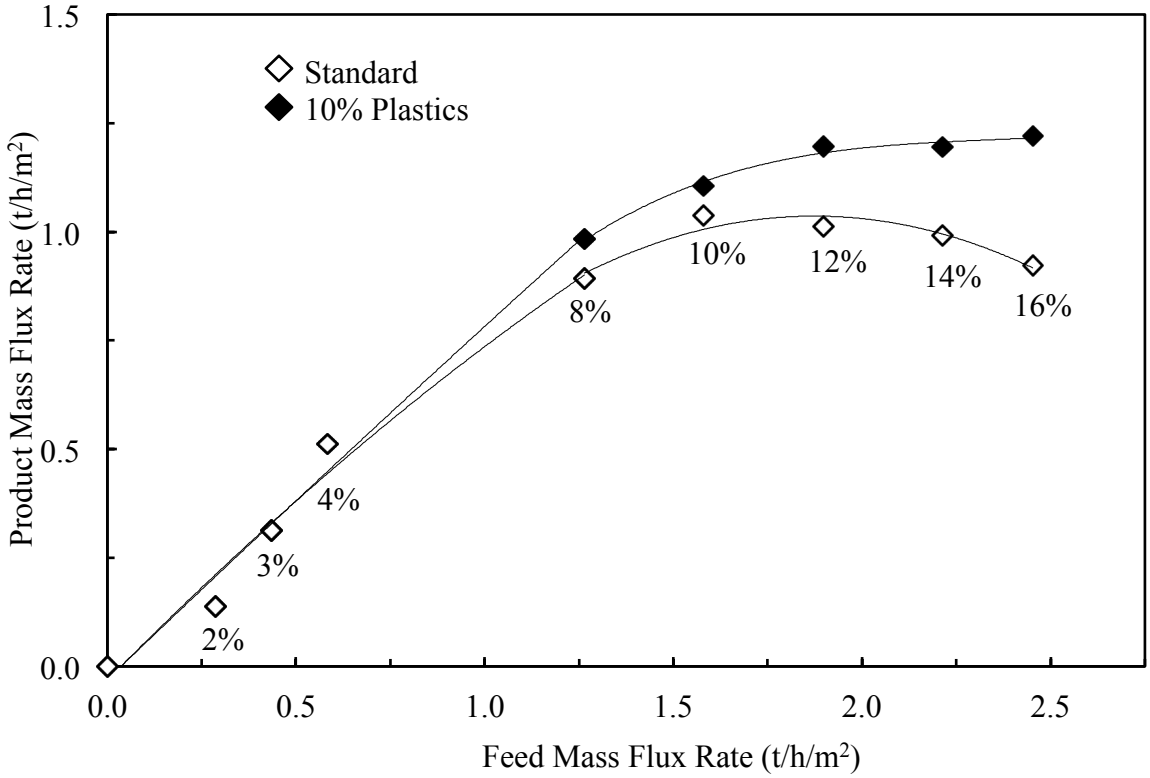


Figure 6.15. The impact of plastic particle addition on carrying capacity characteristics for the Coalburg coal from Kanawha County, West Virginia for different feed solid concentrations.

6.2.2.3. Particle Size-by-Size Flotation

The impact on flotation performance was evaluated on a particle size-by-size basis and plotted against the mass yield, or weight recovery, as shown in Figures 6.16 and 6.17. At 10% (by weight) concentration of plastic particle addition to the feed slurry, weight recovery was improved by more than 30 and 10 absolute percentage points for the coarsest and finest size fractions, i.e. plus 150 microns and minus 25 microns, respectively. One may note that the weight recovery of the coarse and the ultrafine particles during the flotation rate tests were almost equal without plastic particle addition. However, the improvements in weight recovery of the ultrafine particles were significantly less compared that of the coarse particles which agrees well with the findings of the carrying capacity results.

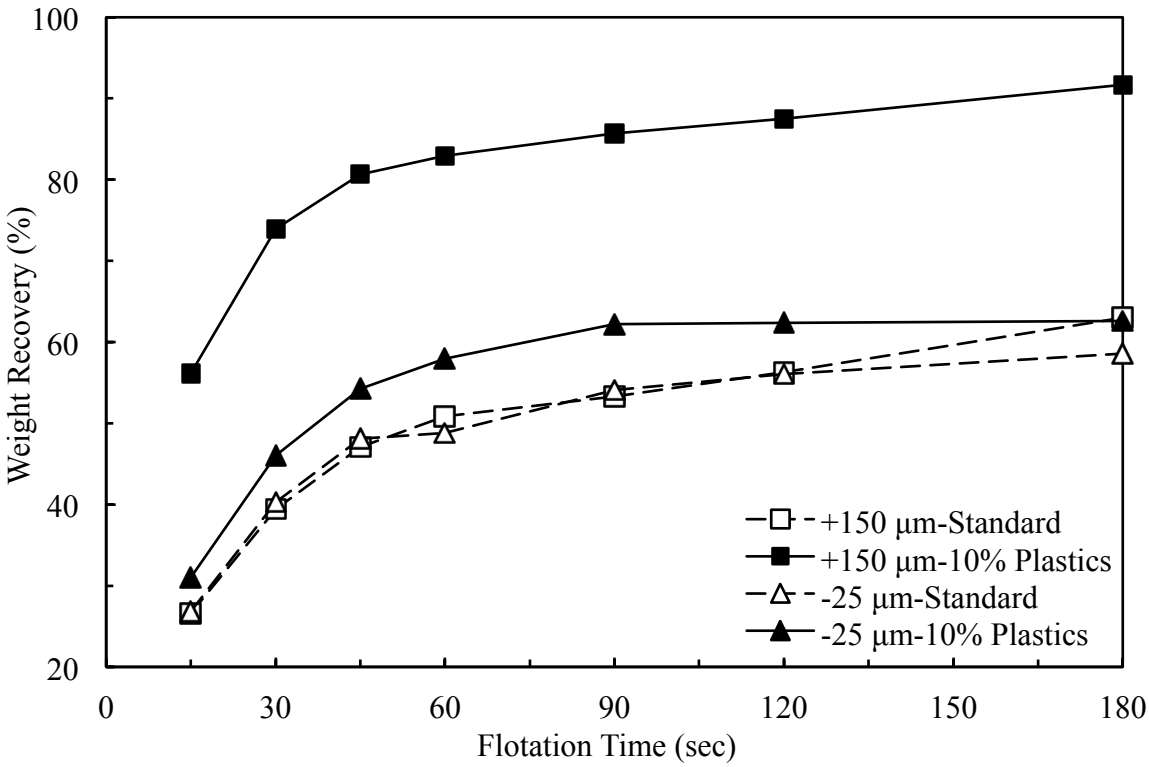


Figure 6.16. Improved mass recovery rates for the coarsest and the finest size fractions of Pittsburgh No. 8 coal with and without the plastic particle addition.

An analysis of the impacts on the particle size fractions between 25 and 150 microns is provided in Figure 6.17. Under the same operating conditions, recovery improvement decreased notably for particle sizes between 150 and 25 microns, compared to that of the coarse coal weight recovery values. Especially for fine size fractions (75 to 25 microns), conventional flotation results showed significantly lower gains of about 5 absolute percentage points after one minute of flotation. After one minute of flotation, the recovery gain for the 150 x 75 micron fraction was about 10 absolute percentage points compared to 5 absolute percentage points for the 75 x 45 micron and 45 x 25 micron size fractions.

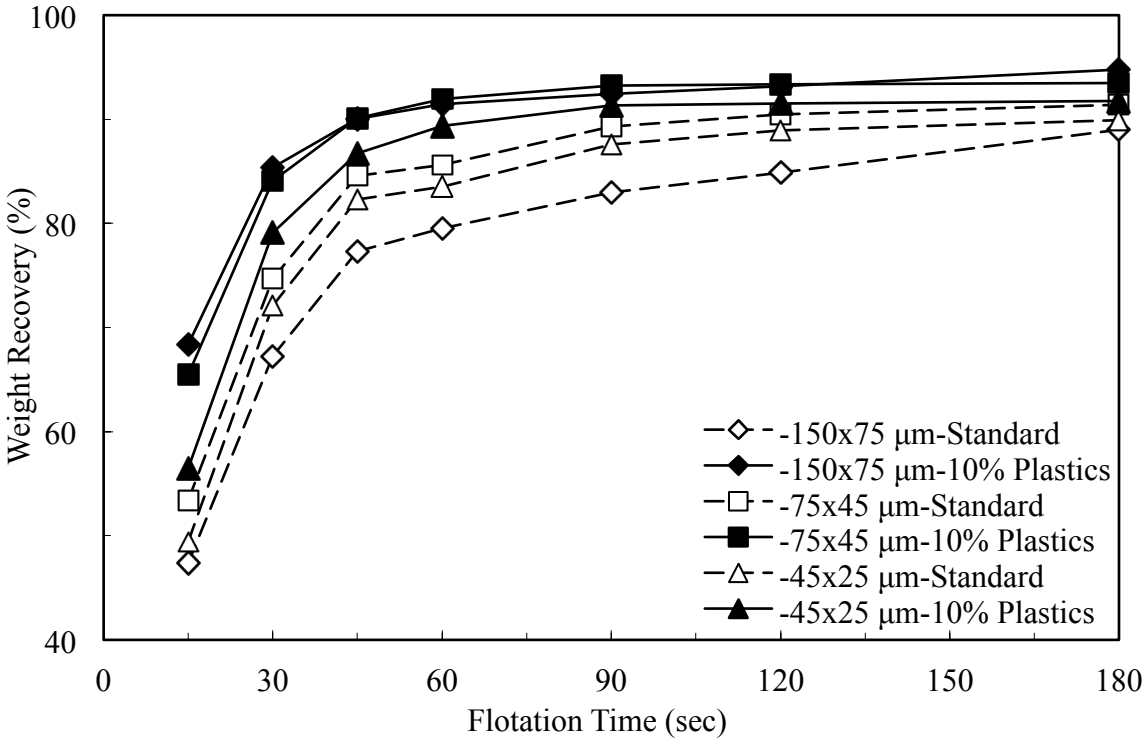


Figure 6.17. Improved mass recovery rates for the intermediate-to-fine size fractions of Pittsburgh No. 8 coal with and without the plastic particle addition.

In addition to the weight recovery response for different size fractions based on flotation time, the potential change in the lower and upper particle size limits of flotation was quantified on a size-by-size basis after one minute as shown in Figure 6.18. As a result of the flotation rate tests, weight recovery of the Pittsburgh No. 8 coal was increased by at least 5 absolute percentage points under both operating conditions, i.e., Tests 1 and 2, with the addition plastic particle at 10% (by weight) concentration. However, the amount of material being recovered as a result was significantly greater for the coarser particle size fractions, which was 30 to 35 absolute percentage points higher for particle sizes of around 150 microns. These results clearly show that the addition of the plastic material preferentially increases the top particle size treatable by flotation and thus enlarges the particle size range of the process.

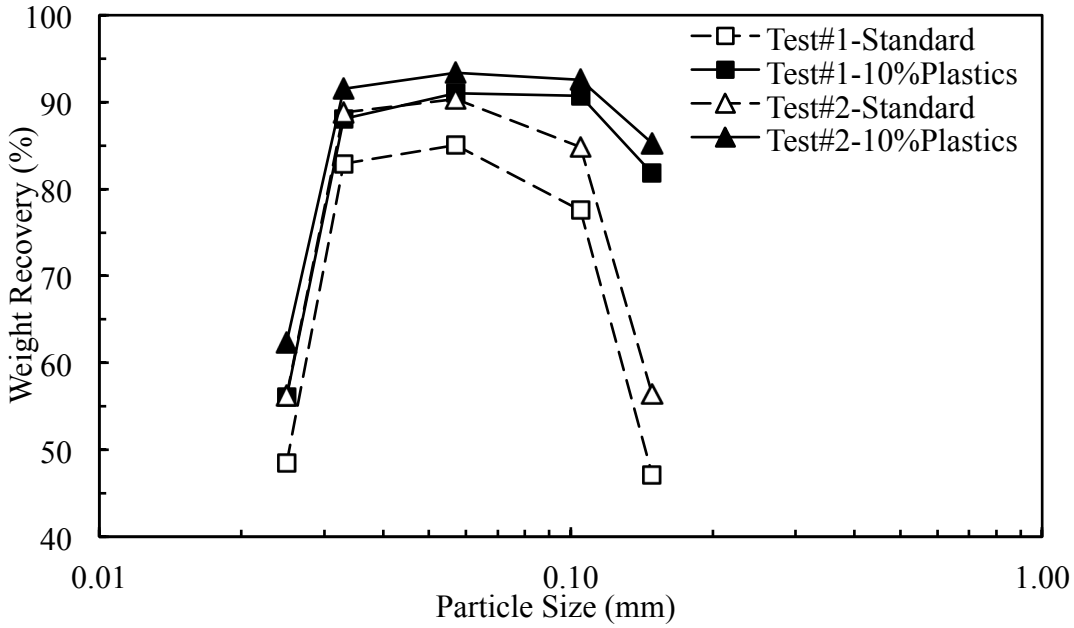


Figure 6.18. Particle size-by-size weight recovery improvements achieved by the addition of plastic particles at 10% concentration by weight on Pittsburgh No. 8 coal.

Following these promising results, flotation feed material from a Coalburg coal source was used in flotation rate tests to evaluate the performance based on different size fractions. Similar to the results from the Pittsburg No. 8 coal (Figure 6.16), the improvement in weight recovery for the coarsest size fraction was significantly higher than that of the ultrafine particles, which was more than 35 absolute percentage points after one minute of flotation as shown in Figure 6.19. The effect on -25 micron recovery was statistically insignificant.

In addition to the finest and the coarsest size fractions, the intermediate-to-fine size fractions, which are thought to be closer to the optimum range of coal flotation, was also evaluated with the addition of plastic particles at 10% (by weight) concentration. As shown in Figure 6.20, the recovery improvement obtained for the 150 x 75 micron size fraction was around 25 absolute percentage points which was of the same magnitude as that realized for the particles coarser than 150 microns. On the other hand, the results for the 45 x 25 fraction was similar to the -25 micron fraction which revealed little to no increase in recovery.

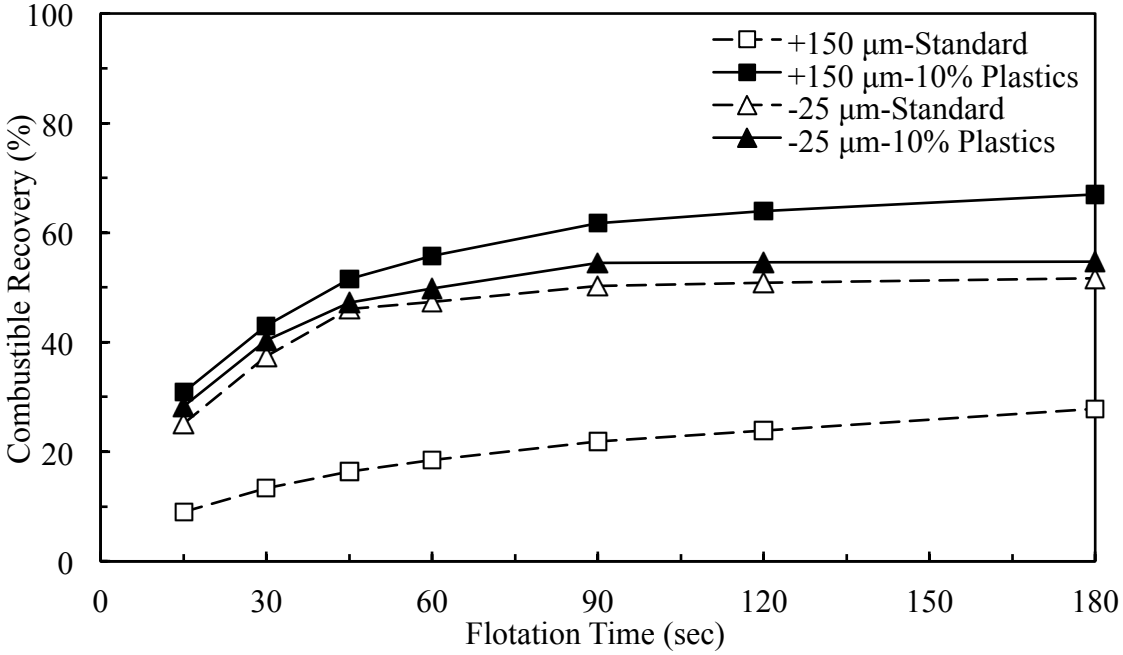


Figure 6.19. Improved mass recovery rates for the coarsest and the finest size fractions of Coalburg coal with and without the plastic particle addition.

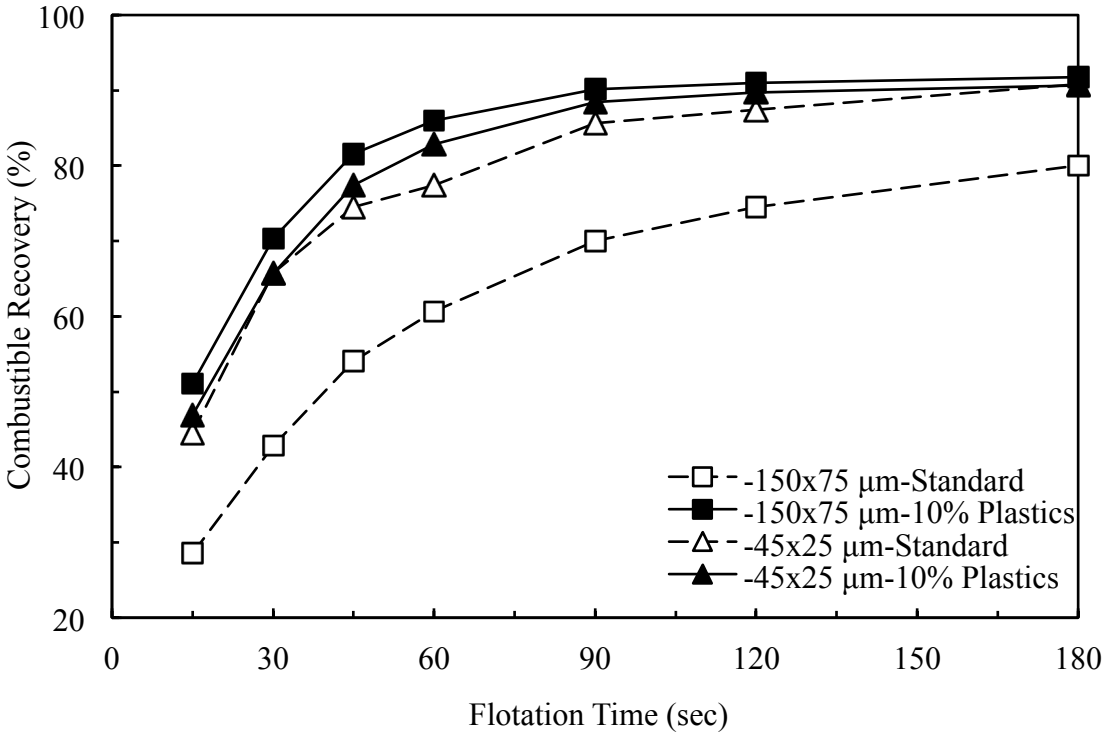


Figure 6.20. Improved mass recovery rates for the intermediate-to-fine size fractions of Pittsburgh No. 8 coal with and without the plastic particle addition.

The preferential coarse particle recovery gain was evident by the flotation rate test results. As previously described, successful attempts to increase coarse particle recovery should enhance carrying-capacity. To evaluate the significance, the samples collected from carrying-capacity tests involving Coalburg coal were sieved and analyzed to assess particle size recovery. As shown in Figure 6.21, the continued upward trend in the product mass flux rate for tests using feed solids content above 10% by weight (Figure 6.16) was a result of a preferential increase in coarse particle recovery. Recovery increased by 10 absolute percentage points for the coarsest particle size fraction when feeding a 16% solid concentration slurry containing 10% plastic particle by weight.

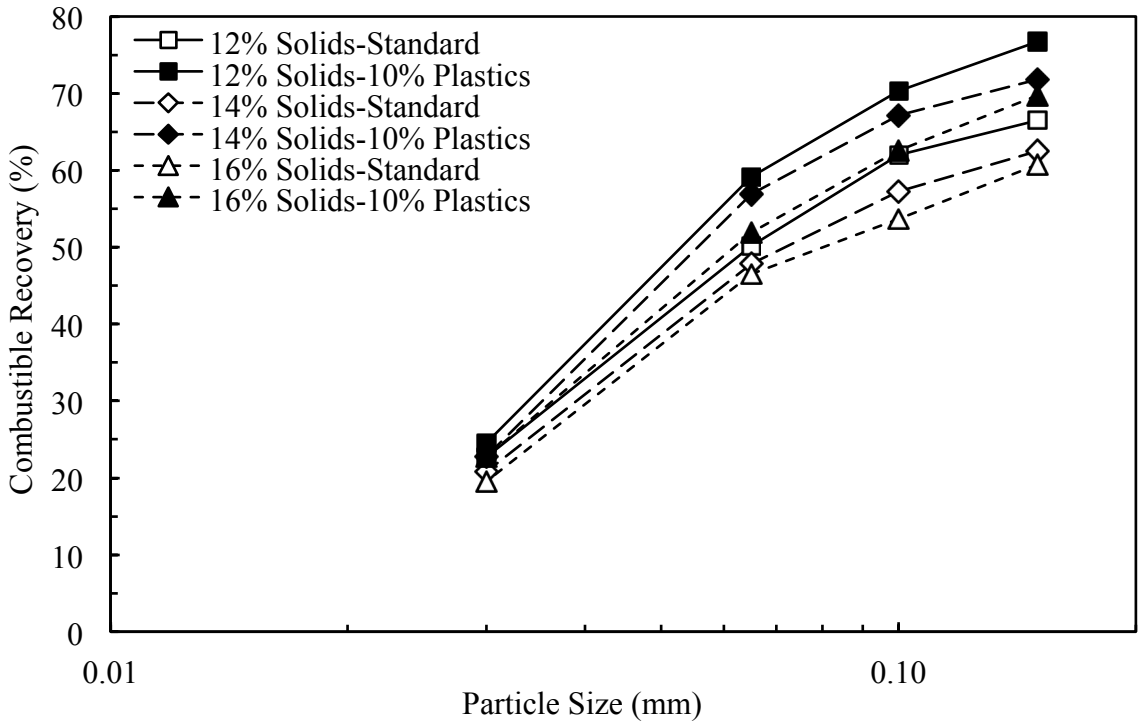


Figure 6.21. The impact of plastic particle addition on combustible recovery for different size fractions following the carrying capacity tests for the Coalburg coal from Kanawha County, West Virginia.

The particle size-by-size performance analyses shows that the addition of the plastic particles has the potential of increasing the upper particle size limits typically associated with the froth flotation process. The impact is believed to be due to improved froth stability which results in higher bubble surface area flux rates and thus reduced detachment of coarse particles in the froth zone. The plastic particles are ideal for this application given a surface hydrophobicity characterized by a contact angle of 84 degrees which is less than the 90 degree criteria that has been identified in previous studies for froth stability (Dippenaar, 1982a, b; Garrett, 1993).

6.3. CONCLUSIONS

Fundamental studies have shown that froth stability can be enhanced by hydrophobic particles that have a contact angle less than 90 degrees. As a result, bubble coalescence is minimized and the bubble surface area flux rate increased which elevates the carrying capacity of a flotation system. Plastic particles having a contact angle of 84 degrees was added to the feed slurry being treated by froth flotation. The plastic was magnetic due to their large composition of magnetite. As a result, the particles can be recovered from flotation froth by a low intensity magnetic separator.

Experiments to evaluate the impact of the plastic particle addition were evaluated in a laboratory semi-batch conventional cell and a continuously operated flotation column. Coals from multiple sources were used in the evaluation to assess the plastic particle addition impact on coal recovery over a range of surface hydrophobicities. The conventional cell experiments were used to assess the effect on flotation rate and to evaluate the effect of plastic concentration, reagent addition and slurry pH. Flotation column tests assessed the impact on volumetric and solids carrying capacity in a continuous process. The plastic particles were recovered from all flotation samples by three cycles through a high-gradient magnetic separator.

Conclusions from the investigation are:

1. The flotation rate of Coalburg coal with a relatively low degree of surface weak hydrophobicity was increased by 56% by the addition of 10% plastic particles by weight. A lower rate improvement of 21% was obtained for a more highly hydrophobic coal with the addition of 5% plastic particles by weight.

2. The flotation rate improvements provided an increase in the one-minute flotation recovery in a conventional cell of about 15 absolute percentage points for the weakly hydrophobic coal.

3. A particle size-by-size analysis of the conventional flotation performance revealed preferential coarse particle recovery gains. For a Pittsburgh No. 8 coal, the recovery increase was over 30 absolute percentage points for the coarsest particle size fraction as compared to around 10 absolute percentage points for the finest particle size fraction.

4. Plastic particles having a size larger than 150 microns were found to provide the greatest flotation improvement whereas the finest plastic particles provided the least impact. This finding indicates that plastic particle attachment to the coal surfaces was not the primary mechanism for the coal recovery gains observed in the coal flotation tests.

5. For a Coalburg coal sample, the addition of plastic particles at a 10% concentration activated flotation at pH values of 4 and 10 under which little to no flotation occurred without the plastic particle addition. At a pH value of 4, flotation recovery gains over 40 percentage points were realized.

6. At a slurry pH of 7.5, the recovery improvement was around 12 absolute percentage points after the addition of 10% plastic particles to the feed stream.

7. Test results obtained from the treatment of a highly hydrophobic coal revealed the potential to substantially reduce collector and/or frother dosages while maintaining a constant combustible recovery value.

8. Tests using a flotation column revealed that near optimum separation performance can be achieved with the plastic particle addition as compared to release analysis results. Improved froth stabilization generally results in an increase in product ash content due to hydraulic entrainment of clay particles. However, the wash water addition in the column froth appears to be able to eliminate hydraulically entrained material.

9. Recovery gains were obtained throughout the range of volumetric feed rates tested and the absolute gain increased with an increase in the volumetric rate. The recovery gains ranged from 5 to 12 absolute percentage points. The results indicate a positive impact on the collection zone flotation rate which may be a result of attachment of the finer plastic particles on the surfaces of the coal which would enhance surface hydrophobicity.

10. The addition of the plastic particle significantly altered the product mass flux rate relationship with the feed mass flux rate. Above a certain feed mass flux rate, product mass flux rate decreases due to preferential detachment of the coarse particles. However, the addition of plastic particles in the feed eliminate any drop in the product mass flux rate and, in fact, provided a gradual increase in the mass flux rate above the critical feed mass flux rate value.

11. Particle size-by-size analysis of the carrying capacity samples showed preferential recovery improvements for the coarsest particle size fractions as expected from the product mass flux and feed mass flux relationship.

CHAPTER 7

SUMMARY AND CONCLUSIONS

In the present study, two different approaches were explored to enhance the froth flotation performance of coal particles finer than 150 microns including samples with poor flotation recovery characteristics. These novel concepts included: i) pretreatment of the flotation feed though a cavitation system, and ii) application of plastic particles with magnetic features in the flotation process.

The first concept involved the pre-aeration of flotation feed using a cavitation system, which was previously proven to enhance flotation recovery in laboratory studies. By injecting feed through a cavitation system, micron-sized bubbles nucleate onto the surface of the coal particles. Collisions between the pre-aerated solid particles produce aggregates with air serving as the bridging agent. The aggregates are more efficiently recovered in a conventional flotation system due to improved collision efficiency with conventional bubbles. In addition, the attachment process may be benefited from the interaction of the nucleated bubbles on the particle surfaces and the conventional bubbles.

A laboratory study was performed to further understand the effect of feed pre-aeration using a cavitation system. The experiments were conducted using fone coal samples that varied from a poorly floatable to highly floatable. Flotation samples were pretreated in the cavitation device before introduction to laboratory conventional and column flotation units.

Based on the positive results from the laboratory studies, a full-scale cavitation system was installed for in-plant testing into a flotation circuit that was comprised of three StackCells placed in series in which the tailings stream produced by one unit was the feed to the next. After installing the cavitation pre-aeration system in the feed pipe to the first StackCell, a detailed full-scale in-plant test program was conducted to optimize

performance, quantify recovery improvement and evaluate the potential of reducing collector dosage.

The other concept utilized hydrophobic plastic material to improve froth stability and thus flotation recovery. The plastic was produced with a blend of magnetite particles, which made the plastic easily recoverable by magnetic separators. Laboratory conventional and column flotation cells were used to collect the necessary data needed to validate and duplicate the promising results from previous research (Munoz-Diaz, 2007). The previous study indicated a significant enhancement in separation performance by the addition of magnetic hydrophobic particles to the flotation process. Flotation rate tests were conducted while varying particle size and the concentration of the magnetic plastic material over a range of slurry pH values. In addition, to assess the benefits on carrying capacity, column flotation tests were performed at different feed solid concentrations while maintaining the volumetric feed flow rate constant.

The conclusions obtained from these investigations are provided as follows:

Cavitation Feed Pretreatment:

1. Preliminary studies of the feed pre-aeration concept were conducted on a coal with excellent floatability characteristics in conventional cell tests. The flotation rate tests revealed a four absolute percentage point improvement in flotation recovery.

2. These tests were followed by an evaluation on a coal source that is known to be difficult to recover using froth flotation. The flotation rate test results indicated the potential to increase recovery by 8 to 10 absolute percentage points using a cavitation tube to pre-aerate the feed to the flotation cell. In addition, evidence was provided that collector dosage requirements could be reduced by as much as 50%. Under different collector and frother dosages, on average, flotation rate was improved by 15% when no air is added and by 30% when a relatively small amount of air is added to the feed to the cavitation system.

3. Following the positive results from the flotation rate tests, continuous laboratory column flotation tests were performed to test the effect on the volumetric feed rate capacity. When treating the difficult-to-float coal, the flotation recovery improvement realized by using feed pre-aeration reached at maximum of around 20 absolute percentage points at the highest volumetric feed rate of 2000 ml/min. Given that all other parameter values were held constant, this finding suggests that feed pre-aeration significantly increases flotation rate by elevating the efficiency of the bubble-particle collision and/or attachment processes. Recent data also suggests the possibility of enhanced attractive interactions between a micron-sized bubble attached to a particle surface and a bubble produced by a conventional generator. This mechanism would provide enhanced flotation rates by improvements in the probability of attachment.

4. The impact on the carrying capacity of a flotation column was also evaluated by increasing the feed solids concentration while holding the volumetric feed rate constant at 1050 ml/min. The pre-treatment through the cavitation tube increased carrying capacity from 0.95 to 1.25 t/h/m^2 or 32%. Projecting this improvement to a typical 4-m diameter industrial column indicates the potential of increasing flotation recovery up to 4 t/h per unit.

5. Particle size analyses of the samples collected from the carrying capacity tests revealed that the improvement achieved by cavitation pretreatment was found to be preferentially achieved on the ultrafine particle size fractions of the feed. The data supports a hypothesis that the feed pre-aeration through a cavitation tube is likely due to aggregation of the ultrafine coal particles resulting from the interaction of the nucleated micron-size bubbles on the particle surfaces with other hydrophobic particles. As such, the nucleated bubbles are serving as the bridging medium. Individual ultrafine particles have low mass and high surface area and thus take up a significant amount of conveying space on air bubble surfaces. By aggregating the ultrafine particles, more mass can be carried per unit of bubble surface area.

6. Based on the positive laboratory results, a full-scale cavitation system developed by Eriez Flotation Divison-USA was installed in the feed pipe of the primary StackCell of a 3-stage flotation circuit in a plant that produces coal for use in the metallurgical market. The volumetric feed rate to the circuit was around 11000 L/min with a solids flow rate of 60 t/h under standard feed solid concentration of around 8.5% by weight. Nearly 50% of the floatable material in the feed to the flotation circuit had a particle size finer than 45 microns. A detailed test program was conducted to assess the potential of using cavitation for enhanced flotation rates and carrying capacities and to evaluate the potential of reducing collector dosage. The pre-aeration system was found to provide greater than 10 absolute percentage points in recovery improvement throughout the test program.

7. When the flotation performance was compared with respect to the collector dosage, identical recovery values were achieved using 50% less collector when utilizing the cavitation system without air addition and 2/3 less collector when injecting 1.4-1.55 m^3/min (50-55 ft^3/min) of air in the feed to the cavitation system. At a constant collector dosage, recovery increased by 10 absolute percentage point using cavitation without additional air and 17 absolute points when additional air was provided to the cavitation system. For the cavitation tests with air addition, decreasing the collector dosage from 0.33 kg/t to 0.11 kg/t showed 46% to 68% improvement in the carrying capacity relative to those obtained with no pretreatments. Furthermore, at the same frother concentrations, air addition prior to the cavitation tube system gave an additional 50% increase in the carrying capacity response.

8. In addition to assessing the collector consumption, frother additions to the flotation circuit was also evaluated in the presence and in the absence of the cavitation pretreatment. Under the same operating conditions, it was found that the frother consumption could be reduced by more than 30% with the cavitation pretreatment while achieving nearly equal recovery values.

9. The impact of cavitation pretreatment with the air addition was shown photographically that bubble sizes reporting to the flotation product were significantly smaller when using the cavitation system with air as compared to the product generated when pretreatment was not used. This evidence suggests higher bubble surface area rates which would provide higher carrying-capacity values.

10. Although the air addition was applied at a very small volume (1.4-1.55 m^3/min, 50-55 ft^3/min), the comparative studies shown that air addition is not required for the improved performance. This point out to the fact that the dissolved air in plant water would be sufficient enough to generate micron-size bubbles on coal surfaces through the cavitation tube, although additional air may further benefit the feed pretreatment due to the micro-bubble population in the system.

11. In summary, feed pre-aeration using a cavitation system with and without air has been proven to provide significant improvements in flotation recovery through laboratory and in-plant test programs. The preferential improvement on the finest particle size fractions indicates that the mechanism is agglomeration of the ultrafine particles using the micron-size bubbles nucleated on the particle surfaces during cavitation treatment as the bridging medium. Substantial reductions in both frother and collector may be realized using this pretreatment concept.

Evaluation of the Magnetic Plastic Particles:

12. To validate and confirm the flotation rate response and the corresponding froth recovery improvement from a previous study (Munoz-Diaz, 2007), conventional flotation tests were conducted in the current research using coal sources with varying degrees of floatability. The addition of 10% (by weight) plastic material to difficult-to-float flotation feed showed significant improvement in combustible recovery response by around 15 absolute percentage points as a result of a 56% increase in flotation rate. These results are close to those from the preliminary studies, which showed a similar impact on coal from the same source.

13. Conventional flotation tests conducted using the plastic material found that flotation rates were significantly increased when evaluating difficult-to-float and easy-to-float coal samples. When using 5% plastic concentration by weight, flotation rate increased from 2.14 to 2.60 min^{-1} for the highly floatable coal which provided a recovery improvement of 5 absolute percentage points. A greater benefit was realized for the difficult-to-float coal with 10% plastic addition by weight. Flotation rate was increased by 56% which improved recovery by about 9 absolute percentage points. A similar finding was reported in the previous study for a more hydrophobic coal source (Munoz-Diaz, 2007).

14. It is well known that the optimum coal recovery in froth flotation typically occurs around the neutral pH values. Similar findings were also realized in this study in which recovery was maximized at around 70% after 3 minutes of flotation for the weakly hydrophobic coal. When plastic particles were added at a 10% concentration, recovery improved by 12 absolute percentage points. At pH values of 4 and 10, virtually no flotation occurred without the addition of plastic particles. Adding the plastic material resulted in activation of the system and the recovery values achieved were between 24% and 50%.

15. At low pH values, the poor recovery is generally believed to be due to clays coating the coal surfaces thereby reducing or eliminating the ability of air bubbles to attach. The substantially improved recovery values at pH 4 when using plastic particles may indicate that either clay adsorption onto the plastic surfaces does not have the same effect or the clay coating is not occurring at the same level. As a result, a stable froth layer is generated which allows recovery of the weakly hydrophobic coal particles albeit at lower rates than that achieved at pH 7.5.

16. It is also feasible that the coal particles are aggregating with the more hydrophobic plastic particles through the strong hydrophobic interaction energy. In this hypothesis, the bubbles attach to the plastic surfaces creating a bubble-coal-plastic

agglomerate that floats due to its relative density. This mechanism may explain the ability to recover the weakly hydrophobic coal at a pH of 10 under which little or no flotation occurred when plastic particles were not added. A similar finding was obtained for a cola having a higher degree of hydrophobicity.

17. On the basis of the promising results obtained from the conventional flotation tests, laboratory column flotation tests were conducted to further evaluate the effect of plastic addition on the volumetric capacity of a flotation system under kinetic-limiting conditions. Recovery values achieved on the more difficult-to-float coal improved from 5 to 10 absolute percentage points over the range of volumetric flow rates tested. Although improved froth stability is believed to be the main benefit of the plastic particle addition, these results support the possibility of advantages gained from the aggregation of fine coal and plastic particles.

18. The test results from a carrying-capacity evaluation provided strong evidence for the hypothesis that the main benefit of the plastic particle addition was improved froth stability. When the feed solids concentration was increased from 2% to 16% by weight, a maximum capacity of 1.2 $t/h/m^2$was achieved at about 12% solids by weight with 10% plastic addition which represents a 20% increase in carrying capacity compared to test using no plastic particles. When no plastic particles were added, the typical decrease in the product mass flux rate was obtained due to selective detachment of the coarse coal particles. However, this trend was not observed when adding plastic particles.

19. Particle size analyses of the products generated from the carrying capacity tests revealed that the recovery improvement was selectively achieved on the coarsest floatable coal particles in the flotation feed. This finding agrees well with the absence of a decrease in the product mass flux rate after reaching a maximum value.

20. A study was performed to determine the significance of the particle size of the plastic material on coal recovery. The results indicate that plastic particles having a particle size larger than 150 microns play the primary role in coal flotation improvement. Plastic particles finer than 45 microns provided minimal improvement. This finding indicates that:

    - Aggregation of plastic particles onto coal surfaces as a mechanism for improving surface hydrophobicity is not the primary reason for the enhanced coal recovery.

    - Stabilization of the froth by the existence of coarse plastic material with a contact angle slightly less than 90° is the most likely mechanism providing the enhanced flotation recovery. Previous studies have shown the particles with similar contact angles provide a viscous water film around the bubble surfaces in the froth which reduces water drainage and thus bubble coalescence. As a result, higher bubble surface area flux rates are realized.

CHAPTER 8

RECOMMENDATIONS FOR FUTURE WORK

The results obtained in the current research demonstrated that there is potential for improved flotation recovery for the finest and the coarsest size fractions that exist in the feed slurry. However, further research is needed from the fundamental perspective and for successful and practical applications of the proposed processes in the mining industry. The following recommendations for future studies were developed to supplement or expand the findings of the research conducted in this study:

Cavitation Feed Pretreatment:

1. During the in-plant testing, the amount of collector and frother dosages were not similar to the other preparation plants, which resulted in lower than expected recovery values due to the plant restrictions that prevented the operators from employing more reagents to the system. In addition to the in-plant tests conducted during this investigation, the cavitation tube system may be tested in another operation, which has already high recovery values in the flotation circuit. This study could provide additional information to test the added benefit of the cavitation tube system on reducing the flotation reagents, especially collector, which would result in both economical and environmental benefits. These tests would also reveal the repeatability of the cavitation tube system in another application and provide additional data for further improvements in the flotation circuit with and without the cavitation tube system. A systematic study for the frother concentration is also needed to draw major conclusions about the benefits of the cavitation bubbles and air addition to the flotation system and their effect on reducing the frother dosage.

2. Fundamentally evaluate the effects of the cavitation bubbles in the liquid and/or on the solid surface in relation to bubble coalescence and the froth stability in flotation. By photographically measuring the bubbles size distribution at different froth depths in the froth zone, after reaching the steady state conditions, the impact of cavitation bubbles on improved flotation performance could be better understood. The effect of particle hydrophobicity on froth stability and the film drainage in the presence and in the absence of cavitation bubbles would be beneficial to determine.

3. Conducting bubble surface area measurements to compare the cavitation- and the conventional-sized bubbles in the flotation slurry and to calculate their impact on the total bubble area flux, S_b, which determines the available bubble surface area to transport particles from the collection zone to the froth zone. Using the superficial gas flow rate, J_g, and the bubble size, D_b, data below and above the froth zone, the bubble surface area flux approaching to and leaving the froth zone could be calculated ($S_b=6J_g/D_b$).

4. Flotation steps, i.e., collision, attachment and detachment, could be fundamentally analyzed from a visual perspective using an atomic force microscopy (AFM) in the tapping mode with and without the cavitation bubbles. The cantilever helps imaging the surface features, including bubbles, by recording force variations while scanning the solid surface topology. In addition, to study the formation, adsorption and stability of cavitation bubbles on solid surfaces of different hydrophobicity, quartz crystal microbalance (QCM) techniques could be used. The vibrational frequency of a quartz crystal is strongly dependent on its mass, in which a frequency shift from a measurement is due to the adsorbed material and, thus, may indicate the hydrophobicity of the surface with and without the cavitation bubble.

<u>Evaluation of the Magnetic Plastic Particles:</u>

5. Fundamentally evaluate the effect of magnetic plastic material on induction time and thus the probability of attachment through surface chemistry studies. The

induction time would be measured experimentally under a given set of conditions, as an indicator of floatability, flotation kinetics and an indirect measure of flotation recovery. Induction time measurements would be conducted under different pH conditions with and without collector (Fuel Oil No. 2) and plastic material addition to evaluate their impact on the surface hydrophobicity and thus the floatability. Distilled water, HCl and NaOH would be used to prepare neutral, high and low pH solutions. In order to assure their accuracy, pH values of the coal-solution mixtures would be continuously measured before and after the tests. Based on these results, fundamental explanations would be addressed on the impact of plastic material on induction time.

6. Visual characterization and qualitative assessment of the impact of the magnetic plastic material on the flotation process, i.e. collision, attachment and detachment, would be studied in microscopic scale using a high-speed camera setup and froth stability measurement equipment. Floatability characteristics of different size and density coal particles would be evaluated for the formation of bubble clusters using a high-speed monitoring device to give an overall view of the flotation principles before and after the hydrophobic enhancement of the surfaces (Ata and Jameson, 2005; Emerson, 2007).

7. Propose a plan for the practical commercial application of the magnetic plastic material by conducting studies to find the best way possible to introduce the material into the existing flotation units in a preparation plant. In addition to adding the magnetic plastic material into the feed stream, investigate other methods for the direct addition into the froth phase and the bubble generation system. Consider studying the degradation of the plastic surface characteristics over time due to recycling from a preparation plant perspective. Define the surface properties of the plastic material after first, second and third time of recycling through the magnetic separator. Use scanning electron microscope (SEM) and other microscopic measurement devices to evaluate the surface characteristics and the plastic coating

properties of the magnetite particles after the recycling process. Evaluate the economics, maintenance and handling of the plastic material addition system from an operative preparation plant perspective.

APPENDIX A

STACKCELL CIRCUIT

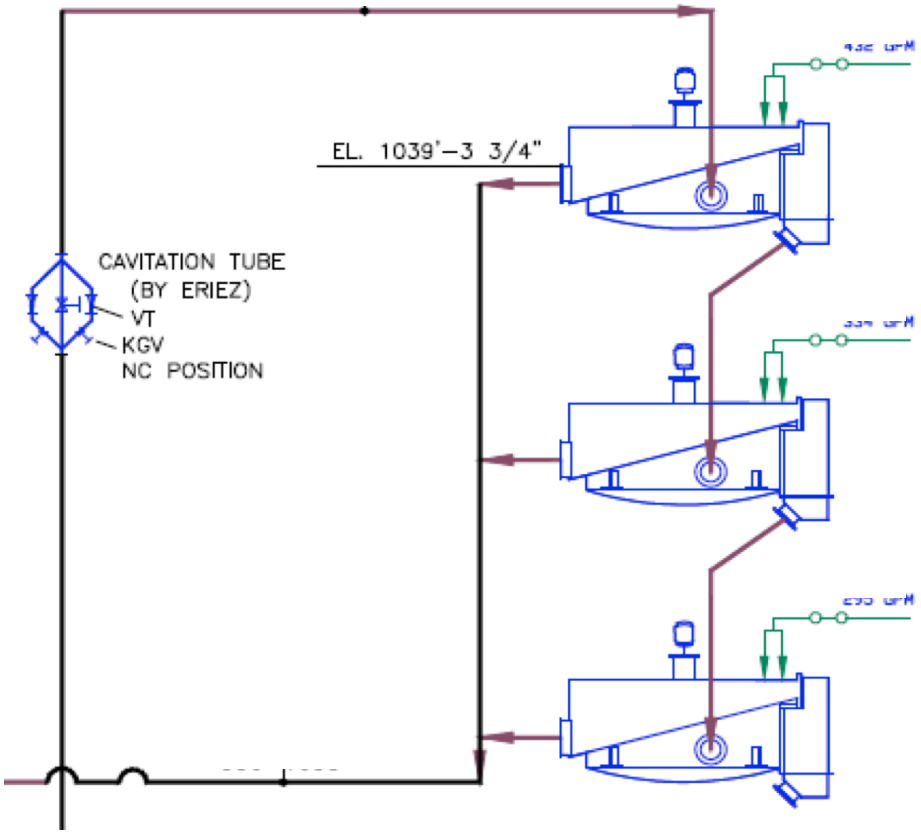


Figure A.1. The addition of cavitation tube system to the existing preparation plant design with the StackCell circuit.

Table A.1. Material and volume balance of the StackCell circuit based on the initial design.

Description	Fluid	Solids (t/h)	Solids (%)	Pulp (S.G.)	Flow (L/m)	Delivery Pressure (kPa)		
						Normal	Max.	Min.
Feed Cell-1	Slurry	60.0	6.7	1.02	13200	-	-	-
Wash Water Cell-1	Process Water	0.0	0.0	1.00	1635	138	207	138
Overflow Cell-1	Froth	15.6	12.0	1.03	1910	-	-	-
Feed Cell-2	Slurry	44.4	5.1	1.02	12925	-	-	-
Wash Water Cell-2	Process Water	0.0	0.0	1.00	1265	138	207	138
Overflow Cell-2	Froth	8.4	10.0	1.03	1240	-	-	-
Feed Cell-3	Slurry	36.0	4.1	1.02	12940	-	-	-
Wash Water Cell-3	Process Water	0.0	0.0	1.00	890	138	207	138
Overflow Cell-3	Froth	5.8	8.0	1.02	1065	-	-	-
Tailings Cell-3	Slurry	30.2	3.5	1.02	12990	-	-	-
Combined Overflows	Froth	29.8	10.4	1.03	4220	-	-	-

APPENDIX B

CAVITATION TUBE SYSTEM

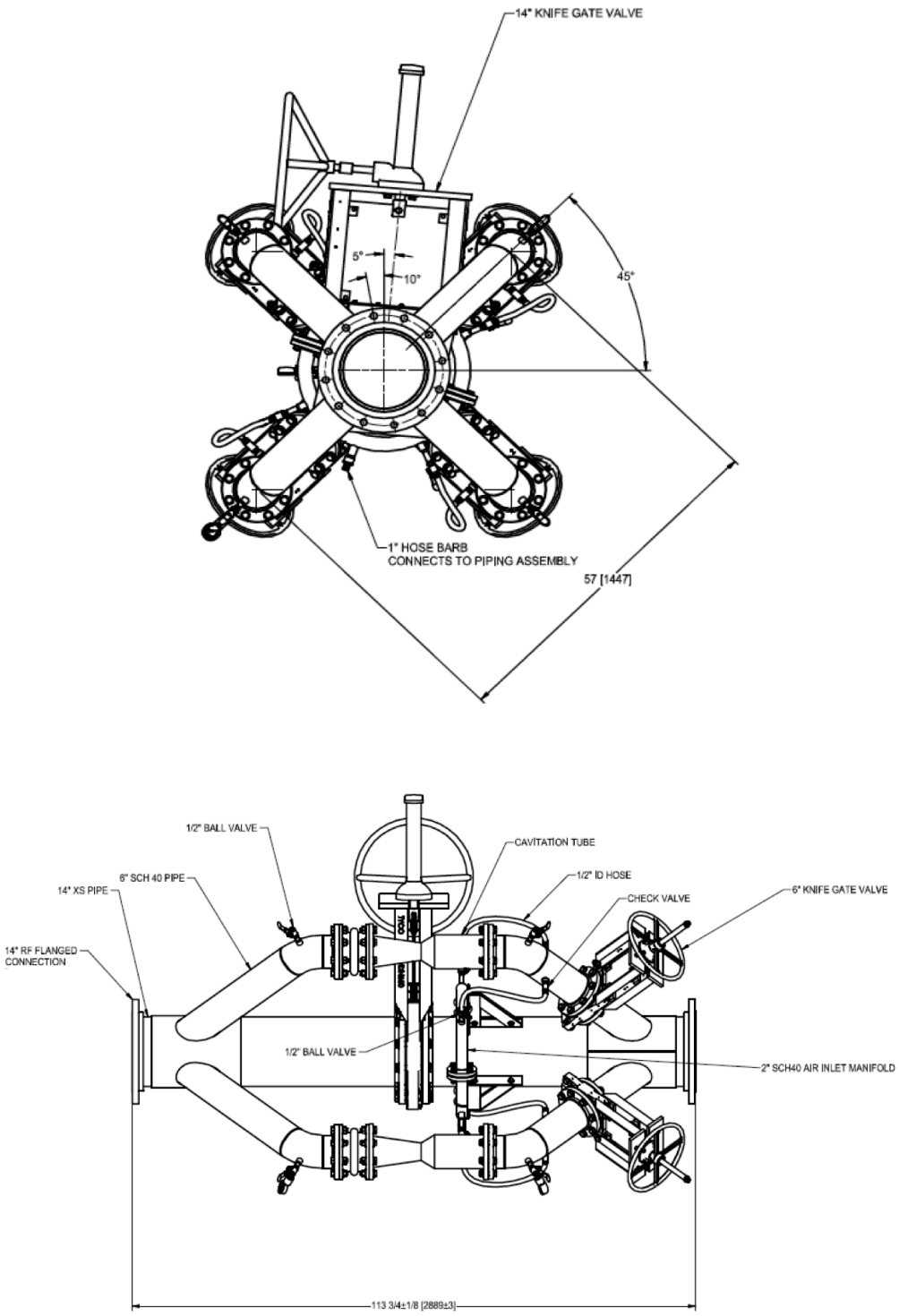


Figure B.1. The detailed design of the cavitation tube system including the knife-gate valves, pressure gauges and air inlet manifolds mounted on a 35.6-cm (14-inch) main pipe.

AUSTRALIAN VENTURI TUBE DESIGN

Australian researchers from CSIRO Energy Technology Division used the British Standards (BS 1042, 1992) to design the Venturi tube (Hart et al., 2002; 2004). According to these standards, three types of convergent sections exist in classical Venturi tubes, i.e., machined, roughcast and rough-welded. Each type specifies a set of ranges for the entrance diameter (D), the diameter (Beta) ratio (β=d/D**)** and the Reynolds Number (Re_D). The Venturi design in this study was specified to have a smooth (machined) internal surface in the convergent section, which is especially important for calculating the discharge coefficient (C) that depends on the surface finish of this section as shown in Figure B-2. If a calculated value for D, β or Re_D falls outside of the specified ranges, the relative uncertainty of the discharge coefficient (C) increases. This can affect the pressure loss across the Venturi tube, which in our case could reduce the probability of cavitation.

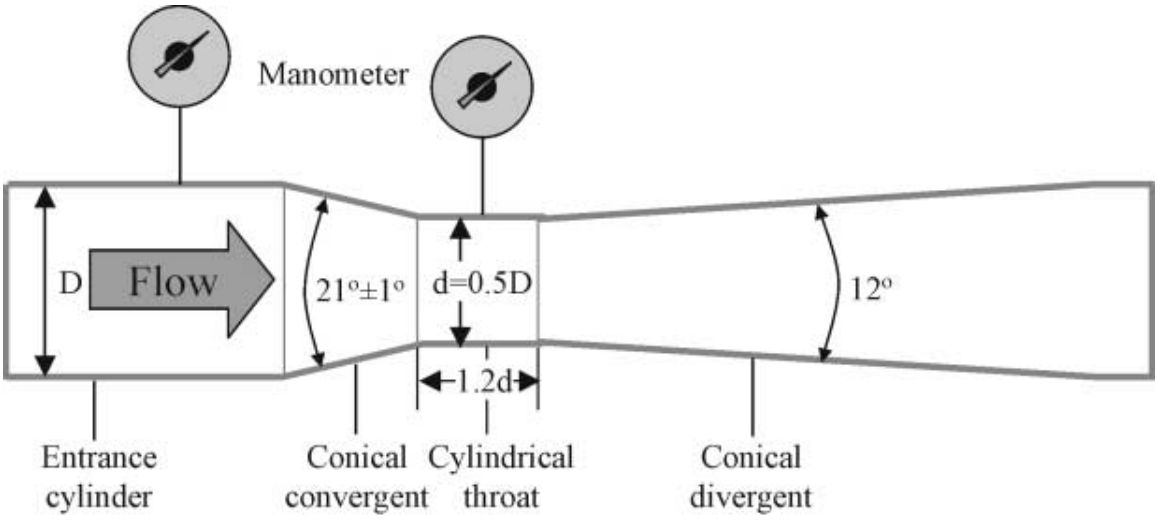


Figure B.2. Venturi cavitation tube with some of the major design parameters (Tao, 2004).

Following are the list of most important design parameters for the Venturi tube, which includes the British Standards (BS 1042, 1992) with some slight deviations that were applied by Hart et al. (2002; 2004):

1. The geometric profile of the conical convergent section of a classical Venturi tube should be 21° (or ±1°),

2. The length of the entrance cylinder to the conical convergent section should be equal to or greater than the internal diameter,

3. The design constraints for a classical Venturi tube with a machined convergent section are as follows (Section 10.1.5.3; BS 1042, 1992):
   - $50 \text{ mm} \leq D \leq 250 \text{ mm}$
   - $0.4 \leq \beta \leq 0.75$
   - $2 \times 10^5 \leq Re_D \leq 1 \times 10^6$
   - Under these conditions the value of the discharge coefficient (C) is 0.995.

4. The geometric profile of conical divergent section should be between 7° and 15°, which was angled at 5° for this study.

5. The length of cylindrical throat section should be equal to the internal diameter. From the pilot scale design, this section was modeled as 15% of the length of the cavitation section.

6. The theoretical pressure drop is taken as the difference between the pressure reading at the entrance cylinder to cavitation tube and at the cylindrical throat, which requires two gauges for the accuracy of pressure measurement. In this study, the main concern was not to determine the flow rates but to generate cavitation on the coal particles. As a result a single pressure tapping was placed at the center of the cylindrical throat section.

REFERENCES

Ahmed, N., and Jameson, G.J., 1989. Flotation kinetics. Mineral Processing and Extractive Metallurgy Review, 5, 77–99.

Anon., 2010. Cavitation sparging system: Enhanced column flotation. Published by Canadian Process Technologies Inc.

Anon., 2011. Cavitation. Submarine, propulsion and propeller lecture notes.

Arndt, R.E.A., and Ippen, A.T., 1968. Rough surface effects on cavitation inception. Journal of Basic Engineering, Transactions of The American Society of Mechanical Engineers, 90, 249-261.

Attalla, M., Chao, C., and Nicol, S.K., 2000. The role of cavitation in coal flotation. In: Proceedings of the Eight Australian Coal Preparation Conference, Port Stephens, Australia, November 12-16, 2000, pp. 337-350.

Attard, P., 2003. Nanobubbles and the hydrophobic attraction. Advances in Colloid and Interface Science, 104, 75-91.

Avery-Edwards, D.J., Elms, R., and Buckingham, A., 1994. Silicone antifoams for nonwoven applications, Tappi Journal, 77 (8), 235-238.

Barnaby, S. W., and Thornycroft, J., 1895, Torpedo boat destroyers, In: Proceedings of the Institution of Civil Engineers, 122, pp. 51-103.

Barnaby, S. W., 1897. On the formation of cavities in water by screw propellers at high speeds. Transactions of the Institute of Naval Architects, 38, 139-144. 103.

Batchelor, G. K., 1951. Pressure fluctuations in isotropic turbulence. In: Proceedings of the Cambridge Philosophical Society, 47, pp. 359-374.

Batterham, R., and Moodie, J.P., 2005. Flotation in the minerals industry – Some observations. In: Proceedings of the Centenary of Flotation Symposium, The Australasian Institute of Mining and Metallurgy, Melbourne, Australia, pp. 3-6.

Butt, H.J., Jaschke, M., and Ducker, W., 1995. Measuring surfaces forces in aqueous electrolyte solution with the atomic force microscope. Bioelectrochemistry and Bioenergetics, 38, 191–201.

Chhabra, R.P., 1993. Bubbles, drops, and particles in non-Newtonian fluids. CRC Press. Boca Raton, Florida.

Cheng, T., and Holtham, P.N., 1995. The particle detachment process in flotation. Minerals Engineering, 8 (8), 883–891.

Cho, Y.S., and Laskowski, J.S., 2002. Effect of flotation frothers on bubble size and foam stability. International Journal of Mineral Processing, 64, 69-80.

Christodoulou, L., 2013. Personal communication.

Cilliers, J., 2007. Column flotation - The froth in column flotation, In: Fuerstenau, M.C., Jameson, G., and Yoon, R.H., (Eds.), Froth Flotation – A Century of Innovation, SME, Littleton, Colorado, pp.708-729.

Craig, V.S.J., Ninham, B.W., and Pashley, R.M., 1993. The effect of electrolytes on bubble coalescence in water. Journal of Physical Chemistry, 97, 10192-10197.

Dahlke, R., Gomez, C.O., and Finch, J.A., 2005. Operating range of a flotation cell determined from gas holdup vs. gas rate. Minerals Engineering, 18 (9), 977-980.

Dai, Z., Fornasiero, D., and Ralston, J., 2000. Particle-bubble collision models – A review. Advances in Colloid and Interface Science, 85, 231–256.

Daily, J.W., and Johnson, V.E., 1956. Turbulence and boundary-layer effects on cavitation inception from gas nuclei. Journal of Basic Engineering, Transactions of The American Society of Mechanical Engineers, 78, 1695-1706.

Dean, R.B., 1944. The formation of bubbles. Journal of Applied Sciences, 15, 446-451.

Deglon, D.A., Sawyer, F. and O'Connor, C.T., 1999. A model to relate the flotation rate constant and the bubble surface area flux in mechanical flotation cells. Minerals Engineering, 12 (6), 599-608.

Deglon, D.A., Egya-Mensah, D., and Franzidis, J.P., 2000. Review of hydrodynamics and gas dispersion in flotation cells on South African platinum concentrators. Minerals Engineering, 13, 235-244.

Derjaguin, B.V., and Shukakidse, N.D., 1960. Dependence of flotability of antimonite on zeta potential. Transactions of the Institute of Mining and Metallurgy, 70, 569-570.

Derjaguin, B.V., Dukhin, S.S., 1961. Theory of flotation of small and medium-size particles. Transactions of the Institute of Mining and Metallurgy, 70, 221–246.

Dippenaar, A., 1982a. The destabilization of froth by solids. I. The mechanism of film rupture. International Journal of Mineral Processing, 9, 1-14.

Dippenaar, A., 1982b. The destabilization of froth by solids. II. The rate determining step. International Journal of Mineral Processing, 9, 15-22.

Dobby, G.S., and Finch, J.A., 1987. Particle size dependence in flotation derived from a fundamental model of the capture process. International Journal of Mineral Processing, 21, 241-260.

Drzymala, J., 1994. Characterization of materials by Hallimond tube flotation. Part 2: Maximum size of floating particles and contact angle. International Journal of Mineral Processing, 42, 153-167.

Dürr-Auster, N., 2008. Formation and stability of a liquid foam prepared from a lamellar surfactant dispersion, Ph.D. Dissertation, Swiss Federal Institute of Technology (ETH), Zürich, Switzerland.

Eisenberg, P., 1950. On the mechanism and prevention of cavitation. In: Report No. 712, U.S. Navy Department, David W. Taylor Basin, pp. 121-128.

Erepan, P., 2004. Investigation of the reasons for copper and gold loss in the cleaner tail, at Ok Tedi, Papua, New Guinea, M.S. Thesis, Curtin University of Technology, Perth, Australia.

Falutsu, M., and Dobby, G.S., 1989. Direct measurement of froth drop-back and collection zone recovery in a laboratory flotation column. Minerals Engineering, 2, 377-386.

Fan, M., 2008. Picobubble enhanced flotation of coarse phosphate particles, Ph.D. Dissertation, University of Kentucky, Lexington, Kentucky, USA.

Fan, M., Tao, D., Honaker, R.Q., and Luo, Z., 2010, Nanobubble generation and its applications in froth flotation (part III): specially designed laboratory scale column flotation of phosphate. Mining Science and Technology, 20, 317-338.

Finch, J.A., and Dobby, G.S., 1990. Column Flotation. Pergamon Press, Oxford.

Finkelstein, Y., and Tamir, A., 1985. Formation of gas bubbles in supersaturated solutions of gases in water. American Institute of Chemical Engineers Journal, 31, 1409-1419.

Firth, B.A., 1998. Australian coal flotation practice. In: Parekh, B.K., and Miller, J.D., (Eds.), Advance in Flotation Technology, pp. 289-307.

Flynn, H.G., 1964. Physics of acoustic cavitation in liquids. In: Mason, W.P., (Ed.), Physical Acoustics Principles and Methods, Vol. 1, Part-B, Academic Press, New York, pp. 57-172. 1419.

French, R.H., and Wilson, D.J., 1980. Fluid mechanics-Foam flotation interactions. Separation Science Technology, 15, 1213-1227.

Fuerstenau, D.W., 1957. Correlation of contact angles, adsorption density, zeta potentials, and flotation rate. Transactions of the American Institute of Mining Engineers, 208, 1365-1367.

Garrett, P.R., 1993. Recent developments in understanding of foam generation and stability. Chemical Engineering Science, 48 (2), 367–392. 1367.

Gaudin, A.M., 1957. Flotation, 2nd edition. McGraw-Hill, New York. 1367.

Gerth, W.A., and Hemmingsen, E.A., 1976. Gas supersaturation thresholds for spontaneous cavitation in water with gas equilibration pressure up to 570 atm. Zeitschrift für Naturforschung (in German), 31a, 1711-1716. 1367.

Gerth, W.A., and Hemmingsen, E.A., 1980. Heterogeneous nucleation of bubbles at solid surfaces in gas-supersaturated solutions. Journal of Colloidal Interface Sciences, 74, 80-89. 1367.

Goel, S., and Jameson, G.J., 2010. Detachment of particles from bubbles in a stirred cell. In: Proceedings of the 25th International Mineral Processing Congress, September 6-10 2010, Brisbane, Australia.

Goel, S., and Jameson, G.J., 2012. Detachment of particles from bubbles in an agitated vessel. Minerals Engineering, 36-38, 324-330.

Gogate, P.R., and Pandit, A.B., 2001. Hydrodynamic cavitation reactors: A state of the art review. Reviews in Chemical Engineering, 17 (1), 1-85.

Gorain, B.K., Franzidis, J.P., Manlapig, E.V., 1995. Studies on impeller type, impeller speed and air flow rate in an industrial scale flotation cell. Part 1. Effect of bubble size distribution. Minerals Engineering, 8 (6), 615-635.

Gorain, B.K., Franzidis, J.P., Manlapig, E.V., 1997. Studies on impeller type, impeller speed and air flow rate in an industrial scale flotation cell. Part 4. Effect of bubble surface area flux on flotation performance. Minerals Engineering, 10 (4), 367-379.

Gorain, B.K., Franzidis, J.P., and Manlapig, E.V., 1999. The empirical prediction of bubble surface area flux in mechanical flotation cells from cell design and operating data. Minerals Engineering, 12 (3), 309-322.

Haas, P.A., and Johnson, H.K., 1967. A model and experimental results for drainage of solution between foam bubbles. Industrial & Engineering Chemistry Fundamentals, 6 (2), 225-233.

Hampton, M.A., and Nguyen, A.V., 2009. Systematically altering the hydrophobic nanobubble bridging capillary force from attractive to repulsive. Journal of Colloid and Interface Science, 333, 800-806.

Hampton, M.A., and Nguyen, A.V., 2010. Nanobubbles and the nanobubble bridging capillary force. Advances in Colloid and Interface Science, 154, 30-55.

Hayward, A.T.J., 1970. The role of stabilized gas nuclei in hydrodynamic cavitation inception, Journal of Physics-D: Applied Physics, 3, 574-579.

Hart, G., Morgan, S., Bramall, N., and Nicol, S.K., 2002. Enhaced coal flotation using picobubbles. Investigation Report to The Australian Coal Association (ACARP), Project No. C9048, Report No. ET/IR535.

Hart, G., Townsend, P., Morgan, S., Morgan, P., and Firth, B., 2004. Scale-up of coal flotation using picobubbles. Final Report to The Australian Coal Association (ACARP), Project No. C12049, Report No. ET/IR720.

Heiskanen, K., 2000. On the relationships between flotation rate and bubble surface area flux. Minerals Engineering, 13 (2), 141-149.

Hennessy, T.R., 1989. On the site of origin, evolution and effects of decompression microbubbles. In: Brubakk, A.O., Hemmingsen, B.B., and Sundnes, G., (Eds.), Supersaturation and Bubble Formation in Fluids and Organisms, The Royal Norwegian Society of Sciences and Letters, The Foundation, Trondheim, Norway, pp. 291-340.

Henry, C.L., 2009. Bubbles, Thin Films and Ion Specificity, PhD Dissertation, The Australian National University, Canberra, Australia.

Hinze, J.O., 1955. Fundamentals of the hydrodynamic mechanism of splitting in dispersion processes. American Institute of Chemical Engineers Journal, 1 (3), 289–295.

Holl, J.W., 1960a. The inception of cavitation on isolated surface irregularities. Journal of Basic Engineering, 82, 169-183.

Holl, J.W., 1960b. An effect of air content on the occurrence of cavitation. Journal of Basic Engineering, 82, 941-946.

Holl, J.W., 1969. Limited cavitation, In: Robertson, J.M., and Wislicenus, G.F., (Eds.), Cavitation State of Knowledge, The American Society of Mechanical Engineers, New York, USA.

Holl, J.W., 1970. Nuclei and cavitation. Journal of Basic Engineering, 92, 681-688.

Honaker, R.Q., 2006. Air eductor flotation feed pretreatment. 2006-2007 Research Summary.

Honaker, R.Q., Ozsever, A.V. and Parekh, B.K., 2006. Selective detachment process in column flotation froth. Minerals Engineering, 19(6-8), 687-695.

Honaker, R.Q., 2008. Course notes: Advances in froth flotation.

Ip, S.W., Wang, Y., and Toguri, J.M., 1999. Aluminum foam stabilization by solid particles. Canadian Metallurgical Quarterly, 38 (1), 81-92.

Ishida, N., Sakamoto, M., Miyahara, M., and Higashitani, K. 2000. Attraction between hydrophobic surfaces with and without gas phase. Langmuir, 16 (13), 5681-5687. 695.

Israelachvili, J.N. and Pashley, R.M., 1984. Measurement of the hydrophobic interaction between two hydrophobic surfaces in aqueous electrolyte solutions. Journal of Colloidal Interface Science, 98 (2), 500-514. 695.

Israelachvili, J.N., and McGuiggan, P.M., 1988. Forces Between Surfaces in Liquids. Science, 241 (4867), 795-800.

Jameson, G.J., Nguyen, A.V., Ata, S., 2008. The flotation of fine and coarse particles. In: Fuerstenau, M.C. (Ed.), Froth Flotation-A Century of Innovation. Society for Mining, Metallurgy, and Exploration, Inc. (SME), USA, pp. 339-372.

Jameson, G.J., 2010. New directions in flotation machine design. Minerals Engineering 23, 835-841.

Jiang, L., 1998. Fluidization of particles by a gas stream through a batch particle/liquid suspension in a tubular bubble column, M.S. Thesis, University of Minnesota, Minneapolis, MN.

Jowett, A., 1974. Resolution of flotation recovery curves by a differential plot method. In: Transactions of the American Society of Mining and Metallurgical Engineers, 85 C263–C266.

Jowett, A., 1980. Fine Particles Processing. In: Somasundaran, P., (Ed.), Proceedings of the International Symposium on Fine Particles Processing, AIME, AIMM, New York, Vol. 1, Chapter 37.

Karaman, M.E., Ninham, B.W., and Pashley, R.M., 1996. Effects of dissolved gas on emulsions, emulsion polymerization, and surfactant aggregation. Journal of Physical Chemistry, 100, 15503-15507. 695.

Kelsall, D.F., 1961. Application of probability assessment of flotation systems. In: Transactions of the American Society of Mining and Metallurgical Engineers, 70, 191-204.

Kempnich, R.J., 2003. Coal preparation – a world review. In: Proceedings of the 20th International Coal Preparation Conference, Lexington, Kentucky, pp. 15–40.

Knapp, R.T., Daily, J.W., and Hammitt, F.G., 1970. Cavitation. McGraw-Hill, New York, USA.

Kohmuench, J.N., and Mankosa, M.J., 2006. An update on the role of column flotation in the coal industry. Coal Preparation Society of America Journal, 5(1), 19-26.

Kohmuench, J., Mankosa, M., Yan, E., Wyslouzil, H., Christodoulou, L., and Luttrell, G., 2010. Advances In Coarse Particle Recovery – Fluidised-Bed Flotation. Proceedings of the 25th International Mineral Processing Congress (IMPC), September 6-10, 2010, Brisbane, Australia.

Krasowska, M., and Malysa, K., 2007. Kinetics of bubble collision and attachment to hydrophobic solids: I. Effect of surface roughness. International Journal of Mineral Processing, 81, 205-216. 19-26. 695.

Krasowska, M., Krastev, R., Rogalski, M., and Malysa, K. 2007. Air-Facilitated Three-Phase Contact Formation at Hydrophobic Solid Surfaces under Dynamic Conditions. Langmuir, 23 (2), 549-557.

Laplante, A. R., 1980. The effect of air flow rate on the kinetics of flotation, Ph.D. Dissertation, University of Toronto, Toronto, Canada.

Lauterborn, W., 1979. Cavitation and coherent optics. In: Cavitation and Inhomogeneities in Underwater Acoustics, Springer-Verlag, pp.3-12.

Leonard, R., and Lemlich, R., 1965. Laminar longitudinal flow between close-packed cylinders, Journal of Chemical Engineering Science, 20, 790-791.

Levenspiel, O., 1972. Chemical Reaction Engineering, Wiley, New York.

Li, S.C., Ed., 2000. Cavitation of hydraulic machinery, 6th Edition, Imperial College Press, London, UK.

Liberato, R., 2011. Personal communication.

Lin, T.J., Tsuchiya, K., and Fan, L.S., 1998. Bubble flow characteristics in bubble columns. American Institute of Chemical Engineers Journal, 44, 545-560.

Luttrell, G., 2010. Personal communication.

Luttrell, G., 2012. Bubble Trouble. Coal Preparation Society of America Journal, 11(3), 9-11.

Luttrell, G., and Yoon, R.H., 1992. A hydrodynamic model for bubble-particle attachment. Journal of Colloid Interface Sciences, 154, 129-137.

Lynch, A.J., 1977. Mineral crushing and grinding circuits: their simulation, optimization and control. In: Fuerstenau, D. W. (Ed.), Developments in Mineral Processing, Vol. 1, Elsevier, Amsterdam, p. 342.

Mankosa, M.J., Luttrell, G.T., Adel, G.T., Yoon, R.H., 1992. A study of axial mixing in column flotation. International Journal of Mineral Processing, 35, 51-64.

Marrucci, G., 1969. A Theory of Coalescence. Chemical Engineering Science, 24, 975-985.

Mao, L., and Yoon, R.H., 1997. Predicting flotation rates using a rate equation derived from first principles. International Journal of Mineral Processing, 51, 171-181. 51-64.

Mason, T.J., 1991. Practical sonochemistry. Ellis Horwood, Chichester, UK, p. 27.

Meloy, T. P., 1983. Analysis and optimization of mineral processing and coal-cleaning circuits – circuit analysis. International Journal of Mineral Processing, 10(1), 61-80.

Munoz-Diaz, C., 2007. Performance And Enhancement Methods For Coal Flotation. M.S. Thesis. University of Kentucky, Lexington, KY.

Nguyen, A.V., Schulze, H.J., and Ralston, J., 1997. Elementary steps in particle-bubble attachment. International Journal of Mineral Processing, 51, 183-195.

Nguyen, A., 2003. New method and equations for determining attachment tenacity and particle size limit in flotation. International Journal of Mineral Processing, 68, 167-182.

Ofori, P., and Firth, B.A., 1998. TurboFlotation for fine coal. In: Partridge, T., (Ed.), Proceedings of 23rd International Coal Preparation Congress, Brisbane, Australia, pp. 746-755.

Honaker, R.Q., and Ozsever, A.V., 2002. Evaluation of the selective detachment process in froth flotation. Presented in: National Energy Technology Laboratory, September 4, 2002.

Ozsever, A.V., 2005. Evaluation of the Selective Detachment Process in Froth Flotation. PhD. Dissertation, University of Kentucky, Lexington, KY.

Parekh, B.K., and Miller, J.D., 1998. Advances in Flotation Technology, SME, CO.

Parker, J.L., Claesson, P.M., and Attard, P., 1994. Bubbles, cavities, and the long-ranged attraction between hydrophobic surfaces. Journal of Physical Chemistry, 98, 8468-8480.

Palmer, L., Cookson, D., and Lamb, R., 2011. The relationship between nanobubbles and the hydrophobic force. Langmuir, 27(1), 144-147.

Parsons, C. A., 1897. The application of the compound steam turbine to the purpose of marine propulsion. In: Transactions of the Institute of Naval Architects, Vol. 38, pp. 232-242.

Parsons, C. A., 1906. The steam turbine on land and at sea. Lecture to Royal Institution, 4 May 1906.

Pease, D.C., and Blinks, L.R., 1947. Cavitation from solid surfaces in the absence of gas nuclei. Journal of Physical and Colloidal Chemistry, 51, 556-567.

Power, A., Franzidis, J.P., and Manlapig, E.V., 2000. The characterization of hydrodynamic conditions in industrial flotation cells. Presented at the 7th Mill Operators` Conference, Australiasian Institute of Mining and Metallurgy, Kalgoorlie, Parkville, Australia.

Prince, M.J., and Blanch, H.W., 1990. Bubble coalescence and break-up in air-sparged bubble columns. American Institute of Chemical Engineers Journal, 36, 1485-1499.

Pyke, B., Fornasiero, D., and Ralston, J., 2003. Bubble particle heterocoagulation under turbulent conditions. Journal of Colloid and Interface Science, 265, 141-151.

Rabinovich, Y.I. and Yoon, R.H., 1994. Use of atomic force microscopy for the measurements of hydrophobic forces. Colloid and Surface Science, 93, 263-273.

Ralston, J. and Dukhin, S.S., 1999. The interaction between particles and bubbles. Colloid and Surface Science, 151, 3-14.

Ralston, J., Dukhin, S.S., Mischuk, N.H., 1999a. Bubble-particle attachment and detachment in flotation. International Journal of Mineral Processing, 56, 133-164.

Ralston, J., Dukhin, S.S., Mischuk, N.H., 1999b. Inertial hydrodynamic particle-bubble interaction in flotation. International Journal of Mineral Processing, 56, 207-256. 3-14.

Ryan, W.L. and Hemmingsen, E.A., 1993. Bubble formation in water at smooth hydrophobic surfaces. Journal of Colloidal Interface Sciences, 157, 312-317.

Sastri, S.R.S., 1996. Technical Note: Carrying Capacity in Flotation Columns. Minerals Engineering, 9 (4), 465-468.

Sayed-Ahmed, A.S., 2013. Bubble-particle interactions in nanobubble enhanced froth flotation. Poster presentation in the 2013 SME Annual Meeting, Denver, Colorado.

Schubert, H., and Bischofberger, C., 1978. On the hydrodynamics of flotation machines, International Journal of Mineral Processing, 5, 131.

Schubert, H., 1999. On the turbulence-controlled microprocesses in flotation machines, International Journal of Mineral Processing, 56, 257.

Schubert, H., 2005. Nanobubbles, hydrophobic effect, heterocoagulation and hydrodynamics in flotation. International Journal of Mineral Processing, 78, 11-21.

Schuhmann, R.J., 1942. Flotation kinetics: I. Methods for steady state study of flotation problems. Journal of Physical Chemistry, 46, 891-902.

Schulze, H.J., 1982. Dimensionless number and approximate calculation of the upper particle size of floatability in flotation machines. International Journal of Mineral Processing, 9, 321-328.

Schulze, H.J., 1984. Physicochemical Elementary Processes in Flotation. Elsevier, Amsterdam.

Sherrell, I. M., 2004. Development of a flotation rate equation from first principles under turbulent flow conditions, Ph.D. Dissertation, Virginia Polytechnic Institute and State University, Blacksburg, Virginia.

Simonsen, A.C., Hansen, P.L., and Klosgen, B., 2004. Nanobubbles give evidence of incomplete wetting at a hydrophobic interface. Journal of Colloid and Interface Science, 273, 291-299.

Smoluchowski, M.v., 1917. Theory of coagulation in colloids. Zeitschrift für Physikalische Chemie (in German) 92, 129-168.

Soto, H.S., Barbery, G., 1991. Flotation of coarse particles in a counter-current column cell. Minerals & Metallurgical Processing, 8 (1), 16-21. 695.

Sposito, G., 1989. Chemistry of Soils. Oxford University Press, New York. 695.

Stinebring, D.R., Billet, M.L., Lindau, J.W. and Kunz, R.F., 2001. Developed cavitation-cavity dynamics. Course Material, Applied Research Laboratory, State College, PA, USA. York.

Stockelhuber, K.W., Radoev, B., Wenger, A. and Schulze, H.J., 2004. Rupture of wetting films caused by nanobubbles, Langmuir, 20, 164-168.

Stumm, W., 1992. Chemistry of The Solid – Water Interface. John Wiley and Sons Inc., New York.

Sutherland, K. L., 1948. Physical chemistry of flotation, XI – Kinetics of the flotation process. International Journal of Physical Chemistry, 52, 394-425.

Tan, S.N., Fornasiero, D., Sedev, R., Ralston, J., 2005a. Marangoni effects in aqueous polypropylene glycol films. Journal of Colloid Interface Science, 286, 719–729.

Tan, S.N., Pugh, R.J., Sedev, R., Ralston, J., 2005b. Foaming of polypropylene glycols and glycol/MIBC mixtures. Minerals Engineering, 18, 179-188.

Tao, D., 2004. Role of bubble size in flotation of coarse and fine Particles – A review. Separation Science and Technology, 39 (4), 741-760.

Tao, Y., Liu, J., Yu, S., and Tao, D., 2006. Picobubble enhanced fine coal flotation. Separation Science and Technology, 41, 3597-3607.

Tao, D., Fan, M., and Honaker, R.Q., 2010. Enhanced fine coal column flotation using cavitation concept. In: Proceedings of the 16th International Coal Preparation Congress, April 25-29 2010, Lexington, KY, USA.

Tomlinson, H.S., Fleming, M.G., 1965. Flotation rate studies. In: Proceedings of the 6th International Mineral Processing Congress. Pergamon, Oxford, pp. 563–579.

Trevena, D.H., 1987. Cavitation and tension in liquids. Adam Hilger, Bristol, UK.

Verbist, G., Weaire, D., and Kraynik, A.M., 1996. The foam drainage equation. Journal of Physics: Condensed Matter, 8, 3715-3731. 695.

Weber, M.E., and Paddock, D., 1983. Interceptional and gravitational collision efficiencies for single collectors at intermediate Reynolds numbers. Journal of Colloid Interface Sciences, 94, 328-335.

Weiss, T., and Schubert, H., 1988. In: Proceedings 16th Mineral Processing Congress, Elsevier, Stockholm, Part A, p. 807.

Westwater, J.M., 1964. Measurement of bubble growth during mass transfer. In: Davis, R., (Ed.), Cavitation in Real Liquids, Elsevier, Amsterdam, pp. 34-54.

Williams, J.J.E. and Crane, R.I., 1983. Particle collision rate in turbulent flow. International Journal of Multiphase Flow, 9 (4), 421-35.

Wu, T.Y., 1969. Cavity flow analysis: a review of the state of knowledge. In: Robertson, J.M., and Wislicenus, G.F., (Eds.), Cavitation State of Knowledge, The American Society of Mechanical Engineers, New York, USA.

Xu, Z., and Yoon, R.H., 1990. A study of hydrophobic coagulation. Journal of Colloid and Interface Science, 134, 2, 427-434.

Yang, J., Duan, J., Fornasiero, D., and Ralston, J., 2003. Very small bubble formation at the solid-water interface. Journal of Physical Chemistry-B, 107, 6139-6147.

Yianatos, J.B., Bergh, L.G., and Aguilera, J., 2000. The effect of grinding on mill performance at division Salvador, Codelco-Chile. Minerals Engineering, 13(5), 485-495.

Yianatos, J.B., Bergh, L.G., Condori, P., and Aguilera, J., 2001. Hydrodynamic and metallurgical characterization of industrial flotation banks for control purposes. Minerals Engineering, 14(9), 1033-1046.

Yoon, R.H., and Luttrell, G.H., 1989. The effect of bubble size on fine particle flotation. Mineral Processing and Extractive Metallurgy Review, 5, 101-122.

Yoon, R.H., Luttrell, G., Adel, G.T. and Mankosa, M.J., 1989. Recent advances in fine coal flotation. In: Chander, S., (Ed.), Advances in Coal and Mineral Processing Using Flotation, Society of Mining Engineers, Littleton, CO, Chapter 23, pp. 211-218.

Yoon, R.H., 1991. Hydrodynamic and surface force in bubble-particle interaction. In: Proceedings of 17th International Mineral Processing Congress, Dresden, Germany, Vol. II, pp. 17-31.

Yoon, R.H., 1993. Microbubble Flotation. Minerals Engineering, 6 (6), 619-630.

Yoon, R.H. and Mao, L., 1996. Application of extended DLVO theory, IV - Derivation of flotation rate equation from first principles. Journal of Colloid and Interface Science, 181(2), 613-626.

Yoon, R.H., Flinn, D.H., Rabinovich, Y.I., 1997. Hydrophobic interactions between dissimilar surfaces. Journal of Colloids Interface Science, 185, 363-370.

Yoon, R.H. and Aksoy, B.S., 1999. Hydrophobic forces in thin water films stabilized by dodecylammonium chloride. Journal of Colloids Interface Science, 211, 1-10.

Yoon, R.H., 2000. The role of hydrodynamic and surface forces in bubble-particle interaction. International Journal Mineral Processing, 58, 128-143.

Young, F. R., 1999. Cavitation. Watford College-Hertfordshire, McGraw-Hill, London, UK.

Zhou, Z.A, 1996. Gas nucleation and cavitation in flotation, Ph.D. Dissertation, McGill University, Montreal, Canada.

Zhou, Z.A, Xu, Z., Finch, J.A., Hu, H., and Rao, S.R., 1997. Role of hydrodynamic cavitation in fine particle flotation. International Journal of Mineral Processing, 51, 139-149.

VITA

I. PERSONAL DATA

Place of Birth: Surmene-Trabzon, TURKEY

II. EDUCATION

Ph.D. University of Kentucky – 2007 to 2013 - Mining Engineering

M.S. University of Kentucky – 2004 to 2007- Mining Engineering

B.S. Istanbul Technical University – 2000 to 2004- Mining Engineering

III. PROFESSIONAL EXPERIENCE

08/04 – 09/13	University of Kentucky, Lexington, Kentucky
01/04 – 06/04	Istanbul Technical University, Istanbul, Turkey

V. JOURNAL PUBLICATIONS

Honaker, R.Q., Jain, M. and Saracoglu, M., 2007. Ultrafine coal cleaning using spiral concentrators. Minerals Engineering, 20 (14), 1315 – 1319.

Honaker, R.Q., Saracoglu, M., Thompson, E., Bratton, R., Luttrell G.H., and Richardson, V., 2008. Upgrading coal using a pneumatic density-based separator. International Journal of Coal Preparation and Utilization, 28 (1), 51 – 67.

VI. CONFERENCE PROCEEDINGS

Honaker, R.Q., Jain, M., Parekh, B. K., and Saracoglu, M., "Optimized Spiral Separation Performance for Ultrafine Coal Cleaning", In *Proceedings of the XV International Coal Preparation Congress*, Beijing, China, October 17-20, 2006, Beijing: China University of Mining and Technology, pp. 502-508.

Honaker, R.Q., Luttrell, G., Bratton, R., Saracoglu, M., Thompson, E., and Richardson, V., "Dry Coal Cleaning Using the FGX Separator". In *Proceedings of the Coal Prep 2007: 24th Annual International Coal Processing Exhibition and Conference*, Lexington, KY, April 30-May 3, 2007.

Saracoglu, M., and Honaker, R.Q., "Evaluating Chemical Needs in Coal Flotation". In *Proceedings of the XIIth International Mineral Processing Symposium,* Cappadocia, Turkey, October 6-8, 2010.

Saracoglu, M., and Honaker, R.Q., "Dry Coal Cleaning Using the FGX Separator". In *Proceedings of the 27th Annual International Pittsburgh Coal Conference,* Istanbul, Turkey, October 11-14, 2010.

Saracoglu, M., Honaker, R.Q., and Bratton, R., "Parametric Evaluation of Air Table Separations For U.S. Coals of Varying Characteristics", In *Proceedings of the 2011 SME Annual Meeting*, Denver, Colorado, February 27 – March 2, 2011.

Honaker, R.Q., Saracoglu, M., Kohmuench, J., and Mankosa, M., "Cavitation Pretreatment of a Flotation Feedstock for Enhanced Coal Recovery". In *Proceedings of the Coal Prep 2011: 28th Annual International Coal Processing Exhibition and Conference*, Lexington, KY, May 2-5, 2011.

Honaker, R.Q., Saracoglu, M., Kohmuench, J., and Mankosa, M., "Cavitation Pretreatment of a Flotation Feedstock for Enhanced Coal Recovery". In *Proceedings of the 22nd World Mining Congress and Expo,* Istanbul, Turkey, September 11-16, 2011.

Honaker, R.Q., Saracoglu, Christodoulou, L., Kohmuench, J., Yan, E., and Mankosa, M., "In-plant Evaluation of Eriez Cavitation Pre-aeration System". In *Proceedings of the Coal Prep 2013: 30th Annual International Coal Processing Exhibition and Conference*, Lexington, KY, April 29-May 2, 2013. n